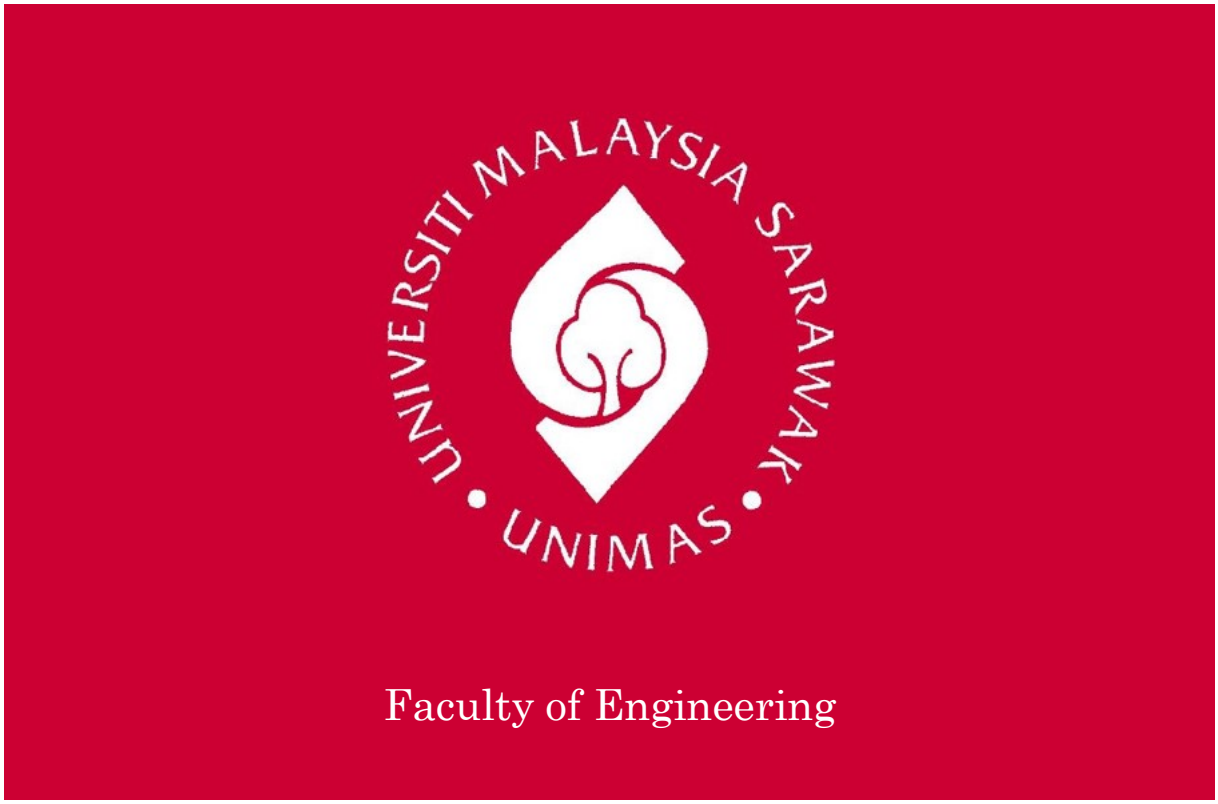

Stress-Strain-Temperature Behaviour of Deposited Cemented Slurry

Ting Wee Kiet

Master of Engineering
2019

Stress-Strain-Temperature Behaviour of Deposited Cemented Slurry

Ting Wee Kiet

A thesis submitted

In fulfilment of the requirements for the degree of Master of Engineering

(Civil Engineering)

Faculty of Engineering
UNIVERSITI MALAYSIA SARAWAK
2019

DECLARATION

I hereby declare that the work embodied in this thesis entitled "Stress-Strain-Temperature Behaviour of Deposited Cemented Slurry" has been carried out by me in the department of Civil Engineering, Universiti Malaysia Sarawak, under direction of Dr Alsidqi Hasan (Supervisor).

The information derived from the literature has been duly acknowledged in the text and list of references have been provided. The thesis has not been accepted for any degree and is not concurrently submitted in candidature for any other degree at this or any other Institution.

Name: Ting Wee Kiet

Student ID: 16020090

Date: 15 May 2019

DEDICATION

Special Dedication to my supervisor, my family, my friends, my fellow colleague and all faculty members for all your care, support and trust in me.

ACKNOWLEDGEMENT

My sincere gratitude to Universiti Malaysia Sarawak (UNIMAS) and Department of Civil Engineering, Faculty of Engineering, UNIMAS for providing the opportunity to pursue my postgraduate study by providing the good facilities, equipment and enhancement program. I would like to acknowledge the research grants provided by UNIMAS under Fundamental Research Grant Scheme FRGS/TK01(01)/1301/2015(18) from Ministry of Higher Education Malaysia.

I wish to express my unparalleled gratitude and earnest appreciation to my supervisor, Dr Alsidqi Hasan for his knowledgeable guidance and support throughout the research period. I wish to extend my thanks to my panels for their contributions, detailed comments and insight which have been an utmost gain for me.

My greatest gratitude and appreciation towards my family members and partner, Winnie Ting Huong Tien for their continuous support and inspiration throughout every highs and lows of my life. Ceaselessly, with all my appreciation to one and all who directly or indirectly contribute to the success of this research.

ABSTRACT

In mine backfill design, the estimation of stress generation from the backfilling material is crucial to ensure the stablity of the underground structure and safety for the underground workers. Under elevation of temperature which may be caused by geothermal gradient and exothermic reaction of cement hydration, cemented paste backfill (CPB) was speculated to generate additional stress towards the confined surrounding. This thesis presents a series of experimental work to explain the mechanism of deposition within narrow wall in terms of stress-strain behaviour under thermal alteration. The physical and mechanical properties of the proposed material is studied. A model was designed and developed to investigate the stress-strain-temperature behaviour of CPB that fulfilled the necessary boundary condition to replicate a mining stope. Preliminary tests were conducted on the model to ensure its accuracy. CPB as the primary sample and uncemented paste backfill (UCPB) as control sample were studied regarding their stress-strain behaviour by applying different heating pattern during and after deposition. Both materials experienced thermal expansion when there is gain in temperature. Under semi-confined condition, the material will exert thermal stress onto the adjacent wall. The final stress can be up to 50% greater than the peak stress estimated by conventional theorem upon elevation of temperature by 30 °C. UCPB and CPB experience different mechanism when there is a change in temperature but generally reflects the behaviour obtained from the full-scale monitoring. The test showed a good correlation with the anomaly observed within full-scale monitoring. Based on the finding, an empirical formulation is established to explain and predict the stress behaviour throughout the slurry-paste deposition.

Keywords: Mine backfill, cemented paste, stress-strain behaviour, thermal effects, arching

Tingkah Laku Terikan-Tegasan-Suhu Isian Buburan Simen

ABSTRAK

Dalam reka bentuk lombong, anggaran penjanaan terikan dari bahan penyangga adalah penting untuk memastikan kestabilan struktur dan keselamatan pekerja bawah tanah. Dalam keadaan bersuhu tinggi yang disebabkan oleh sumber suhu seperti geoterma dan reaksi eksotermik penghidratan simen, pes simen (CPB) dijangka untuk menghasilkan terikan tambahan ke arah sekelilingnya. Tesis ini membentangkan satu siri eksperimen untuk menerangkan mekanisme pemendapan dalam keadaan terkawal dari segi tingkah laku tegasan dan terikan dengan perubahan haba. Model yang memenuhi beberapa syarat replikasi yang diperlukan untuk mewakili keadaan perlombongan telah direka bentuk dan dibina untuk menyiasat kesan suhu atas tingkah laku buburan CPB. Sifat fizikal dan mekanikal bahan cadangan telah dikaji. CPB sebagai sampel utama dan pes lumpur yang tidak bersimen (UCPB) sebagai sampel kawalan telah dikaji dengan menggunakan pola pemanasan yang berbeza. Kedua-dua bahan mengalami pengembangan termal apabila terdapat kenaikan suhu. Di bawah keadaan separa terkurung, bahan akan menimbulkan terikan haba ke dinding bersebelahan. Peningkatan terikan sebanyak 50% dari anggaran teorem setelah mengalami peningkatan haba sebanyak 30 °C. UCPB dan CPB mengalami mekanisme yang berbeza apabila terdapat perubahan suhu tetapi pada amnya mencerminkan tingkah laku yang diperoleh dari pemantauan skala penuh. Eksperimen ini menunjukkan korelasi yang baik dengan anomali yang diperhatikan dalam pemantauan skala penuh. Berdasarkan penemuan itu, satu rumusan empirikal ditubuhkan untuk menjelaskan dan meramalkan tingkah laku terikan sepanjang pemendapan pes lumpur.

Kata kunci: *Penambangan lombong, pes simen, tingkah laku terikan-tegasan, kesan haba, lengkungan*

TABLE OF CONTENTS

LIST OF TABLES

LIST OF FIGURES

LIST OF ABBREVIATIONS

2D	Two-Dimensional
3D	Three-Dimensional
AMD	Acid Mine Drainage
ASTM	American Society for Testing and Materials
BS	British Standard
CIS	Cast In-Situ
CMS	Cahya Mata Sarawak
CPB	Cemented Paste Backfill
CTE	Coefficient of Thermal Expansion
DAQ	Data Acquisition
FS	Factor of Safety
HF	Hydraulic Fill
HTE	Half Through Element
IFC	Interfacial
INT	Internal
KB	Kanowna Bell Gold Mine
OPC	Ordinary Portland Cement
NW	Narrow Wall
PC	Precast
PF	Paste Fill
PSD	Particle Size Distribution
PWP	Pore Water Pressure
RF	Rock Fill

RL	Raleigh Mine
SEM	Scanning Electron Microscope
SF	Silica Flour
SNM	Savannah Nickel Mine
THMC	Thermo-Hydro-Mechanical-Chemical
UCPB	Uncemented Paste Backfill
UCS	Unconfined Compressive Strength

LIST OF SYMBOLS

σ_v	Vertical stress
σ_h	Horizontal stress
K	Coefficient of lateral earth pressure
ε	Strain
R^2	Determination Coefficient
u	Pore water pressure
σ'	Effective stress
E	Elastic Modulus
A	Cross-sectional area
γ	Unit Weight
w/c	Water to Cement Ratio
c	Cohesion
ϕ	Internal Friction Angle
δ	Interface Friction Angle

CHAPTER 1

INTRODUCTION

1.1 Background

Stress distribution of fill material within narrow wall such as silo has drawn considerable attention from physicist (Landry et al., 2004). Such analysis also had been extended to explain the mechanism within paste backfill in the underground mine stopes. The stress distribution was first formulated by Janssen (1895), who discovered that the total weight of the fill material within the narrow wall was not equivalent to the total weight recorded at the bottom of the narrow wall. The mechanism was described as an arching effect. The arching effect was found to be more pronounced as the wall was narrower (Janssen, 1895) or higher (Ting et al., 2011).

Silo is fabricated using steel, or reinforced concrete has been commonly used as a storage chamber for all sorts of granular material (Jarrett, 1991). It was originally designed to be cylindrical, but due to its drawback on space management and cost of fabrication, the rectangular silo is now more commonly adopted in large scale industries (Goodey et al., 2003). Both silo and mine stope have similar geometry, i.e. width to height ratio but different properties of the fill material. Granular material such as corn is usually stored in a silo while fine material such as paste is usually filled in mine stope.

The increase in demand on mining products to be used for improving and sustaining human civilisation has led to a growth burst on mining activities around the world (Sheshpari, 2015). Mining is an activity to seek and extract valuable minerals embedded within the Earth's crust (Yilmaz et al., 2003). Due to the scarcity of minerals around the ground level, deep mining is the next challenge for the mining companies to maintain their profit margin and safeness during the recovery of ores (Nasir and Fall, 2008; Sheshpari, 2015).

Underground ore extraction would create mined-out spaces (stopes) in form of narrow rectangle with plan dimensions of 15-40 m and heights of 50-100 m and above (Helinski et al., 2007; Rankine and Sivakugan, 2007) that could reduce the ground stability and indirectly giving impact to ore recovery rate and safety issues (Ghirian and Fall, 2015).

Mining activities generate huge quantities of waste rock stockpiling and tailings impoundments (Li and Yang, 2015). 3500 tailing ponds had been generated globally (Davies, 2002) and 26 tailing pond failures had been recorded in the past century (James et al., 2011). Previously, the tailings pond was a counter-measure towards the waste generated from mining, but it was not an ideal solution as tailings with sulphide minerals content would chemically react with oxygen (oxidation) and water to form acid mine drainage that could contaminate the surrounding (Potvin and Thomas, 2005). The new environmental legislation requires the mining industries to improve their tailings management by removing the existing environmental impact. Thus, a solution was introduced which is mine backfill that is much more beneficial compared to tailing impoundments (Belem et al., 2002).

Mine backfill is a new tailings management to make use of the dewatered slurries as cemented or uncemented paste (Benzaazoua et al., 2004). Cemented paste backfill (CPB) is widely adopted in the underground mining industry around the world due to its technical, environmental and economical strongpoints (Belem et al., 2002; Yilmaz et al., 2003; Benzaazoua et al., 2004; Fall et al., 2008; Huang, 2009; Li and Yang, 2015). CPB is a process of utilising dewatered tailing waste, binding agent and water to create a free-flowing slurry to be filled into stopes and hardened as adjacent underground mine support (Helinski et al., 2007; Fall et al., 2008; Ghirian and Fall, 2015; Sheshpari, 2015). CPB is well renowned by its ability to act as support to improve the stability of ground surface and provide safer working platform during extraction process which indirectly maximise ore recovery rate and

reduce environmental impact such as land expropriation and oxidation risk (Belem et al., 2002; Yilmaz et al., 2003; Benzaazoua et al., 2004; Rankine and Sivakugan, 2007; Fall et al., 2008; Huang, 2009; Li and Yang, 2015; Liu et al., 2015; Sheshpari, 2015; Yang and Li, 2015; Li et al., 2016).

As beneficial as CPB could be, there are complications in CPB mix design as the material itself has transient properties which are strongly affected by thermal, hydraulic, mechanical and chemical factors (Belem et al., 2002; Ghirian and Fall, 2015; Li et al., 2016). From December 2003 to December 2004, more than seven incidents of failure occurred due to design capability of the structure as it did not consider all of the possible factors throughout the whole filling and curing process (Helinski et al., 2007). Such failure has become a serious concern as it has a great impact on the mining operation, workers' safety and extreme penalty in cost and time (Yang and Li, 2015).

Mine backfill is conducted within a limited space or narrow wall. Most experimental research such as physical, chemical, mechanical behaviour of paste backfill had been conducted at laboratory scale due to the cost associated with the full-scale study. Although some discrepancies between laboratory test and full-scale test were evident (Fahey et al., 2011), laboratory tests are still superior in term of the ability to control. For example, temperature change due to the heat generated from exothermic hydration reactions could be monitored and simulated in the laboratory model (Belem et al., 2000; Orejarena and Fall, 2008; Abdul-Hussain and Fall 2012; Ghirian and Fall, 2014, 2016; Wu et al., 2016).

Stress propagation anomaly had been observed in the full-scale monitoring of CPB (Thompson et al., 2009, 2012; Hasan et al., 2014; Doherty et al., 2015). The stress which should reduce and remain at the rest period unexpectedly showed an incremental trend. It was recently shown by various researchers who conducted full-scale monitoring on different

mine and all showed the same propagation anomaly. It was speculated that the stress increase was due to the temperature increase. However, the data obtained from the full-scale study were not able to explain on this anomaly.

1.2 Problem Statement

Stress distribution was first explained in a theory proposed by Janssen (1895). Vertical stress (σ_v) and horizontal stress (σ_h) of deposited material, could be expressed as:

$$\sigma_v = \frac{W}{A} = \gamma h \qquad \text{[Equation 1.1]}$$

$$\sigma_h = K\sigma_v + u \qquad \text{[Equation 1.2]}$$

$$K = \frac{\sigma_h'}{\sigma_v'} \qquad \text{[Equation 1.3]}$$

where, W is the total weight of the depositing material (kN), A is the cross-sectional area of deposition (m^2), γ is the unit weight of the depositing material (kN/m^3), h is the height of deposition (m), K is a constant, u is pore water pressure (kN/m^2), σ_v' and σ_h' is the effective vertical and horizontal stresses (kN/m^2), respectively.

Equations 1.1 and Equation 1.2 are valid and applicable in standard engineering literature for evaluating total stress of material within infinite space and frictionless walls. When deposition took place in narrow opening within friction walls (narrow walls) such as mine stopes and silos, Janssen (1895) showed that the total vertical stress was lower than the result calculated by Equation 1.1 (Janssen's effect). The reduction in the vertical stress was due to the stress transfer from the depositing materials to the surrounding walls (called arching), which depended on the frictional properties between depositing materials and walls.

Modern experiments which were conducted in the centrifuge system using total stress sensors had further confirmed the Janssen's effect (Take and Valsangkar, 2001). For the non-cemented slurry application, finite element models had been carried out and confirmed with the presence of arching mechanism (Fahey et al., 2009).

For cemented slurry application, Janssen's effect, as well as Equation 1.1 and Equation 1.2, could not fully explain the deposition mechanism. Published recent findings from full-scale studies of cemented slurry deposition (in mine stopes) showed supporting results (Thompson et al., 2012; Hasan et al., 2013, 2014; Doherty et al., 2015). In these full-scale experiments, total stress sensors were installed at the bottom of mine stopes to measure the total stress during deposition. The measurements showed that as the height of deposition increased the total stress increased (propagated), when deposition stopped (called rest period) the total stress decreased for a moment, and afterwards the total stress started to gain some increase without addition of slurry. One of the recorded anomalies in the total stress increase is shown in Figure 1.1 and more observation from other literature is shown in Appendix A.

It was previously shown by researchers that conduct monitoring on different mines, and all showed the same anomaly. These results showed that the current theory on stress distribution needed to be improved to give a better explanation on the behaviour of CPB during its deposition within narrow wall by investigating the temperature change during the curing of CPB as there is still no experimental evidence to prove it.

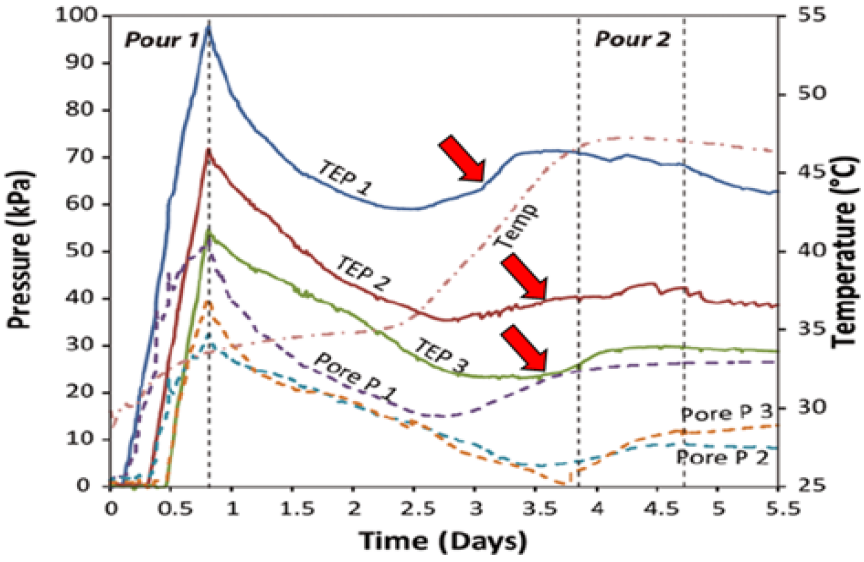

Figure 1.1: Full-scale monitoring results from published literature (Thompson et al., 2012)

1.3 Hypothesis

Based on the problem statement in Section 1.2, the anomaly could be due to the increase in temperature from various sources of heat such as exothermic cementation process/hydration of binders, geothermal gradient from the underground mine rock mass/wall and human-induced activity. The temperature caused the backfill material to expand in volume and generates thermal stress to its adjacent wall due to arching effects. This phenomenon had been speculated by Thompson et al. (2012), Hasan et al. (2013, 2014), and Doherty et al. (2015) but there is yet to be an experimental approach to explain this anomaly. By conducting the present study, the anomaly of the total stress increment could be disclosed to improve stress estimation design for mine backfilling.

1.4 Objectives

This research aims to investigate the effects of temperature on the stress-strain behaviour of laboratory prepared CPB using the designed narrow wall model. The specific objectives are as follows:

i. To determine the physical and mechanical properties of CPB.
ii. To investigate the effects of temperature on CPB geotechnical properties.
iii. To develop a narrow wall model with temperature control and monitoring system.
iv. To evaluate the effects of temperature on CPB based on stress and strain behaviour during and after deposition.
v. To propose an empirical model to improve current stress distribution theory based on the experimental findings.

1.5 Scope of Study

In this experimental research, the proposed experimental model was at laboratory scale by fulfilling most of the crucial boundary conditions to replicate the actual mining stope backfilling condition accurately. It had been established that the scale factor should not affect the results of this study based on the finding discussed in Section 2.5.2.1, Section 2.6.4 and Section 2.7.1.1. The backfill material used was a replacement for actual CPB where tailing was replaced with silica flour. The substitution of material was widely accepted and thoroughly explained in Section 2.7.3 and tested in Section 4.2. The variety of temperature pattern was limited to two main types where the first temperature pattern was performed after factoring out other stress altering mechanism while second temperature pattern was to replicate the actual temperature profile of mining stope. Another material namely uncemented paste backfill (UCPB) was also tested similarly with CPB to serve as a control sample.

CHAPTER 2

LITERATURE REVIEW

2.1 General

This chapter presents relevant material reported in the past that were related to this study. There are mainly four subsections which are discussed. The chapter focuses on cemented paste backfill (CPB) background, analytical approach of stress distribution, stress-strain behaviour of CPB within narrow wall (NW) and evidence in NW modelling.

2.2 Underground Mining

Underground mining is a process of ore recovery through deep excavation beneath the earth crust (Hustrulid and Holmberg, 1991). The process involves excavation for tunnel and rooms for mining operation which is costly and complex in term of safe design. The extracted material is transported to the processing facilities, leaving enormous underground voids at multiple regions due to scattered ore deposit. Therefore, the mine design is generally focused on ground support, accessibility, and extraction procedure corresponding to the pattern of the deposited ore (Hartman, 1992).

2.2.1 Terminology and Methods

Ore deposits were extracted via mining for century (Hustrulid and Holmberg, 1991). Common mining terminologies are shown in Table 2.1 and illustrated in Figure 2.1.

Table 2.1: Terminology used in underground mining

Terminology	Definition in underground mining
Drive	Horizontal, vertical and incline passage as access to the working area
Shafts	Vertical passage that is excavated from top to the bottom of mine
Incline	Sloping passage excavated inward from a hillside
Drifts	Horizontal underground passages that follow the trend of an ore body
Stope	Mine-out space created after ore removal
Back	The roof of mine out void
Pillar	Supporting rock mass (adjacent wall) of a stope

The open-stope method is commonly used where an open-stope is created with the support of pillars (Belem and Benzaazoua, 2008). Such method creates a mined-out void (stopes) that is in narrow-rectangular shape with a cross-sectional area of 15-40 m and height of 50-100 m and above (Helinski et al., 2007; Rankine and Sivakugan, 2007) that could significantly affect the overall stability (Ghirian and Fall, 2015).

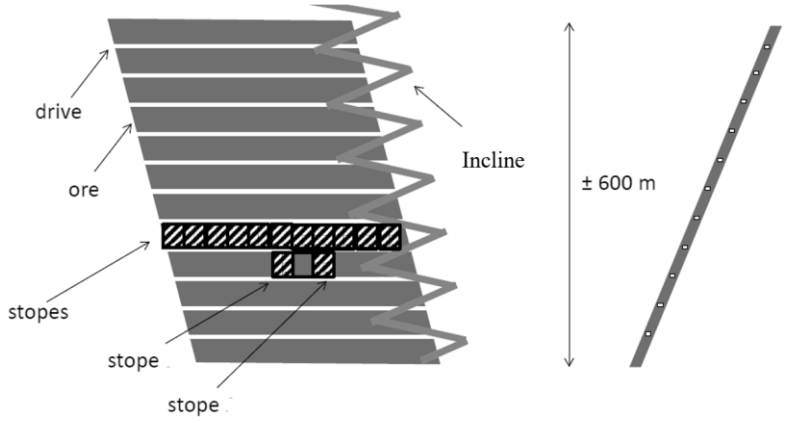

Figure 2.1: Generic schematic of underground mining
(Hasan et al., 2012)

Backfill was introduced as solution to improve engineering stability of the underground structure by filling up the void with waste material thus minimising the amount of waste to be disposed on the surface of the earth. Therefore, the benefit of backfilling has gained wide acceptance as essential solution for mining around the world (Witteman, 2013).

2.2.2 Development in Mine Backfill

Mine backfill provides a method for the proper management of mine waste and assists in the stability of mining-related voids. Backfill usually uses waste rocks or dewatered tailings as its primary materials, sometimes mixed with cement or other binders to achieve higher strength. As of today, there are three types of backfilling which are hydraulic fill (HF), rock fill (RF) and paste fill which is also known as cemented paste backfill (CPB) which their main benefits are summarised below;

i. Limiting excavation exposure and ensuring long-term regional stability: large excavations could easily lead to collapse with time. In this case, backfill could be applied as a bulking agent to occupy the voids and thus mitigates the risk of collapsing. For example, if the excavation becomes unstable and loosening material starts falling from the excavation boundary, backfill would prevent further loosening.

ii. Waste disposal: mine backfill is increasingly perceived as an environmentally friendly option to manage mine waste. Underground storage allows a reduction of surface storage of mine waste up to 60%. Studies also show that once captured underground, chemicals within mine waste tends to remain in an inert state, and most reactions are inhibited.

iii. Improving recovery rate of minerals: in most underground mining systems, pillars or walls have to be left behind to support the roof. However, with the application of mine backfill to supply the extra support, these areas could be exploited, thereby allowing a maximum recovery rate.

Fresh backfill is usually prepared in a plant located not far from a mine on the surface and is delivered either by truck, pumping, and gravity or combined ways to underground cavities. Figure 2.2 shows a schematic of a stope-mining operation, showing the interactions of the mining, processing and backfilling stages as they occur in a typical operation. Figure 2.3 shows a schematic of a typical stope-filling scenario, where the fill is deposited from the top of the stope and confined by a constructed barricade across the opening or drawpoint at the base, through which the ore was initially removed. The fill material is contained from entering the mine workings by a containment barrier called a barricade. Barricades are engineered to be permeable barriers made of waste rock and concrete aggregate mixtures for preferential drainage (Witteman, 2013).

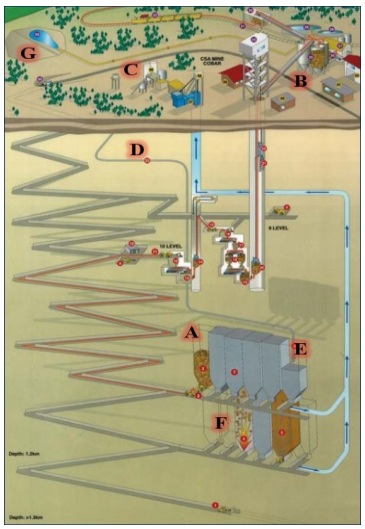

A. Ore extraction from stope.
B. Concentrator and thickener where ore is processed and full stream tailings produced
C. Backfill plant where the fill components are mixed.
D. Delivery system, transporting the fill from the backfill paste plant to the stope.
E. Backfill deposition into an excavated stope.
F. Blasting of a stope, exposing adjacent backfill.
G. Tailings storage facility

Figure 2.2: Schematic on typical stope-mining sequence with the use of CPB (After Helinski et al., 2007)

Historically, backfilling has utilised waste rock or coarse tailings material, mixed with water and cement, or other binding agents, due to the complexities associated with the use of finer tailings fraction. Considering the weakness of HF and RF, CPB has been introduced to the mine backfill with its own practical strength as shown in Table 2.2.

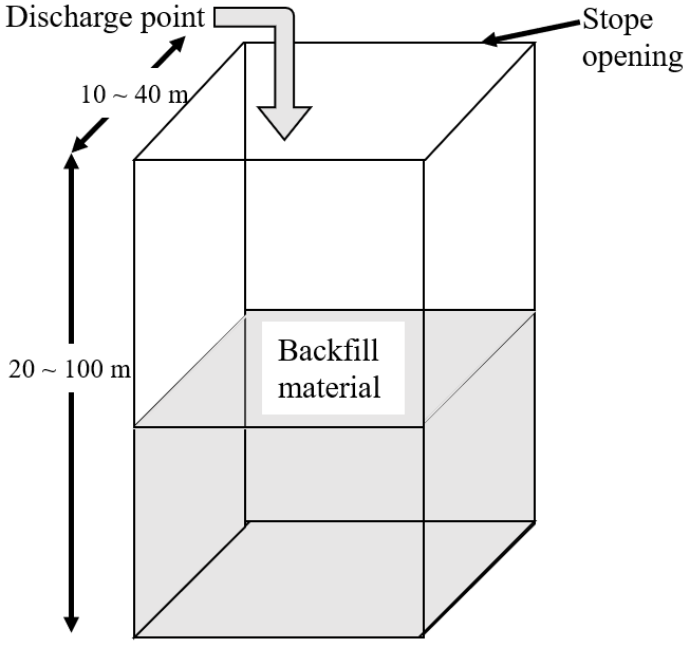

Figure 2.3: Typical stope backfilling with typical dimensions

Table 2.2: Comparisons of backfilling methods
(Hassani and Archibald, 1998)

Properties	Hydraulic Fill	Cemented Paste Fill	Rockfill
Placement State	60% to 75% solids (by weight)	75% to 85% solids (by weight)	Dry
Underground Transport System	Borehole/pipeline via gravity	Borehole/pipeline via gravity, could be pumped	Raise, mobile equipment, separate cement system
Binder Application	Cemented or uncemented	Cemented only	Cemented or uncemented
Water to Cement Ratio (w/c)	High w/c ratio, low binder strength	Low to high w/c ratio. Low to high binder strength	Low w/c ratio, high binder strength
Placement Rate	100 to 200 Tonne/hr	50 to 200 Tonne/hr	100 to 400 Tonne/hr
Segregation	Slurry settlement and segregation, low strength development	No segregation	Stockpile and placement segregation, reduced strength and stiffness
Stiffness	Low stiffness	Low or high stiffness	High stiffness if placed correctly
Tight Filling	Cannot tight fill	Easy to tight fill	Difficult to tight fill
Binder Quantity	Requires large quantity of binder	Lower quantity of binder required	Moderate binder quantities
Barricades	Expensive	Inexpensive	Not necessary
Water Runoff	Excessive water runoff	Negligible water runoff	No water runoff
Capital Costs	Low capital costs	High than for slurry fill	Moderate capital costs
Operating Costs	Low distribution costs; lowest cost for an uncemented fill	Lowest cost for a cemented fill	High operating costs

2.2.3 Cemented Paste Backfill (CPB)

CPB is used as a filling material in paste fill which is more beneficial than conventional HF. Cured and hardened CPB in stopes create stronger ground support for the operation in underground mines compared to HF (Yilmaz et al., 2004; Sheshpari, 2015).

CPB and HF both serve as mine backfilling technique which both could be beneficial as the aforementioned benefits but each technique has different intensity of effects on the benefits mentioned such as CPB used up more tailings (75 to 85% solids by weight) in its

typical mix design compared to hydraulic fill (60 to 75% solids by weight) which is able to reduce surface disposal by effectively returning it into mine stope (Hassani et al., 2008). CPB also favours in cost reduction in contract with cemented hydraulic fill as it requires a lesser amount of binder which is a major cost in backfilling. CPB could be pumped through the pipeline without worries of segregation, and it could be equally (tightly) filled into mine stope compared to HF and RF. Other benefits could be seen from the comparison provided by Hassani and Archibald (1998) referring to Table 2.2.

However, designing CPB is somewhat complicated due to its time progressive behaviour (Belem et al., 2002; Ghirian and Fall, 2015; Li et al., 2016). Analysis on backfill design parameters (e.g. internal pressure development, required strength, and mix optimization), transportation requirement (consistency and rheological) and design of optimal barricade are required for safety assurance and optimal cost (Chang, 2016).

2.2.3.1 Preparation and mix design of CPB

Underground backfill material could be differently prepared, transported and placed in mining according to fill type mining method and infrastructure (Helms, 1988). CPB materials may be from different in types of tailing and binders used, but it generally undergoes the same process of preparation. First, the mill tailings are formed from dewatered slurries by thickening and filtering process to acquire filter cake of 70 – 85% solids by weight. These solid particles are commonly mixed with one or more types of cement as a hydraulic binder such as Portland cement, sulphate-resistance cement, and ground granulated blast furnace slag, (if these materials show pozzolanic behaviour) and water was added to produce high slump (18 – 25 cm) for transportation of the paste to the underground (Helms, 1988; Brackebusch, 1995; Benzaazoua et al., 1999; Fall et al., 2005; Orejarena and Fall, 2011; Yilmaz et al., 2014). Nowadays, other additives could be added to improve the

flowability of CPB within pipeline rather than the usage of sulphide material (Sheshpari, 2015). One of the CPB preparation plants is shown in Figure 2.4.

Figure 2.4: CPB preparation plant in Chihong mine (Sheshpari, 2015)

In order to achieve a good CPB design, there are specific criteria need to be considered, which including mechanical and environmental performance, durability and barricade stability. At first, an excellent mechanical performance indicates the capability of CPB to withstand certain loading stresses after being loaded. Secondly, barricades are necessary to maintain their stability by employing suitable CPB hydraulic conductivity for drainage and suitable permeability for barricades to allow the pore water to be drained.

Apart from that, environmental performance and durability are another two essential CPB design criteria which could be altered by controlling CPB's permeability matrix. Sulphide mineral components in the CPB allows oxidation to produce acid mine drainage (AMD), a major pollutant from mining site which could contaminate the underground water (Fall et al., 2009; Wu et al., 2013). Long-term exposure of sulphide product could damage the microstructural properties of CPB (Walske, 2014). Therefore, the CPB mix composition design is essential. Depending on the required strength, hydraulic conductivity and slump, the required composition of the CPB mixture were different in terms of grain-size distribution and chemical components of the tailings, type and ratio of the binder agent, water and additives (Sheshpari, 2015). The typical percentage of binder and tailings in CPB mixture is 3 to 7% (by weight for binder) and 70 to 85% (for tailings). Besides, the water to

cement ratio of CPB is between 2.5 to 7%, which is much higher than other cement-based material. The higher water content of CPB is to ensure the smooth flow through the transportation pipeline. An adequate number of fine particles should be mixed together in CPB mixture to prevent the phenomenon of settlement and particle segregation.

Depends on the different function underground, the strength design requirement also varies for CPB (Witterman, 2013; Sheshpari, 2015; Chang, 2016). The unconfined compressive strength (UCS), is defined as the maximum axial compressive strength value that a material could withstand before its failure. Sometimes, it is also known as uniaxial compressive strength. Previously, there are many researchers reported the different range for UCS of CPB, as demonstrated in Table 2.3 below.

Table 2.3: Unconfined compressive strength (UCS) of CPB

UCS of CPB	References
• Free-standing CPB applications: UCS < 1MPa • Common applications range: 0.2MPa-5MPa when surrounding rock mass has UCS of 5 MPa – 240 MPa	Sheshpari (2015)
• Common applications range: 0.1MPa-5MPa to avoid liquefaction potential • Target strength: 1MPa • Suggested early-age curing period: ≥ 28 days	Witterman (2013)
• Common applications range: 0.7MPa-2MPa	Chang (2016)

Equation 2.1 was established to estimate the UCS under the simplest condition, at which only vertical support of the backfill to be considered (Belem and Benzaazoua, 2008):

$$UCS_{design} = E_P \left(\frac{\delta H_P}{H_P}\right) FS \qquad \text{[Equation 2.1]}$$

where, E_P is the elasticity modulus of the pillar, δH_P is the deformation of the strata, H_P is the initial height of the strata, and FS is the safety factor. According to the assumption made that any vertical loading that cause in-roof deformation was shown in Figure 2.5 which proves that CPB must have sufficient strength to remain free-standing.

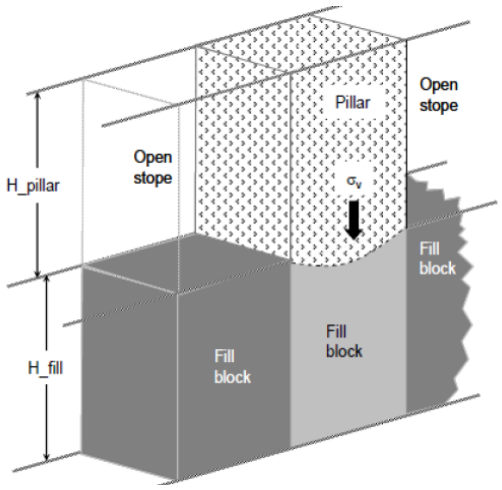

Figure 2.5: Deformation of roof due to the vertical load of pillar (Belem and Benzaazoua, 2008)

Large amount of CPB is prepared in a batching plant which is further away from the filling point, proper design and consideration on the flowability of CPB must be taken into account as it ensures the flowing of CPB to be efficient and clogging-free. Operation of CPB cost 20% of the average of total mine operating cost (Fall et al., 2008). Pipe clogging will cause delays as pipeline network is needed to be investigated and disassembled for clearing the blockage which results in more operating cost (Wu et al., 2013). During the maintenance, clogged material as well as the batched material will be wasted as hydration commence as soon as mixing commenced. Therefore, pipe clogging must be avoided at all cost by considering all influencing factors that may hinder the flowability of CPB.

Rheology of CPB depends on its slump value, mix ratio, and density as internal factors and external factors would be the effects of temperature and time progression due to hydration process (Wang et al., 2004; Yin et al., 2012). Figure 2.6 also show the source of heat that is significant during transportation of CPB is heat generation from frictional contact between CPB and pipeline and the surrounding temperature of the pipeline which is strongly dependant on the location of the mine and the embedment depth of pipeline design (Fall and Samb, 2009).

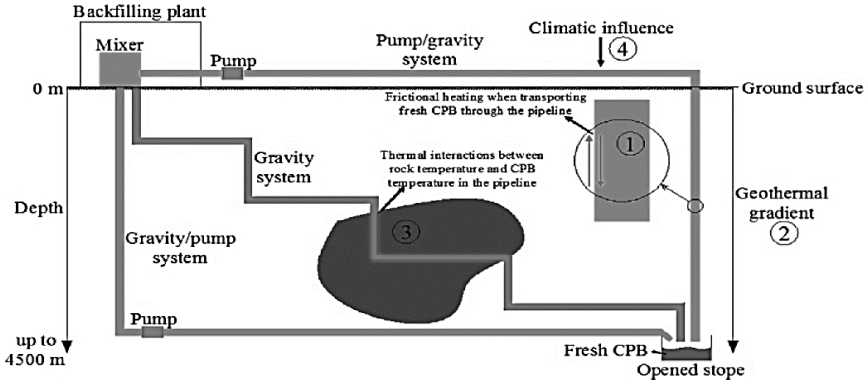

Figure 2.6: CPB transportation to underground voids and its influencing factors

2.2.3.2 Method and rate of backfilling

The rate of filling is the volume of CPB that is filled into the stope with respect to time. The rate of filling plays an important role as it controls the total stress generation (El Mkadmi et al., 2013) and evolution of pore water pressure (Thompson et al., 2012) towards the structure of the mining stope. Depending on the design requirement, different rate of filling and filling strategies could be incorporated accordingly (Nasir and Fall, 2010; Cui and Fall, 2015). The rate of the pumping CPB into the stope could be defined as the rate of backfilling. The rate of pumping by Equation 2.2 could be converted to the rate of increase in the height of backfill structure which mainly depends on the cross-sectional area (A_r) of the stope (Nasir and Fall, 2009).

$$\frac{\Delta H}{\Delta t} = \frac{\Delta V/\Delta t}{A_r} \qquad \text{[Equation 2.2]}$$

where, is the $\Delta H/\Delta t$ is the rate of backfilling (m/h) and $\Delta V/\Delta t$ the pumping rate (m^3/h).

In the mining industry, multiple stages of backfilling were usually applied to reduce the stress generated on the barricade. Depending on the fill condition, sometimes it is not necessary to have multiple stages backfilling as it prolongs the filling total duration with initial plug rest time which shows an increase in the operational cost of backfilling. Table 2.4 shows examples from two mines are presented (Helinski et al., 2011).

Table 2.4: Example of mine backfilling rate at KB and SNM mine

Mine			Kanowna Bell Gold Mine (KB)	Savannah Nickel Mine (SNM)
Details	**Parameter**	**Unit**		
CPB mix	Solid	%	75	75
	Cement	%	3.1	3.1
Geometry	Shape	-	Rectangular prism	Rectangular prism
Dimension	Height	meter	40	23
	Width	meter	15	10
	Length	meter	18	12
Backfilling rate and steps	Plug fill	meter/hour	0.2-0.5	0.04
	Plug height	meter	10	6
	Rest period	hour	24	24
	Remain fill	meter/hour	0.3-0.6	0.1
	Total time	hour	184	300

Sequential backfilling investigated by El Mkadmi et al. (2013) in his study on the effects of multiple placements of fills with different rate of filling on the stress generation. From Figure 2.7, that the initial and final stress value is greater with higher rate of filling.

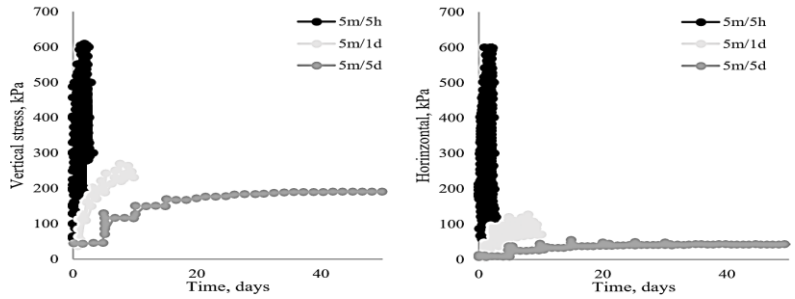

Figure 2.7: Rates of filling vs change of the total (a) vertical and (b) horizontal stresses (After El Mkadmi et al., 2013)

2.2.3.3 Hardening process of CPB

Variation of chemical composition and the presence of organics in tailings caused the hardening process of CPB to be more complex compared to concrete (Mozaffarindana, 2011). Multiple researchers had investigated the hardening process by either monitoring the mechanical properties, such as Simon (2005) or looking at the microstructure of the sample of which has been done by Ramlochan et al. (2004) and both at once by Benzaazoua et al.

(2004) which concludes that from the result of the dissolution test, the hardening process of CPB also experience precipitation of hydrated phases from pore water of CPB rather than conventional cement hydration in concrete or mortar.

Immediately after mixing all paste constituents, CPB behaves like a viscous non-Newtonian fluid (Simon, 2005). CPB hardening consists of two stages which are shown in Figure 2.8. At first stage (< 2 min), the initial dissolution of Ordinary Portland Cement (OPC) grains occurs, resulting in an amorphous semi-permeable gel on the cement surface that prevents dissolved ions from entering the bulk pore fluid (Mozaffarindana, 2011) until reaching super-saturation. During this period (known as the induction or dormant period), the paste is still plastic and workable. At the second stage (> 2 min), there will be two phenomena. First is the direct hydration of the cement residual which forms hydrates in the process. Second is the precipitation of hydrated secondary phase from the super-saturation which is controlled by water consumption in direct hydration (Benzaazoua et al., 2004).

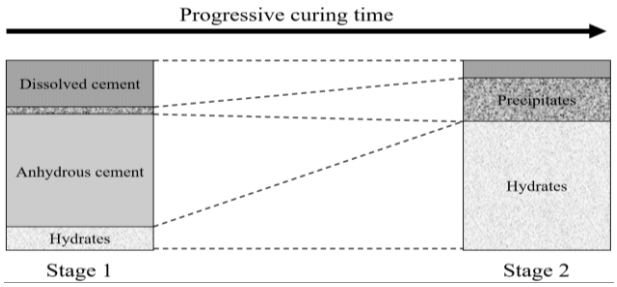

Figure 2.8: Time depending reaction of dissolution and precipitation of binder

2.3 Hydration Behaviour of CPB after Backfilling

CPB is a geotechnical material where its mechanical behaviour such as shear strength is dependent on its characteristics like cohesion and internal friction angle (Sheshpari, 2015). Studies have been done by Ghirian and Fall (2014) where the internal friction angle does not have significant change with time whereas its development in shear strength primary relies on the improvement of cohesion due to cement hydration.

The factor is dependent on the percentage of solid, binder, water content, heat load due to different sources of heat, the presence of admixture, and curing time (Sheshpari, 2015). Fall et al. (2010) investigated on the mechanical behaviour of CPB with different composition in mix design and found that change in curing temperature played a significant role in the development of modulus of elasticity and strength. Similarly, curing at higher temperature could lead to gain in strength at the early stage but resulting in lower final strength development.

The stress behaviour is connected to three mechanisms during curing such as deformation associated with chemical shrinkage and thermal expansion of CPB (Thompson et al., 2011; Cui and Fall, 2015), self-desiccation associate with cement hydration process and self-weight consolidation associated with drainage (Helinski et al., 2011). The effects of these mechanisms are crucial for the stress distribution on the walls (pillar) and barricade to ensure that CPB is capable of self-supporting during filling and curing as well as does not produce excessive stress that overload the design capacity (Sheshpari, 2015). The effect of hydration on volume reduction is interrelated with reduction in pore water pressure and chemical shrinkage phenomenon which is similar to the self-desiccation mechanism in concrete (Grabinsky and Simms, 2006; Helinski et al., 2007a). Walske (2014) state that thermal expansion needs to be significant to overcome other stress-reducing mechanisms such as chemical shrinkage and reduction in pore water pressure. As shown in Figure 2.9, cementation or hydration is an important influential factor that contributes to total stress generation from its own effect of hydration and contribution as a source of heat for thermal deformation. An understanding in the hydration process is necessary for its significance towards total stress of CPB and is discussed thoroughly in Section 2.3. Mechanism of CPB strain or deformation and its impact on effective stress generation is discussed in Section 2.4.

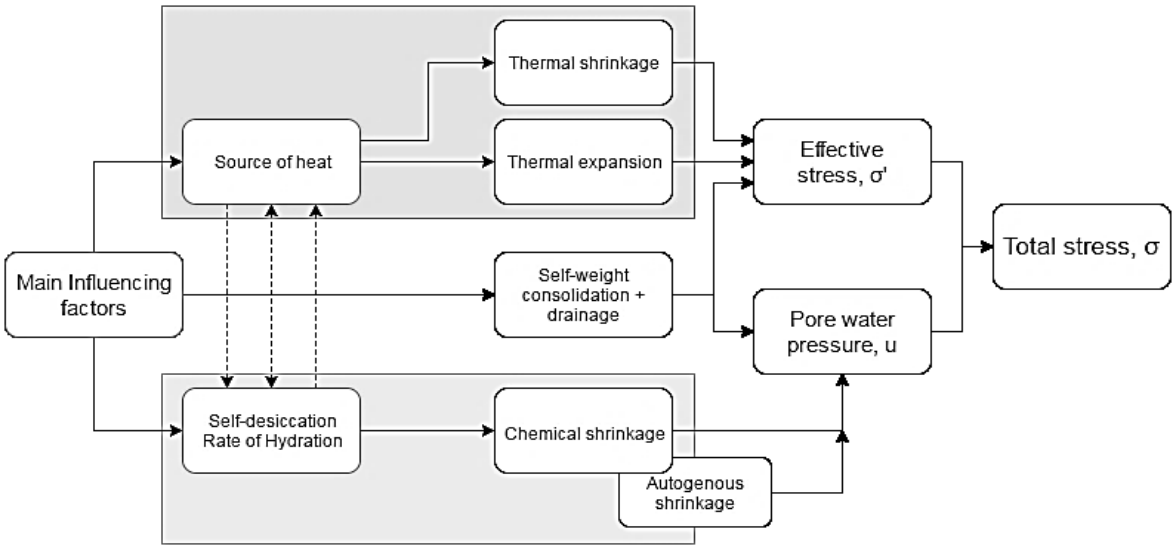

Figure 2.9: Main influencing factors on total stress generation

2.3.1 Background of Cement and its Hydration Process

Cement refers to a kind of building material made by grinding calcinated limestone and clay to a fine powder, which could be mixed with water and poured to set as a solid mass or used as an ingredient in making cement paste or concrete. Portland cement, developed from hydraulic limes, is one of the most common types of cement used around the world. According to ASTM C150, there is five common Portland cement which are types I, II, III, IV, and V. Composition of Portland cement may be different due to the different sources but it is still commonly made up of four primary types of minerals which is shown in Table 2.5. A proper balance in the composition of these minerals could provide desired properties such as strength development rate and workability.

Table 2.5: Four important minerals of Portland cement

Name	Chemical formula	Oxide composition	Abbreviation
Tricalcium silicate (alite)	Ca_3SiO_5	$3CaO.SiO_2$	C_3S
Dicalcium silicate (belite)	Ca_2SiO_4	$2CaO.SiO_2$	C_2S
Tricalcium aluminate	$Ca_3Al_2O_4$	$3CaO.Al_2O_3$	C_3A
Tetracalcium aluminoferrite	$Ca_4Al_2Fe_2O_{10}$	$4CaO.A1_nFe_{2-n}O_7$	C_4AF
Abbreviation notation: C=CaO, S=SiO_2, A=Al_2O_3, F=Fe_2O_3			

Hydration is a process of cement gaining its strength through a set of chemical reactions with the presence of water. There are two stages in hydration which are dissolution on stage one and precipitation on stage two (Benzaazoua et al., 2004). Firstly, ionic constituents (OH^-, Ca^{2+} and $H_2SiO_4^{2-}$) is released into the solution during cement and water interaction until the solution is supersaturated (no more ions could be dissolved). At this point, hydration products are formed from precipitation of excess ion. Calcium Silicate Hydrate (C-S-H) is the main product, and Calcium Hydroxide (CH) is the side product at the end of the hydration process. The detailed hydration process is shown in Appendix B.

The degree of hydration is dependent on various variables such as the ratio of water to cementitious material, type of supplementary cementing material, curing conditions, presences of admixture, and age (Mozaffarindana, 2011).

2.3.2 Contributing Factors on CPB Hydration Process

Hydration is very receptive to chemical-temperature changes and the physical characteristics of the material used in the mix design. Geochemistry of tailings used for CPB mix is usually chemically complex as it is exposed to various chemical during the mining process. Process water from mining operation have complex chemical composition, and due to utilisation purposes, it is usually used as water for CPB preparation (Sheshpari, 2015).

It gets complicated as CPB mix undergoes hydration process which many different compounds might be formed compared to ordinary cement paste or concrete. The properties and behaviour of the CPB from the beginning of mixing until its curing process in stope are continually changing due to the progression of hydration. Change due to hydration will be minimised after 28 days of curing but this subjected to change due to both physical (i.e. stress and temperature) and chemical conditions (Walske, 2014). Thorough understanding of each factor that influences hydration is vital to the understanding of CPB behaviour.

2.3.2.1 Effect of properties of hydrated cement compounds

Cement is usually made up of the four compounds mentioned in Table 2.6, and each product of the compound plays its own significant role after a series of reaction. Figure 2.10 shows that the early strength of cemented materials derives from the hydration products of C_3S and ultimate strength are provided by the hydration products of C_2S. C_3A is the main contributing compound towards heat generation.

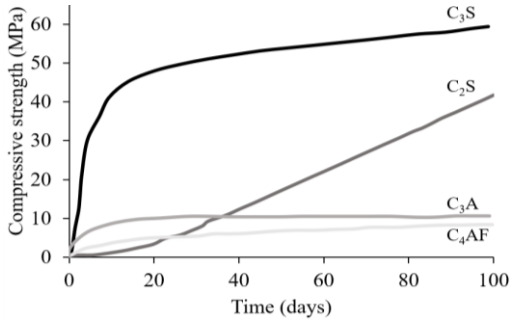

Figure 2.10: Compressive strength of pure cement compound (After Mozaffarindana, 2011)

Table 2.6: Function of cement compound

Compound name	Functions
Tricalcium silicate (alite), C_3S	• Hydration and hardening occur rapidly • Responsible for initial early strength on long-term strengths
Dicalcium silicate (belite), C_2S	• Hydration and hardening occur slowly • Contributes to the strength of later age (after 7 days)
Tricalcium aluminate, C_3A	• Releases a huge amount of heat in the first few days • Contributes slightly to the early strength • Responsible for initial set
Tetracalcium aluminoferrite, C_4AF	• Hydration occurs intensively without contribution of strength • Ferrite Hydration causes the colour to change to grey

2.3.2.2 Effect of physical properties of tailings and binder used

Greater specific surface area of finer cement particles will also promote hydration process (Bouasker et al., 2008). CPB that contains excessive number of fine tailings will reduce the void space for hydration products and hence lowing the strength outcome (Fall et al., 2005). The cement content has a good agreement with the increase in strength (Helinski

et al., 2007b). Strength increase due to density could be observed from the higher ratio of solid content used (Cayouette, 2003; Rankine and Sivakugan, 2007), It also has the effect of reducing the water to cement ratio of the mix which indirectly increases the cement content in term of the ratio (Revell, 2004).

2.3.2.3 Effect of chemistry

The chemical composition of the CPB design affects the cementation process (Benzaazoua et al., 2004; Fall and Benzaazoua, 2005). Considering the presence of sulphide is important in mine backfill with sulphide rich tailings. Sulphides could increase early strength as its precipitate could reduce the porosity by filling up the void (Cayouette, 2003; Fall and Benzaazoua, 2005; Fall and Pokharel, 2010) but it may hinder the ability of cement particles to hydrate and cause a reduction in the rate of hydration and strength. Expansion caused by sulphide oxidation could be deleterious to the CPB microstructure (Walske, 2014).

2.3.2.4 Effect of water content

From Appendix B, water is required during the hydration process to produce C-S-H. The amount of water required for concrete is preferably to be kept lower than 0.5 g and for complete hydration of cement to be 0.23 to 0.25 g of water for every gram of cement used. Insufficient water for hydration of the cement will limit the dispersion of cement within the mix due to higher yield strength thus hindering the rate of hydration (Walske, 2014). CPB has higher water content to every 1g of cement used as additional water is added to account for the flow requirement of the pipeline (Mozaffarindana, 2011).

2.3.2.5 Effect of temperature

Temperature is an important factor in the rate of hydration as it helps to modify the strength of the cementitious material. Effects of temperature are observed at every phase of hydration throughout the slow long-term process. Optimal temperature condition should be

controlled for a sufficient time to provide the needed activation energy for the reactions to occur (Mehta and Monteiro, 2006). A curing temperature of (< 35°C) favours binder consumption, which contributes to cost savings (Chang, 2016). Higher temperature accelerates the hydration process. Therefore, it promotes early strength development but results in lower ultimate strength for a long-term consideration as shown in Figure 2.11.

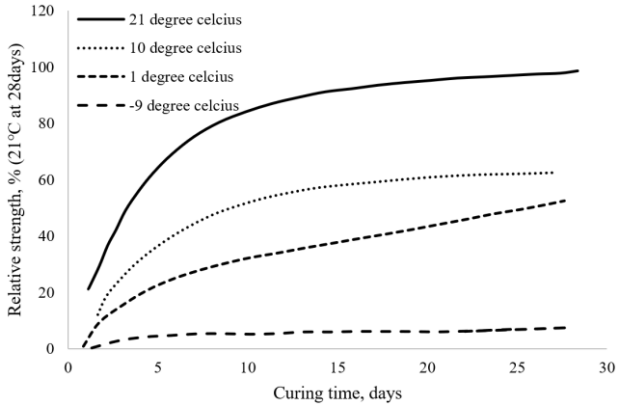

Figure 2.11: Effects of curing temperature on cement hydration

Numerous laboratory, numerical and field studies conducted on CPB agree with effect of curing temperature on the development of material properties by showing significant improvement in the mechanical properties at higher curing temperatures (Fall et al., 2007; Nasir and Fall, 2009; Fall et al., 2010; Nasir and Fall, 2010; Thompson et al., 2011, Thompson et al., 2012). Fall et al. (2007, 2010) show that regardless of the mix design, the rate of increment in strength is promoted by higher curing temperatures while the value of strength is still dependent on the curing time. More hydrate formed due to higher curing temperature will be filled into the void and improve the pore structure (Fall et al., 2010; Pokharel and Fall, 2011). It is also concluded that higher temperature promotes early strength gain but results in lower ultimate strength where it is caused by the reduction of diffusion rates which hinder the movement of hydrate products and continuity of hydrate formation (Kjellsen et al., 1991).

Nasir and Fall (2010) is able coupled the effects of hydration with temperature in a model to estimate the strength for different mixes with varying cement content, initial temperature, stope size and rate of backfilling but did not consider the effects of consolidation and self-desiccation as factors in strength and effective stress generation (Helinski et al., 2007a; Fahey et al., 2011). The failure mode of CPB will be changed due to the higher peak strength acquired but with lower post-peak strain thus giving quasi-brittle failure mode. Besides strength development, curing temperature is also very influential in effective stress development within the cementitious material (Walske, 2014).

Understanding the effect of curing temperature on the rate of CPB hydration and subsequent properties development is crucial for both in-situ and laboratory. Effective stress generated from pore water pressure reduction because of hydration must be considered for accurate estimation of stress.

2.4 Strain Behaviour of Backfill Material

Unlike UCPB, CPB could be treated as a multiphase porous medium which consists of liquid (capillary water and physically adsorbed water), gaseous (pore air) and solid (binder, tailings and hydration products) phases. The strain behaviour of CPB on its microstructural changes is explained based on the mechanical process with consist of initial consolidation, mechanical strain (plastic and elastic strain), chemical shrinkage and thermal expansion.

Chemical shrinkage is a measurement of the overall volume change of a cementitious material that occurs during hydration due to the reduced volume of the final hydrated products compared with the unhydrated constituents (Powers, 1935; Tazawa et al., 1995). Chemical shrinkage may be measured in one of two ways: volumetric method (ASTM Standard Test Method C1608-07), where the volume of water absorbed in the specimen gives a direct measurement of the volume change associated with chemical shrinkage, or

examination of the change in buoyancy of a hydrating specimen submerged in a liquid (Sant et al., 2006; Lura et al., 2010). While the latter method is easy to automate, it is a more expensive option due to the requirement of a high precision balance.

With the consumption of water in the reactive porous media of the CPB, the meniscus of the liquid-gaseous interface will gradually form and result in a progressive increase in capillary pressure. Consequently, the skeleton of the CPB will suffer increasing compression and the volume of the solid skeleton will decrease (called chemical shrinkage). Based on a previous study on cement paste (Powers and Brownyard, 1947), two sources that contribute to chemical shrinkage are identified as chemically combined water induced by hydration reactions and physically absorbed water by cement gel. The volume of these two types of water is less than the volume of the capillary water with the same mass.

In addition to chemical shrinkage, autogenous shrinkage is a subset of chemical shrinkage which is regard to the potential for cracking via the measurement of the bulk strain generated in closed hydration system. Autogenous shrinkage only occurs with conventional self-desiccation, where no free water exists within the system, and moisture migration is prevented from occurring (Tazawa et al., 1995; Sant et al., 2006). Self-desiccation typically occurs where the water to cement ratio is less than 0.4, (Powers and Brownyard, 1947; Geiker and Knudsen, 1982) although this number varies slightly for different cement types. Due to the very high *w/c* ratio of CPB ($w/c > 5$) self-desiccation never truly occurs, and rather the self-desiccation refers only to the reduction in pore water pressure. As such, autogenous shrinkage is not seen to occur in the hydration of CPB (Walske, 2014).

Cui and Fall (2015) stated that due to the exothermal binder hydration, temperature gradients occur inside the CPB structure which results in the development of thermal stress. Based on previous studies on cementitious materials (e.g. mortar, cemented soil and

concrete) (Emanuel and Hulsey, 1977; Mindess et al., 2003; Sellevold and Bjøntegaard, 2006), the evolution of the coefficient of thermal expansion (CTE) is controlled by solid constituents (e.g. aggregate and cement), moisture content and degree of hydration. The coefficient of thermal expansion shall be estimated from the volumetric change of backfill sample via potentiometer during deposition test.

Post-consolidation CPB strain behaviour could be analysed by considering the following factors. The water consumption caused by binder hydration (self-desiccation) could lead to skeleton changes (i.e. chemical shrinkage). In addition, thermal expansion induced by the temperature gradient in the CPB is taken into consideration in this study as well (Cui and Fall, 2015). Equation 2.3 shows the total strain, ε generated in the CPB structure consists of four components, which are elastic, ε_e, plastic, ε_p, thermal, ε_T, and chemical, ε_c strains which obey the theory of superposition.

$$\varepsilon = \varepsilon_e + \varepsilon_p + \varepsilon_T + \varepsilon_c \qquad \text{[Equation 2.3]}$$

Whereas, UCPB which is inert and free from any forms of chemical reaction does not need to take chemical shrinkage into account while analysing its strain behaviour. The volumetric change of solid or paste (semi-solid) shall incur additional stress to the surrounding wall (confinement) and needs to be considered while estimating the stress distribution of backfill material within stope.

2.5 Stress Distribution of Backfill Material

Stress distribution of fill material within silo has drawn great attention on physics researcher (Landry, 2004). From granular material storage to soil backfill, the distribution of stress must be considered for retaining structure design such as silo for granular material or liquid and backfilling for geotechnical application. Excessive stress shall deform and damage the designed retaining structure and result in spillage or containment of filled

material. In order to prevent such catastrophe event, stress distribution theory has been developed to assist in engineering design application.

2.5.1 Stress Distribution Theory within Narrow Wall

Stress distribution differs depending on the geometry of filling, material properties, wall surface properties, and storing condition such as temperature, static or dynamic, and presence of external stress. The following subsections show the development of stress distribution theory until today. The state of art stress distribution theory developed by Pirapakaran and Sivakugan (2007) is still unable to explain some of the anomalies found in the recent full-scale monitoring of CPB deposition at different mine around the world.

2.5.1.1 Janssen's theory

An experimental approach has been conducted by Janssen using maize as a granular material to be filled into a rectangular NW namely silo. Janssen conducted a few experiments by altering the width of his model, but the fill material and wall surface roughness remained to be the same throughout tests. The outcome of the experimental approach shows that the recorded bottom weight of the maize is less than the apparent mass of the total maize filled. Hypothesised on the fictional angle of the wall and the maize had caused an occurrence of a phenomenon namely the arching effect. The correlation between arching effect and the width of the rectangular silo model could be seen from his research where the arching effect is less significant as the broader or wider the space between silo walls. The stress distribution is illustrated in a free body diagram shown in Figure 2.12.

Janssen is able to derive a basic function stating that within a continuous medium of static fill material, a constant fraction, K of vertical stress is transferred to the wall as horizontal stress. There are several factors that could break the assumption of constant K throughout the filling height which are the variety of wall friction value, wall deformation,

and homogeneity of filled material. Minor deviation of the aforementioned factors does not have a significant effect on the total stress recorded.

Another assumption has been made where due to the difficulty of measuring internal stress within the fill material in the past, it is assumed that the vertical stress is independent on the height of the silo mould which is also known as incipient failure.

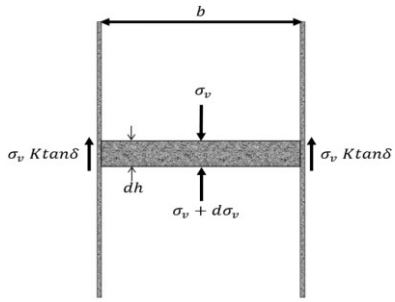

Figure 2.12: Diagram of an infinitesimal filled material (dh) within narrow friction wall.

Solving the above free body diagram by considering four side walls via integrating δh and $\delta \sigma_v$, the total vertical stress σ_v is expressed as (Janssen, 1895):

$$\sigma_v = \Gamma b \frac{1-e^{-(\frac{4K \tan \delta h}{b})}}{4K \tan \delta} \qquad \text{[Equation 2.4]}$$

where Γ is the bulk unit weight of the material (kN/m^3), b is the distance between the walls (m), h is the height of deposition (m), δ is the angle of interfacial friction between material and wall (degree), and K is the ratio between horizontal stress and vertical stress (dimensionless). Equation 2.4 contains the exponential function of K, δ, h and b. As we could see, the height of deposition (h) only exists within the exponential term. Thus, the total stress saturates as the height of deposition (h) increases.

Modifications and extensions of the theory for granular material applications have been proposed to improve Janssen's formulation based on experimental evidence (Vanel and Clement, 1999; Vanel et al., 2000; Ovarlez et al., 2003). For example, in the case of maximum shear stress (Mohr-Coulomb) threshold has been surpassed, the total stress found

to be lower than Janssen's equation due to the slip of the material along the walls (Ovarlez et al., 2003). This is known as overshoot effect resulting from overburden stress equal to saturation mass applied.

2.5.1.2 Arching effect

The arching effect was introduced by Terzaghi in 1943, but it has been around ever since Janssen's theory based on his experiment on corn pressure in silo cells. In Figure 2.13, Janssen shows that the arching effect is there when the fill material is consolidated. It induces shear between the wall and the filling material over every horizontal section which transfers some of the vertical pressure of the consolidated material towards the static wall.

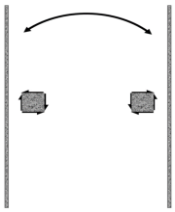

Figure 2.13: Janssen arch

Soil arching is a universal phenomenon which is ubiquitous within the yielding soil shear stress transfer to other adjoining static material (Terzaghi, 1943). As shown in Figure 2.14, the shearing resistance between static mass and yielding soil oppose any relative movement and thus transfer some pressure from the yielding mass towards the static mass.

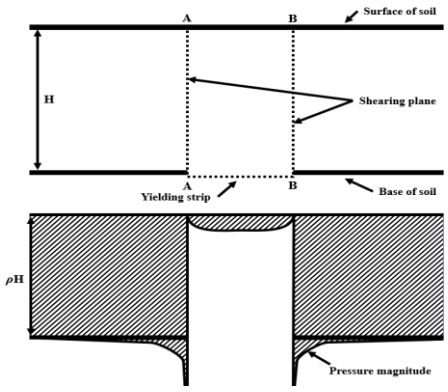

Figure 2.14: Terzaghi's pressure distribution over yielding strip

Pirapakaran (2008) provides a diagram (Figure 2.15) showing the effects of arching within mine stope as the yielding section (CPB) possess any downward movement, an increase of stress could be seen at the static support (rock mass) which prevent downward movement of yielding mass due to shear resistance and thus lowering the stress at the base.

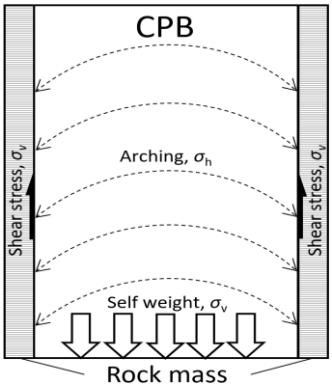

Figure 2.15: Diagram showing the arching effect in backfilled stopes (After Pirapakaran, 2008)

Horizontal pressure is to be considered as the barricade is located at the side of the filling zone. Horizontal pressure could be determined from the analytical which are Marston's 2D model, Marston's modified model (Aubertin et al., 2003), Terzaghi's model with cohesion consideration, Van Horn (1963) 3D model and Belem and Benzaazoua (2008) 3D longitudinal stress model.

An understanding in this phenomenon is crucial in understanding the pressure distribution within narrowly confined soil such as trenches, retaining wall, mining stope and even more of the geotechnical application in the world (Chevalier, 2011; Xie, 2016).

2.5.1.3 Remarkable development of stress distribution theory

Silo which is usually made of reinforced concrete or steel has been commonly used as a storage chamber for all sorts of granular material (Jarrett, 1991). The silo is originally designed to be cylindrical in shape, but due to its drawback on space management and cost of fabrication, rectangular silo is now more commonly adopted in large scale industries

(Goodey et al., 2003). Basically speaking, both silo and mining stope have similar geometry which is their width to height ratio but different in the properties and behaviour of fill material. As stated by Ghirian and Fall (2015) cemented paste is a complex geotechnical material used in mining stope backfill is much more complicated as the behaviour of the cemented paste are to be considered during stress estimation in structural design. Thus, the stress distribution theory from the silo is adapted and modified to be applicable for stress estimation on CPB design, and it is still under improvement until today. From Janssen's Equation 2.4, it has been derived by Marston (1930) as a 2D arch analysis to calculate horizontal pressure, σ_h along the side wall of the excavated trench.

$$\sigma_h = \frac{\gamma B}{2\mu'}\left[1 - exp\left(-\frac{2K_a\mu' H}{B}\right)\right] \quad \text{[Equation 2.5]}$$

The vertical pressure, σ_v and parameter K_a are as follows:

$$\sigma_v = \sigma_h / K_a \quad \text{[Equation 2.6]}$$

$$K_a = tan^2(45° - \varphi/2) \quad \text{[Equation 2.7]}$$

where γ = fill bulk unit weight (kN/m^3); B = stope width (m); H = fill mass height (m); μ' = tan δ = sliding friction coefficient between fill and sidewalls (δ is the wall friction angle, generally assumed at between $\varphi/3$ and $2\varphi/3$, and ranging from 0° to 22°); φ = fill internal friction angle (degree); and K_a = active earth pressure.

Some of the boundary condition of mine stope is different from silo. It is shown in Figure 2.16 where additional compressive force, C is subjected compared to silo case. H is the height of backfill and B is the width of the stope. At depth h, the horizontal layer element is subjected to lateral compressive force C, shearing force S, and vertical forces V and $V + dV$. The weight of the backfill in this layer is given by:

$$W = \gamma B dh \quad \text{[Equation 2.8]}$$

where γ is the unit weight of the backfill, and dh is the thickness of the layer element. The global equilibrium of the layer element also gives:

$$W = dV + 2S \qquad \text{[Equation 2.9]}$$

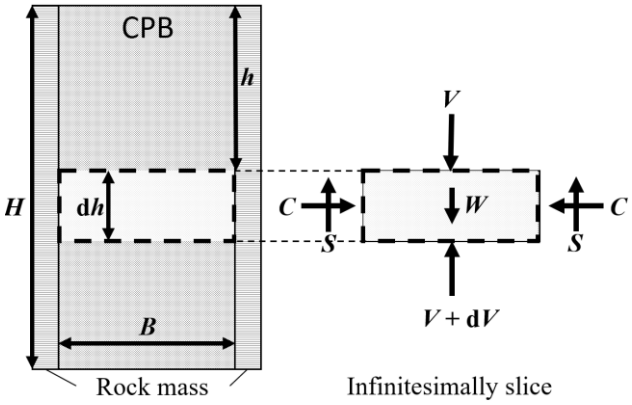

Figure 2.16: 2D free body diagrams of backfill and force acting on an infinitesimal slice

Aubertin et al. (2003) then modified Marston's 2D arch analysis to predict effective horizontal pressure, σ'_{hH} along pillar sidewalls at a depth H corresponding to the stope bottom and effective vertical pressure, σ'_{vH} of cohesionless material:

$$\sigma'_{hH} = \frac{\gamma B}{2\tan\varphi'_f}\left[1 - exp\left(-\frac{2KH\tan\varphi'_f}{B}\right)\right] \qquad \text{[Equation 2.10]}$$

$$\sigma'_{vH} = \sigma'_{hH}/K \qquad \text{[Equation 2.11]}$$

where γ = fill bulk unit weight (kN/m^3); B = stope width (m); H = fill height (m); φ'_f = fill effective internal friction angle (degree); and K = earth pressure coefficient. Earth pressure coefficient K corresponds to three different states: K_a (active), K_0 (at rest), and K_p (passive), given by the following relationships:

$$K = K_0 = 1 - \sin\varphi'_f \qquad \text{[Equation 2.12]}$$

$$K = K_a = tan^2\left(45° - \varphi'_f/2\right) \qquad \text{[Equation 2.13]}$$

$$K = K_p = tan^2\left(45° + \varphi'_f/2\right) \qquad \text{[Equation 2.14]}$$

According to Brooker and Ireland (1965), coefficient K_0 must vary from 0.4 to 0.6; K_a must vary from 0.17 to 1.0, and K_p must vary from 1.0 to 10. However, in a filled stope, the active earth pressure condition (K_a) seems improbable because the paste backfill has insufficient internal pressure to push out the stope walls. Thus, prevailing earth pressure conditions will probably be at rest and passive pressure only.

2D arch analysis by Terzaghi (1943) is able to predict horizontal pressure, σ_h along static walls at the bottom of backfilling on cohesive material:

$$\sigma_h = \frac{(\gamma B - 2c)}{2\tan\varphi}\left[1 - exp\left(-\frac{2KH\tan\varphi}{B}\right)\right] \qquad \text{[Equation 2.15]}$$

And cohesionless material:

$$\sigma_h = \frac{(\gamma B)}{2\tan\varphi}\left[1 - exp\left(-\frac{2KH\tan\varphi}{B}\right)\right] \qquad \text{[Equation 2.16]}$$

The vertical pressure σ_v at the bottom of the stope:

$$\sigma_v = \frac{\sigma_h}{K} \qquad \text{[Equation 2.17]}$$

$$K = \frac{1+sin^2\varphi}{cos^2\varphi+4tan^2\varphi} = \frac{1}{1+2tan^2\varphi} \qquad \text{[Equation 2.18]}$$

where K = earth pressure coefficient; γ = fill bulk unit weight (kN/m^3); c = fill cohesive strength (kPa); B = stope width (m); H = depth below fill toe (m); $tan\ \varphi$ = fill internal friction coefficient; and φ = fill internal friction angle (degree).

The three-dimensional solution proposed by Van Horn (1963) for vertical stress at depth, h considering width, B and breadth, L and interfacial friction angle between backfill and wall, δ is predicted by the equation:

$$\sigma_v = \frac{\gamma}{2k_r\tan\delta}\left(\frac{BL}{B+L}\right)\left[-2k_r\tan\delta\frac{h(B+L)}{BL}\right] \qquad \text{[Equation 2.19]}$$

where c = fill bulk unit weight (kN/m^3); h = fill height in the stope below the surface (m); B = stope width; L = stope strike length (m); and $k_r = \sigma_h/\sigma_v$; δ = interfacial friction angle (°) between backfill and stope wall.

Pirapakaran and Sivakugan (2007) provide good reviews on the current state-of-the-art analytical solutions on the stress development with particular reference to the non-cemented slurry, which includes Marston (1930), Terzaghi (1943), Aubertin et al. (2003) as well as numerical model using FLAC. These analytical solutions are expressed as extended forms of Marston's theory with particular attention to material friction angles, effect of cohesion, coefficient of lateral pressure, as well an extension to the 3D problems.

Determining forces within mine backfill could be approached analytically by solving the equilibrium of forces in the three-dimensional free body diagram on an infinitesimally thin slice of backfill surrounded by four walls as illustrated in Figure 2.17. The slice of thickness *dh,* length *l* and width *w* are in static equilibrium within the walls. The slice is subjected to vertical forces from the overlying backfill (*V*) and its own weight (*dV*). It exerts a horizontal force (*dC*) acting against the walls. Consequently, the shear force (*dS*) is generated on the side walls, which acts against the downward force of the overlying backfill.

Weight of the slice:

$$dW = \gamma w l dh \qquad \text{[Equation 2.20]}$$

where γ = fill bulk unit weight (kN/m^3).

Compressive forces acting on the vertical face:

$$dC = 2(w + l)dh\sigma_h \qquad \text{[Equation 2.21]}$$

Shear force *S*:

$$dS = 2(w + l)dh\sigma_h tan\delta \qquad \text{[Equation 2.22]}$$

Vertical stress σ_v:

$$\sigma_v = \frac{V}{wl} \qquad \text{[Equation 2.23]}$$

Earth pressure coefficient *K*:

$$K = \frac{\sigma_h}{\sigma_v} \qquad \text{[Equation 2.24]}$$

Thus, the relationship could be established from Equations 2.20 to Equation 2.24:

$$dV = \gamma wldh - 2(w+l)K\tan\delta\frac{V}{wl}dh \qquad \text{[Equation 2.25]}$$

$$\int_0^h dh = -\int_0^V \frac{1}{\left[2\left(\frac{w+l}{wl}\right)KV\tan\delta - wl\gamma\right]}dV \qquad \text{[Equation 2.26]}$$

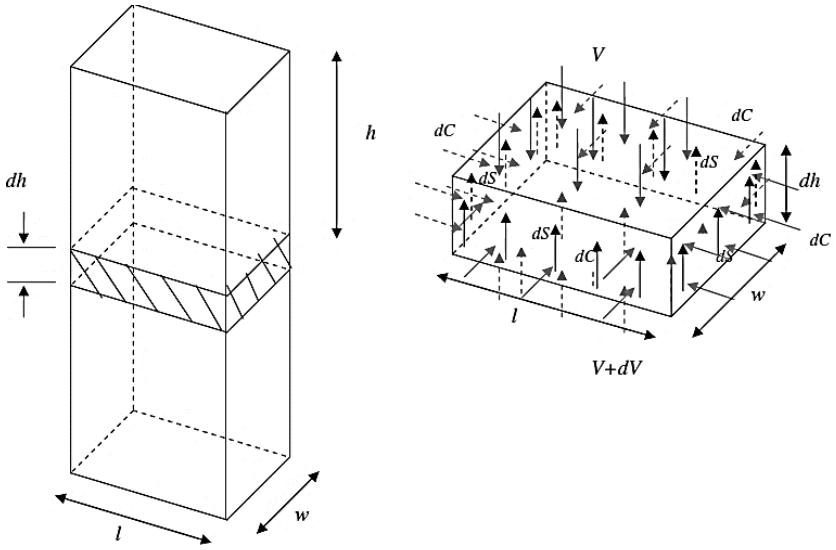

Figure 2.17: 3D (a) free body diagrams of stope and (b) an infinitesimal slice of backfill (Pirapakaran and Sivakugan, 2007)

The equilibrium of forces in the free body diagram could be solved by integrating *dh* over the entire depth of backfill. The vertical and the horizontal force and stress could be rewritten as:

$$F_v = \gamma l^2 w^2 \frac{1-\exp\left\{-2K\tan\delta h\frac{(l+w)}{lw}\right\}}{2K\tan\delta\,(l+w)} \qquad \text{[Equation 2.27]}$$

$$F_h = \gamma l^2 w^2 \frac{1-\exp\left\{-2K\tan\delta h\frac{(l+w)}{lw}\right\}}{2\tan\delta\,(l+w)} \qquad \text{[Equation 2.28]}$$

And

$$\sigma_v = \gamma lw \frac{1-\exp\left\{-2K\tan\delta h\frac{(l+w)}{lw}\right\}}{2K\tan\delta\,(l+w)} \qquad \text{[Equation 2.29]}$$

$$\sigma_h = \gamma lw \frac{1-\exp\left\{-2K\tan\delta h\frac{(l+w)}{lw}\right\}}{2\tan\delta\,(l+w)} \qquad \text{[Equation 2.30]}$$

Rock mass is stiffer than backfill materials by around 100 times of CPB stiffness resulting in very small (negligible) wall movement upon completion of backfilling, CPB would be at rest condition ($K=K_0$). For loose backfilling, the wall frictional is considered 2/3 of backfill frictional angle. There are two assumptions made for this analytical solution: first, the vertical forces in the backfill are assumed to be uniformly distributed from side to side at any depth; second, the value of K is undetermined (Pirapakugan and Sivakugan, 2007). These two assumptions could result in inaccurate estimation of the force distribution within a backfill mass and thus of the force acting on retaining barricades. From the input of the stress distribution theory shown, all factors need to be taken into consideration while formulating, establishing and experimenting with the stress distribution behaviour of CPB.

2.5.2 Factors Affecting Stress Distribution

In-situ properties of CPB are different from the laboratory CPB material based on the ability to replicate the boundary condition by controlling the contributing factors. CPB deposited into mine stope is under the factor of NW geometry, transient behaviour of the material, surface roughness for different type of rock wall with uncontrolled curing temperature and in static condition unless of any seismic event occurrence. Understanding the behaviour of in-situ CPB is vital for optimisation in structural and CPB design.

The differences in field and laboratory behaviour could be due to the geometry of stope (Walske, 2014), geotechnical properties of fill and wall (Sheshpari, 2015), coupled thermo-hydro-mechanical-chemical (THMC) phenomenon in CPB (Abdul-Hussain and Fall, 2012; Ghirian and Fall, 2014) and filling rate (El Mkadmi et al., 2013).

2.5.2.1 Geometry of stope

Stress distribution across a variety of regular and irregular shape is different. In silo, the wall is usually designed to have a regular cross-section across the entire height except

for the discharge point of the silo. In mining stope, rectangular shape void is usually formed during recovery by blasting and others forms of extraction, but it is irregular on the surface of the wall. Size of the cross-section of the silo and mining stope determines the significance of arching effect which will alter the stress distribution. Janssen (1895) had shown the difference in apparent mass recorded at the bottom of the silo is much lesser with narrower silo model which had been proved by Li et al. (2003) that greater stress is observed at the centre of the filling. State-of-the-art stress distribution theorem showed that the stress could be predicted at any scale and it showed that the scale does not affect the stress distribution (Pirapakaran and Sivakugan, 2007; Sivakugan et al., 2014).

The difference in size of laboratory cast CPB (typical sample size, 200 cm^3 and backfill modelling for this research, 60000 cm^3) in contrast with actual stope deposits (typically 45,000 m^3) (Walske, 2014), the rate of heat dissipation is slowed by the large mass resulting in higher the net temperature gain from exothermic reaction as heat dissipation is less significant (Fall et al., 2007). Indirectly, an increase in curing temperature will significantly affect hydration rate and thus the effective stress generated.

2.5.2.2 Friction angle of fill material and wall-fill interface

Arching which is a frictional cause relies mainly on the friction generated between the fill material itself and with the surrounding wall. Interfacial friction angle between backfill and rock mass is an important parameter of arching effect estimation in CPB (Marston, 1930). Interfacial friction angle, δ is usually used during analysis (Terzaghi, 1943; Li et al., 2003) with agreement with two assumption which the interfacial friction angle is higher than internal friction angle, φ of CPB because of irregularity on the surface of rock mass that results in greater roughness which cause shear failure to occur along CPB instead of CPB and rock mass (Sheshpari, 2015). Nasir and Fall (2008) performed a direct shear test

on trimmed rock mass which has a smooth surface and shows that the internal friction angle of CPB is higher compared to interfacial friction angle of smooth rock mass and CPB. With the presence of significant pressure and heat, foliation of rock will occur and reduce the surface roughness and thus resulting in an overestimation of the arching effect (Mitchell et al., 1982). Consequently, overestimation will lead to failure and incur major loss.

2.5.2.3 Thermo-Hydro-Mechanical-Chemical (THMC) behaviour of CPB

The cemented slurry is a heterogeneous material as its properties will be altered with time through cement hydration. A coupled behaviour approach proposed by Cui and Fall (2015) shown in Figure 2.18 shows an interaction between THMC behaviour of CPB.

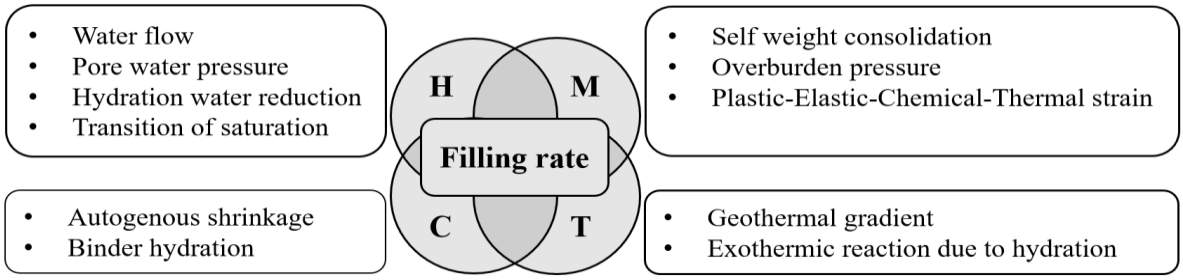

Figure 2.18: Schematic interaction within CPB's behaviour

THC have a direct contribution towards the mechanical behaviour of CPB such as heat generation and reduction of pore water pressure due to hydration. Thus, mechanical strain deformation of CPB is mainly caused by chemical shrinkage, thermal shrinkage and thermal expansion where chemical shrinkage is a result of self-desiccation and thermal expansion or shrinkage are the results of curing temperature variation with curing time. Net volumetric change within an unconfined NW will induce or reduce the stress exerted onto adjacent wall due to arching.

2.5.2.4 Filling method and its rate

Backfilling from a greater height will create a greater impact pressure due to the free-falling distance for the CPB to accelerate. For granular material, the height of filling affects

the packing fraction due to different intensity of impact. Figure 2.19 shows the result from the test conducted by Vanel and Clement (1999) to show the difference in vertical pressure with different filling method. Packing fraction is not significantly affected by filling method if CPB is used instead. Moreover, plug and pour method (usually explained as the rate of backfilling) has more significance in total stress recorded during stope backfilling. The hardened properties of CPB could significantly reduce vertical and horizontal stress recorded by allowing a designed portion of CPB (Plug fill) to harden and archive stability between supporting rock masses prior the rest of the filling. Figure 2.7 shows the relationship between the rate of filling and stress generated.

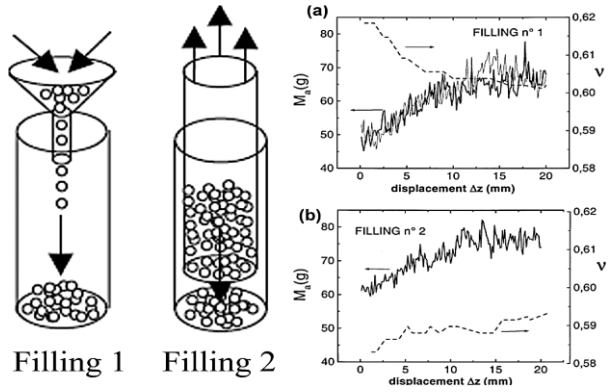

Figure 2.19: Apparent mass and packing fraction of (a) Filling 1 (b) Filling 2 (Vanel and Clement, 1999)

2.5.3 Improving the Stress Distribution Theory

According to Section 2.5.2, some of the contributing factors such as the geometry of stope, friction angle, unit weight of fill material and height of backfilling were incorporated in the state-of-the-art stress distribution theorem by Pirapakaran and Sivakugan (2007), but the effects of temperature change were yet to be considered in the theorem. The effects of temperature on the strain behaviour CPB could alter the total stress induced onto the wall of stope due to arching. Therefore, the effect of temperature must be studied and taken into consideration while predicting the stress distribution of backfilling.

2.6 Stress-Strain Condition on CPB under the influence of Curing Temperature

Cemented paste backfill (CPB) has been observed to achieve different characteristic or behaviour when cured in-situ compared with equivalent mix composition cured and tested in a laboratory environment (Revell, 2004; le Roux et al., 2005; Fahey et al., 2011). The significant differences between in-situ and laboratory curing are the curing temperatures. The in-situ cured CPB possess higher temperature due to the heat generated from exothermic hydration reactions which occur as the material cures. Temperature increases do not typically occur in a laboratory-cured specimen due to the small specimen size cured under atmospheric conditions.

Temperature is also known to play a critical role in the process of cement hydration and mechanical strain for both cement pastes and concrete. Higher temperatures increase the rate and extent of hydration reactions, which in turn positively affects the strength development in comparison to curing at lower temperatures. Numerical modelling and laboratory studies (Fall et al., 2007; Nasir and Fall, 2009; Fall et al., 2010; Nasir and Fall, 2010) as well as in-situ data recovered from field studies (Thompson et al., 2011, Thompson et al., 2012) indicate these benefits also extend to CPB material, despite the lower cement content compared with cement pastes or concrete.

2.6.1 The Curing Environment

Heat generated in an underground mining environment may come from a variety of sources including backfill hydration, mining machinery, lighting or blasting as well as geographical location and geothermal gradient where temperatures rise with progressively deeper mining (Fall et al., 2010). In locations where permafrost conditions exist (i.e. northern Canada) or geological conditions where self-heating due to exothermic sulphide reactions may increase rock mass temperatures to the vicinity of 400°C (in rare circumstances)

(Bernier and Li, 2003). These extreme temperatures are not encountered frequently, as indicated by the in-situ data mentioned previously, which showed typical temperature increases up to 50°C (Grabinsky and Thompson, 2009; Thompson et al., 2011, 2012; Hasan et al., 2012, 2013; Doherty et al., 2015). Table 2.7 below summarises the heat sources in underground mine and backfill operation, as reported by Sheshpari (2015) and Chang (2016). Figure 2.20 shows the temperature profile of the earth crust at various location.

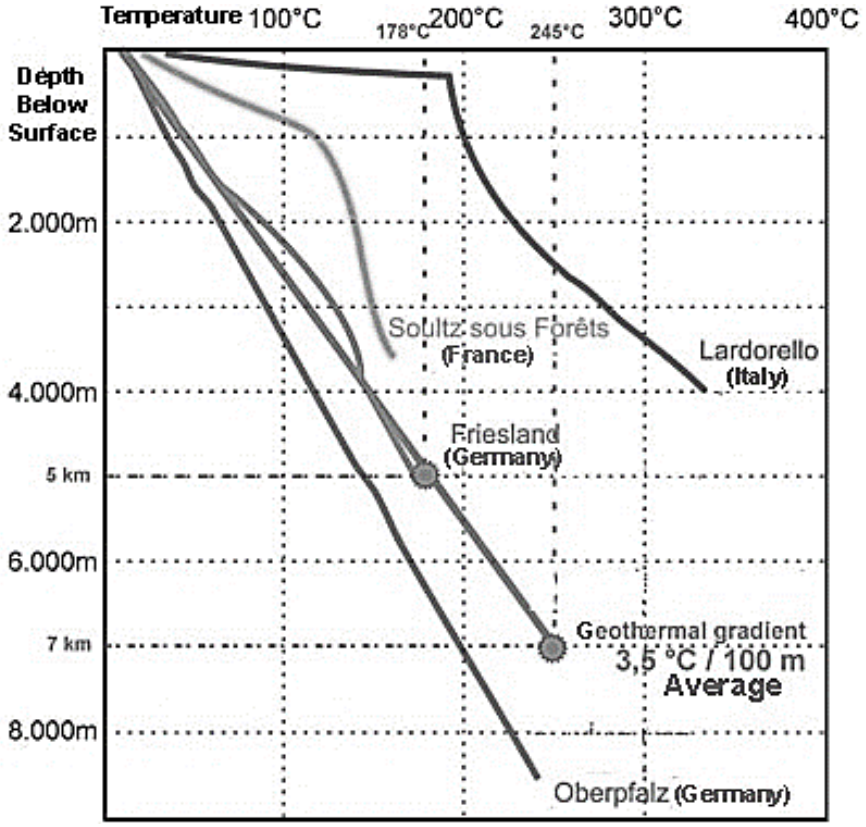

Figure 2.20: Thermal profile with respect to depth
(Battery and Energy Technologies, 2017)

Due to the lower ambient temperatures and the small specimen sizes used in laboratory testing, any heat generated due to hydration is dissipated quicker than it could be produced, preventing any temperature rise. Due to the size of the CPB mass and the insulation provided by the underground environment, the heat generated by the exothermic reactions associated with the hydration process became significant.

Table 2.7: Heat sources in underground mine and backfill operation

Heat sources	Mine depth	Geographical location	Cement hydration	Backfill transportation	Self-heating mechanisms	Man-induced temperature
Description	• The temperature rise is proportional to the mine depth, due to the natural heat influx by geothermal gradient • Estimation of temperature rise of 3.5℃ per 100m of most land depth in the world • The deeper the mine depth, the longer CPB backfilling transport distance and longer time for hydration initiating of fresh CPB	• Different region experiences different climate or seasonal change • Climate change will significantly influence a relatively shallow mine • e.g. northern Canada, as a permafrost area, low temperature will influence CPB temperature in surface mixing plants, transportation and hydration thermal load • Temperature variation due to seasonal change also brings impact to the temperature of the water component of CPB	• Cement hydration is an exothermic reaction, which produces a significant amount of heat to the underground surrounding • Heat accumulation especially in the central part of the structure, due to the slow heat dissipation rate within the massive size of the cemented backfill structure • Cemented backfill temperature could achieve 50℃ after 4 days of curing	• Friction loss is the main heat contributor • Friction between transferring pipe and cemented paste • Friction between cemented paste and hosting rock walls	• Abnormally high temperature (>400℃) was observed in some Canadian underground mines due to the exothermic reactions of sulphide minerals • Sulphide minerals such as pyrrhotite rich in many Canadian mines, present in the rock mass or cracked backfill structures • Not yet well understood	• Heat released by some mining operations such as machinery, blasting operations, lighting ventilation, res, etc • Heat production limited small area

2.6.2 In-Situ Mine Backfilling Monitoring

For a better understanding on the difference in properties between in-situ and laboratory cured material, several field instrumentation studies have been conducted (Thompson et al., 2009; Helinski et al., 2011b; Thompson et al., 2012; Hasan et al., 2013, 2014). Such studies have included extensive instrumentation of stopes prior to filling. Instruments were installed at multiple targeted locations within the stope to collect the data of the behaviour of CPB at different location and elevation of mining stope.

Total stress, temperature, negative pore pressure sensors and pore pressure transducers (PPT) allow real-time monitoring of the changes in conditions as the stope is filled and then as curing progresses. Where both pore pressures and total stress have been monitored, results of these studies have indicated that initially, stope filling occurs under undrained conditions and thus the loading on the barricade, at its maximum, is hydrostatic (Helinski et al., 2011b; Thompson et al., 2012). As time and filling of the stope progress, the pore pressure will begin to reduce as compared with the total stress measurements as indicated in Figure 2.21. The effective stress generated as a result is determined by the difference between curves labelled σ_v and u. The third curve presented, labelled "σ_v no arching" will be discussed subsequently.

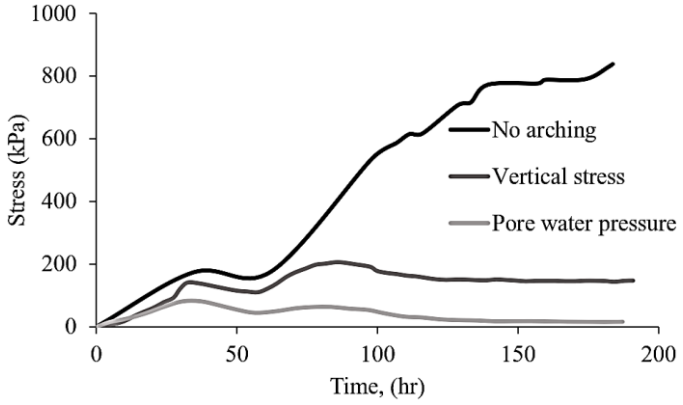

Figure 2.21: In-situ measurement of total stress and pore pressure (After Helinski et al., 2011)

This reduction in pore pressure (u) with respect to total stress (σ_v) generates effective stress (σ_v') within the material is expressed in Equation 2.31.

$$\sigma_v' = \sigma_v - u \qquad \text{[Equation 2.31]}$$

Temperature monitoring during fill and curing indicated that the temperature within the fill is within the range of 30 to 50 °C that is higher than laboratory temperatures (~23°C) at which laboratory-prepared CPB are cured (Thompson et al., 2012). Elevated temperature positively influence cement hydration reactions, increasing the rate and ultimate extent to which they occur (Fall et al., 2010). Similar temperature increases to those measured by Grabinsky and Thompson (2009). Thompson et al. (2011) and Thompson et al. (2012) shows similar in-stope monitoring at SNM and KB (Helinski et al., 2011). Details regarding these CPB mixes were provided in Table 2.4. Unfortunately, no in-situ temperature data was available from a KB stope. Given the similar mine type and location of the RL and KB mines in the Goldfields region of Western Australia, it could be assumed that the temperatures generated in each mine are likely to be similar. KB stopes are much larger in size (~20 m by 80 m) compared with SNM stopes (~6 m by 10 m). An increase in bulk size could have a positive effect in generating higher temperatures due to reduced heat dissipation.

The temperature increase observed in the SNM stope is far more modest by the use of 1.5% Minecem (a low-heat proprietary binder used in the SNM CPB mix), compared with 5% of Ordinary Portland cement (OPC) (Walske, 2014). Thompson et al. (2012) had conducted fieldwork at the Cayeli Mine (Cayeli Bakir Isletmeleri A.S), which is an underground mine, owned by Inmet Mining Corporation and is located in northeast Turkey, close to the town of Cayeli- Rize. The mining method is long-hole stoping. The instruments were installed for the monitoring of total earth pressure (stress) and pore water pressure with respect to current mine temperature. One of the data collected was shown in Figure 2.22.

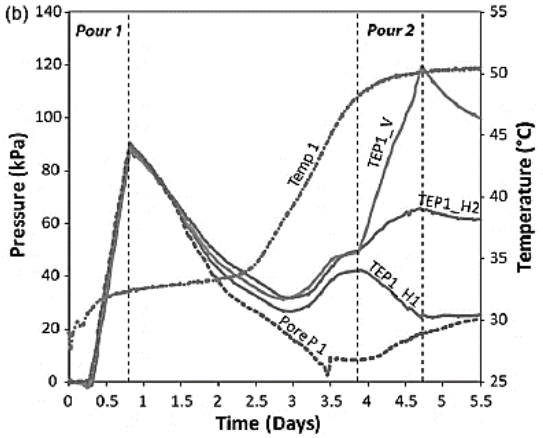

Figure 2.22: Measurement of pressure and temperature in Caliye mine (Thompson et al., 2012)

This behaviour is the opposite of expected stress behaviour after the completion of filling. Due to consolidation and/or self-desiccation of the mix, the pore pressures should initially be seen to reduce. This would be especially true if the self-desiccation mechanism was the primary means of pore pressure reduction, as the elevating temperatures will enhance the hydration process as discussed previously. If thermal expansion was responsible for this total stress increase, it would need to be significant to overcome the other stress-reducing mechanisms. Further investigation into the relationship between curing temperature and effective stress generation may offer further insight into these processes.

2.6.3 Laboratory and Numerical Studies

CPB has been studied not only from the full-scale monitoring but also through laboratory approach and numerical analysis. Helinski et al. (2007) improved a program namely MinTaCo to CeMinTaCo that is capable of developing a constitutive model, a permeability model and the concept of self-desiccation relative to the consolidation process. CeMinTaCo is a one-dimensional model that could not account for the arching effects.

Li et al. (2003) used FLAC-2D a numerical modelling software as shown in Figure 2.23 to show that the vertical and horizontal stress have non-uniform distribution without

considering temperature as one of its function. Across the depth, longitudinal distance away from the centre of filling possess lower stress. Additionally, Li et al. (2003) also showed the correlation between their numerical modelling and analytical methods of Marston theory which shows some underestimation from analytical method.

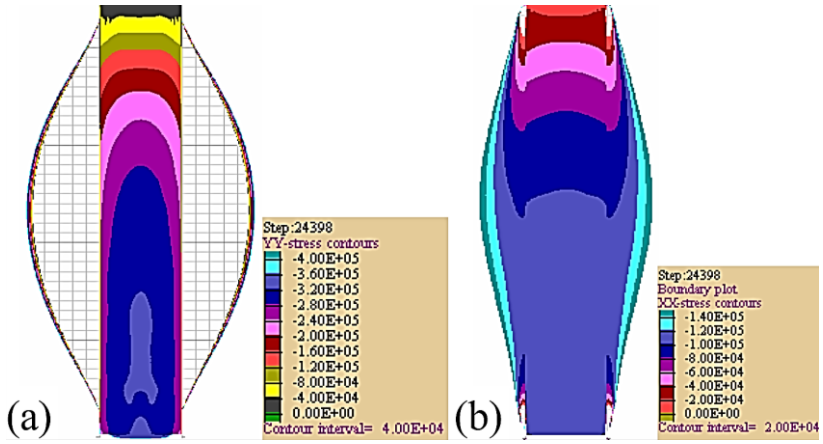

Figure 2.23: Pattern of stress distribution in stope, a) vertical stress, b) horizontal stress (Li et al., 2003)

Numerous laboratory investigation has been conducted on CPB. CPB behaviour based on its consolidation (Belem et al., 2008; Yilmaz et al., 2008), hydraulic conductivity (Fall et al., 2009), thermal conductivity (Célestin and Fall, 2009), mechanical behaviour (Belem et al., 2000), hydration behaviour (Nasir and Fall, 2009) and mix proportioning (Fall et al., 2008) as few examples to show the numerous amount of study that has been conducted. While the published literature clearly shows the significant positive effects of elevated curing temperature on the development of CPB mechanical properties, nowhere has this effect been coupled with the known benefits of effective stress generation. To truly represent in-situ conditions in a laboratory environment, these two effects must be considered in conjunction (Walske, 2014).

2.6.4 Importance of Temperature-Stress behaviour of CPB

It has been established that from the curing environment of CPB within mining stope, it shall be subjected to temperature change based on the heat sources as stated in Section 2.6.1. The stress anomaly observed in full-scale monitoring is speculated to be caused by the change in temperature (Section 2.6.2). Numerous researches are conducted on CPB via laboratory testing and numerical modelling, but none of them considers the effect of temperature on effective stress generation (Section 2.6.3). As scale factor would not distort the stress distribution analysis, laboratory scale replication of stope model with temperature control was required to study the effect of temperature on the stress behaviour of CPB when deposited into the NW (stope). The ability to replicate in-situ conditions in a laboratory environment (Section 2.7) offers feasible studies on the behaviour of CPB without incurring major cost.

2.7 Evidence in Narrow Wall Modelling

Variety of NW set-up has been introduced to investigate the behaviour of fill material. Following are the evidence of NW design, influential boundary condition and filled material considered by the other researchers.

2.7.1 Narrow Wall Model

NW model is a scaled-down set-up that is used to replicate stope backfilling. This enables researchers to study the stress distribution of backfilling material based on the controlled factors.

2.7.1.1 Size

NW height must be more than the double of diameter or side length (Jarret, 1991). The size of the mining stope fulfils the requirement of NW with its width to height ratio. Such ratio is widely used in laboratory testing and numerical modelling where the scale

factor is not an issue. It is not practical for laboratory approach to be conducted on the scale of mining stope as it requires a larger scale of heat generating devices to control the curing temperature and the monitoring equipment is practically non-recoverable as they are embedded within the hardened CPB.

2.7.1.2 Shape

During ore extraction, the mine-out void generated is usually in irregular rectangular shape. Rectangular wall is much more beneficial if the deformation of both bending and stretching (including linear thermal expansion) is more viable compared to cylindrically shaped wall. Stress distribution model (Belem and Benzaazoua, 2008) and recent numerical modelling (Li and Aubertin, 2010) cases studies are generally based on rectangular stope. Generally, all circular, square, and rectangular shaped wall has been used in the previous research (Jarret, 1991; Rotter, 2002; Goodey, 2006) and in terms of numerical modelling (Goodey, 2003; Li et al., 2003; Pirapakaran and Sivakugan, 2007; Li and Aubertin, 2008, Li and Aubertin, 2010)

2.7.1.3 Material

Construction material for silo is usually made up of steel or concrete (Jarret, 1991). The wall support of mine backfill is earth rock mass where its interfacial friction angle, δ will be different if another material is used as the wall instead. It is not viable to extract undisturbed rock mass to replicate the interfacial friction angle thus other materials are usually used as a replacement. Some example on usage of Perspex (Jarret, 1991; Widisinghe and Sivakugan, 2014) or variety of steel (Rotter, 2002; Goodey, 2003) as seen from the previous attempt on the experimental model and numerical model.

2.7.2 Boundary Condition

Deposited cemented slurry within a NW or stope is affected by multiple factors which are shown in Figure 2.24. The boundary condition of actual backfilling is important and need to be considered during laboratory testing. The following are the crucial boundary condition of mine backfill.

2.7.2.1 Fixed and static wall

The rock mass wall surface is irregular but is usually generalised as a regular rectangular NW. The rock mass possesses a great modulus of elasticity after being consolidated within the earth's crust for centuries which could be up to 90GPa (Hoek and Diederichs, 2006). CPB is in a static condition provided that there is no vibration from natural phenomena such as earthquake and human-induced activity such as blasting.

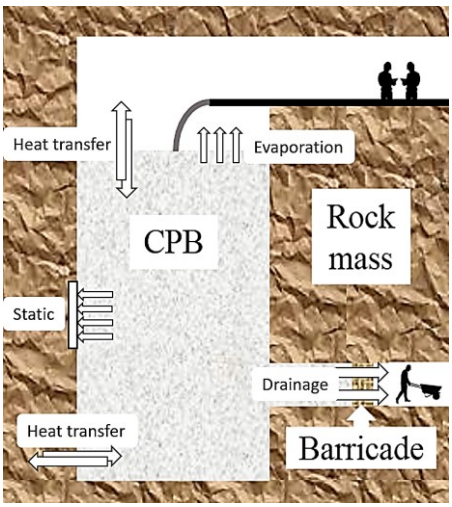

Figure 2.24: Schematic diagram of the phenomenon during backfill

2.7.2.2 Drainage

In mining stope, the barricade is usually designed to be able to drain excess water to reduce pore water pressure. But in order to attain maximum stress, the condition needs to be kept in the hydrostatic state (Thompson et al., 2009; Helinski et al., 2011b; Thompson et al., 2012). The surrounding rock mass is very low in hydraulic conductivity which will not cause

any significant drainage from CPB. Undrained condition enables investigation of the total stress behaviour without any deviation due to reduction in pore water pressure, but some pore water is used up during the hydration process (Ghirian and Fall, 2015). With excess water due to high water content of CPB design, autogenous shrinkage could be neglected.

2.7.2.3 Confinement

The backfilling process of mining stope is usually exposed to the atmosphere (not confined) where evaporation of excess water is allowed to reduce excess pore water pressure and heat loss or heat gained through convection is not controlled (Ghirian and Fall, 2015). Under a high curing temperature, the rate of evaporation of water is higher, and the reduction of pore water pressure will be more significant. During the investigation of CPB's behaviour, evaporation must be controlled to prevent unnecessary inaccuracy.

2.7.2.4 Curing temperature

CPB is usually cured at an uncontrolled curing environment where heat is free to be generated, transferred to and received from the surrounding. Sources of heat are described in Section 2.6.1. Thermal expansion of confined material shall exert addition stress to its surrounding. Semi-confined static material especially liquid and gas shall not exert any additional stress to its surrounding, but frictional paste and solid shall exert additional stress due to volumetric expansion and arching.

To understand the effects of curing temperature on the behaviour of CPB, the curing temperature needs to be controlled throughout the investigation. As heat dissipation is greater than heat generated from hydration in the laboratory-scale specimen, an external source of heat needs to be supplied to CPB to investigate its behaviour at higher curing temperature (Walske, 2014).

2.7.3 Fill Material

Fill material for mine backfilling are generally tailing waste generated from mining, binder and wastewater. For laboratory approaches, tailings made up of silica flour (varies among manufacturer) is commonly used for its similarity in mineralogical composition, inert towards chemical reaction (Fall et al., 2010; Ghirian and Fall, 2015) and resistance in high temperature (Souza et al., 2012). Manufactured silica flour comes with good consistency in particle shape and size for repeatable result. Silica flour is also used for tailing replacement due to its similarity towards the particle size distribution of nine Canadian mines (Nasir and Fall, 2008; Fall et al., 2010; Abdul-Hussain and Fall, 2012; Ghirian and Fall, 2015).

CPB mix proportion is usually in between of 3 – 7% by weight for binder and 70 – 85% for tailings (Landriault, 1995; Nasir and Fall, 2009; Orejarena and Fall, 2011). CPB have high water content (*w/c* ratio of 2.5 to 7%) which exceed the water needed for completed hydration of cement, because it is required to be pump through a pipeline without causing clog (Ramlochan et al., 2004). Mixing could be done with a concrete mixer or food mixer for 7 minutes or until it is homogenised (Cui and Fall, 2015). After mixing, slump test needs to be conducted for rheology check. The most common slump value used in CPB prior transportation to backfilling site is about 18 cm (Fall et al., 2007; Ghirian and Fall, 2015).

The filling method of the deposited material is targeted to produce isotropy distribution and reduce the effects of segregation throughout the filling process. In actual mine stope filling, CPB is poured from a given height at a steady rate. Jarret (1991) had conducted a test on distributed filling from a different height and noticed that the density at the pit and the top of the silo only shows a small deviation which is approximately 4%. CPB is not significantly affected by methods of filling, but it still has to be acknowledged.

2.7.4 New narrow wall model with temperature control

There is still no published literature on the behaviour of backfill material within NW under thermal alteration. None of the previously designed NW was used for backfilling material (paste with fine particles). Thus, a new NW model was designed with reference to the previous literature and modifications are implemented to fulfil the boundary conditions and to establish the objective of this research. CPB is prepared with references to previous literature and used as the fill material into the NW.

2.8 Summary of Review

Underground mining is inevitable due to the scarcity of resources at shallow level. Stopes or void is generated from mining activities, and the best solution is by cemented paste backfill. The THMC properties of CPB and stress distribution of fill material within NW were well established, but stress distribution anomaly was still observed during the full-scale monitoring. Stress anomaly could cause failure in mine backfill structure which usually resulted in fatality in humans' life and major loss in production (i.e. clogged access due to backfill failure, clogged pipeline due to halted production, and wasted batched material). Temperature change during the curing of CPB was speculated to be the cause of stress anomaly, but there is still no experimental evidence to prove it. Based on Section 2.7.4, an improved NW and fill material could be designed. Temperature effects on the stress-strain behaviour of CPB were studied with the proposed NW model. Experimental design and approach to achieve the objective of this research were discussed in Chapter 3.

CHAPTER 3

METHODOLOGY

3.1 General

In this chapter, the experimental approach to investigate the stress-strain-temperature behaviour of deposition within a NW was discussed. Material characterisation, model design, instrumentation, system calibration, preliminary test, deposition test procedure and test plan were explained. The effects of temperature were studied by implying a range of temperature heating pattern throughout the curing process. Figure 3.1 shows the flow of this research.

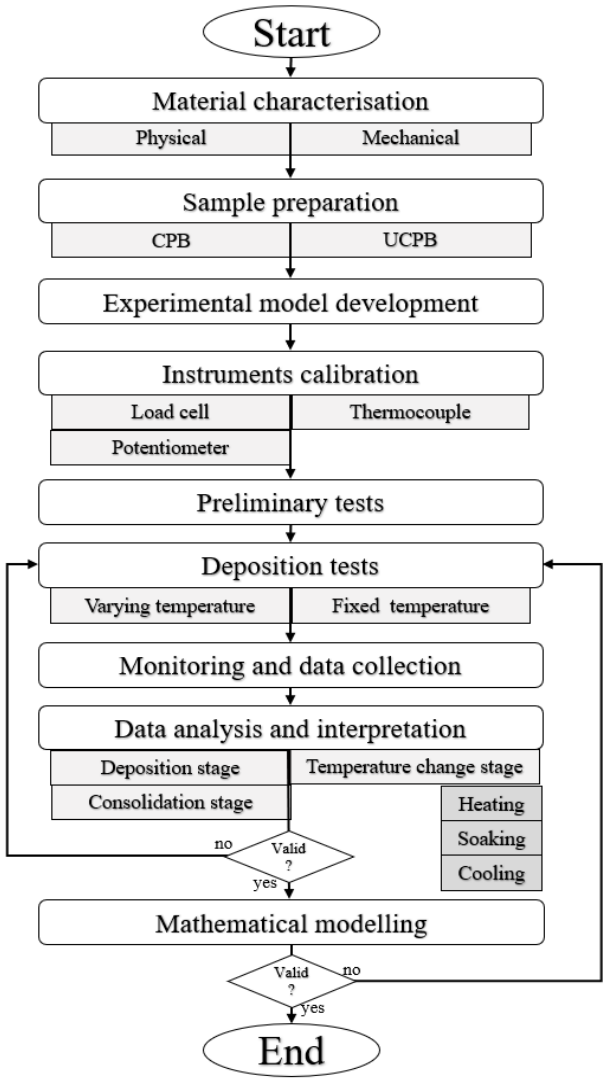

Figure 3.1: Flowchart of this research

3.2 Selection of Fill Material

With references to Section 2.7.3, the fill material was reproduced by using silica flour, cement and water. The specification of cement, water as well as silica flour used was provided by its manufacturer. To ensure that the silica flour complies with the requirement as replacement material for tailings, characterisation test were conducted (Section 3.3). The mix design was controlled to ensure the reproducibility of the sample for every test.

3.2.1 Ordinary Portland cement (OPC)

OPC was commercially obtained from Cahya Mata Sarawak (CMS) (Figure 3.2). As claimed by the manufacturer, the quality of cement was satisfactory as CMS cement exceeded the standard requirement specified in Malaysian Standard MS EN 197-1 which is equivalent to ASTM C150.

Figure 3.2: CMS Portland cement

3.2.2 Water

Tap water was used for mixing, which was neutral in pH, free from chemical residual, low total dissolved solids and no salinity as stated in the quality control standards (Kuching Water Board, 2000). The water pH, the total dissolved solids and the salinity were 6.84, 74.3 ppm and 0.0627 ppt, respectively. These data were obtained from water quality tests using PCSTestr35, EUTECH Instruments.

3.2.3 Silica flour as tailings

Silica flour is a finely ground crystalline silica which mainly consists of silicon dioxide was commercially obtained from SILVERBOND® Malaysia as shown in Figure 3.3. SILVERBOND® crystalline silica is produced from high purity quartz with SiO_2 of 99.38%. The manufacturer claimed that it is inert and neutral in pH. Thus, it would neither be reactive nor degrade upon extreme temperature. Silica flour had been extensively used when subjected to high temperature due to its capability to prevent strength retrogression. It had a chemically inert property which does not react even if subjected to high temperature thus providing a better assurance to be used as tailing replacement in this experimental approach.

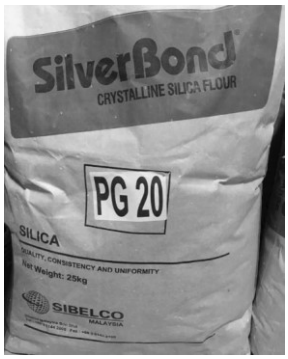

Figure 3.3: Crystalline silica flour

3.3 Material Characterisation

The silica flour used may be different from the silica flour used by the previous researchers in terms of its physical properties, microstructure, and mechanical behaviour. The silica flour used for this research was reinvestigated for its characteristic by conducting the following test. This was performed to provide experimental evidence on the characteristic of the silica flour although specification was provided by the manufacturer.

3.3.1 Physical properties

The properties testing that had been conducted were shown in Table 3.1. Silica flour was classified via the Unified Soil Classification System (USCS).

Table 3.1: Physical properties testing and method

Physical properties	Testing Method
Specific gravity, G_s	Density Bottle (Small Pycnometer) method (BS 1377: Part 2: 1990: 8.3)
Particle size distribution	Simple dry sieving and hydrometer analysis (BS 1377: Part 2: 1990: 9.3 and 9.5)
Liquid limit, LL	Cone penetrometer (BS 1377: Part 2: 1990: 4.3)
Plastic limit, PL	(BS 1377: Part 2: 1990: 5.3)
Water content, *w*	Oven drying at 105 ˚C (BS1377: Part 2: 1990)

3.3.2 Soil microstructure with scanning electron microscope (SEM)

SEM test was conducted to investigate the particle condition of silica flour. Under different resolution of lenses, different magnification could be archived. This test was conducted according to ASTM E2809.

3.3.3 Mechanical behaviours

The mechanical behaviour of silica flour played an important role in the deposition test within the NW. Behaviour such as friction angle, cohesion, strain deformation, and shear stress were needed for a better understanding of its effects during the NW deposition test.

3.3.3.1 Unconfined compressive strength test

Unconfined compressive strength (UCS) (ASTM D2166-16) was conducted for mix design clarification purposes. Proposed mix of CPB sample was needed to be able to archive a targeted strength as actual CPB used in mine backfilling as reviewed in Section 2.2.3.1. The sample was prepared under a range of cement content (3-7%) cured in a controlled humidity for 3 days with three replicates for optimal result.

3.3.3.2 Yield stress test

Yield stress was determined with fifty cent rheometer (Phasias and Boger, 1996). The yield stress of the sample was in the range of the actual application where the sample was able to flow and fill without any disturbance caused.

3.3.3.3 Modified direct shear test

Rapid-small shear box test (ASTM D3080) was referred and modified accordingly. Direct shear test could determine the shear strength of the soil under limitation and suitability. Direct shear test was conducted to determine the lower and upper limit of the internal friction angle of the fill material.

Figure 3.4 summarises the importance of the paste backfill mechanism within the stope wall when there is thermal expansion due to temperature increase. As the backfill takes place within a stope, vertical stress was transferred to the sidewalls due to arching. Exothermic reaction from the cement hydration and other sources of heat contributed to the expansion, and thus arching is intensified.

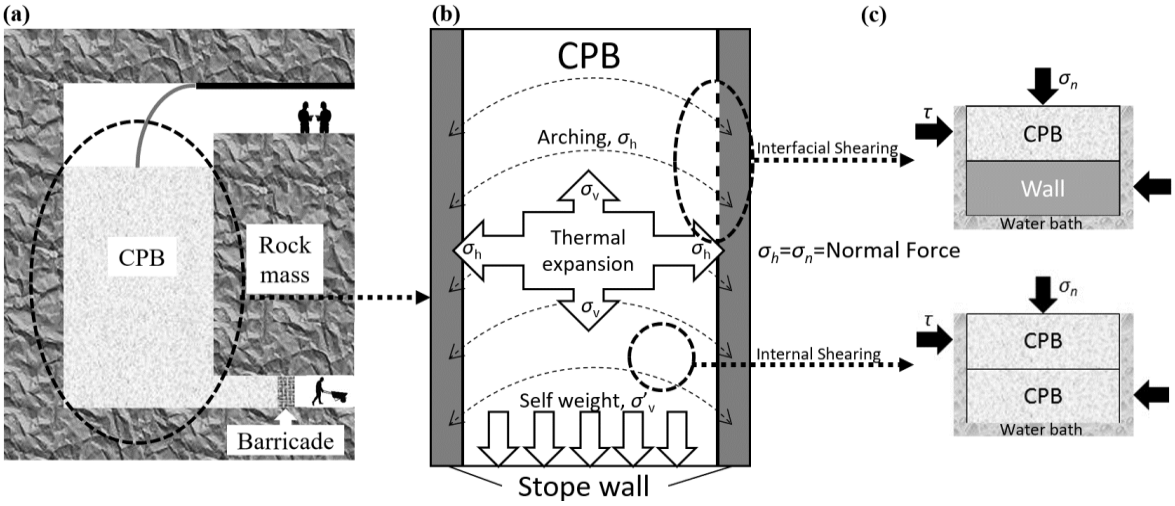

Figure 3.4: Schematic diagram for direct shear sample

Silica flour was suitable for rapid test using small shear box as in ideal condition, dry silica flour should not have any cohesion. Normal stress was back calculated from the condition of NW without any overburden stress or arching effects. The greatest normal stress would be the specific weight of the fill material across the total height of filling. The proposed normal stress was 16 kN/m^2 and with a factor of 200% and 300% which were 32 kN/m^2 and 48 kN/m^2. The shearing rate was selected based on the longest time required for

UCPB or CPB samples to achieve 90% consolidation (t_{90}), which is measured at about 0.5 min (ASTM D3080-11). The total elapsed time to failure was 5.8 min, and the horizontal displacement at failure was about 6 mm. Thus, the maximum displacement rate suitable for these experiments was 1.03 mm/min.

For the interfacial shear test, the mould was modified such that only the upper half (top) is filled with sample whereas the lower half (bottom) was replaced with an aluminium plate to simulate the stope sidewalls. An aluminium plate with dimensions of 60 mm wide, 60 mm long and 5 mm thick was used. The sample and the aluminium surface had to be exactly at the shearing plane. Aluminium material was used since it has an elastic modulus of about 70 GPa which is in the range of the elastic modulus of the rock mass (20 to 100 GPa) in mine stopes. For every attempt, a new aluminium plate obtained from the same material was used to ensure similar surface roughness.

The direct shear test was performed with ELE International digital direct shear apparatus used as the main apparatus. A temperature controlling system was incorporated in the direct shear apparatus, which consists of a digital temperature controller, two heating elements, and a thermocouple. During the test, the shear box was filled with water to keep the sample saturated throughout shearing. Water heating elements were immersed inside the shear box to generate heat into the sample. The temperature was controlled and monitored with a temperature controller and thermocouples. Such incorporation of temperature controlling system as shown in the illustration (Figure 3.5) did not caused disturbance towards the shearing process. The shearing temperature selected was ranging from room temperature (25 °C) to highest testing temperature for the deposition test (70 °C). Normal stress was applied accordingly, and the sample was sheared at the rate of 1 mm/min until 15% shear strain was achieved. A photo of the setup was shown in Figure 3.6.

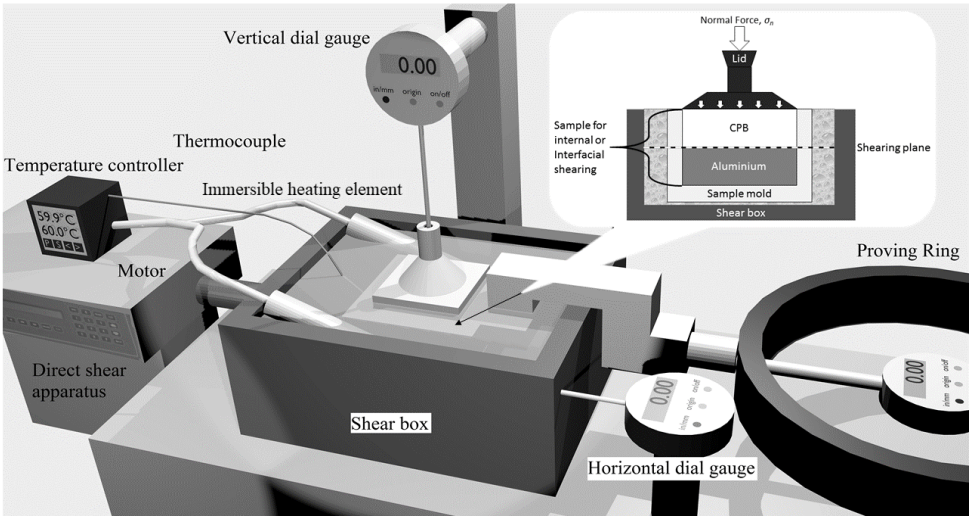

Figure 3.5: Illustration of thermal shear setup

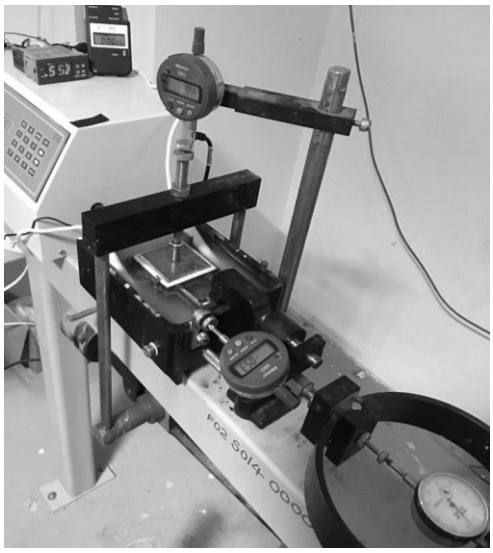

Figure 3.6: Photo of thermal shear setup.

Table 3.2 enlists the number of tests conducted. CPB samples were prepared using cast-in-situ (CIS) and precast (PC) method. CIS samples shows the effect of cementation bonding between CPB and it's shearing surface whereas PC samples prevent the formation of bonding during curing. Table 3.3 shows the direct shear test at elevated temperature.

Section 3.10.1 shows the mix design of UCPB and CPB. Same mix design of UCPB and CPB was used for both direct shear test and deposition test. The PC sample was prepared by pouring the mix into a 60 mm by 60 mm mould (the same size as the direct shear mould),

while CIS CPB was prepared by casting it directly into a well-prepared direct shear box. Figure 3.7 show samples before testing. Prior casting onto the aluminium surface, it was important to ensure that there was no gap in between the aluminium plate and the direct shear box to prevent unnecessary formation of gripping mechanism when CPB fills into the gaps.

The CPB sample was cured under high humidity for 2 days and cured under saturated condition for the remaining 1 day. The binder content and curing time were maintained for every test as the internal and interfacial shear behaviour is significantly affected, but it does not apply to the CPB samples that are prepared using PC method (Nasir and Fall, 2008; Koupouli et al., 2016).

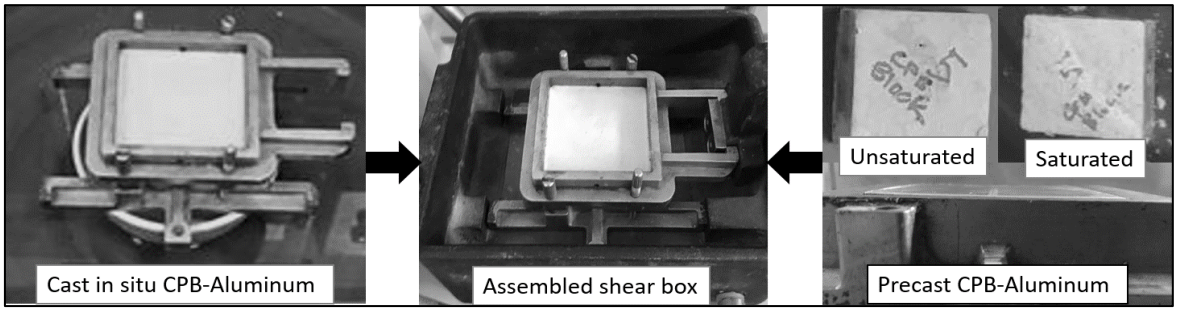

Figure 3.7: Preparation of CPB samples prior to testing with direct shear apparatus

Table 3.2: Test plan for direct shear test at room temperature

Specimen	UCPB				CPB					
Shearing condition	Dry		Saturated		Dry			Saturated		
	UC-UC	UC-A	UC-UC	UC-A	C-C	CIS-A	PC-A	C-C	CIS-A	PC-A

*Note that UC is UCPB, C is CPB, CIS is cast in situ CPB, PC is precast CPB and A is aluminium.

Table 3.3: List of direct shear test at elevated temperatures

Specimen	**UCPB**		**CPB**		
Shearing condition	Internal	Interfacial	Internal	CIS interfacial	PC interfacial
Shearing temperature (°C)	25	25	25	25	25
	50	50	50	50	50
	70	70	70	70	70

3.4 Design Consideration for Deposition Test System

The test model was designed and modified according to the previous literature on NW to suit the current studies on the behaviour of deposition. Factors were considered, but some of the factors were controlled to ensure the reproducibility of the result. The differences in full-scale and laboratory model could be due to the geometry of stope, geotechnical properties of fill and wall, coupled thermo-hydro-mechanical-chemical phenomenon in paste backfill, and filling rate. Based on Section 2.7, a wall with its height that is more than the double of its own width is considered a NW. Therefore, the NW system was designed to be in rectangular shape with 0.8 m height, 0.15 m width, and 0.05 m breadth as the shape of mining stope was generally rectangular. Lightweight aluminium plate was used to construct the NW due to easier handling and processing. The elastic modulus of aluminium is 70GPa, and it was in the range of rock mass at mining level (20-100GPa). The tensile strength of 241MPa prevents deformation due to additional stress generated. Aluminium was also used for its ability to conduct and transfer heat effectively within the wall material and onto the deposited material. In term of its surface properties, it was durable and easy to be cleaned after each usage as the surface roughness was one of the contributing factors towards arching.

The NW system was designed to be able to store the deposited material in a hydrostatic state. The barricade was usually designed to be able to drain excess water to reduce pore water pressure. However, the hydrostatic state was kept in laboratory condition to attain maximum stress. The upper end of the NW was covered to reduce water evaporation.

Vertical and horizontal stress could be reduced by allowing a designed portion of CPB (Plug fill) to harden and archive stability between supporting rock masses prior the rest of the filling. One-time pour was preferred to investigate the greatest stress generation but with a controlled filling rate of 0.0001 m^3/s to 0.0002 m^3/s.

The targeted range of temperature alteration was in between 30 ℃ to 60 ℃. The curing temperature was controlled by an automated temperature controller which supply heat to the system by referring to the input temperature and the present temperature indicated by the thermocouple. The curing temperatures were to be controlled throughout the experiment as heat dissipation was greater than heat generated from hydration in the laboratory-scale sample.

Upon changes in temperature and time, the stress distribution and volumetric changes were monitored using load cell and potentiometer. The aluminium NW was fixed to prevent horizontal expansion of the backfill material. The expansion of the backfill material was monitored from the top which it was not confined. A potentiometer was used for observation of thermally expanding volume of backfill material. A load cell was used to monitor the vertical pressure induced at the bottom plate. A thermocouple was connected to the temperature controller to monitor present temperature of the experiment.

Temperature controller provides direct current to the connected ceramic heaters when the present temperature of the model is lower than the set temperature based on the test plan. A data acquisition unit was used for data logging purposes. Load cell, potentiometer and thermocouple were connected to the data logger for a real-time monitoring and data logging. Data logged was in terms of voltage differences and calibration was required to convert voltage recorded to the desired unit such as stress and deformation.

3.5 Parts Acquisition, Fabrication and Assembly of Narrow Wall

Materials were purchased and fabricated into the desired dimension. Fabricated parts were assembled to construct the model for the deposition test. Appendix C shows the specification of the fabricated parts. Assembled model was shown in Figure 3.8, 3.9, 3.10 and 3.11.

The model was designed with an adjustable level for the entire model. Four 21.6 mm diameter steel all thread rods were installed at four sides of the rectangular base. The height of the base was adjustable from four corners, and the level of the NW could be checked with a spirit level. Mild steel was used as the bottom base for stability concern such as the risk of overturning upon impulsive contact with the NW. The load cell was installed onto an adjustable steel plate which could prevent errors such as non-uniformly distributed stress from the NW to the load cell which may result in complex data and a risk of damaging the load cell. Four 6 mm diameter thread steel rods were installed at the four corners of the steel plate for adjustable level purpose. The load cell was bolted to a 5.5 mm diameter steel thread rod as per required by OMEGA load cell design to be connected to a rigid platform. Two 21.6 mm diameter steel thread rods were installed as vertical support for the NW to restrain the NW's self-weight and arching induced downward force from transferring to the load cell. Illustration and specification for the base of the model are shown in Figure 3.8 below.

The wall was constructed with four pieces of aluminium plate and forms a rectangular hollow wall. The aluminium wall was bolted with an L-shaped high tensile steel plate at both sides, two at a different height to be connected to the vertical steel thread rod mentioned before. This design ensures that no force other than the weight transferred to the bottom plate was transferred to the load cell (considering various stress transfer such as arching). This allowed modification as the entire level of narrow wall was adjustable.

It was common for metal to expand upon thermally heated. The expansion in terms of displacement was low but when it was confined, the expansion would induce a great amount of thermal stress on all direction. Although the aluminium wall was fixed at a few locations where expansion could be controlled, there was still a small portion of open-ended span of aluminium wall that will expand freely due to thermal expansion. Stress generated

from NW expansion was undesirable as the main investigation was on the behaviour of fill material itself. As the fill material consists of water and other very fine material, leaving a gap between wall and bottom plate as Jarret, (1991), Vanel and Clement, (1999), Di Felice and Scapinello, (2009), and Ting et al., (2011) was not applicable. Therefore, an expansion gap was designed as shown in Figure 3.9 below to absorb the expansion and sealed to prevent the backfill material from escaping through the gap.

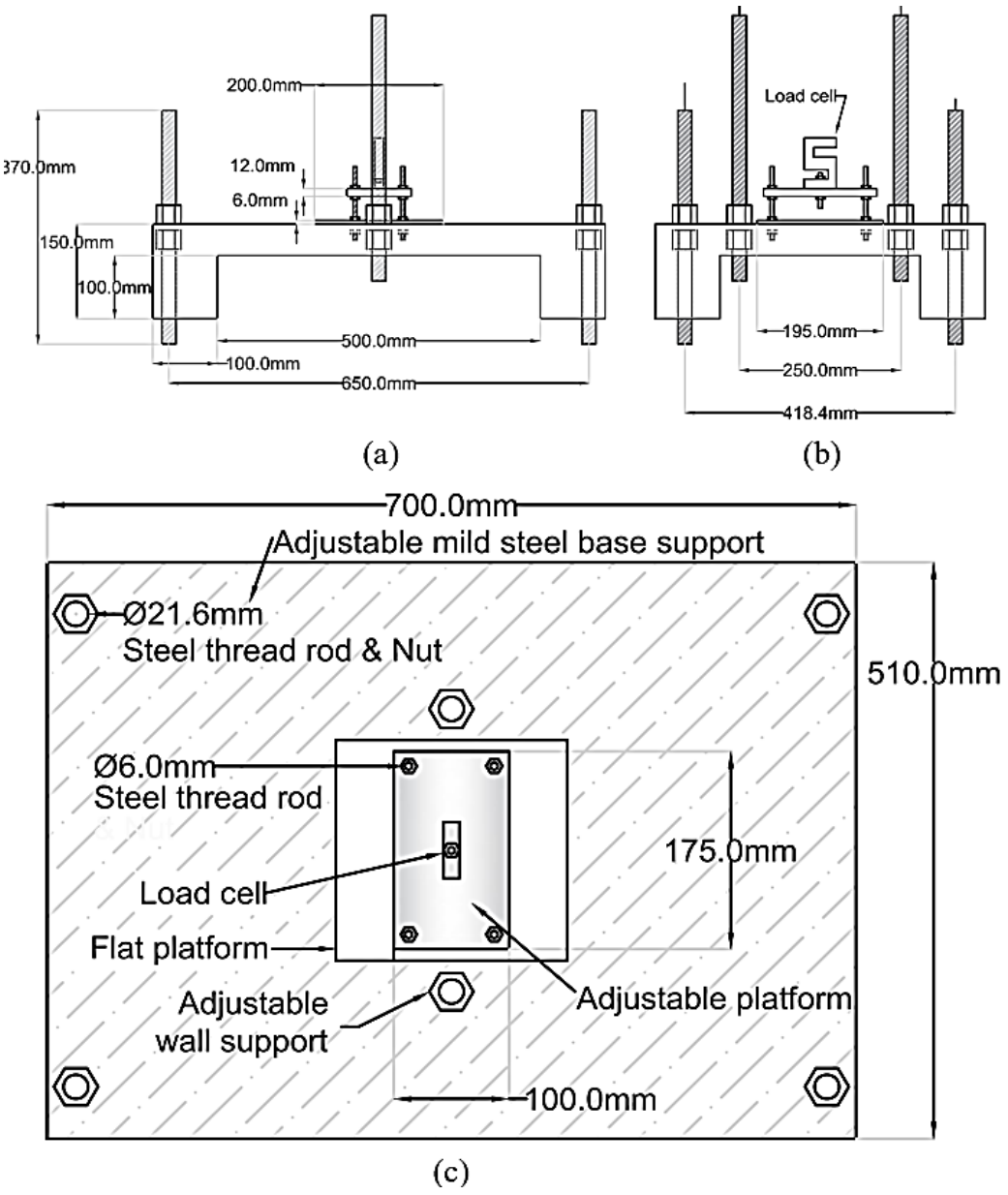

Figure 3.8: Schematic diagram of base platform for narrow wall support (a) side, (b) front, and (c) top view

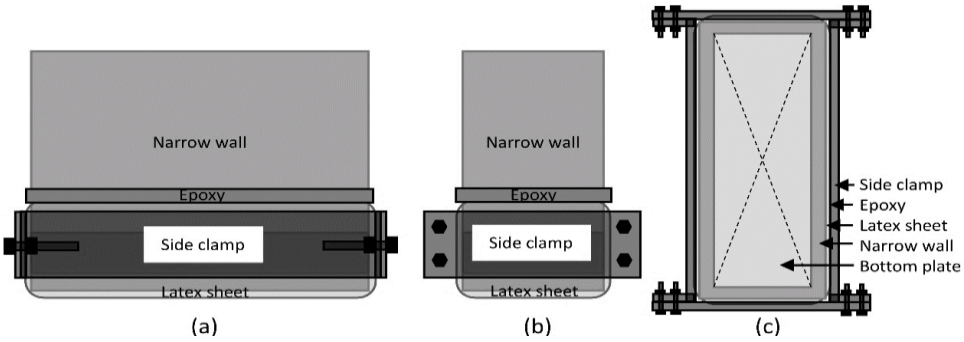

Figure 3.9: Schematic diagram of expansion joint (a) front, (b) side, and (c) top view

U-shaped aluminium tray was used as a holder for the ceramic heater. Both holders on the different side will be bolted together and create a grip on the surface of the NW. The placement height of the ceramic heater was predetermined by ratio and altered after trial or preliminary heating test to have an equivalent distribution of heat. Illustration and specification for the upper half of the model were shown in Figure 3.10 below. Figure 3.11 shows the assembled isometric illustration and actual model set-up.

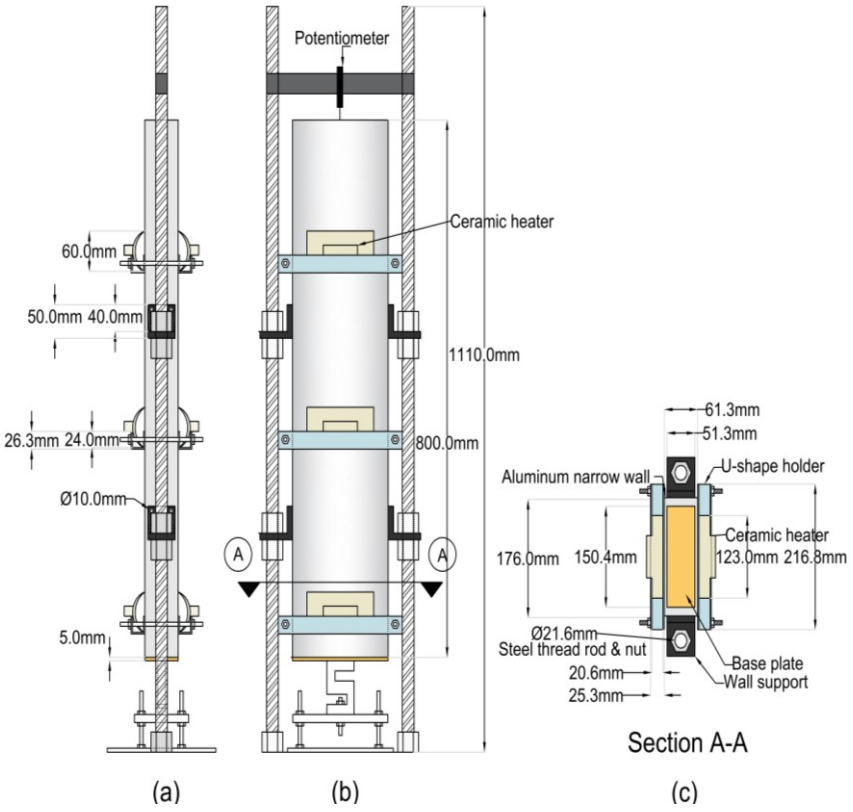

Figure 3.10: Schematic diagram of narrow wall (a) Side, (b) Front, and (c) Top view.

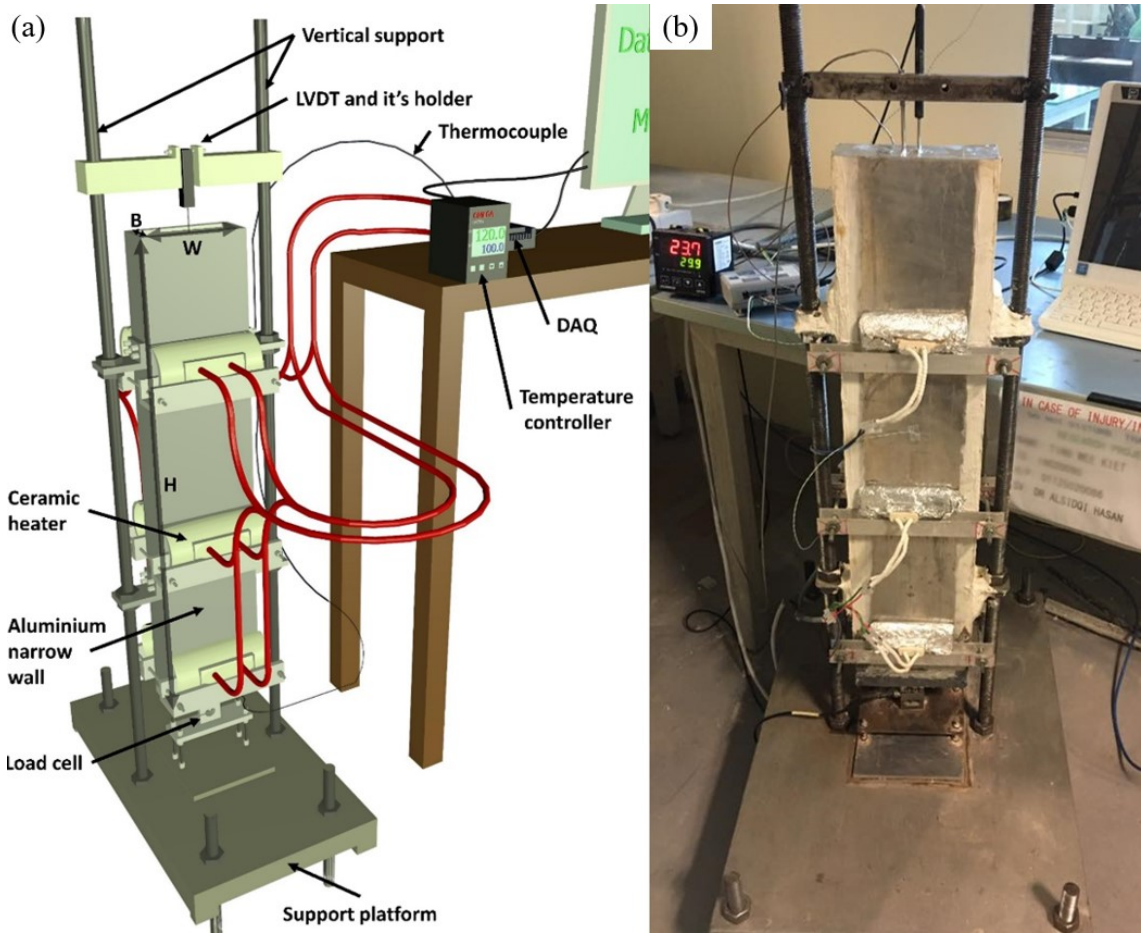

Figure 3.11: Assembled model and components (a) Illustration and (b) Actual model.

3.6 Instrumentation Selection and Installation

Instruments were selected based on the limited condition of the test model such as availability of space for the instrument, the operating temperature of the instrument, design capacity of the instrument, and cost-effective wise. The instruments are shown in Appendix D with its manufacturer, model and function. In-depth specification of instrument selection is discussed in Appendix E. Placement of the instruments is shown in Figure 3.11 and wiring connections in Figure 3.12. All of the instruments required a set amount of power to be operated. The data acquisition unit and temperature controller were compatible with Malaysia power supply standard of 230-240 V 50 Hz. The power supply for other instruments was controlled by data acquisition unit and temperature controller output. Load

cell, potentiometer and thermocouple basically relies on the voltage supply (<10 V) from the data acquisition unit to operate. They basically function as an indicator by showing the difference in voltage and was needed to be compared to calibration data.

Temperature controller used a thermocouple as its very own present temperature indicator and was able to supply up to 250 VCA 5 A (1250 Watts) on its output. Each ceramic heater was used for heat generation. With six ceramic heaters of 750W, there was a spare of 500W for additional needs in the future. Standard 13 A power cable was used to connect the ceramic heater to the temperature controller. A computer was used as its serial port could detect data transfer for data acquisition unit and temperature controller. With a suitable converter such as RS-485 to USB converter, the issue of availability of serial port was solved by using USB port instead. The data acquisition model that was selected for this study comes with its own data to USB cable. Figure 3.12 illustrates the connection of the instruments.

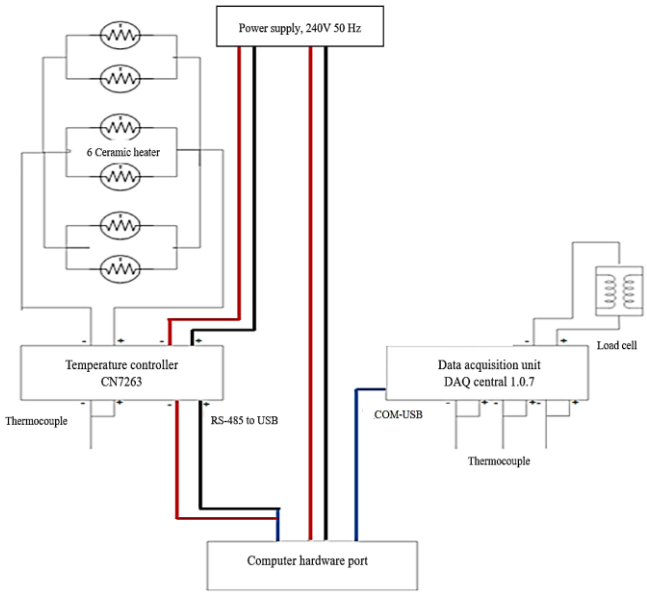

Figure 3.12: Simple schematic on connections of instruments

3.7 Model and System Calibration

The model was calibrated for every repetition of the actual and preliminary test to ensure that the result is consistent and reproducible.

3.7.1 Instrument Calibration

The instruments were calibrated by implying a known value on them. Although a manufacturer calibration was provided to the user, it was proper to ensure that the instrument was functioning correctly to the calibration. Weight from 0 kg to 25 kg with an increment of 1 kg will be applied to the load cell. The linear voltage reading was recorded for each weight, and the relationship between weight and linear voltage could be established for our future monitoring purposes. Same goes for the potentiometer by attaching it to a digital vernier calliper to calibrate the relationship of displacement toward the value of linear voltage shown. All thermocouples were calibrated by placing them in the same water bath with a standard mercury-in-glass thermometer, and any deviation will be adjusted using the DAQ software.

3.7.2 Level of Model

The level of the model must be at an exact upright position as any inclination will result in different arching effect, stress distribution, and flow of material. The steel thread rod which penetrates at four corners of the base support was adjustable by rotating the nut at an appropriate direction for inclination or declination. A spirit level for both directions was set on the top opening of the NW for level adjustment reference. Once the level was centred, the load cell level was adjusted to perfectly touch the bottom plate of the NW throughout the surface of the load cell. The weight of 25 kg was applied to the top of the NW to ensure that the vertical support was properly secured and no force could be transferred other than the apparent mass of the filling.

3.7.3 Heat Distribution

The aluminium wall was required to archive an equally thermal distributed state where it should be calibrated by setting the ceramic heaters on both sides at geometrically equivalent height. As the heating commenced, it was monitored by thermocouple on the

distribution of the heat within the aluminium NW. The adjustment was made, and additional ceramic heaters were added to improve the rate of heating and distribution of heat. Water was used as a mock medium to store the heat between the walls instead of convection to the open atmosphere. The heat transfer was less effective on downward direction but instead, most of the heat has been transferred to the upward part of the medium. Upon adjustment, the finalised location of ceramic heaters was shown in Figure 3.10.

3.8 Preliminary Test

Preliminary tests were required to ensure that the conceptual design of the setup could capture the behaviour of CPB accurately. The challenges were to ensure that only stress generated by the backfill itself was recorded, to control the backfill from leaking and at the same time to allow flexibility so the stress transfer could be recorded accurately.

3.8.1 Stress-Strain Generated from Narrow Wall due to Thermal Expansion.

The functionality of the vertical support was checked by placing 25 kg weight on top of the NW. This was performed to ensure that the NW was properly secured as the arching effects could drag the NW towards the gravitational direction to where the load cell was placed. Such occurrence would cause unnecessary stress to be recorded by the load cell. Therefore, by placing a weight of 25 kg which was significantly higher than the downward force created due to arching effects between backfill material and NW could show that the vertical support was tightened properly. The functionality of the expansion gap was checked during the trial heating. The pressure generated from the expansion of open-ended aluminium wall could be identified by referring to the load cell and potentiometer during the heating process. The cooling process was also recorded for the sake of its ability to return to its initial state. The potentiometer was installed on the NW as shown in Figure 3.13 measures the expansion of the side wall, not the expansion of the backfill.

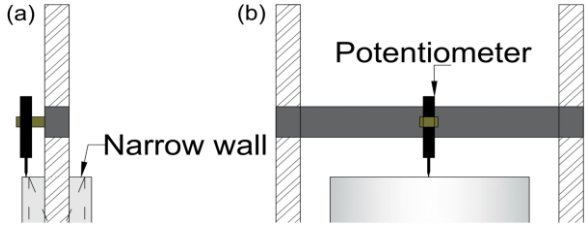

Figure 3.13: Placement of potentiometer during expansion check

3.8.2 Restraining Capability of Latex at the Expansion Gap

The model was required to be tested for the significance of the latex sheet in its modulus of elastic due to the force required for the initiation. Calibration was performed with water as there is insignificant value of arching when the water is in static condition within the NW. By adding the water at a steady rate, the load cell would detect the stress induced on the bottom plate. The water was needed to be completely drained before the actual deposition test. In this case, a vacuum pump with a modified nozzle was used to remove the water steadily. As the water was totally drained, the reading of the load cell should return to its original range of value. The value of restraining force was made known for every new test by calibrating with water. The force required to allow contact between the load cell and bottom plate was used during the analysis as an offset value.

3.9 Precaution

The following are some precautions before conducting the experiment:

i. The thermocouple from the temperature controller was insulated as some current could be discharged into the model that could cause faulty reading and malfunction.

ii. The thermocouple was needed to have good contact with the paste.

iii. Avoid any forms of contact onto the NW to avoid data inconsistency and inaccuracy.

iv. The model could create discomfort due to the surrounding thermal gradient generated from the ceramic heater, and there might be a risk of electrocution from the wiring connection joint around the model.

3.10 Deposition Test

The deposition test via the NW designed previously with the proposed fill material were discussed. CPB was one of the targeted material as it was commonly used as backfill material in mine backfilling. In this study, UCPB was also tested as a control sample to shows the significance of CPB behaviour.

3.10.1 Sample Preparation

Fresh silica flour consists of less than 0.2% bulk water content (from the bag) was used for the preparation of all sample. A series of slump tests and UCS tests were performed to acquire the most suitable mix design for both UCPB and CPB, which were explained in Section 4.3. Mix composition of 72% solid content and 28% water content were used for UCPB and CPB. The cement binder content for UCPB and CPB are 0% and 5%, respectively for all tests. The water-cement ratio for CPB was 7.7. UCPB and CPB samples properties are summarised in Table 3.4.

Table 3.4: Sample mixture characteristic

Sample	Binder content (%)	Solid mass content (%)	Water content by total (%)	Water to cement ratio	UCS (kPa)	Yield stress (Pa)
UCPB	0	72	28	-	48	70
CPB	5	72	28	7.7	314	115

The material could be mixed manually or preferably using automated mixer until homogenised for around 7 minutes depending on handling speed. For CPB, the mixing should not be delayed to avoid an increase in yield stress that would interfere with the filling process. With the same mix design, both CPB and UCPB mix design was used for the direct shear test for internal friction angle and modification were made for interfacial friction angle between sample and aluminium surface at a range of shearing temperature.

3.10.2 Test Plan

The scope of the study was limited to the effect of constant curing temperature and change in temperature during curing with respect to CPB and UCPB as the fill material. It was first investigated under the effect of room temperature to show a laboratory cured behaviour. Typical temperature increase in-situ condition was up to 50°C (Grabinsky and Thompson, 2009; Thompson et al., 2011; Thompson et al., 2012). A set of temperature variant was shown in Test 1-5 in Table 3.5 to identify the effect of constant curing temperature on CPB stress-strain behaviour. The sample cured at a fixed temperature from the starting of deposition until no change was observed on its stress-strain behaviour.

For the effects of temperature change during curing, the sample was deposited and allowed to consolidate until stable stress was indicated by the load cell. The sample was heated (ramp) with different heating pattern and allowed to remain at constant temperature (soak) or cool (dwell) to lower temperature. Detailed temperature change is shown in Table 3.5. From Test 6-12, UCPB was tested under the same temperature variant as a control sample to show the significance of CPB behaviour. The recommended procedure for test preparation and paste backfilling was shown in Appendix F.

Table 3.5: Test plan for deposition test

Backfill					**CPB**				
Test	1	2	3	4			5		
Step	-	-	-	-	1	2	3	4	5
Ramp	RTP - 30	RTP - 40	RTP - 50	RTP - 60	RTP - 30	30 - 40	40 - 50	50 - 60	30 - 60
Soak	30	40	50	60	30	40	50	60	60
Cool	-	40 - 30	50 - 30	60 - 30	-	-	-	60 - 30	60 - 30
Backfill					**UCPB**				
Test	6	7	8	9			10		
Step	-	-	-	-	1	2	3	4	5
Ramp	RTP - 30	RTP - 40	RTP - 50	RTP - 60	RTP - 30	30 - 40	40 - 50	50 - 60	30 - 60
Soak	30	40	50	60	30	40	50	60	60
Cool	-	40 - 30	50 - 30	60 - 30	-	-	-	60 - 30	60 - 30

CHAPTER 4

CHARACTERISTIC OF BACKFILL MATERIAL

4.1 General

This chapter shows and discusses the findings on the characteristic of the backfill material through the proposed testing shown in Section 3.3. The tests were conducted according to the standard method enlisted in Table 3.1. The findings serve as an understanding and assist in the analysis of the behaviour of silica slurry (UCPB) and cemented silica slurry (CPB) during deposition test. The findings are comparable with the established research on the characteristic of the backfill material.

4.2 Physical Properties of Silica Flour

The silica flour (SF) used was obtained from three new bags of silica flour. Each of the physical property tests were performed thrice. The average of the results was tabulated in Table 4.1. The result was comparable with manufacturer datasheet and test conducted by other researchers (Célestin and Fall, 2009; Fall et al., 2010; Ghirian and Fall, 2015).

The usability of SF had been checked with the average of nine Canadian mine tailing size with our particle size distribution (PSD) data, as shown in Figure 4.1. Table 4.2 shows

Table 4.1: Physical properties and mechanical behaviour result of silica flour

Physical properties	Result	Specification	Literature
Specific gravity, G_s	2.67	2.65	2.7
Particle size distribution	Silt	-	Silt
Coefficient of uniformity, C_u	3.66	3.65	16.2-16.6
Coefficient of gradation, C_c	1.17	-	1.3
Initial water content	< 0.2%	0.2%	-
Liquid limit, LL	23.83%	-	-
Plastic limit, PL	22.22%	-	-
Plasticity index, PI	1.61%	-	-
Shrinkage limit, SL	5.31%	-	-
USCS classification	Low plasticity silt	-	Low plasticity silt

the physical properties of silica flour. The physical properties of silica flour used was similar other than the coefficient of uniformity where the silica flour in this study was well graded. The mean particle diameter of silica flour is 25 μm. According to Potvin et al. (2005), the paste fill should contain at least 15% of passing with particle size of 20 μm. Therefore, the proposed silica flour was suitable as tailing replacement for the mix design of CPB sample.

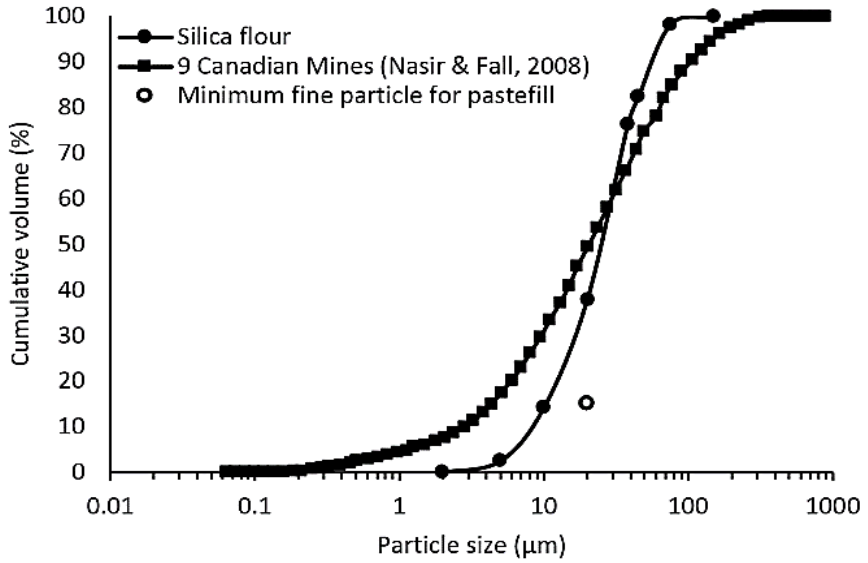

Figure 4.1: PSD of SF and the average PSD from 9 Canadian mines

Table 4.2: Physical properties of silica flour

Parameter	G_s	D_{10}	D_{30}	D_{50}	D_{60}	D_{90}	C_u	C_c	Δ
Unit	-	μm	μm	μm	μm	μm	-	-	-
Value	2.67	8.2	17	25	30	56	3.66	1.17	1.91

The microstructure of SF is shown in Figure 4.2 at different magnifying scale. From Figure 4.2, silica flour possessed fine and coarse particles that were in the shape of quartz. The silica flour was loosely packed and free from any forms of moisture at its surface.

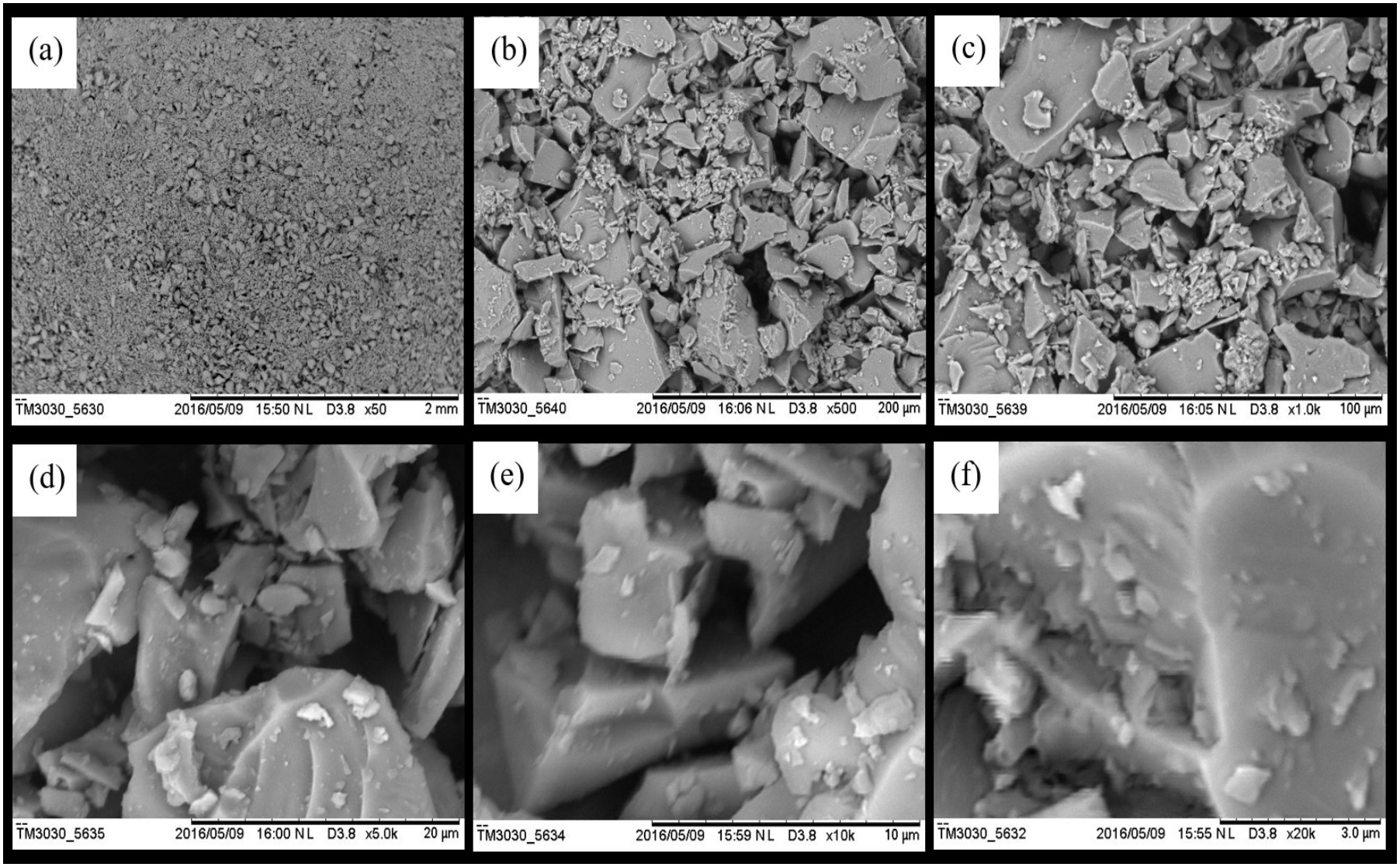

Figure 4.2: SEM images of SF at magnifying scale of (a) 50, (b) 500, (c) 1000, (d) 5000, (e) 10000, and (f) 20000 times

4.3 Mechanical Properties of Backfill Material

The mechanical behaviours of UCPB and CPB were investigated through UCS test, slump test, and direct shear test with consideration of temperature change. UCS value of the CPB was required to ensure the correlation between the laboratory made CPB and the actual CPB used in mine backfilling. As the strength of CPB exhibited a direct relationship with its shear strength, the appropriate binder content was to be determined through UCS test and was kept constant throughout the test. With arching effect as the main phenomenon that affects the stress distribution of backfill, the known contributing factors towards arching such as unit weight, internal friction angle, apparent cohesion of backfill, and interfacial friction angle between backfill material and its adjacent wall were needed to be identified. The CPB also had to be designed in a way that its yield stress complied with the flowability requirement of actual transportation pipeline. The findings on the aforementioned parameters are discussed in the following subsection.

4.3.1 Uniaxial Compressive Strength

UCS test was conducted on CPB samples to determine the appropriate amount of binder used to reproduce the CPB mix that complied with the standard practice. UCS test showed the UCS of the sample by allowing the material to be compressed until failure. The peak compressive strength of the sample was compared with the rest of the samples with different binder content but with the same curing duration and environment.

A linear relationship between uniaxial compressive strength (kPa) and binder used (%) was observed from Figure 4.3. The higher the binder content, the greater the uniaxial compressive strength of the CPB sample. The strength of CPB was directly related to the shear strength of the sample too (i.e. cohesion). Cohesion, frictional angle and unit weight of the samples is partially controlled by the binder content, and these parameters are crucial

in affecting the intensity of arching effects. Thus, the binder content must be controlled and fixed throughout every testing program (i.e. direct shear test and deposition test).

UCS of CPB was usually between 200 kPa to 5000 kPa, but the common target strength in practice was 1000 kPa at 28 days or 300 kPa at 3 days (Sheshpari, 2015). Ghirian and Fall (2016) and Wu et al. (2016) also showed similar findings, where at 3 days of curing, the UCS should be around 300 kPa. From Figure 4.3, 5% of binder was chosen to obtain the UCS at around 300 kPa after 3 days of curing. The amount of OPC, $B_w(\%)$ used was decided by the percentile of dry mass of solid as shown in Equation 4.1.

$$B_w = \frac{W_B}{W_{Dry-S}} \qquad \text{[Equation 4.1]}$$

where W_B is the weight of binder and $W_{Dry\text{-}S}$ is the dry weight of solid.

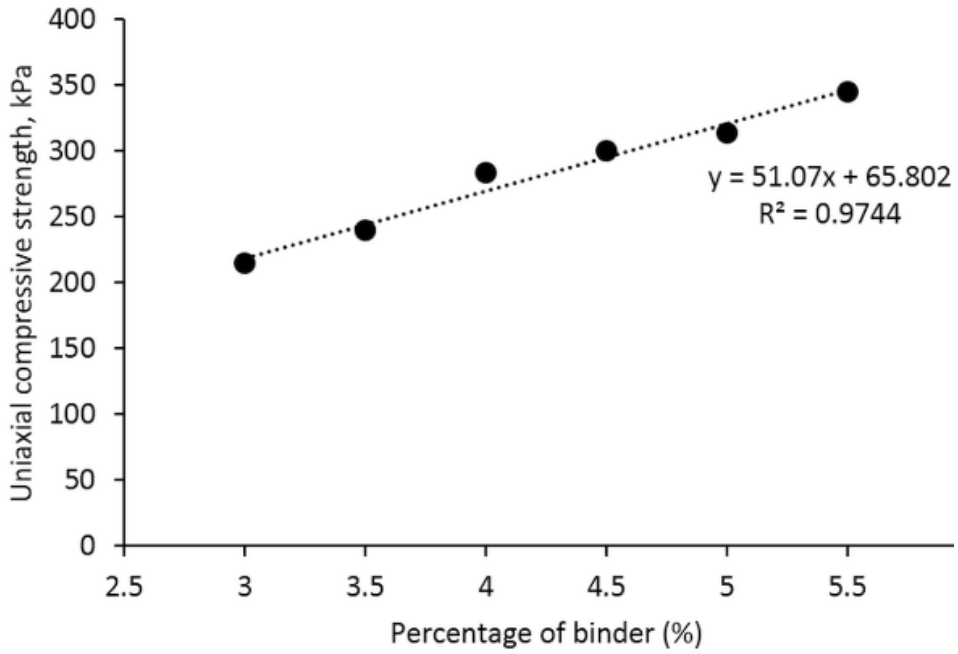

Figure 4.3: Graph showing UCS value for different amount of binder used

4.3.2 Yield Stress and its Flowability

Figure 4.5 shows the relationship between three variables, namely solid content, yield stress and normalised slump height (z/H) for samples with 5% binder content. Note

that z is the slump and H is the height of the sample. A range of normalised slump height (z/H) versus yield stress estimation is also shown in Figure 4.4. Slump test was conducted with different solid content designed for the sample, and its respective normalised slump height was recorded. From the Atterberg's limits of the silica flour, the expected range of water content could be predicted from its liquid limit and plastic limit. The change in the material phase was critical as it had a low plasticity index of 1.61%. Therefore, by referring to Figure 4.5, the normalised slump height changed significantly in the range of 72% to 75% solid content. It was evident that from the addition of cement, the plasticity index of ML soil would be affected depending on the amount of binder added (Bayat et al., 2014). With the normalised slump height, the dimensionless yield stress could be estimated from Figure 4.4 using the exact theoretical solution curve. The yield stress, τ_y could be calculated using Equation 4.2 below.

$$\tau_y = Normalized\ slump\ height\ \times\ \rho g H \qquad \text{[Equation 4.2]}$$

where, ρ is the density of the sample, g is the gravity acceleration constant, and H is the total height of the slump cone. The estimated yield stress corresponding to the normalised slump height for different solid content is plotted and shown in Figure 4.5. Yield stress below 200 Pa was recommended for a clog-free flow within the pipeline (Cooke, 2008). Thus, 72% solid content with 115 Pa of yield stress was chosen as CPB sample mix design. At 72% solid content, the estimated yield stress for UCPB sample was obtained and it is found to be lower than the yield stress of CPB which was 70 Pa. The addition of cement into the backfill material would increase the yield stress and retard its flowability. It was found to be true for both UCPB and CPB that with higher solid content, the yield stress would be higher.

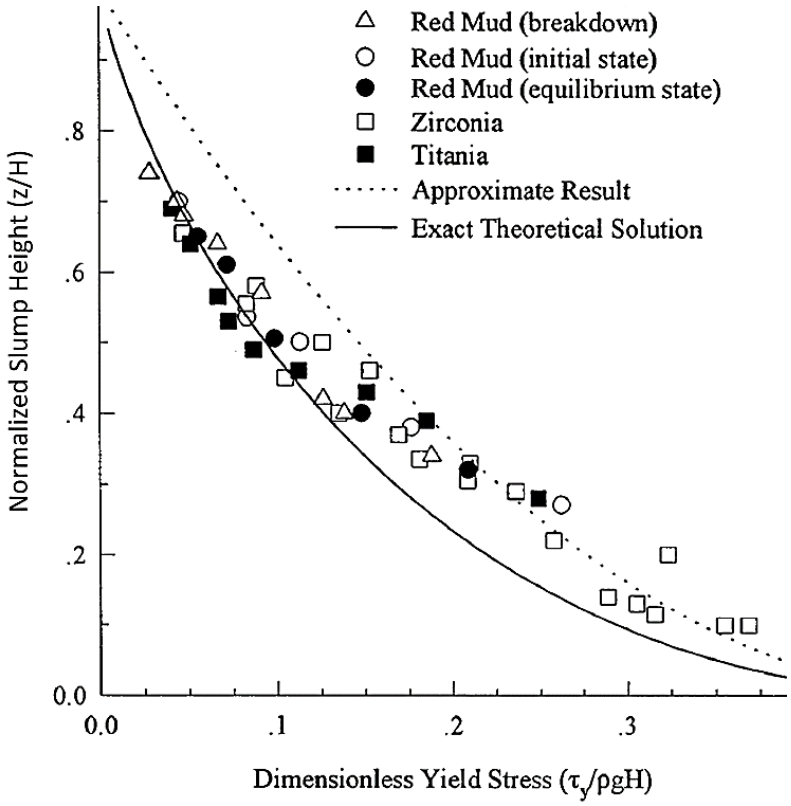

Figure 4.4: Normalised slump height of soils with theoretical prediction (Pashias et al., 1996)

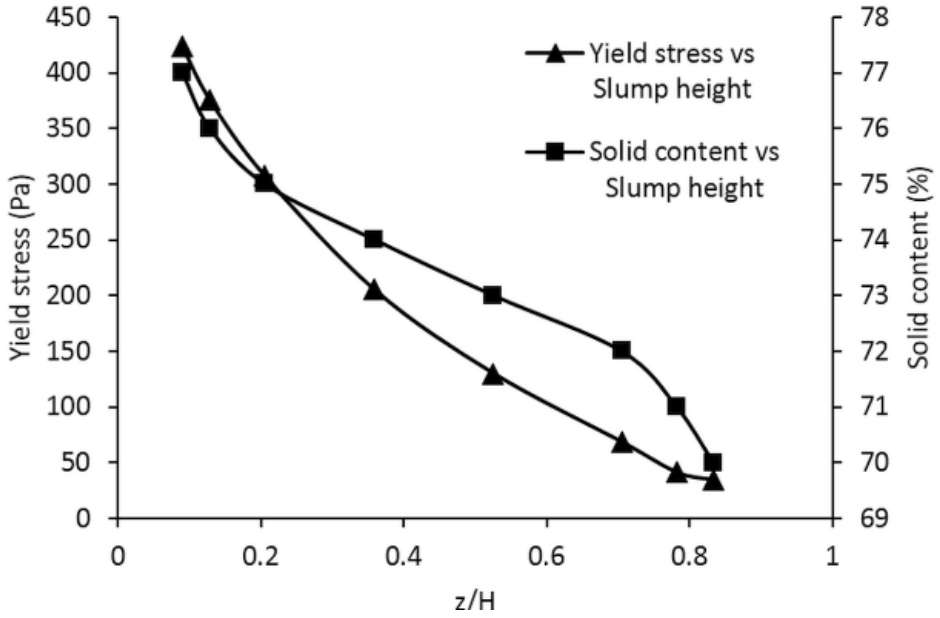

Figure 4.5: Yield stress corresponding to the solid content (%) and slump height

4.3.3 Shear Behaviour of Backfill

The direct shear test was performed on UCPB and CPB under different shearing condition according to Table 3.2. The direct shear results were presented in terms of shear stress-strain, and Mohr-Coulomb envelope that showed apparent cohesion and friction angle parameter. The shear stress-strain curves of UCPB and CPB are shown in Figure 4.6 and Figure 4.7 respectively. Generally, two types of curves could be observed which were nearly perfect plateau elastoplastic curve (Figure 4.6a, Figure 4.6b, and Figure 4.7) and elastoplastic curve with strain hardening (Figure 4.6c and Figure 4.6d).

Each test in Figure 4.6 was investigated under different density, but only the one initial packing of 1.75 g/cm^3 was discussed in the present study because it correlated with the density of the mix design for UCPB and CPB used. Figure 4.6a and Figure 4.6b show the internal shear stress-strain behaviour of dry silica flour and interface shear stress-strain behaviour of dry silica flour with aluminium surface without water for saturation whereas Figure 4.6c and Figure 4.6d are sheared under a saturated condition. Specimens in Figure 4.6a and Figure 4.6b behaves like a fine granular remoulded sample. Shear stress-strain behaviour of remoulded specimen normally behaves like elastoplastic curve with strain hardening where peak stress was not presented as overconsolidated. The internal shear stress of UCPB-UCPB was greater than UCPB-A interface by 56.0%, 53.4% and 51.0% with respect to the normal stress of 16 kPa, 32 kPa and 48 kPa. When saturated, the silica flour tended to behave like a block of paste although no cement binder was added. The greater initial gain in shear stress as shown in Figure 4.6c and Figure 4.6d compared to dry silica flour was partly due to the formation of minor cohesion within UCPB and adhesion between UCPB and aluminium surface. After overcoming the shear strength from the adhesive/cohesive behaviour, lubrication effect due to the presence of water would reduce

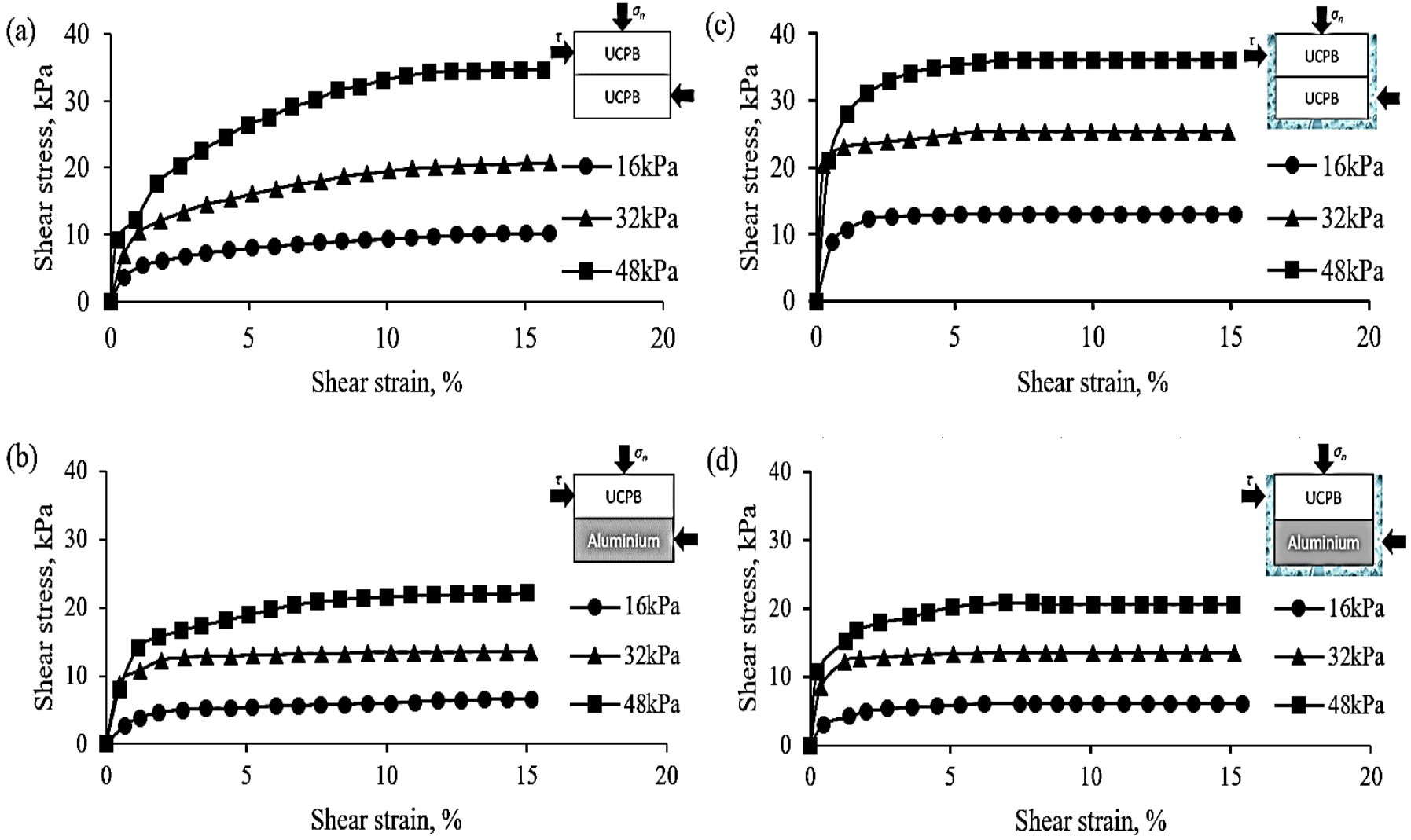

Figure 4.6: Shear stress-strain of UCPB under different shearing condition (a) Dry UCPB-UCPB (b) Dry UCPB-A (c) Saturated UCPB-UCPB (d) Saturated UCPB-A

the friction and thus resulting in a minor gain in shear stress after 2% shear strain. The ultimate shear strength for the saturated case was slightly higher due to the minor adhesion and/or cohesion.

Figure 4.7a to Figure 4.7c show the internal shear stress-strain behaviour of CPB and interface shear stress-strain behaviour of CPB-A under different casting method whereas Figure 4.7d to Figure 4.7f show the same tests but under saturated condition. Binder content and curing time was kept to be constant throughout the tests since the interface shear stress-strain behaviour was significantly affected by binder content if the shearing occurred within CPB and within a cast in-situ CPB-A interface shear (Nasir and Fall, 2008) although it had been established that the interface shear stress-strain behaviour was insignificantly affected by binder content and even less affected by curing time (Koupouli et al., 2016). Figure 4.7c and Figure 4.7f show similar shear stress-strain behaviour as Figure 4.6b and 4.6d but possess higher shear stress throughout the shearing. Similar behaviour was probably due to the same contact in between specimen and aluminium, but the difference in shear stress value was most likely due to the greater surface roughness of CPB compared to UCPB which was rather soft and does not have the ability to control its surface roughness. The interface shear stress of precast CPB-A did not vary much from each other due to the counterbalance effect as mentioned in UCPB-A interface.

Figure 4.7a, Figure 4.7b, Figure 4.7d and Figure 4.7e show shear stress-strain behaviour in between CPB-CPB and CPB-A interface under saturated and unsaturated condition. First peak shear stress could be seen at region less than 3% shear strain for both unsaturated and saturated CPB-A interface which is due to the failure of the cementation bond between CPB-A interface. This was supported by post-shear observation where a very thin frictional layer of CPB remained on the aluminium surface. It was confirmed that there

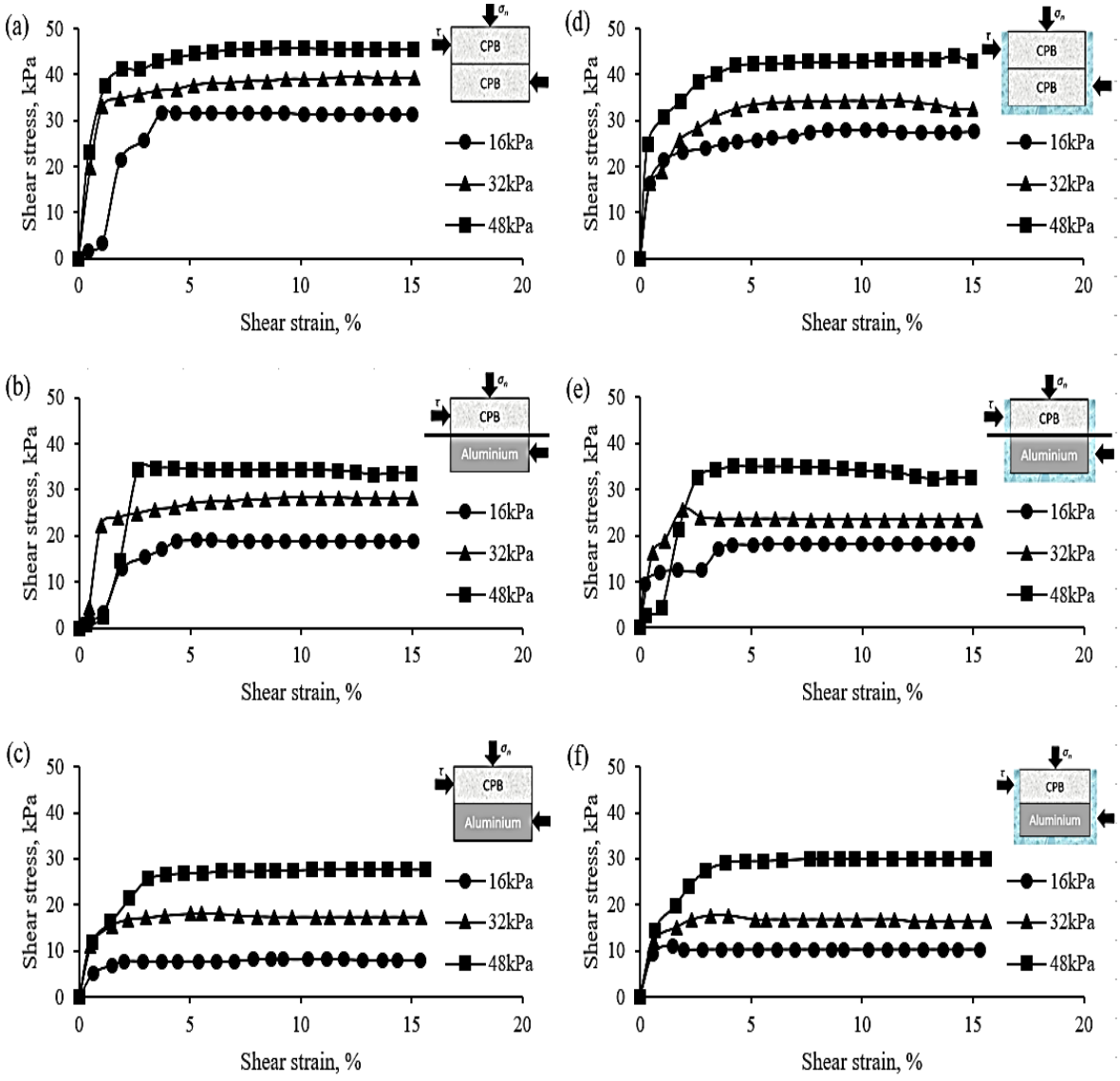

Figure 4.7: Shear stress-strain of CPB under different shearing condition (a) Dry CPB-CPB (b) Dry Cast in-situ CPB-A (c) Dry Precast CPB-A (d) Saturated CPB-CPB (e) Saturated Cast in-situ CPB-A (f) Saturated Precast CPB-A

was bonding in between cast in-situ CPB as the layer cannot be easily removed from the surface of aluminium. After the peak shear stress, the shear stress remained or slightly increased beyond 3% shear strain. For CPB-CPB shear, shear stress had reached its peak at around 1% shear strain then it remained or slightly increased for the rest of the shearing. The internal shearing of CPB possessed the highest shear strength regardless of the saturation condition, followed by cast in-situ CPB-A interface and precast CPB-A interface. The effect of saturation on shear strength was trivial as it slightly affects the friction angle and cohesion.

Figure 4.8 shows the Mohr-Coulomb envelope of UCPB and CPB under different shearing condition, and Table 4.3 shows the cohesion and friction angle obtained from Figure 4.8. These envelopes were produced by fitting a linear regression line for each dataset and all regression line was more than 0.967. Every shear failure envelope obeyed the Mohr-Coulomb failure criterion where the increase in shear stress was linear to the normal stress induced. Friction angle (φ) and cohesion (c) under our range of normal stress (σ_n) and shear stress (τ) recorded were obtained from Equation 4.3.

$$\tau = c + \sigma_n \tan(\varphi) \qquad \text{[Equation 4.3]}$$

It was expected that there should not had any cohesion for cases other than CPB-CPB and cast in-situ CPB-A. Cohesion obtained in the range of -2.7 kPa to 1.8 kPa were obtained as results of curve fitting. The hypothesis was made to explain these small deviations by understanding the shearing condition and the trend of the cohesion value. As mentioned before, saturated shearing condition had the tendency to create a paste-like block where a minor adhesive behaviour could be created in between the material itself and towards another surface. It was notable from the UCPB Mohr-Coulomb envelope that the minor cohesion created was higher when the specimen is saturated, and the adhesive was greater in between of the paste-like material itself rather than in between UCPB-A interface. Minor adhesion in saturated UCPB specimens was lower at saturated precast CPB as the particles of CPB had a greater tendency to be bonded and remained within CPB itself rather than creating a minor adhesive effect by sticking to the aluminium surface as UCPB did. A cohesion of 0.7 kPa was still observed because the surface of CPB was slightly dissolved due to saturation and hence some of the soften parts behaved like paste and thus creating a weaker adhesive behaviour compared to saturated UCPB.

The cohesion obtained from CPB-CPB shearing was greater than the adhesion obtained from the cast in-situ CPB-A interface shear by 110.2% for unsaturated condition and 104.3% for saturated condition. Aforementioned specimen at unsaturated condition generally had higher cohesion than saturated condition. The presence of water could promote minor adhesion to non-cohesive material but at the same time, it would also reduce the bonding strength of CPB and thus reducing the cohesion value.

The friction angle of the UCPB material was tested under different initial density. The internal friction angle of UCPB was in between 27.85 ° to 37.45 °, and interfacial friction angle of UCPB was in between 23.20 ° to 26.13 °. The highest friction angle for all cases of UCPB shearing was shown in Table 4.3. The friction angle of unsaturated UCPB was greater than saturated UCPB by 5%. Such reduction in friction angle was due to the lubrication effect of water and particles. The friction angle of UCPB-A interface was significantly lower due to the smooth surface of the aluminium platform.

The friction angle of precast CPB-A interface was higher than UCPB-A interface as the surface roughness of CPB was higher than UCPB. The friction angle of the specimens with cohesion was affected by the high initial shear stress due to cementation bond. Thus, less shear stress was gained from the variation of normal stress applied and friction angle of the material was reduced upon obeying the linear law of Mohr-Coulomb envelope. As the CPB was sheared under a saturated condition, the cohesion reduction of CPB shows higher friction angle.

Table 4.3: Specimen cohesion and friction angle under each shearing condition

Specimen	**UCPB**				**CPB**					
	Dry		Saturated		Dry			Saturated		
Shearing condition	UCPB-UCPB	UCPB-A	UCPB-UCPB	UCPB-A	CPB-CPB	Cast in-situ CPB-A	Precast CPB-A	CPB-CPB	Cast in-situ CPB-A	Precast CPB-A
Cohesion (kPa)	-2.7	-1.6	1.8	1.2	24.8	11.8	-1.7	19.2	9.4	0.7
Friction angle (°)	37.45	26.13	35.68	24.73	23.83	25.96	31.60	26.94	27.91	30.47

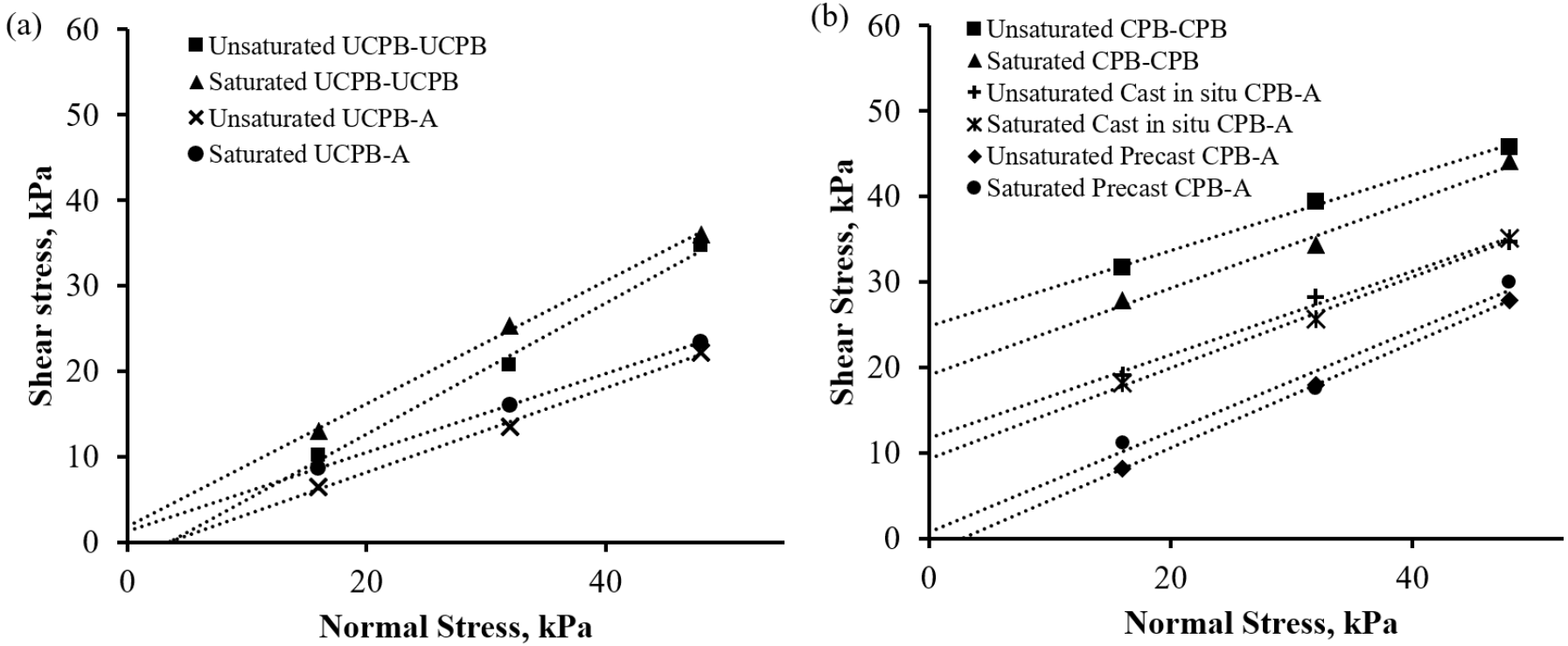

Figure 4.8: Mohr-Coulomb envelope of (a) UCPB and (b) CPB under different shearing condition

Nasir and Fall (2008) showed the interfacial friction angle and adhesion of cast in-situ CPB (dry, binder = 4.5%, w/c = 7.6 and cured at 3 days) and smooth limestone rock was found to be 24.78 ° and 27.06 kPa. The adhesion was higher than the results in the present study as the surface roughness of aluminium was smoother than the rock that was claimed to be smooth. Formation of minor gripping mechanism due to hardening of CPB was more significant at the rougher surface. As the bonding failed due to shearing, the surface of the aluminium and limestone (compressive strength of 27 MPa) was not likely to be damaged whereas CPB failed and formed a thin and evenly distributed layer of CPB on aluminium surfaces and (Nasir and Fall, 2008) rock surfaces. Thus, the shearing occurs between CPB and the thin layer of CPB on the surface of other material, so the interfacial friction angle was similar.

Koupouli et al. (2016) showed the interfacial friction angle and adhesion between precast CPB and smooth granite rock were 38 ° and 8 kPa respectively. The rather soft behaviour of CPB (4.5% binder and 3 days of curing) would deform at 100 kPa applied pressure and above (Yilmaz et al., 2008). Koupouli et al. (2016) applied up to 200 kPa of normal stress on CPB sample which had the tendency to cause deformation and took the shape of the surface roughness of the granite used. Thus, some shear strength required to break the bonding formed due to deformation of CPB. The surface of aluminium was smoother than granite, so the resulting interfacial friction angle is lower.

This study explains the shear stress-strain behaviour of the internal and interfacial friction of the backfill system. UCPB or fully saturated silica flour was nearly cohesionless and adhesionless under fully saturated condition, but CPB possessed a cohesion of 19.2 kN/m^2 and adhesion of 9.4 kN/m^2. Saturated UCPB and CPB possessed an internal friction angle of 35.7 ° and 26.9 ° and interfacial friction angle of 24.7 ° and 27.9 °. The values of

shear strength, cohesion, and friction angle and some comparisons were reported. A thorough analysis was made on each dataset obtained then the following conclusion could be drawn:

i. The shear failure envelopes of both internal and interfacial tests fit the Mohr-Coulomb failure criterion.
ii. The presence of water could alter the final shear strength depending on initial material condition.
iii. The interfacial friction angle of CPB-A was higher than the shear strength of CPB-CPB shearing by a factor of 1.06.
iv. The interfacial friction angle of UCPB-A was lower than the shear strength of UCPB-UCPB shearing by a factor of 0.69.
v. The interface shear behaviour for both cast in-situ and precast CPB-A were comparable with the previous finding on interface shear behaviour of cast in-situ and precast CPB-rock.

Data that were presented in this study would be useful for the understanding of stress distribution of CPB in simulating the CPB-rock wall behaviour in actual stopes.

4.3.4 Effect of Temperature on the Shear Behaviour of Backfill

As the deposition test was conducted at different temperatures, the shear behaviour of the backfill material at the range of the imposed temperature had to be determined. UCPB and CPB were tested according to Table 3.3 where changes in shearing temperature were implemented as Figure 3.18.

The results were presented in terms of stress-strain behaviours and Mohr-Coulomb envelopes that determined apparent cohesion and friction angle. Generally, stress increased as the strain increased until peak stress was reached after which the stress became constant.

Peak stresses were mostly shown for CPB samples, where the stress slightly diminished and became constant at residual. At higher temperature, the expansion of UCPB and CPB were evident from the vertical displacement dial gauge measurement as shown in Figure 4.9. The stress-strain curves for UCPB and CPB are shown in Figure 4.10 and Figure 4.11.

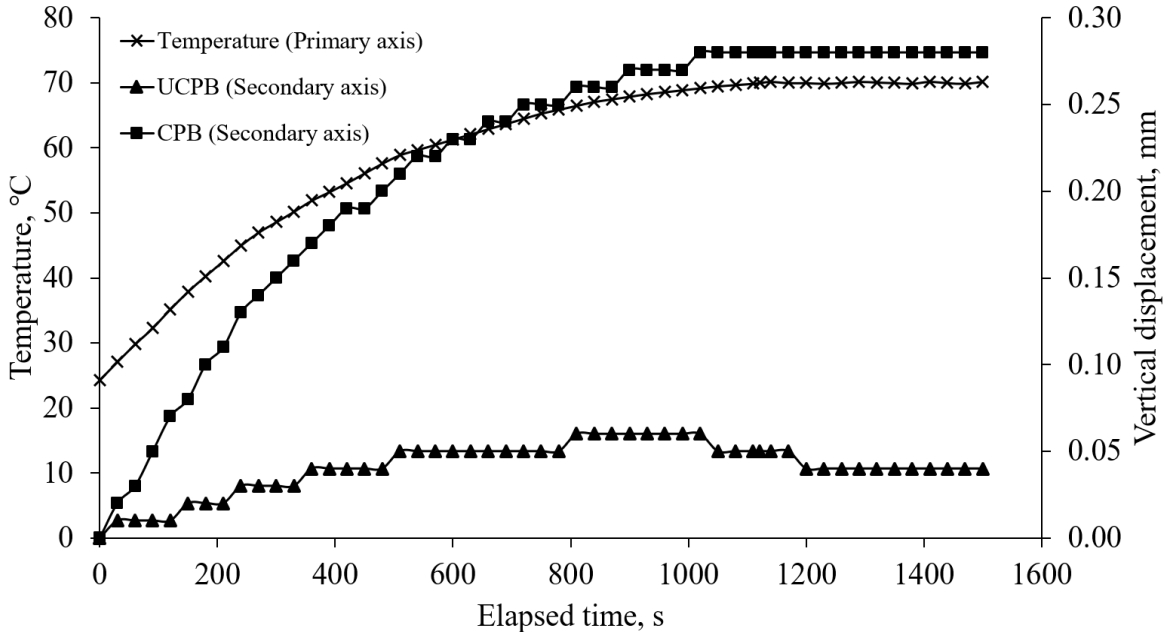

Figure 4.9: The change in vertical deformation with respect to temperature

Figure 4.10a to Figure 4.10c show the internal stress-strain behaviour of the UCPB while Figure 4.10d to Figure 4.10f show the interfacial stress-strain behaviour between UCPB and aluminium plate at varied temperature. The initial density of the UCPB samples was 1750 kg/m^3. In average, the peak stress of interfacial UCPB was lower than peak stress of internal UCPB by an average of 32.25%.

Upon reaching the desired temperature, non-cohesive material such as UCPB was able to reconsolidate to balance out the change in volume caused by thermal expansion. After reconsolidation, the net stress within the sample would be lower and caused the material to behave slightly like over-consolidated sample. Therefore, small differences in peak-residual strength were observed at 50 ℃ and 70 ℃. Figure 4.10 shows that the stress for internal

shearing was more significant than the stress for interfacial shearing. For internal UCPB, there was a total gain of stress by 16.36% from 25 ℃ to 50 ℃ and by 10.40% from 50 ℃ to 70 ℃ which equivalent to an average gain of 0.156 kPa/℃. As for the interfacial shearing, there was a total gain of stress by 18.52% from 25 ℃ to 50 ℃ and by 11.38% from 50 ℃ to 70 ℃ which equivalent to an average gain of 0.098 kPa/℃.

Figure 4.11a to Figure 4.11c show the internal shear stress-strain behaviour of CPB at different temperature whereas Figure 4.11d to Figure 4.11i show the interfacial shear stress-strain behaviour of CPB and aluminium plate using different casting method namely cast in-situ and precast sample preparation. The peak stress was observed at region less than 3% shear strain for both internal and interfacial shearing. It was observed during the experiment that there was obvious cement bonding seen in between cast in-situ CPB and the surface of the aluminium. The interfacial shear stress of cast in-situ interfacial CPB was lower than the internal shear stress by an average of 36.26%. During post interfacial shear test, the sample was inspected and found that every sample had nearly perfect failure occurring exactly on the shearing plane although some small irregularities were observed.

After the peak stress was reached, the stress remained or reduced to the residual state after 3% shear strain. internal CPB possessed the highest shear strength then followed by cast in-situ interfacial CPB and precast interfacial CPB.

For internal CPB, there was a total gain of stress by 36.96% from 25 ℃ to 50 ℃ and by 27.26% from 50 ℃ to 70 ℃, with an average gain of 0.583 kPa/℃. As for interfacial CPB, there was a total gain of stress by 17.38% from 25 ℃ to 50 ℃ and by 11.40% from 50 ℃ to 70 ℃, with an average gain of 0.176 kPa/℃.

Figure 4.11g to Figure 4.11i show similar stress-strain behaviour as Figure 4.11d to Figure 4.11f but possessed higher stress with an average of 12.46%. Similar behaviour was

probably due to the similar contact (i.e. non-cohesive) in between sample and aluminium but different in stress value that was because of the greater surface roughness of CPB compared to UCPB.

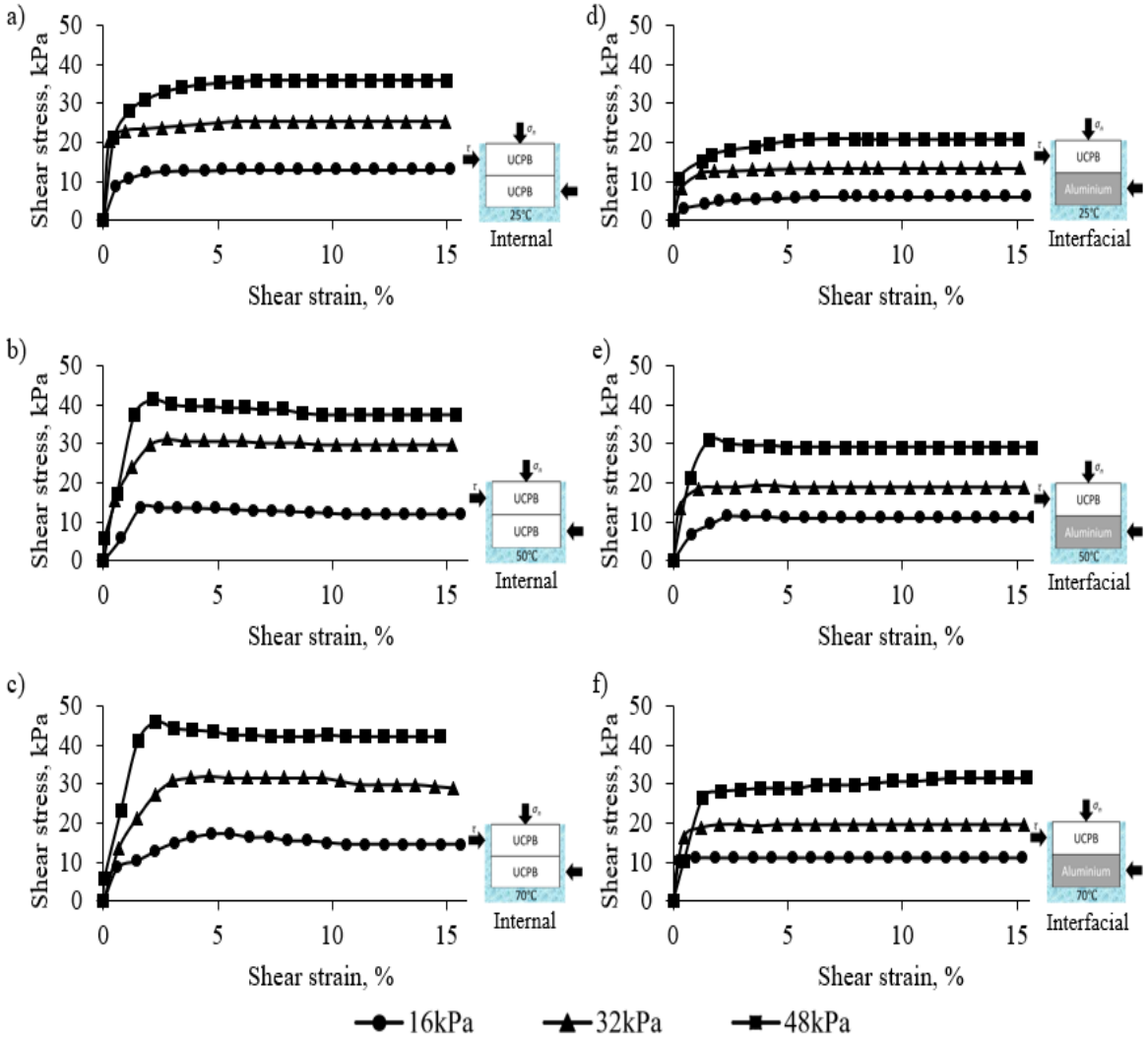

Figure 4.10: Shear stress-strain of UCPB under different shearing condition (a) Internal UCPB at 25 ℃ (b) Internal UCPB at 50 ℃ (c) Internal UCPB at 70 ℃ (d) Interfacial UCPB at 25 ℃ (e) Interfacial UCPB at 50 ℃ (f) Interfacial UCPB at 70 ℃

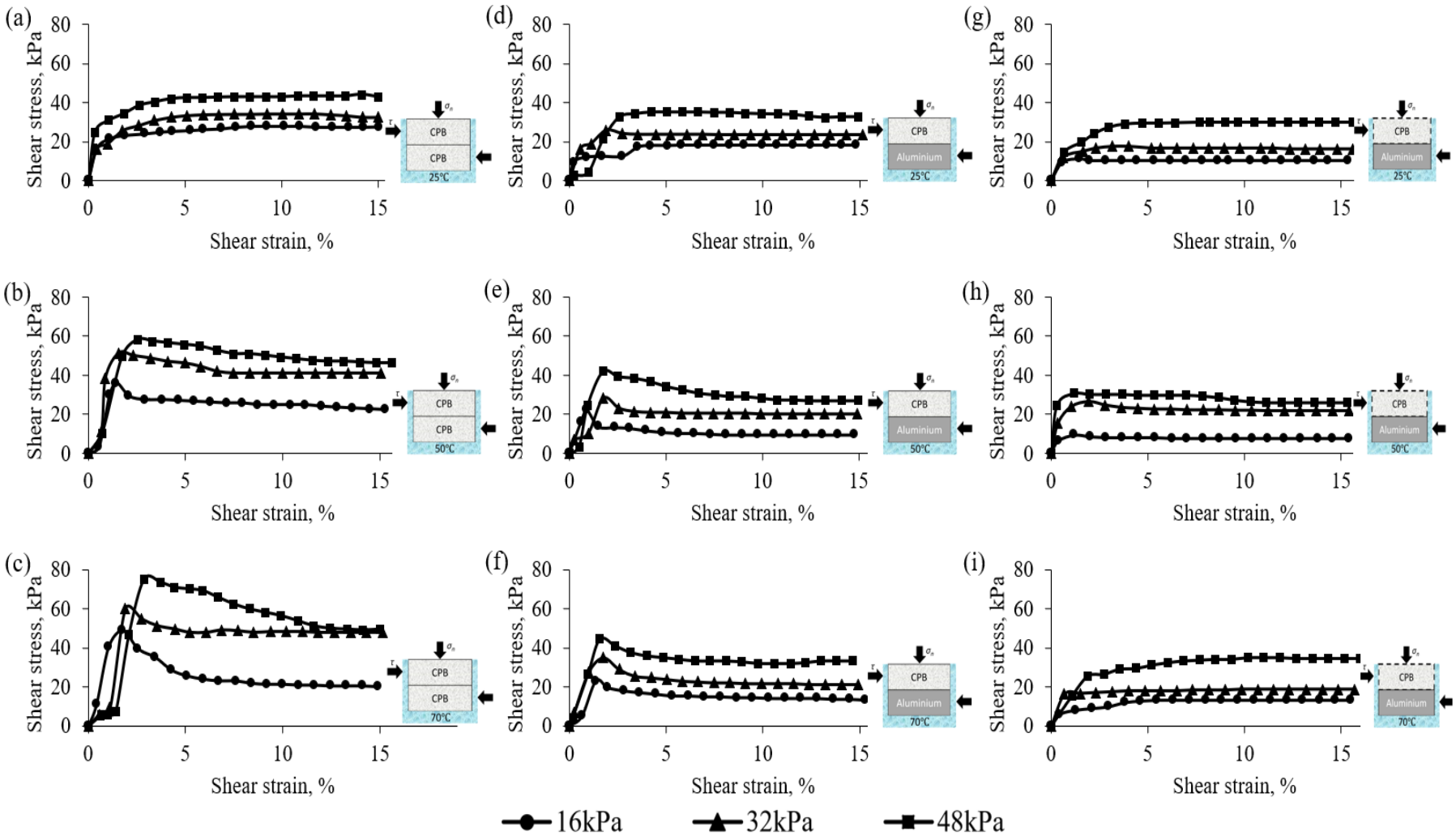

Figure 4.11: Shear stress-strain of CPB under different shearing condition. (a) Internal CPB at 25 ℃ (b) Internal CPB at 50 ℃ (c) Internal CPB at 70 ℃ (d) Cast in-situ interfacial CPB at 25 ℃ (e) Cast in-situ interfacial CPB at 50 ℃ (f) Cast in-situ interfacial CPB at 70 ℃ (g) Precast interfacial CPB at 25 ℃ (h) Precast interfacial CPB at 50 ℃ (i) Precast interfacial CPB at 70 ℃

Overall, CPB samples possessed higher stress than UCPB samples at higher temperature. Internal CPB showed stress with an average of 85.95% higher than internal UCPB whereas same increment applied for interfacial CPB by an average of 69.25% as compared to interfacial UCPB. The effect of temperature on internal CPB and cast in-situ interfacial CPB tests showed higher shear strength increment whereas only showing slight inconsistent increment on internal UCPB, interfacial UCPB, and precast interfacial CPB tests. The peak-residual stress was more significant for CPB in comparison to UCPB as CPB is cementitious material.

Figure 4.12 shows the Mohr-Coulomb envelope of UCPB and CPB under different shearing condition, and Table 4.4 lists values of the apparent cohesion and friction angle obtained from Figure 4.12. These envelopes were produced by fitting a linear regression line for each dataset. Every shear failure envelope obeyed the Mohr-Coulomb failure criterion where the increase in stress was linear to the normal stress induced.

It was expected that the apparent cohesion was negligible (or zero) for cases other than internal CPB and cast in-situ interfacial CPB. Minor apparent cohesion in the range of 0.3 to 2.7 kPa was obtained as results from curve fitting. It was noticeable from the UCPB Mohr-Coulomb envelope that the minor apparent cohesion created was higher in internal UCPB shearing compared to interface UCPB. Precast CPB at 3 days was found to be dissolved slightly by the water during saturation. The dislodgement of CPB particles caused the surface of CPB to be slightly adhesive. Therefore, an apparent cohesion value of less than 1 kPa was observed. The apparent cohesion obtained from internal CPB shearing was greater than cast in-situ interface CPB by 104.6% at 25 °C, 135.7% at 50 °C and 171.1% at 70 °C. Figure 4.13 shows that higher temperature had a positive effect on the apparent cohesion value of cast in-situ interfacial CPB sample and greater influence on internal CPB

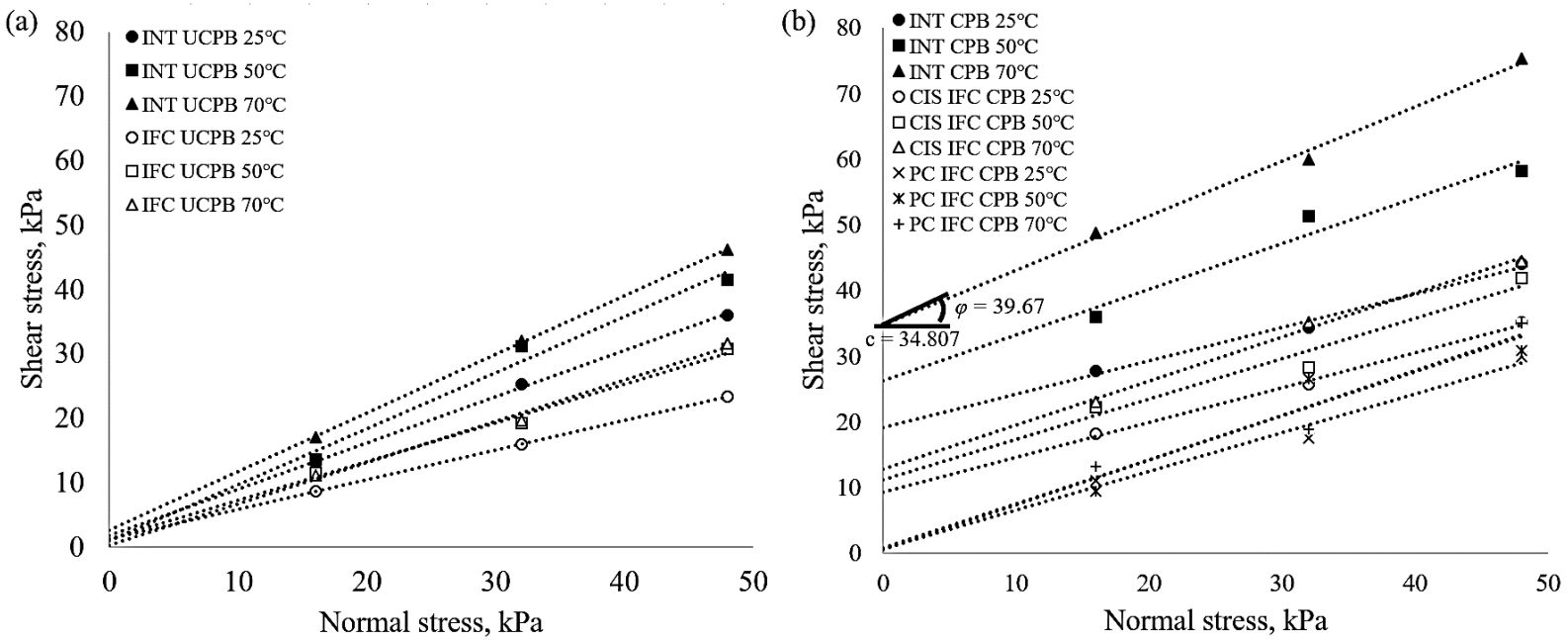

Figure 4.12: Mohr-Coulomb envelope on (a) peak stress of UCPB, (b) residual stress of UCPB, (c) peak stress of CPB and (d) residual stress of CPB at different shearing condition

Table 4.4: Apparent cohesion and friction angle under each shearing condition

Material	**UCPB**						**CPB**								
Shearing condition	**Internal**			**Interfacial**			**Internal**			**Cast in-situ Interfacial**			**Precast Interfacial**		
Temperature, °C	25	50	70	25	50	70	25	50	70	25	50	70	25	50	70
Peak friction angle, °	35.7	41.0	42.3	24.7	31.0	32.7	26.9	34.8	39.7	27.9	31.6	33.7	30.5	33.8	34.3
Residual friction angle, °	35.7	38.7	41.0	24.5	29.3	32.7	25.7	36.3	42.3	23.9	28.7	30.5	31.6	29.9	33.8
Peak cohesion, kPa	1.8	1.0	2.7	1.2	1.3	0.3	19.2	26.2	34.8	9.4	11.1	12.8	0.7	0.9	0.6
Residual cohesion, kPa	1.8	0.9	0.9	-1.2	1.7	0.3	18.8	13.1	10.0	10.4	1.3	3.4	-0.9	0.1	0.9

sample. The effect of temperature on the apparent cohesion value of the remaining sample was assumed to be negligible. For internal CPB, there was a total gain of apparent cohesion by 37.06% from 25 to 50 °C and by 32.61% from 50 to 70 °C, with an average gain of 0.356 kPa/°C. For interfacial CPB, there was a total gain of stress by 18.99% from 25 to 50 °C and by 15.29% from 50 to 70 °C, with an average gain of 0.078 kPa/°C.

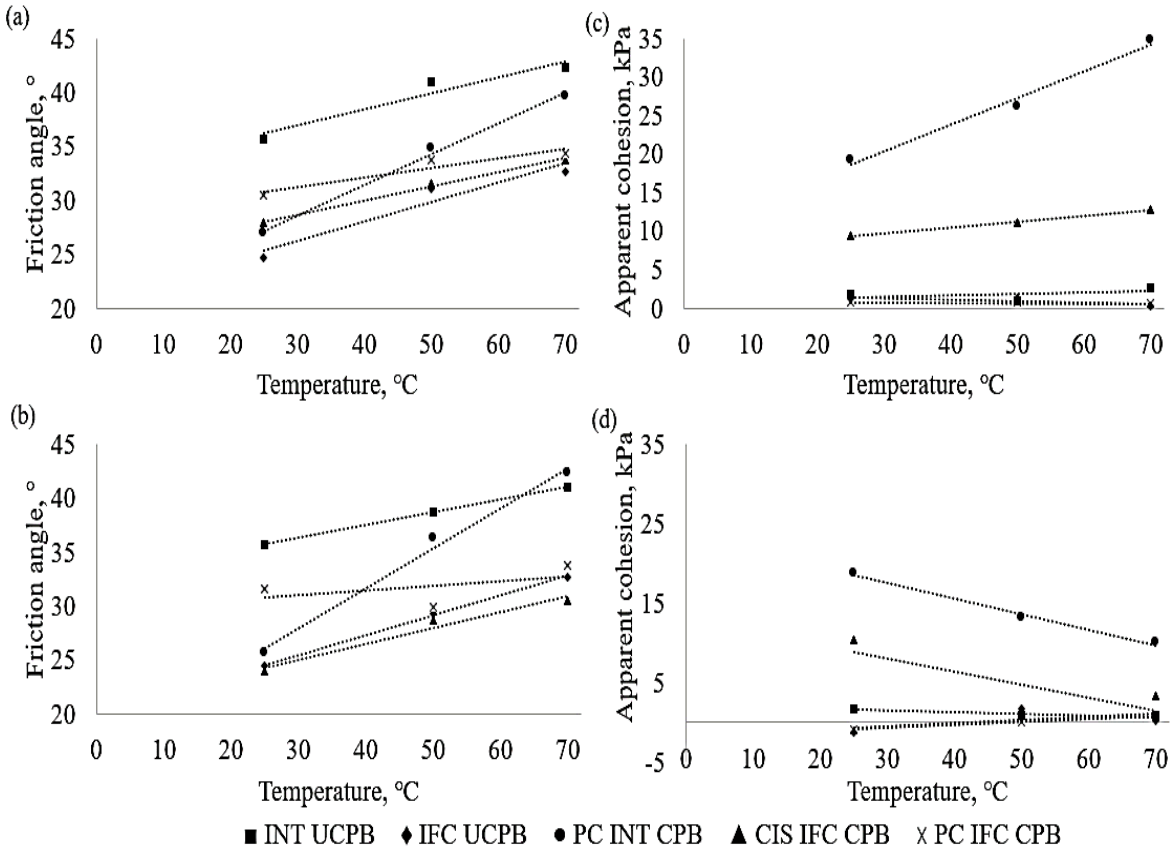

Figure 4.13: Effects of temperature on (a) peak friction angle, (b) residual friction angle, (c) peak apparent cohesion and (d) residual apparent cohesion

The friction angle generally increases with the increase of shearing temperature, but the increment of friction angle varies according to material and shearing condition. The friction angle of internal UCPB was significantly lower by an average of 25.64% due to the smooth surface of the aluminium platform in comparison to the friction angle of internal CPB. The friction angle of precast interfacial CPB was higher than interfacial UCPB by an

average of 11.38% as the surface roughness of CPB was higher than UCPB. Although internal CPB acquired the greatest gain in friction angle at higher temperature (0.23 °/°C), UCPB or non-cohesive sample generally possessed greater friction angle although the gain (0.07 to 0.14 °/°C) due to temperature was less significant as shown in Figure 4.13. Cohesive material (i.e. internal CPB and cast in-situ interfacial CPB) possessed lower frictional angle because of the higher initial stress was needed to overcome cementation bond. Thus, less stress gain was shown from the variation of normal stress applied and reduces the friction angle of the material upon obeying the linear law of Mohr-Coulomb envelope. Based on Figure 4.14, the effect of change in temperature on the change of friction angle and apparent cohesion could be clearly seen.

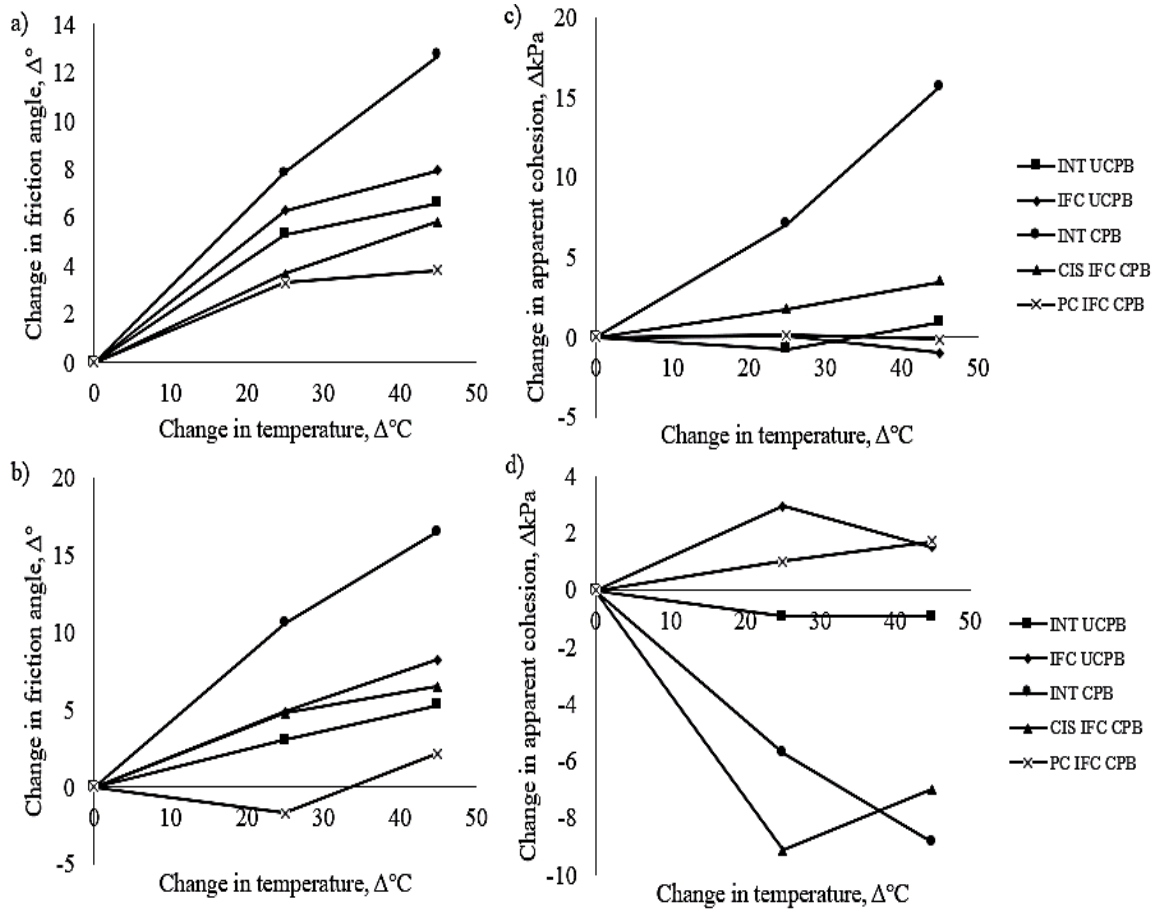

Figure 4.14: Effect of change in temperature on the change of (a) peak friction angle, (b) residual friction angle, (c) peak apparent cohesion, and (d) residual apparent cohesion

Some of the findings on thermal shearing using different material, shearing plane, and temperature range were used to be compared with the findings from this study (Figure 4.15). Different types of sand and clay had been used to investigate the effect of temperature on its shear behaviour, but none had performed such testing on CPB. The clay was slightly affected by the change in temperature, but its effect on the friction angle change was inconsistent as reported by Hueckel and Baldi (1989, 1990), Burghignoli et al. (2000), Cekerevac (2003), and Yavari et al. (2016). The effect of temperature on interfacial shearing was discussed by Karademir (2011) by varying the surface with High-density polyethene (HDPE) and Polyvinyl Chloride (PVC) with Blast sand and Ottawa sand. The findings showed a clear increment of friction angle with the increase in shearing temperature for every variation. Such findings as discussed above were comparable to internal UCPB and interfacial UCPB. The interfacial friction angle at the backfill-aluminium was lower than the internal friction angle of the backfill itself with an average factor of 0.69 at room temperature in comparison to 0.67 which was commonly used.

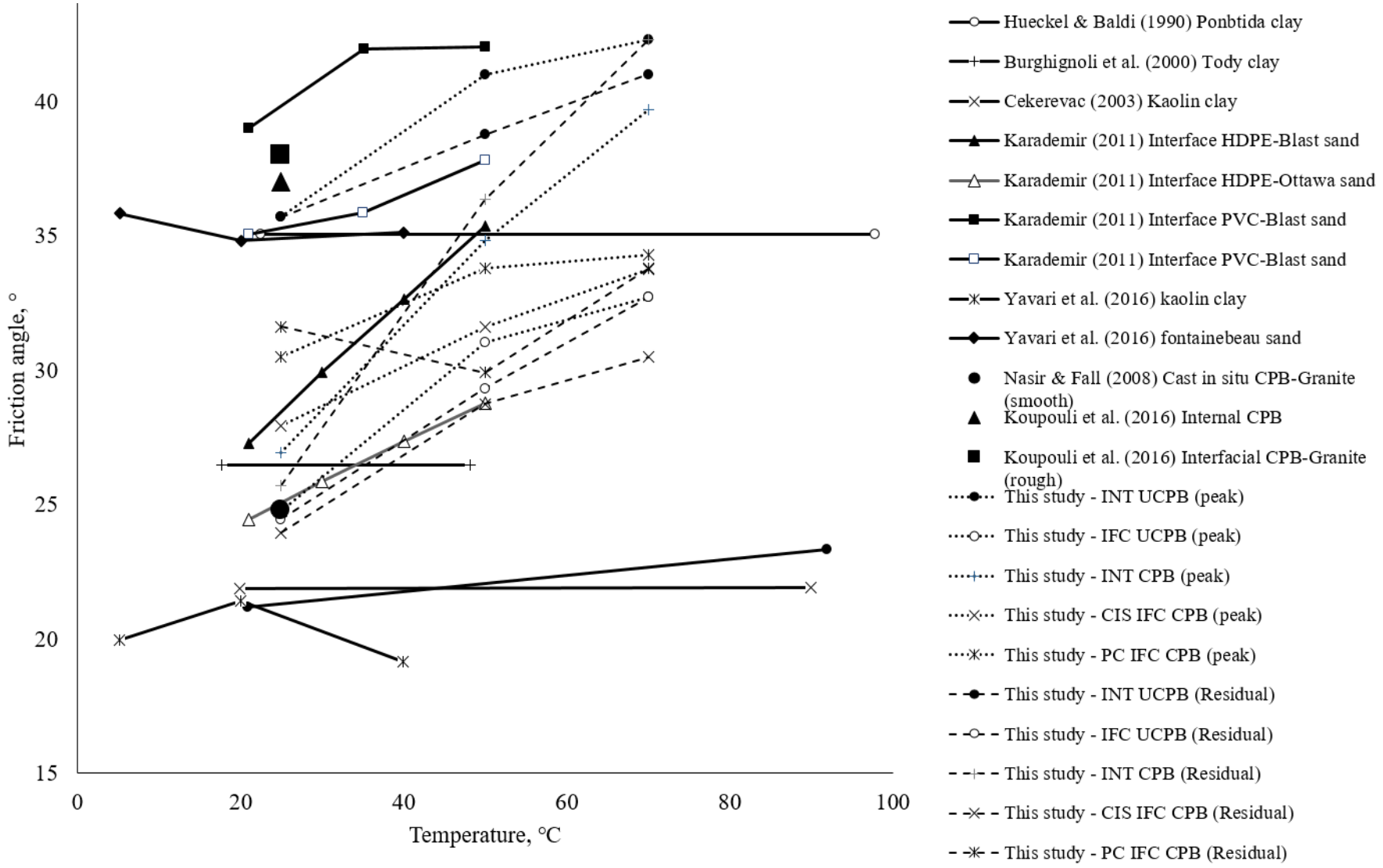

Figure 4.15: Summary of findings from stated researchers on different material, shearing plane, and temperature range

This study presents the shear behaviour of internal and interfacial friction between UCPB and CPB at the temperature of 25 ℃, 50 ℃ and 70 ℃. Comparisons between these findings and related published data were reported. A thorough analysis was made on each dataset obtained then the following conclusions could be drawn:

i. The shear failure envelopes both internal and interfacial tests at all temperature fit Mohr-Coulomb failure criterion.

ii. The internal and interfacial shear strength parameters of CPB, i.e. apparent cohesion (c) and friction angle (ϕ) value increased with the increase in temperature. Its behaviour at room temperature was comparable to the previous finding.

iii. The interfacial shear parameters for both cast in-situ and precast interfacial CPB-A were comparable with the previous finding on the interfacial shear behaviour of cast in-situ and precast CPB-rock (assumed to be at room temperature of 25 ℃).

This study shows the significance of accurate design parameters such as shear strength, apparent cohesion, and friction angle at different temperature for realistic and safer stress distribution estimation on mine backfill design.

CHAPTER 5

STRESS-STRAIN-TEMPERATURE BEHAVIOUR UPON DEPOSITION TEST

5.1 General

This chapter discusses the experimental findings of deposition test based on the proposed experimental framework from Table 3.5. Every calibration and preliminary tests were performed appropriately to ensure that there are no discrepancies occurred from the accuracy of the equipment and the design. The implementation of temperature change for the deposition test was performed according to the test plan. The execution of variation for the deposition test relies on the real-time monitoring of the behaviour of the deposited material which showed that it is not performed according to time.

5.2 Narrow Wall Calibration

As the NW model is completed and ready to be used, the ability of the NW model to capture the behaviour of the deposition for both CPB or UCPB were clarified through preliminary functionality check and actual deposition check. Calibration was performed on the instruments to ensure that it is accurate and consistent after multiple usages over time. The instruments were supplied with a manufacturer calibration. The instruments were recalibrated with the suggested method of calibration in Section 3.7.1 to ensure that the instrument could provide the most accurate data for the proposed experiment. The findings on the calibration were presented accordingly.

5.2.1 Load Cell

The load cell was calibrated by tightening it to a sturdy platform that shall not be deformed under our range of loading. A known weight of 1 kg (with a deviation of 0.005 kg) was placed on the load cell. The placement of weight must be stable to avoid the risk of

having collapsed weight due to instability. An illustration of the calibration of the load cell is shown in Figure 5.1.

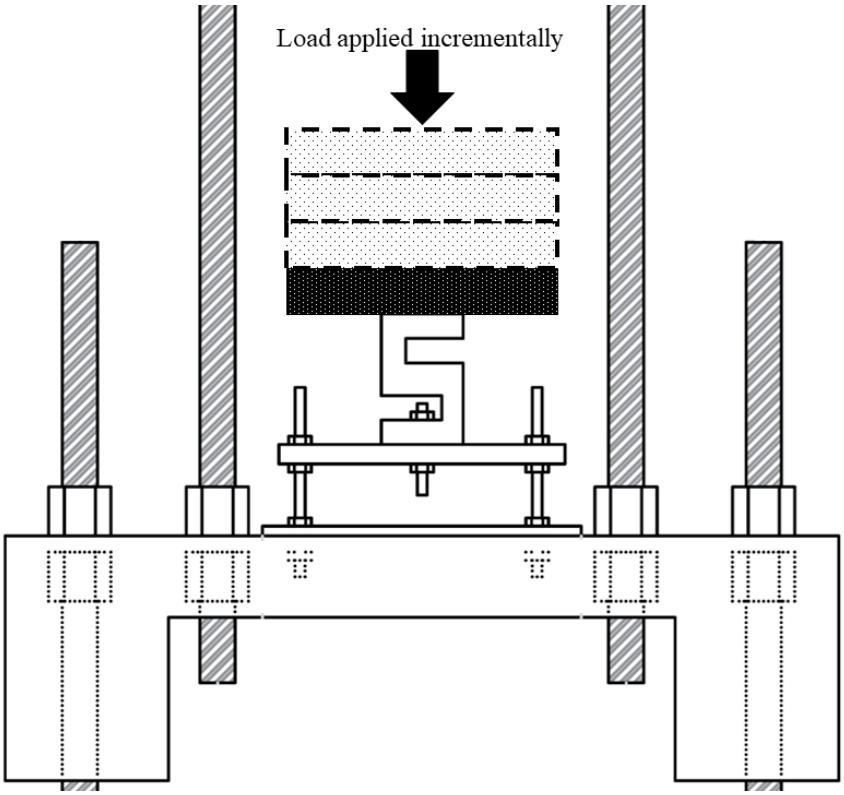

Figure 5.1: Illustration of load cell calibration

At 0 kg load (i.e. no load applied on the load cell), the load cell value was set to its origin (zero) before applying the next load. The load cell detected the differences by loading when the loading caused the strain gauge in the load cell to deflect and showed changes in values of resistance. With the supplied voltage from the data acquisition, the change in resistance was increased or decreased the receiving voltage from the load cell. The values of the voltage at different loading was recorded, and a calibration curve was plotted from it. A calibration curve showing the linear relationship between voltage and load applied in the range of 0-25 kg is shown in Figure 5.2. A function shown in Figure 5.2 was obtained from the calibration curve and to be used for the conversion of voltage to load and to stress for the actual deposition test.

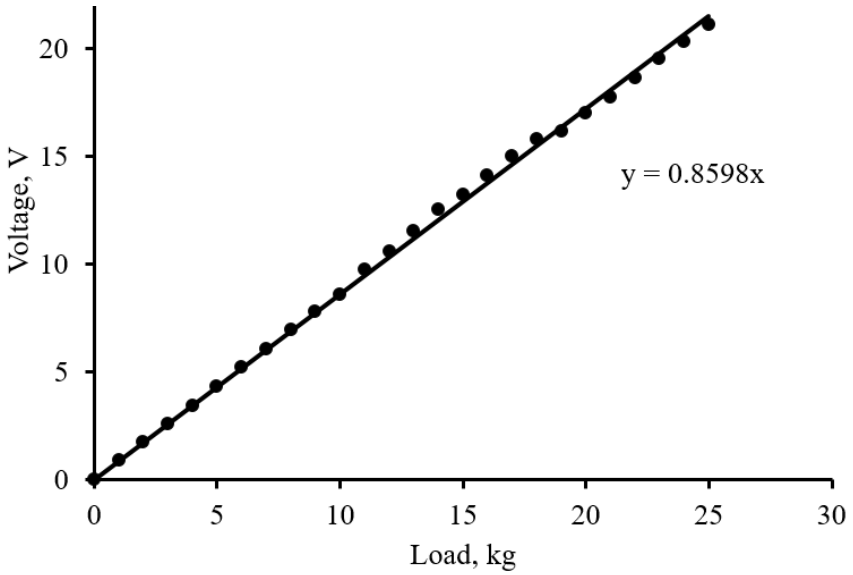

Figure 5.2: Calibration curve of the load cell

5.2.2 Potentiometer

The linear potentiometer was calibrated by attaching the housing to one end of the Vernier calliper external jaw and the extension probe to another end of the external jaw. The connecting adhesive used must be firm and removable. The setting up of the potentiometer and Vernier calliper is shown in Figure 5.3. The potentiometer and the Vernier calliper must be set to zero before the calibration commences. The responding voltage from the potentiometer to the data acquisition unit will vary according to the displacement of the probe which will alter the resistivity within the housing of the potentiometer. Thus, the responding voltage was calibrated with a known displacement (i.e. the displacement of the Vernier calliper in mm), and a calibration curve was obtained and is shown in Figure 5.4. The equation shown in Figure 5.4 was used for the conversion of voltage recorded by the potentiometer to displacement or vertical deformation of the deposition test sample. The calibration was conducted for the whole designed extrusion length of the potentiometer, and it was found that the relationship between voltage and displacement is linear which showed that the instrument is in good working condition.

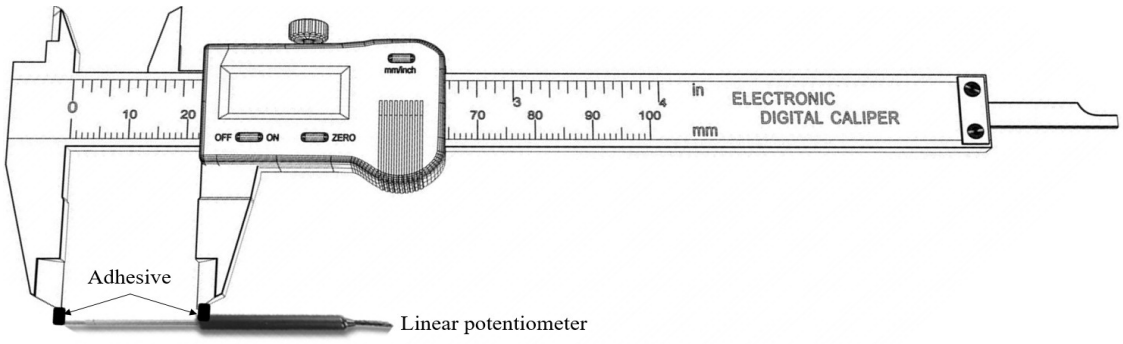

Figure 5.3: Illustration of potentiometer calibration

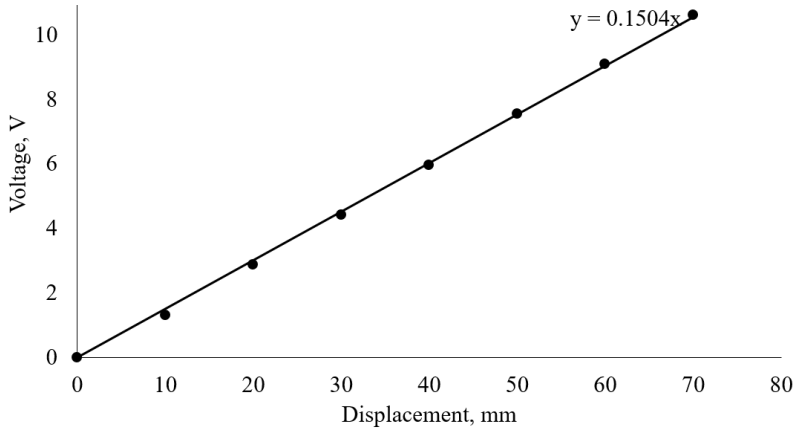

Figure 5.4: Calibration curve of potentiometer

5.3 Preliminary Test

Preliminary tests were conducted to ensure that the design of the setup is capable of collecting the desired data accurately. The preliminary test results were shown and discussed in the following subsection.

5.3.1 Stress-Strain Generation during Temperature Change

The vertical support was properly tightened for every test as the placement of a total of 25 kg weight on top of the NW did not show any stress transfer to the load cell. This was clarified by monitoring the reading of the load cell while placing the load on top of the NW. After the vertical support check, the setup was heated to the maximum temperature which iss 60 °C according to the test plan. The temperature of the NW, stress reading of the load cell and the expansion of the aluminium wall were recorded and shown in Figure 5.5.

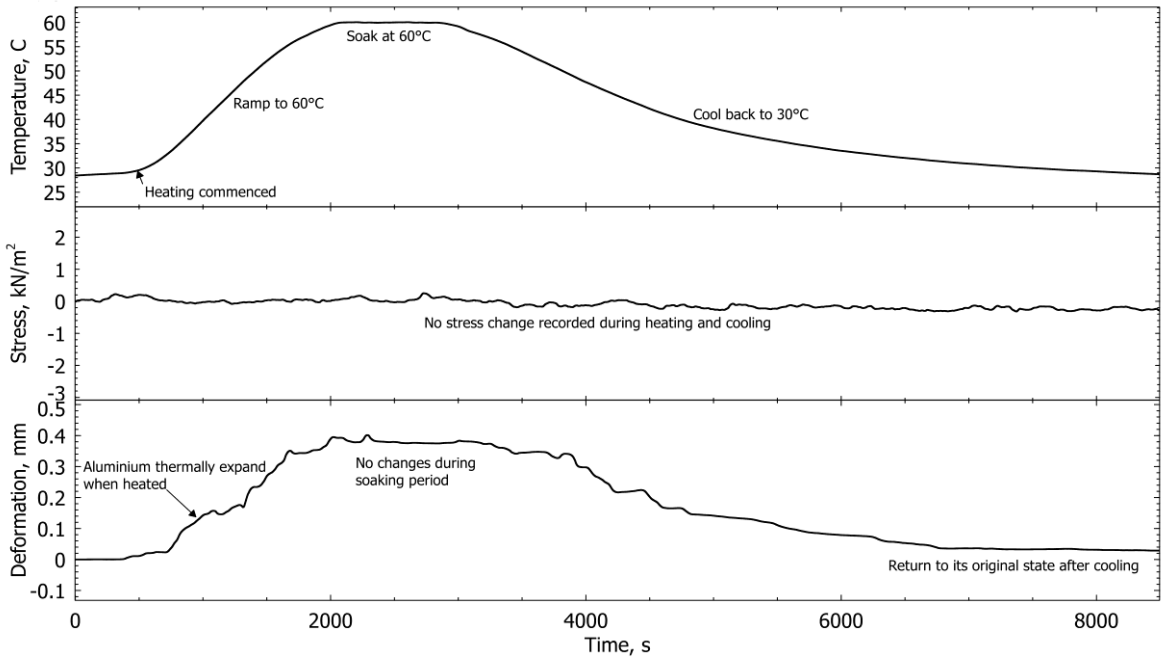

Figure 5.5: Resulting data from expansion check upon thermally altered

As the temperature increases, there were no changes in the load cell reading which proves that the expansion gap was functioning properly whereas the LDVT proves that the NW was expanding with a maximum displacement of 0.4mm for a 30 °C change in temperature. As the span of the upper open-ended of the NW is the same as the lower portion, 0.4 mm linear expansion is within the range of the expansion gap which is about 10 mm. During the cooling phase, there were still no changes observed from the load cell, and the NW could return to its original state based on the deformation recorded by the potentiometer.

5.3.2 Restraining Capability of Latex Sheet

The setup was originally designed to be sealed with silicone sealant, but the restraining capability of silicone sealant was too great which resulted in a great reduction of stress recorded by the load cell. As the expansion gap is required to prevent stress generation caused by the thermal expansion of the bottom open-ended of the NW, latex sheet was proposed as it is flexible, impermeable, and durable. For every new testing (i.e. the reconstruction of expansion gap), the expansion gap was tested by filling the NW up with

water. Water was used considering there is no arching effect when the water is in a static condition. One of the load cell reading of the preliminary test on the restraining capability of latex sheet is shown in Figure 5.6.

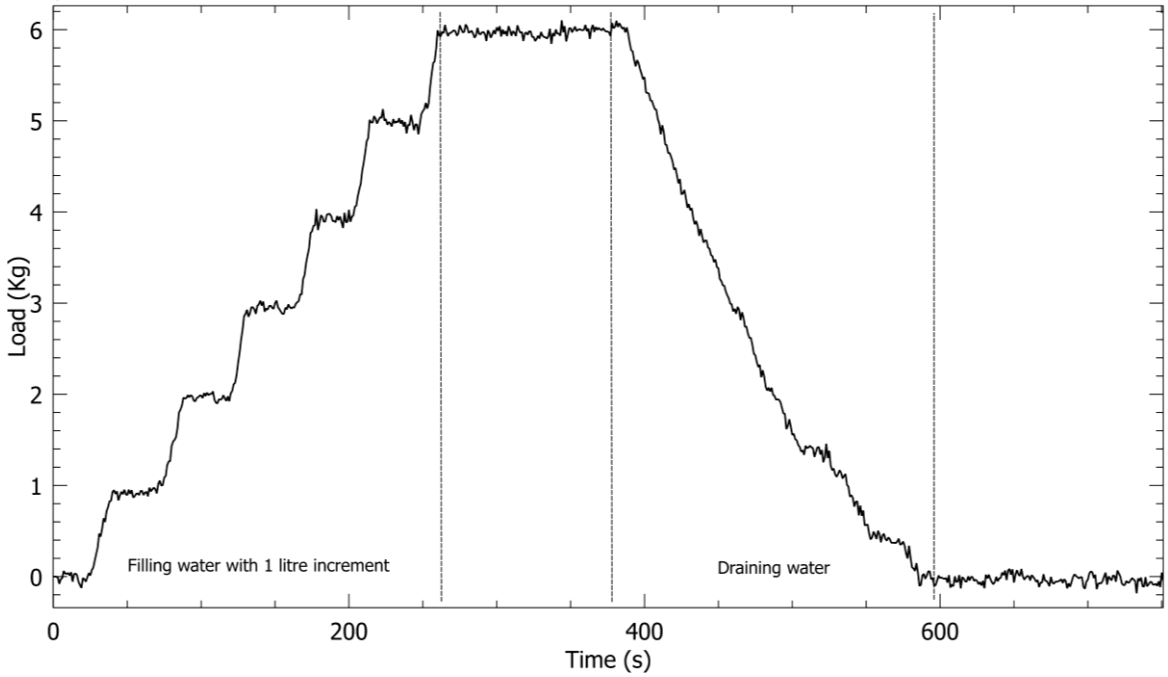

Figure 5.6: Stress generation from the filling and draining of water

The same checking had been done on other sealing method (i.e. silicone sealant), and resulting offset was around 2-3 kg which was too much (20% form total expected weight) considering the deposition mass was only around 12 to 15 kg depending on the density of the backfilling material. From this method of sealing, around 0.05 kg was used in overcoming the elasticity of the latex sheet. For the rest of the increment, it showed an accurate gain in total weight recorded which was 1 kg for every 1 litre of water filled which sums up to a total of 5.95kg. The sealing method only requires 0.3% offset based on the expected total weight of the backfill material. Thus, the offset value obtained from every preliminary test conducted on the restraining capability of the latex sheet was considered.

5.4 Deposition Test

The deposition test was conducted with the NW setup and the prepared sample. With the availability of materials, the mix design of UCPB and CPB had been determined with the rheology test (yield stress and slump height) and unconfined compressive strength test. Upon completion of the calibration and preliminary test, the deposition test was conducted according to the test plan shown in Table 3.5 according to the suggested procedure shown in Appendix F. In a total of 12 attempts, deposition test was conducted to investigate the effects of temperature and temperature change on the stress-strain behaviour of backfill. For further insight, approximately 15 working days were required to complete each deposition test. Usually, it required 5 working days for setting up, calibration and preliminary tests, 3 working days for dismantling and cleaning prior next usage, and 3 to 7 days (including the weekend) to monitor and control the test. The testing was monitored and controlled through the computer using the software of data acquisition unit and temperature controller. Remote access allowed the testing to be observed and adjusted from time to time. The value of stress was generated based on the downward force generated by the filling over the area of the bottom plate which was 0.0075 m^2. The force was assumed to be equally distributed at the surface of the bottom plate. The volumetric change of the filling was measured in linear height and it was assumed that the deformation was the same across the opening of the NW.

5.4.1 Varying the Temperature

The stress-strain behaviour of both UCPB and CPB within NW under temperature alteration were discussed. Such heating pattern was introduced to provide more understanding on the behaviour of backfill material that may be subjected to frequent change in temperature of the mine. Unlike in the actual mine, the temperature change was only induced after the consolidation of the backfill material via referencing to the stress-strain

change over time. This was performed to rule out the stress altering mechanism that was caused by consolidation to allow a better understanding of temperature change effect alone on stress change. The backfill material was investigated by multiple steps ramp and one-time ramp. Section 5.4.1.1 and Section 5.4.1.2 show the effects of temperature variation and filling material that were investigated through the proposed model and discussed with respect to stress behaviour and volumetric deformation.

5.4.1.1 Uncemented Paste Backfill

Figure 5.7 shows the monitoring of stress-strain temperature behaviour of UCPB against the elapsed time from the initiation of deposition until 84 hours after. Before the deposition, the data acquisition was started to ensure that no stress was recorded, LVDT was offset, and to allow preheating monitoring. As the fill material was mixed at room temperature, the system was preheated to a higher temperature depending on the initially targeted temperature upon filling by considering the net temperature transfer. For this case, it was preheated to 34 °C and cooled back to 30 °C after deposition. The deposition was left for a complete consolidation under a controlled temperature of 30 °C. Reduction of the volume was observed as the material consolidate. The rearrangement of the particle during consolidation caused the friction at the side walls to be mobilised that contribute to a phenomenon namely arching. Arching reduces vertical stress by transferring it horizontally to the side wall and towards the platform through the vertical support rod. A steep reduction from 15 kN/m^2 to an equalised value of 7.5 kN/m^2 showed a total reduction of 50% from the original stress value. This phenomenon was also observed in full-scale monitoring (Thompson et al., 2009, 2012; Hasan et al., 2014; Doherty et al., 2015). Such changes were made to control the ramping behaviour because coupled phenomenon from the consolidation and expansion of particles might cause complication in the analysis.

To further studies the effects of temperature, the system was ramped (heated) and soak (maintained) to three level of ramp and soak steps. The temperature was ramped up to 40 °C and maintained until the consolidation reached T_{90} based on the values of load cell prior to the next ramped up steps to 50 °C and 60 °C. Volumetric change complies with the change in temperature where the material expanded during heating and maintained when the temperature was kept constant. The trend was rather irregular that may be due to rearrangement (relaxation) of particles while trying to expand. This phenomenon was not observed when CPB was used as the filling material. The stress increased when the temperature increased, but the reduction of stress occurred when the temperature was maintained. During the heating, particles will expand and while bring restrained by arching thus generating addition stress. As the temperature was maintained and the expansion stops, where the particles were allowed to relax from thermal stress slowly and thus reducing the stress generated. Thermal stress and relaxation mechanism are discussed in Section 5.5.3.

During the cooling phase, the stress reduced due to the instant cooling and caused the material to shrink rapidly. During reconsolidation at high temperature, the initial peak stress was altered due to particle rearrangement (relaxation) and results in lower net stress. With lower net stress but with the same reduction in temperature for the same material resulted in lower final net stress compared to initial stress at the same temperature.

Figure 5.8 shows a replicate testing of UCPB 1 namely UCPB 2. The material was prepared with the same mix design and procedure. The mix was backfilled with a similar rate of backfilling into the narrow up to the same total height. Similarly, the sample was left to consolidate at a constant temperature of 30 °C until the stress-strain behaviour stabilised. UCPB 2 experienced reduction in stress and volume during consolidation. As UCPB 2 was ramped for every increment of 10 °C, the material expanded which resulted in the increase

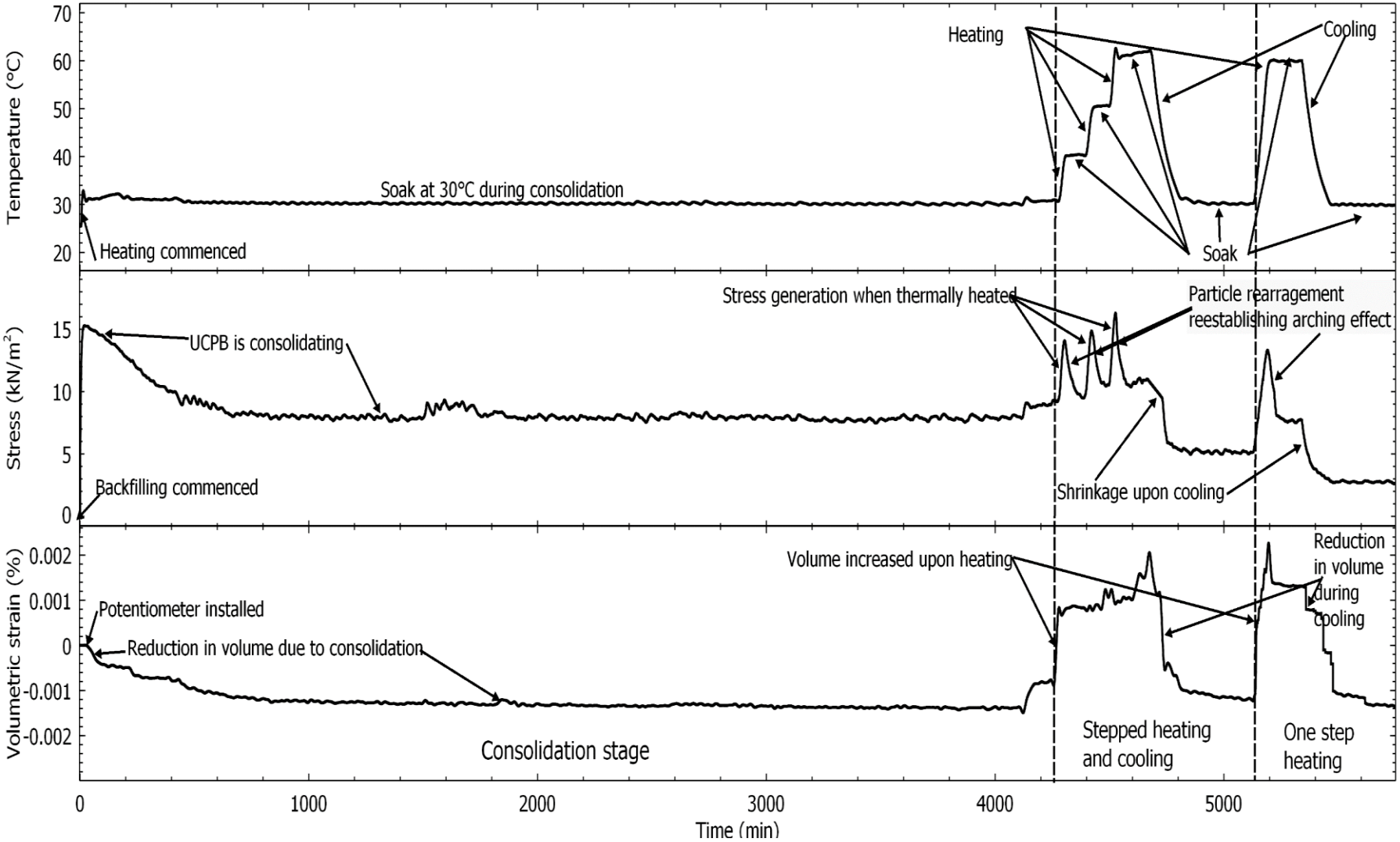

Figure 5.7: Resulting data from UCPB 1 deposition

in total volume and exertion of additional stress onto the load cell. As the sample was soaked at a constant temperature after heating, it experienced a reduction in stress and volume without any reduction in temperature. During cooling, the particles of the sample shrunk and resulted in the reduction of total volume. As the volume decreases, the additional stress generated due to thermal expansion was also relieved. During the increment of 30 ℃, UCPB 2 behaves according to the behaviour experienced during 10 ℃ increment heating pattern but at a different magnitude.

Generally, UCPB 1 and UCPB 2 showed similar stress-strain behaviour according to the applied temperature change pattern, but the only difference is the intensity or magnitude of change in stress and strain.

5.4.1.2 Cemented Paste Backfill

Figure 5.9 and Figure 5.10 show the stress-strain temperature behaviour of CPB against the elapsed time from the initiation of deposition until 204 hours mark with consolidation/hydration stage, steps heating stage, and one step heating stage. CPB was deposited into the NW at 33 ℃ and controlled at 30±1 ℃ throughout the consolidation and hydration phase for 48 hours. Some reduction in volume was observed at the first 25 hours which was due to the primary consolidation upon pouring and net volume change upon chemical shrinkage. Reduction in stress from 20 kN/m^2 to 15 kN/m^2 (25% reduction) was due to the arching effect during the consolidation phase where the particle was still in paste form, and it was not possible anymore when it was hardened after the first 8 hours.

Steps heating from 30 ℃ to 40 ℃, 50 ℃ and 60 ℃ were conducted soon after the stress recorded stabilised. Each step of heating showed a gain in stress recorded. The reduction in stress during soak reduced as time progress. This was due to the hydration where the material was getting stronger, and movement of the material was more restrained at later

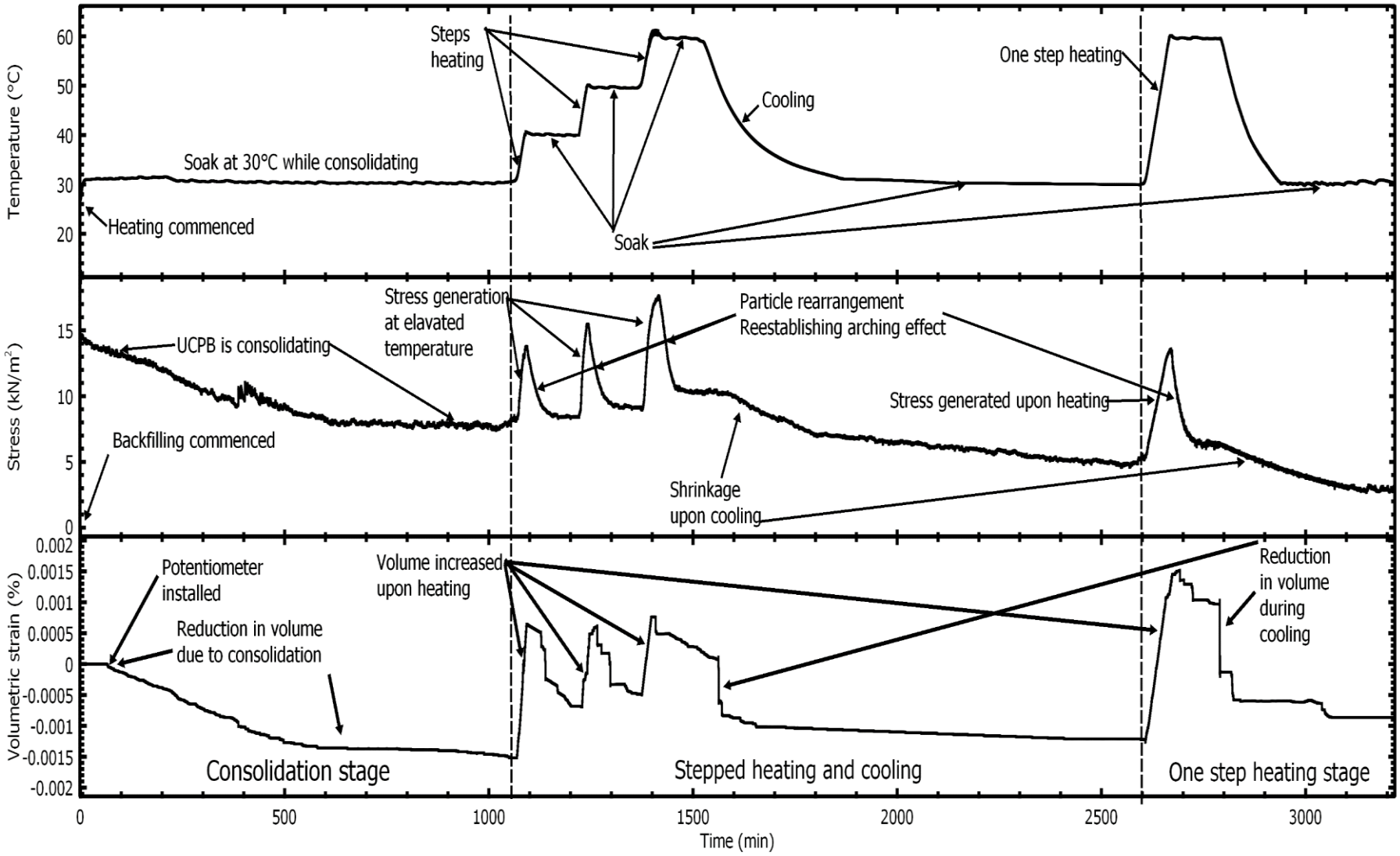

Figure 5.8: Resulting data from UCPB 2 deposition

time. At 4000 minutes mark, the CPB behaved like an elastic material corresponding to temperature change. Before the 4000 minutes mark, there was still reductions in net stress where it significantly reduced the final net stress value by another 25% after cooling back to 30 °C. After 4000 minutes mark where it behaves like elastic material, no reduction in total stress was recorded during the constant temperature period after each heating pattern. A slight reduction in stress recorded was due to the slight overheating when the system was ramped with a big temperature gap due time lag for the heat to be distributed across the medium and reach the respective point where the thermocouple was located.

As for the volumetric change recorded by the potentiometer during the heating and cooling phase, it behaved as the law of expansion where it will expand upon thermally heated and shrunk when cooled. The total net volume was reduced by 2 cm^3 where in terms of linear height displacement, it is only reduced by 0.267 mm. Once harden, the elastic behaviour of CPB tends to archive the same volumetric gain upon heated and revert to same initial volume when cooled to initial temperature.

Figure 5.10 shows the repetition of CPB conducted with the same temperature pattern as CPB 1. The duration of the testing had been shortened as the test is originally independent on time. Therefore, once the stress-strain behaviour after completion of deposition stabilised, heat was induced similarly to CPB 1. As the temperature increase, the vertical stress and volume also increased. During soaking, the stress and strain slightly reduce while there is no change in temperature. As time elapsed, the reduction of stress and volume during soaking diminished. As CPB behaved elastically when it hardens, the stress-strain was able to return to its initial state after heating and cooling. Generally, CPB 1 and CPB 2 behaved the same with respect to temperature change, and the only difference is the slight deviation in terms of values of stress and strain change.

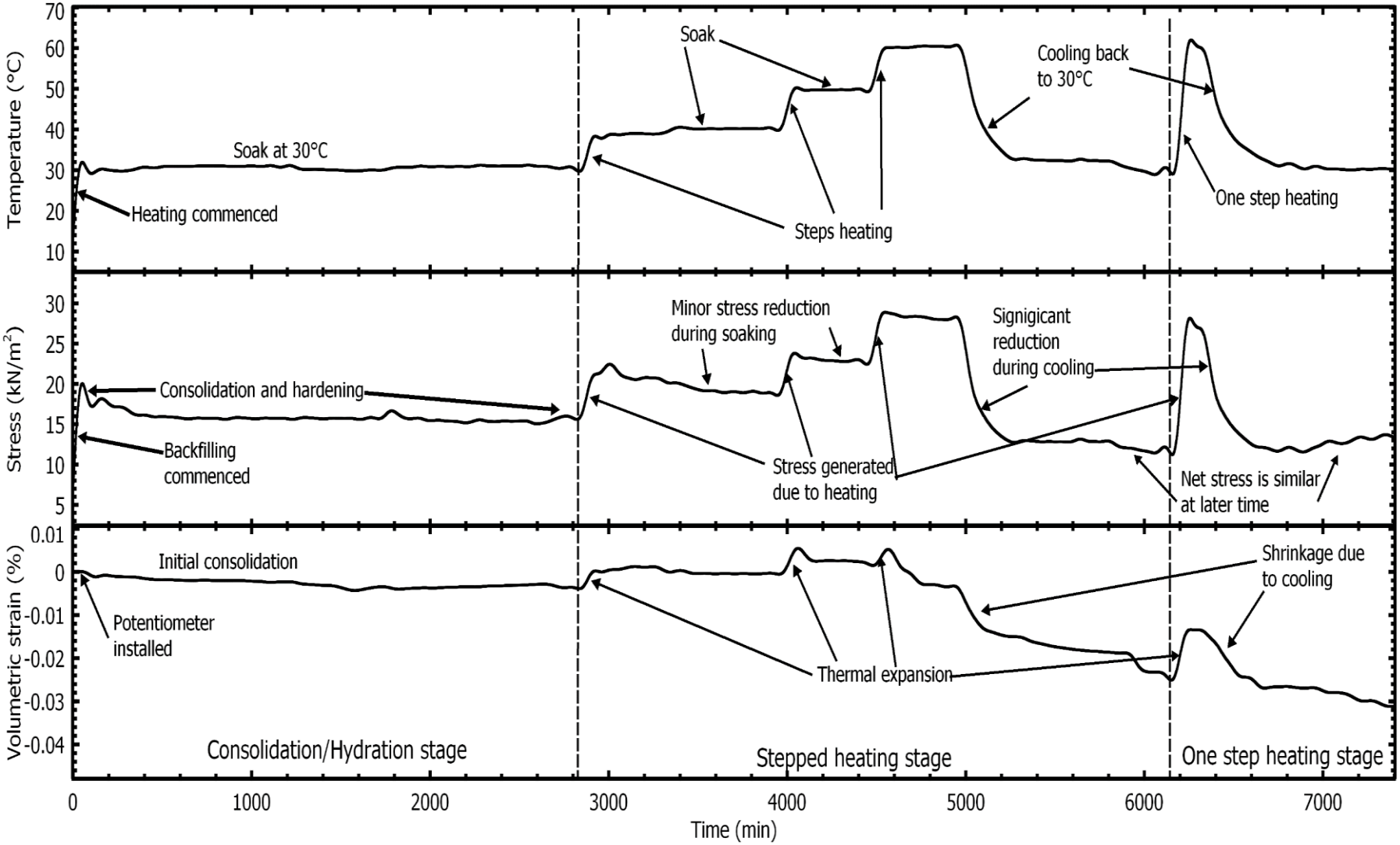

Figure 5.9: Resulting data from CPB 1 deposition

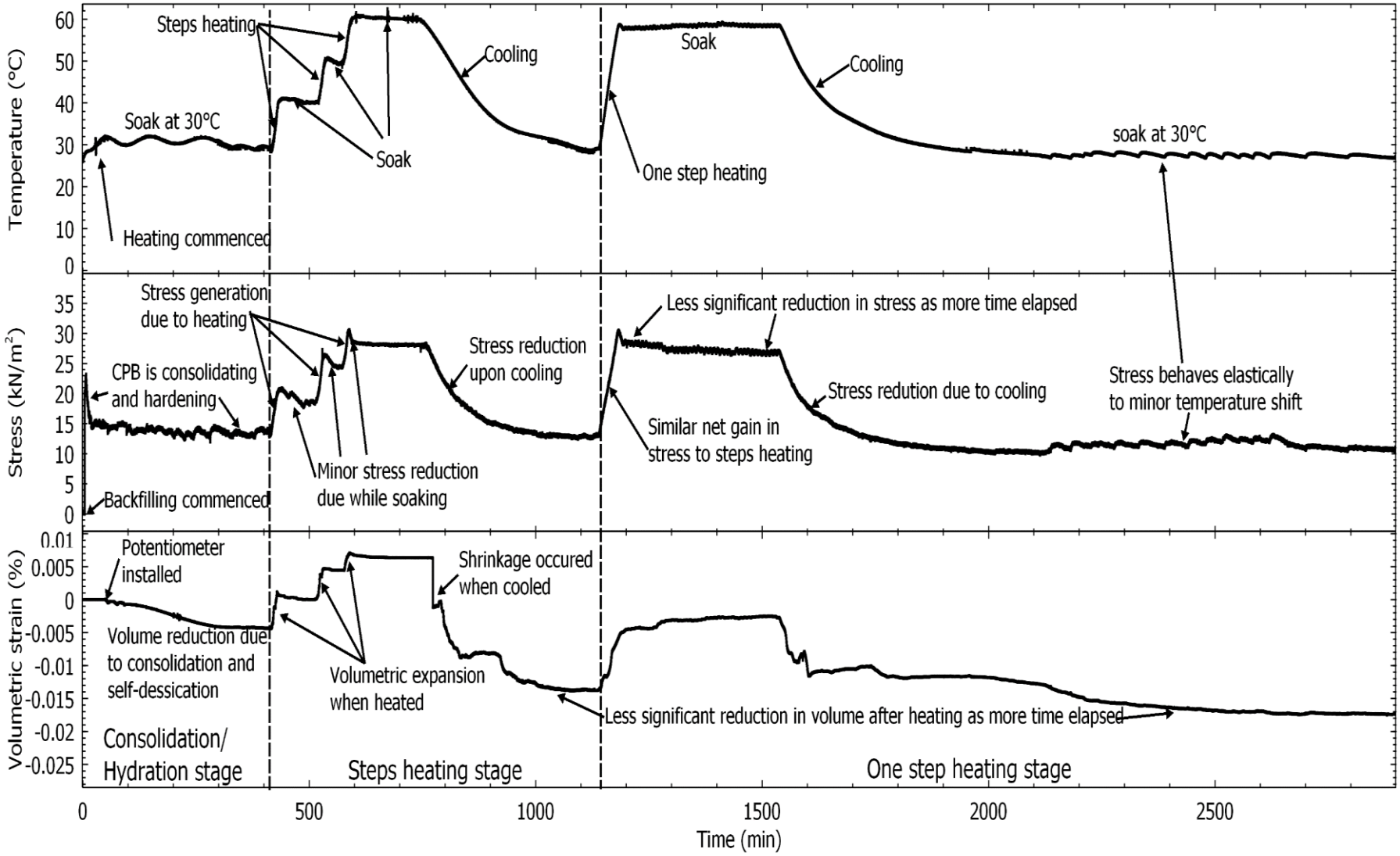

Figure 5.10: Resulting data from CPB 2 deposition

5.4.2 At Fixed Temperature

The stress-strain-temperature behaviour of UCPB and CPB when backfilled into a NW were investigated at a range of controlled temperature. The backfill material was prepared at room temperature. Thus, it required some heating time for the backfill material to reach targeted backfilling temperature. Preparing the backfill material at higher initial temperature was not recommended as it promotes greater loss of water through evaporation at elevated temperature. With the change in water content, the yield stress of the backfill material will be different for every initial temperature variation. Thus, resulting in different intensity of arching and ultimately affects the stress distribution of the backfill material. Additionally, the backfill material was usually prepared at room temperature (may vary from one mine to another) and transported to the backfilling stope where the stope may be initially hotter or colder than the backfill material itself. Depending on the initial temperature of the stope, heat transfer will occur into or out of the backfill material. The heat transfer will change the temperature of the backfill material and cause volumetric change due to thermal expansion or shrinkage. Therefore, this showed that the backfill material (both UCPB and CPB) shall be prepared at room temperature and backfill into the NW that was initially heated to the required temperature. The behaviour of the backfill material when backfilled into the NW at elevated temperature was discussed and presented in the following subsection.

5.4.2.1 Uncemented Paste Backfill

The backfilling test was conducted at four different constant temperature which were 30, 40, 50, and 60 °C. Generally, every UCPB sample were backfilled and heated to the targeted temperature. Upon reaching the targeted temperature, the backfill material was set to soak at a constant temperature until no further change in stress and strain was observed.

A moment after reaching stabilised state, the UCPB samples (other than 30 ℃ test) were cooled to 30 ℃ to observe its behaviour during the cooling phase.

The behaviour of UCPB sample at 30 ℃ is shown in Figure 5.11. The sample is initially prepared at 25 ℃ and heated to 30 ℃ to fulfil the temperature requirement of the first investigation. With an increase in 5 ℃ in the first 10 minutes, the backfill material does not show any abnormal increase in stress. The highest stress recorded is 16.8 kN/m^2 and was slowly reduced to 9 kN/m^2 due to the consolidation of the backfill material that established greater arching effects. A reduction of stress by 46% could be observed mainly due to the consolidation of UCPB at 30 ℃. The consolidation took about 900 minutes (15 hours) to stabilise. The potentiometer shows that the sample was shrinking (reduction in volume) which was likely due to self-weight consolidation. After 900 minutes, the change in volumetric strain stabilised and showed a total of 0.002% reduction from total volume (0.006 m^3). At a constant temperature of 30 ℃, no significant expansive behaviour of UCPB was observed from this testing.

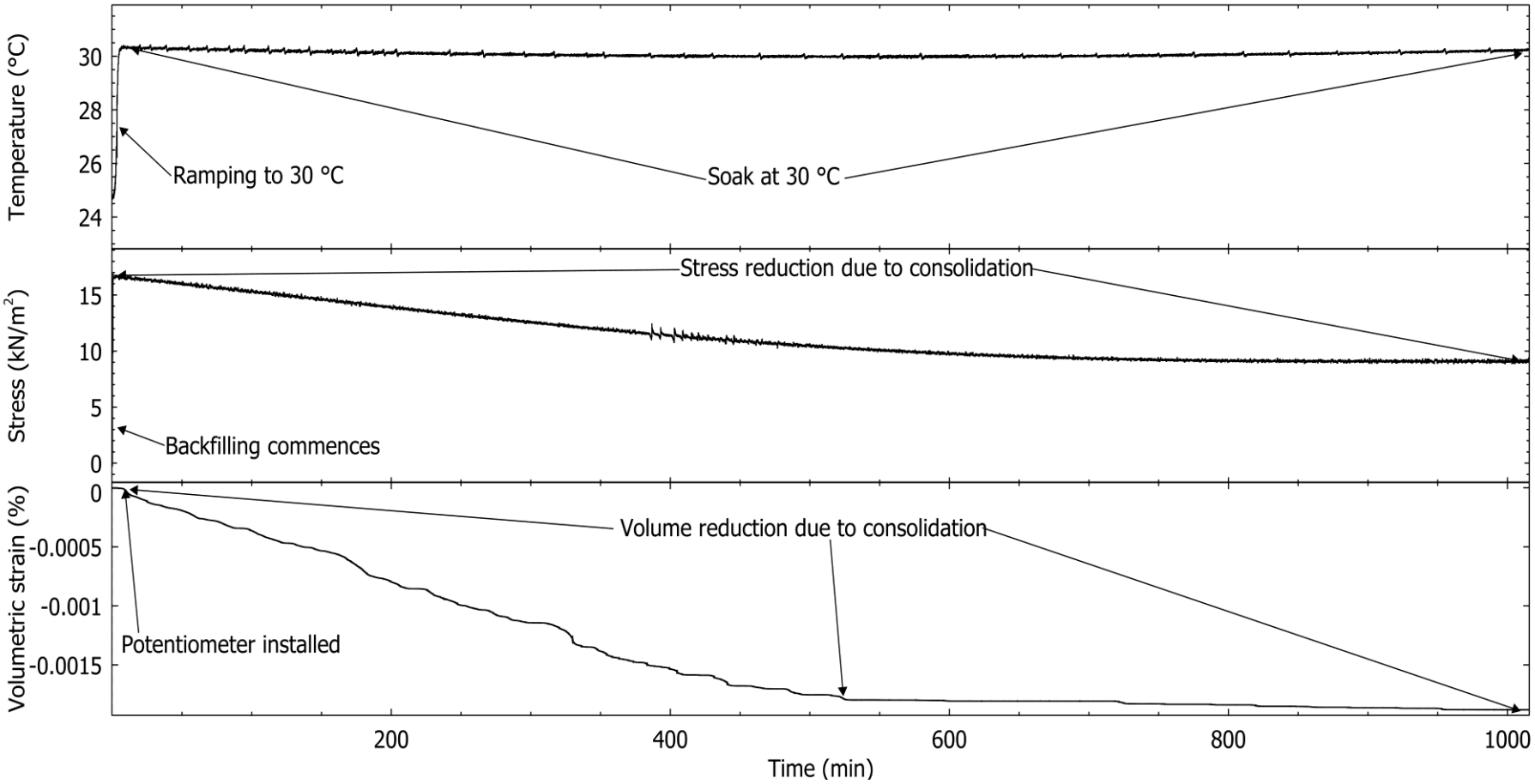

Figure 5.11: Behaviour of UCPB sample at 30 °C

The behaviour of UCPB at 40 °C is shown in Figure 5.12. As the sample was prepared at room temperature, significant time was required for the heating system to heat it up to 40 °C. The heating process began concurrently with the initiation of backfilling which was similar to actual backfilling of backfill material into stope that is hotter than the backfill material itself. As the UCPB was being backfilled into the NW, the heat transfer from the NW to the UCPB began until the UCPB had reached 40 °C. The change in temperature from about 24 °C to 41 °C (slight overheating due to heat transfer delay) caused the UCPB to expand by 0.001% of its total volume. As there was expansion characteristic shown in the UCPB sample, there was no increase in stress observed. This was due to the reduction in stress by the establishment of arching is more significant than the minor increase in stress due to expansion. When the increase of temperature was absent or slowed down, the expansion of UCPB stopped, and consolidation was observed during soaking at 40 °C. The reduction in stress and volume stabilised at 900 minutes mark where the stress reduced by 50% which is from 16 kN/m^2 to 8 kN/m^2 and the volumetric strain after the expansion decrease by 0.001% from 0.0011% to 0.0001%. The reasoning behind the greater reduction in stress in comparison to 30 °C backfilling test was explained in Section 5.5.3.2. When no more changes could be observed, the UCPB was set to be cooled to 30 °C and soaked at 30 °C. The stress reduced by 4 kN/m^2 due to cooling at a rate of 0.4 kN/m^2 / °C while the volume was further reduced by 0.0005% to -0.0004% from original volume.

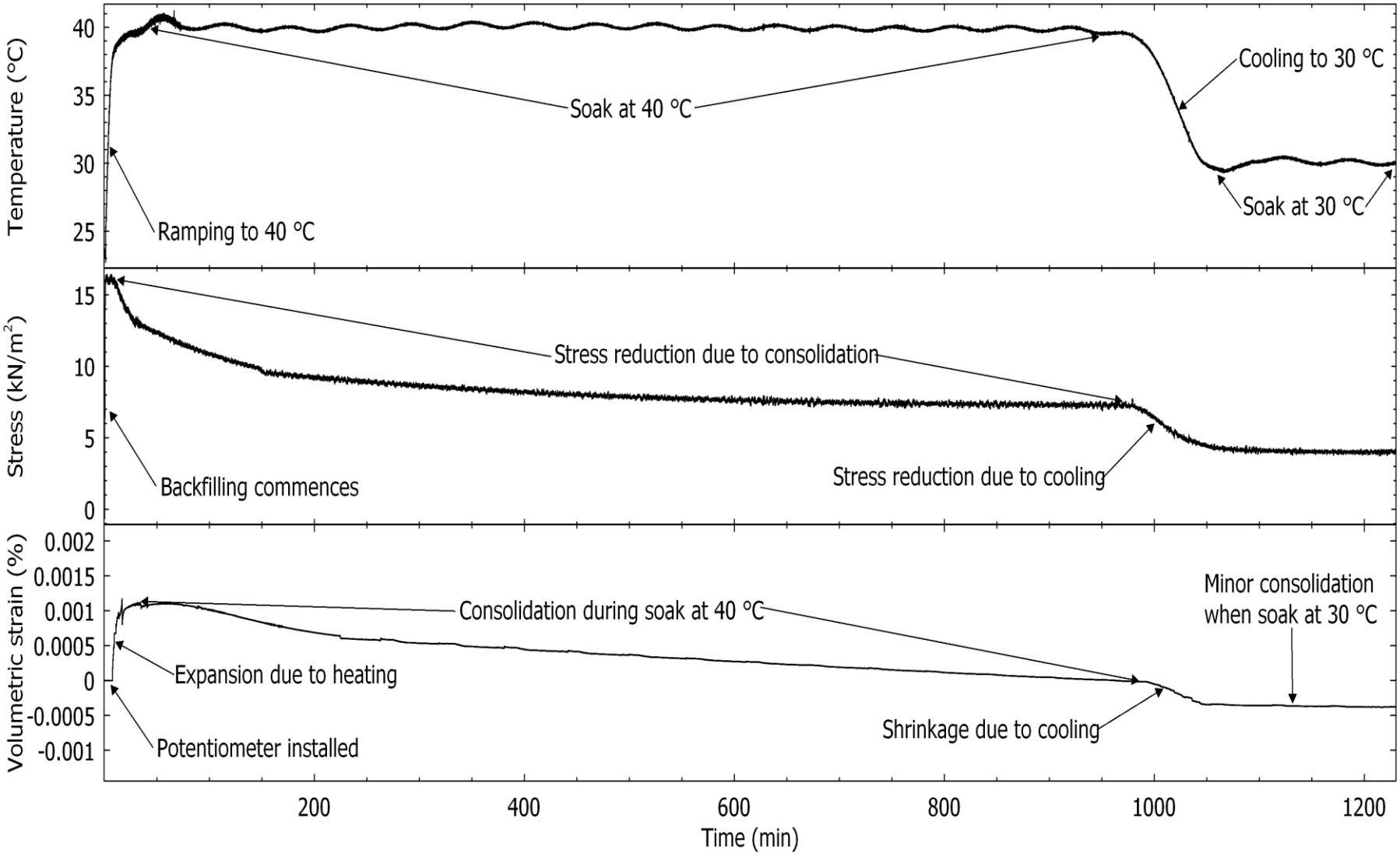

Figure 5.12: Behaviour of UCPB sample at 40 °C

The behaviour of UCPB at 50 ℃ is shown in Figure 5.13. Longer time was required for the heating system to heat it up to 50 ℃ as the temperature difference is about 25 ℃. It took about 40 minutes to reach 50 ℃. The change in temperature was from an initial temperature (about 27 ℃) to 52 ℃ (overheating due to heat transfer lag). Thus, UCPB expanded by 0.0014% of its total volume. As there was expansion characteristic shown in the UCPB sample, there was no increase in stress observed. Although there was no obvious increase in stress observed from this study, the reduction in stress seems to be lesser in comparison with UCPB at 40 ℃. While heating to 50 ℃ (0 to 30 minutes), There was no significant reduction of stress despite the completion of backfilling (i.e. no more increment of self-weight). Such behaviours remained until the increase in temperature is not significant anymore (40 minutes mark) then the reduction of stress due to consolidation became more significant that the increase in stress due to expansion. The reduction in stress by 6.5 kN/m^2 from 14 kN/m^2 to 7.5 kN/m^2 was the least in comparison to both UCPB at 30 and 40 ℃. The lesser reduction in stress was due to the coupled stress altering mechanism from thermal stress and establishment of arching effects.. From the volumetric strain monitoring, it could be seen that the UCPB continued to expand upon heating and slowed down when the increase in temperature is insignificant thereafter. Once the contribution to thermal expansion due to heating is insignificant, the reduction of volumetric strain due to consolidation was observed at 500 minutes mark. As the UCPB stabilised at 50 ℃, it was cooled back to 30 ℃ for its cooling behaviour. With reduction of 20 ℃, the stress reduced by 3.5 to 4 kN/m^2 which was about 0.175 kN/m^2 / ℃. The volumetric strain changed from 0.00125 to 0.0008% which shows that the UCPB shrunk upon cooling.

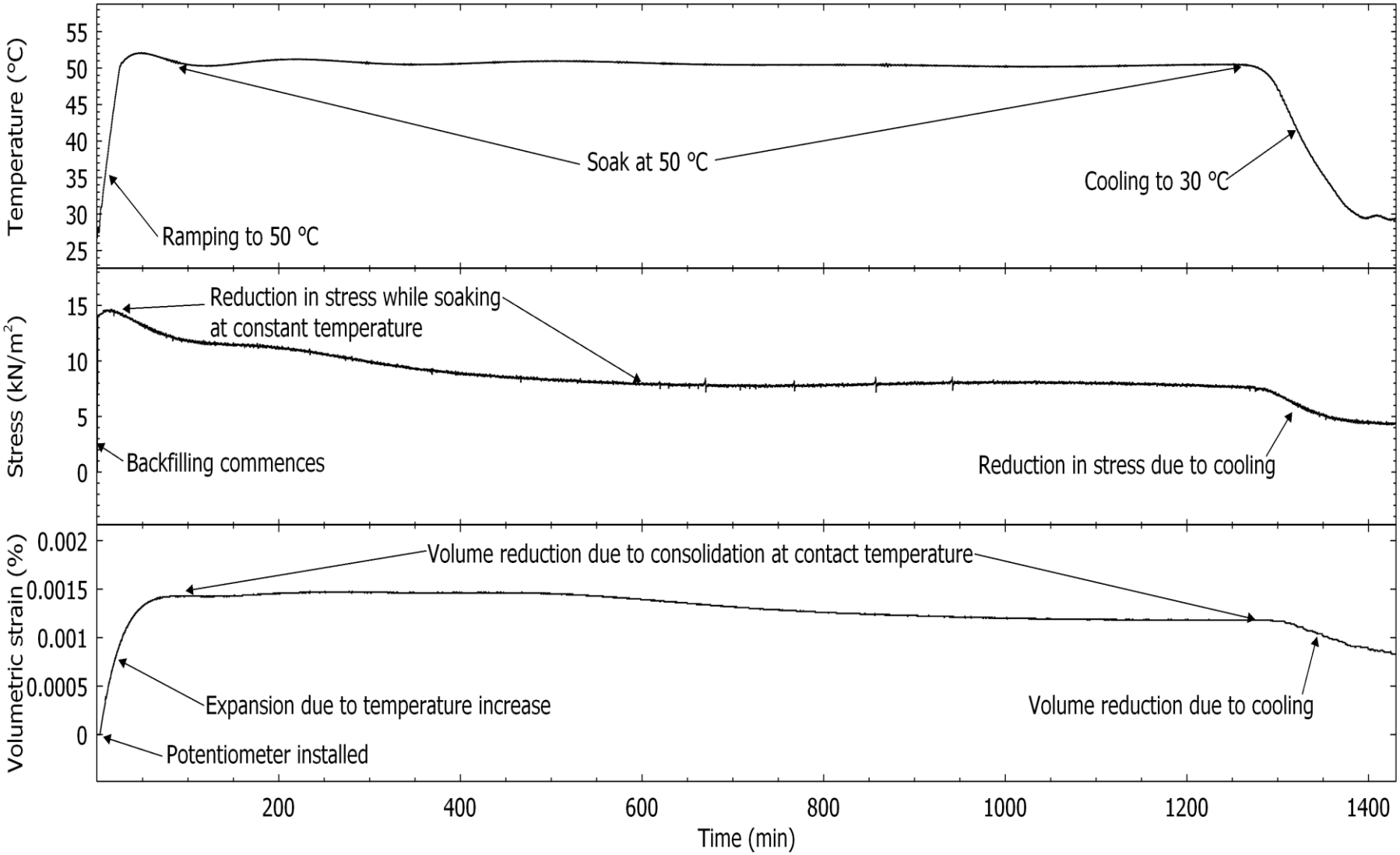

Figure 5.13: Behaviour of UCPB sample at 50 °C

The UCPB was also tested at 60 °C, and the finding is shown in Figure 5.14. With a 35 °C change in temperature, an interesting change in the stress and strain behaviour were observed form this testing. While heating to 60 °C, the UCPB showed a rather common increase in volumetric strain due to thermal expansion, but the increment is somehow delayed with the temperature increase. A sudden expansion trend is observed at 44 minutes mark which was speculated to be caused by the change in the state of the UCPB into a more elastic state instead of free-flowing paste. The consolidation and thermal expansion occurred simultaneously at the first 44 minutes causing the UCPB to be densely packed within its initial volume. At 44 minutes mark, the UCPB itself was dense enough to allow actual volumetric expansion in either upward direction or downward direction where the side of the NW was fixed from any deformation. This was possible as from the reading of the load cell, it showed that the UCPB managed to exert more stress onto the load cell that exceeded the reduction of stress due to the establishment of arching effects.

As for the stress behaviour, the stress reduction is controlled while heating and increase in stress was observed at prolonged heating to a higher temperature. During the soaking period, there was a great reduction in stress and volumetric strain are observed, and similar findings were also observed while testing UCPB by varying the temperature. Upon cooling back to 30 °C, the stress was reduced from 11.5 to 7 kN/m^2 by 4.5 kN/m^2 which was 0.15 kN/m^2 / °C. The volumetric change of UCPB from 60 to 30 °C was by 0.0003% from 0.0012 to 0.0009%.

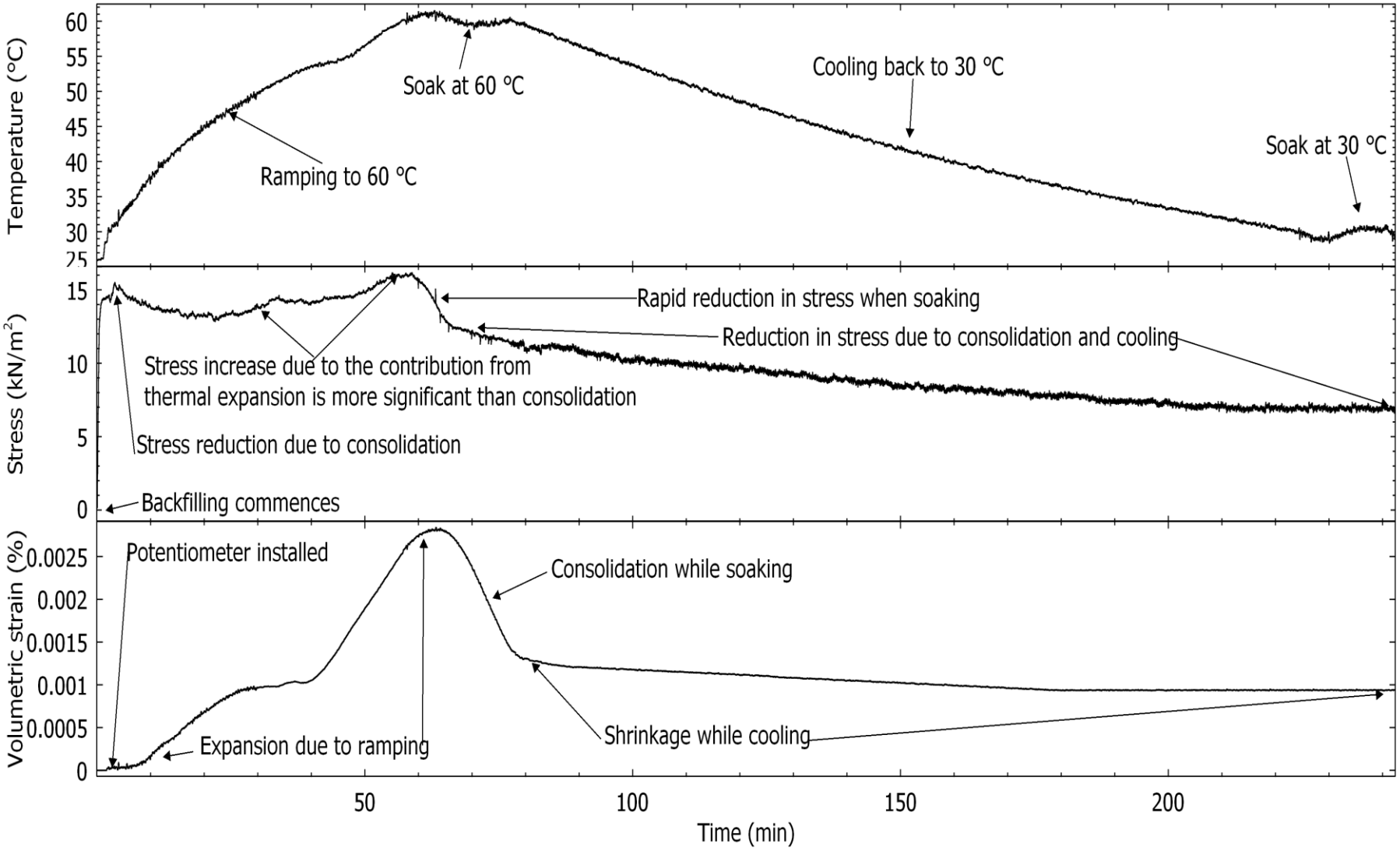

Figure 5.14: Behaviour of UCPB sample at 60 °C

5.4.2.2 Cemented Paste Backfill

The backfilling test for CPB is also conducted at four different constant temperature which are 30, 40, 50, and 60 °C. The temperature change pattern was the same as backfilling test for UCPB. The main differences between CPB and UCPB were the presence of cement hydration in the backfill sample that will alter the state, phase, shear strength and coefficient of thermal expansion. Generally, with the addition of cement of 5% will slightly increase the self-weight of the CPB in comparison to UCPB. With 45 Pa differences in yield stress, the initial establishment of arching could be different. The coupled effect from initial self-weight and yield stress showed slightly higher initial stress in comparison to UCPB sample.

The CPB sample was first tested on 30 °C. The stress and strain behaviour was captured and shown in Figure 5.15. The CPB was prepared and was initially 31 °C upon backfilling. It was allowed to cool down to 30 °C by dissipating heat to the surrounding environment. Upon backfilling, the stress increased due to self-weight induced at the load cell, but upon consolidation of CPB (slurry-state), the stress reduces due to the establishment of arching. The reduction of volume showed that the CPB was indeed consolidating. Backfilling of CPB without any significant increase in temperature showed 50% reduction from 18 kN/m^2 to 9 kN/m^2. Continuous reduction in volume may be due to the remaining consolidation that did not contribute to the changes in stress, self-desiccation and chemical shrinkage. Some irregularities in the stress curve were caused by the shift in temperature between 29 to 31 °C due to heating/cooling hysteresis. As the CPB was getting more elastic as it hardens over time, the effect of temperature on stress change due to thermal deformation was more significant at the later time in comparison with UCPB sample.

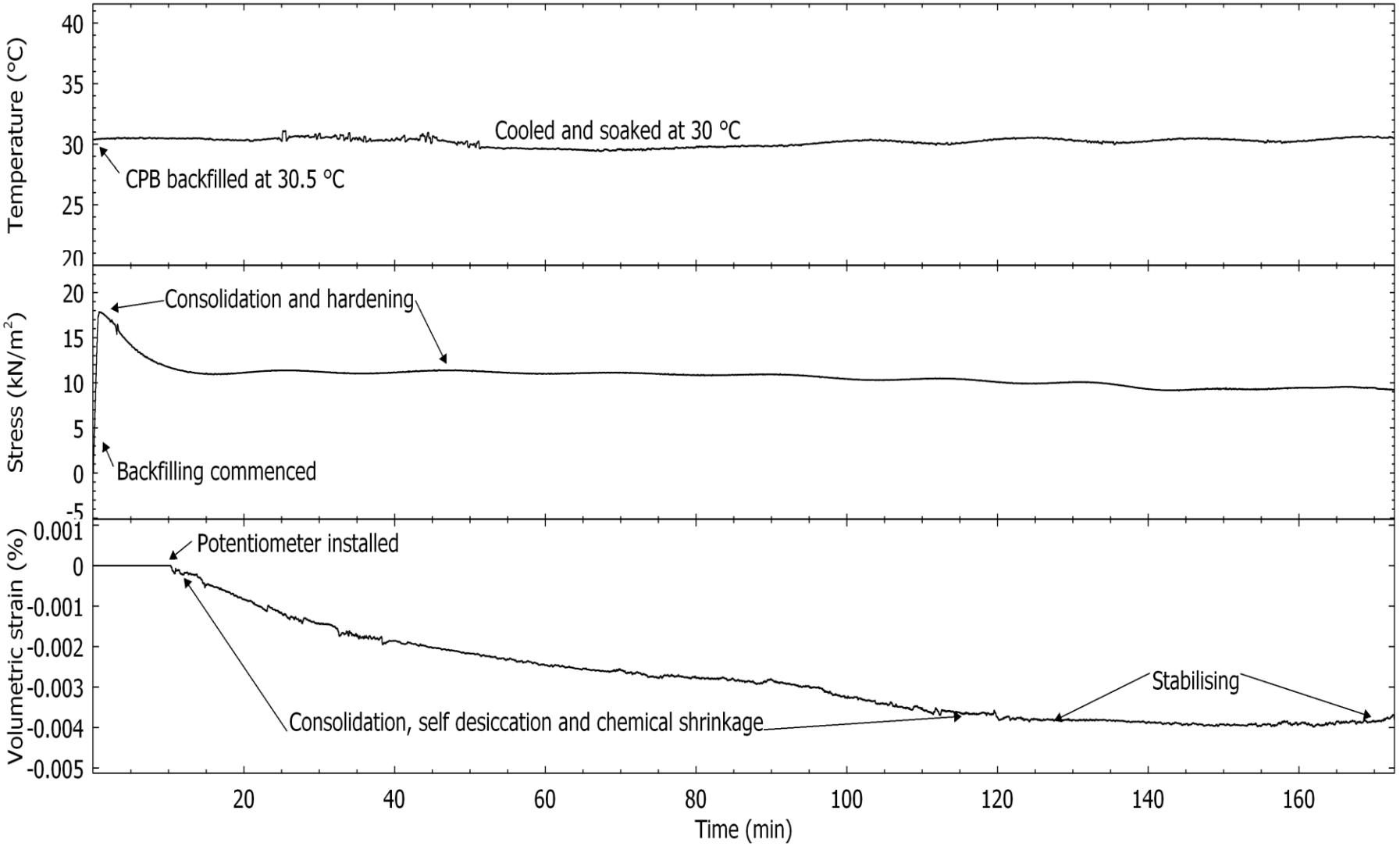

Figure 5.15: Behaviour of CPB sample at 30 °C

Another CPB sample was used to be investigated on 40 ℃ curing temperature, and the findings on its behaviour were shown in Figure 5.16. As the CPB was initially prepared at 30.5 ℃, it had to be heated to 40 ℃. The heating commenced concurrently with the backfilling of CPB into the NW. Upon backfilling, the peak stress recorded due to the self-weight of CPB was 18 kN/m^2. The stress only reduced by approximately 20% in comparison to CPB tested at 30 ℃. Such reduction was possibly due to some thermal expansion that contributes to the stress increase while heating but not significantly to affect the overall trend of stress change due to greater stress reduction caused by the establishment of arching. Initially, reduction in volume due to the consolidation of CPB was observed until the expansion of volume due to temperature increase became more significant than the reduction due to consolidation. A spike of gain in volume was noticed while the CPB was being heated to 40 ℃. As the CPB was cured at 40 ℃, a slight increase in stress could be seen between 100 to 300 minutes mark. Later after 300 minutes mark, the stress slightly reduces which might be due to the heating/cooling hysteresis that allows movement of the particle while expanding or shrinking that contribute to the increase in arching effects. Same as CPB tested at 30 ℃, the heating/cooling hysteresis caused the stress behaviour to behave according to the temperature shift. As this test duration was longer than 30 ℃ test, the behaviour of stress change was getting more dependent on the temperature shift due to prolong hardening that caused CPB to be more elastic.

From the volumetric strain change which is recorded at the open end of the backfilling, it shows that the CPB sample was expanding freely until 600 minutes mark where slight reduction of volume occurred until it was stabilised at 850 to 1000 minutes mark. The CPB sample is then cooled to 30 ℃ and remained at it until stabilised. With the

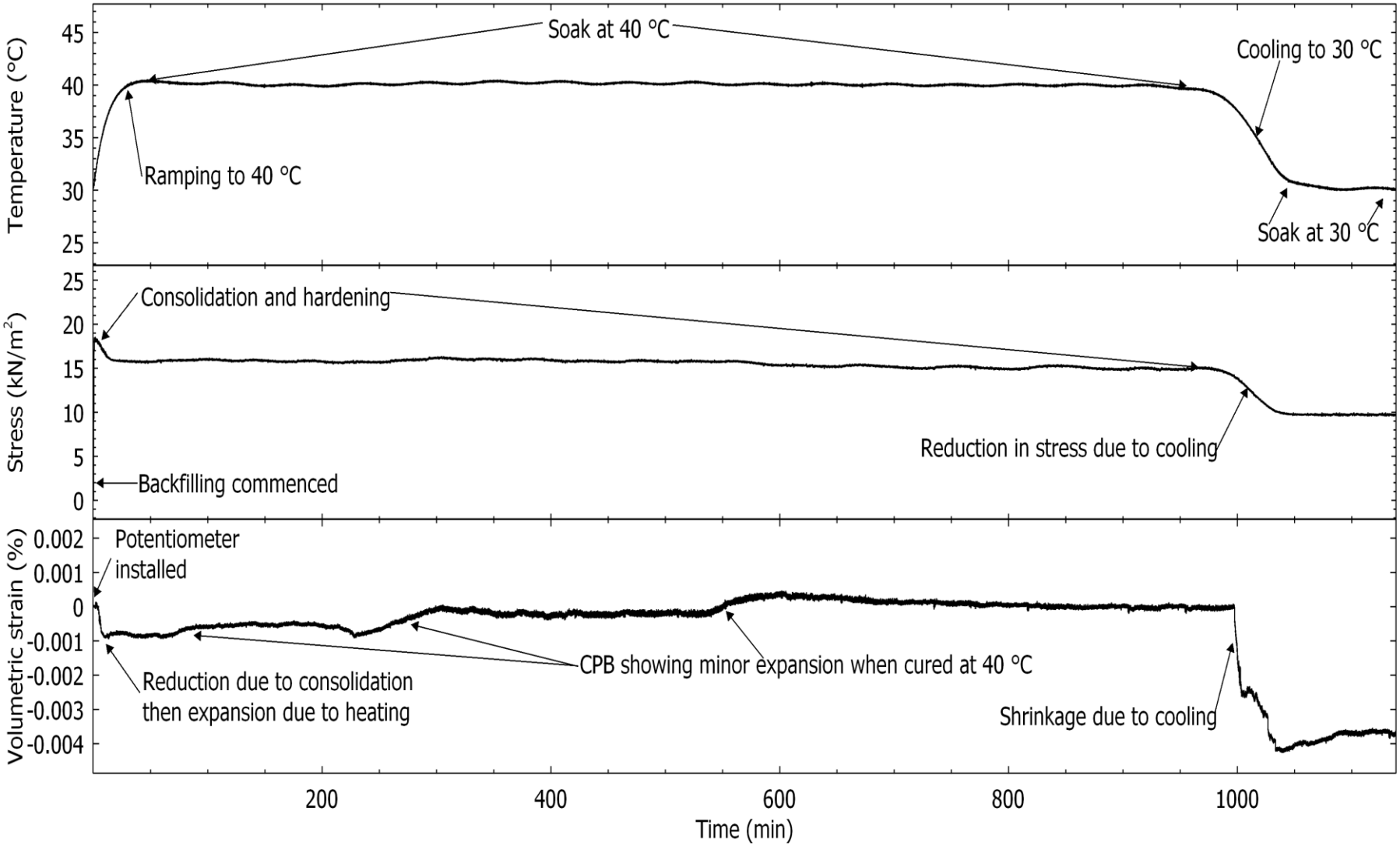

Figure 5.16: Behaviour of CPB sample at 40 °C

change in 10 ℃, the stress further reduces by 5 kN/m^2 which shows a total reduction of 45% that shows slightly higher final stress value if compared to CPB cured at 30 ℃ without any changes in temperature. Reduction in volumes of CPB shows that the CPB sample was shrinking due to cooling. As it is soaked at constant 30 ℃, the CPB abnormally expand slightly then stabilised. A possible cause for this unexplained phenomenon needs to be thoroughly investigated in the future.

Figure 5.17 shows the behaviour of CPB at 50 ℃. The initial stress recorded seems to be lesser in comparison to CPB at lower temperature (i.e. 30 and 40 ℃). This may be due to the heat transfer occurred from the aluminium NW to the lower fill of the CPB while the rest of the filling was yet to be completed. The aluminium wall was preheated to reduce the total heating time, and to correlates with high-temperature stope. This cause the CPB to be rapidly heated and the shear behaviour of the CPB was speculated to behave according to the temperature change. The thermal shear test showed that the increase in temperature will increase the shear strength as well as the frictional angle of CPB and the interfacial frictional angle between CPB and aluminium wall. Thus, the arching effects were intensified during the backfilling, and slightly greater reduction in stress due to arching was observed.

CPB is heated from 30 ℃ to 50 ℃ by 20 ℃ in 40 minutes time. When the system was heating at the first 40 minutes, the CPB does not shows any significant reduction in stress as the stress recorded was in between 17.1 kN/m^2 to 17.2 kN/m^2. As the CPB had reached 50 ℃, The CPB continues to heat up due to the lag time for the heat to be transferred to the centre of the CPB sample where the thermocouple was placed. As the temperature increase slowed down and soon to be cooled back to 50 ℃, significant reduction in stress was observed as there was no significant contribution to stress from the thermal expansion of CPB whereas the consolidation of CPB was still on its way as CPB was still in paste state

at this time of the backfilling (40 to 400 minutes mark). The reduction of stress due to consolidation halted in between 500 to 1500 minutes mark which showed a constant 15.5 kN/m^2 that was only about 1.7 kN/m^2 reduction during soaking at 50 ℃. This was considerably lesser in comparison to CPB at 40 ℃. The lesser reduction in stress during the soaking phase could be explained by its cooling behaviour. Upon cooling to 30 ℃, the stress reduced greatly to 10.5 kN/m^2 that was considerably more than CPB at 40 ℃ because the CPB was initially thermally expanded due to 20 ℃ temperature differences and the net stress generated by thermal expansion would be greater than 10 ℃ temperature change. The final stress reading at 30 ℃ was around the values of CPB tested at 30 ℃, and CPB cooled from 40 ℃ to 30 ℃.

After the completion of backfilling, the expansive behaviour of CPB due to temperature increase was observed. The CPB expanded until the heating slowed down and soaked at 50 ℃. During the soaking, CPB behaved according to the temperature hysteresis but generally showed minor volumetric reduction that was probably due to self-desiccation, chemical shrinkage and consolidation at an early stage. Upon cooling back to 30 ℃, the CPB shrunk further by 0.008% of its original volume. As the CPB is considerably hardened after 800 minutes mark, no significant reduction due to consolidation and hydration could be observed during the soaking phase at 50 ℃ (after 800 minutes mark) and 30 ℃.

Lastly, the CPB was tested at 60 ℃ and its corresponding behaviour is shown in Figure 5.18. The CPB was prepared at 28 ℃ and heated for 50 minutes until it reached 60 ℃ and peaked off with excess heating at 60.3 ℃. The CPB was then allowed to soak at 60 ℃ until the stress and strain reading was found to be stable via real-time monitoring. The CPB was cooled off to 30 ℃ which takes 150 minutes to reduce 30 ℃.

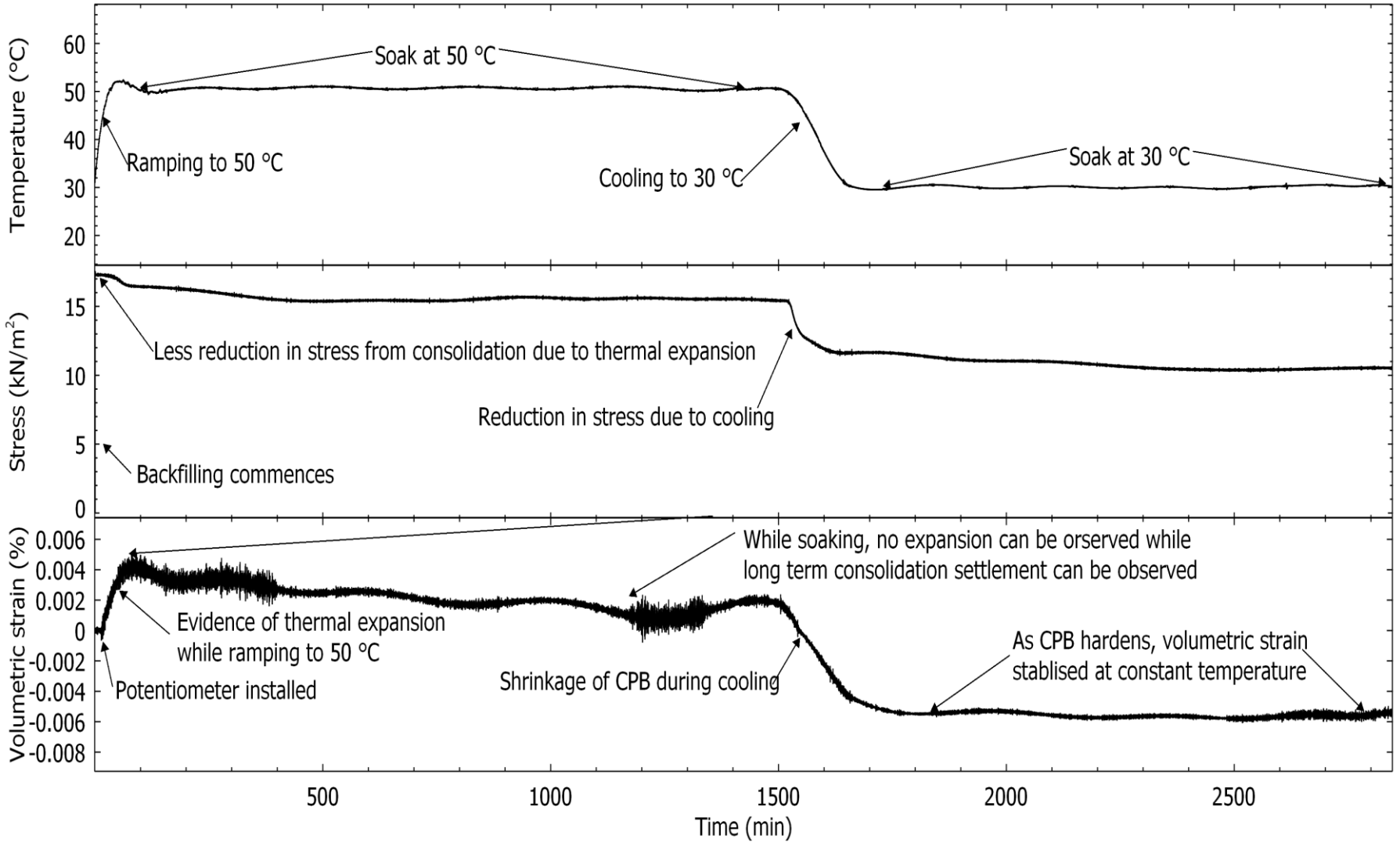

Figure 5.17: Behaviour of CPB sample at 50 °C

The total stress generated from backfilling was 18.6 kN/m^2. Rather than usual stress reduction due to the establishment of arching, heating caused the stress to increase within the 50 minutes timeframe. This behaviour showed that the stress generated from the expansion of CPB slurry exerts stress to the surrounding of the wall was greater in comparison to the reduction of stress due to consolidation. With the increase in temperature, the CPB continues to expand until the heating slowed down and stopped at 60 °C. The stress reading peaked at 22.3 kN/m^2 and the yet to be hardened CPB was allowed to consolidate which cause the stress to reduce to 19 kN/m^2. The CPB seems to be generating additional stress at 150 to 450 minutes mark which was speculated to be caused by the hydration at high temperature that may further promote exothermic reaction and expansion of CPB particles. As the CPB was cooled off by 30 °C, the stress was significantly reduced to 13.4 kN/m^2 that was a reduction of 40%. While soaking at 30 °C, no significant change in stress could be observed. Once again, the final stress at 30 °C was higher in comparison to the final stress at 30 °C of the previous testing temperature of CPB.

Upon installation of the potentiometer, the expansion of CPB was observed corresponding to the heating period. When the temperature of CPB reached the targeted temperature of 60 °C, no expansion of CPB could be observed whereas some minor reduction while the CPB was still in paste state showed the possibility of reduction in volume due to consolidation. As the time progress, the CPB consolidation halted at 300 minutes mark and started to show some expansion until 550 minutes mark. The CPB was allowed to cool back to 30 °C, and the final volumetric strain change of CPB recorded is -0.004% less than its original volume. The volume of CPB at 30 °C after cooling from a different set of curing temperature was found to be similar which is around -0.004%.

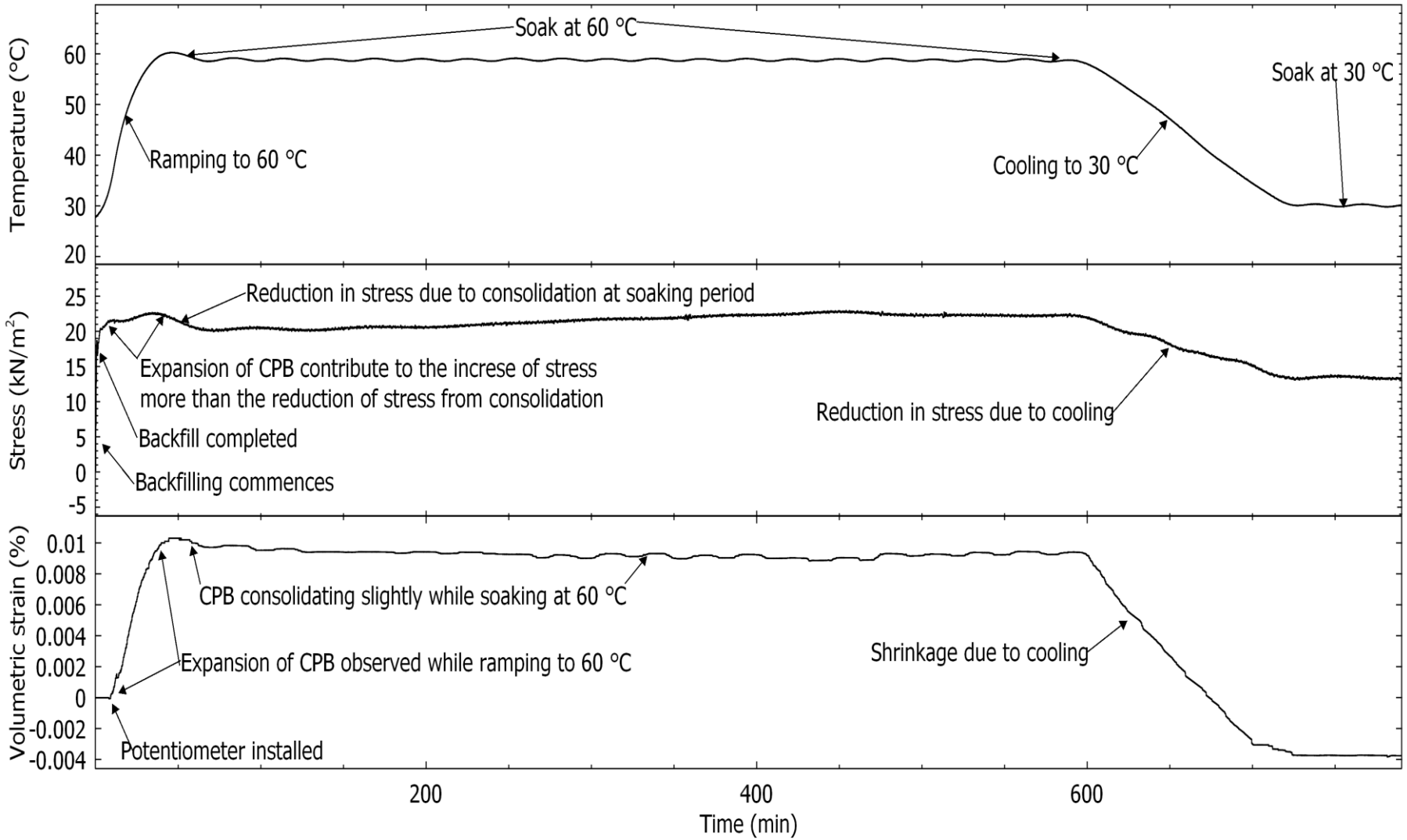

Figure 5.18: Behaviour of CPB sample at 60 °C

5.5 Data Analysis

From the collected data of deposition test above, a thorough analysis was conducted on each specific region (i.e. backfilling, consolidating, heating, soaking, and cooling phase) to further understand the effect of temperature on the stress-strain behaviour of backfill material. Since UCPB was used in this experimental program as a control sample, some of the notable differences were investigated and discussed. In terms of the properties of the material, UCPB and CPB possessed different state of material as time progress, and shear behaviour (frictional angle and/or cohesion). Such differences caused the stress-strain-temperature behaviour to vary between UCPB and CPB. The effect of temperature change, initial curing temperature, type of backfill sample were investigated and presented at the following subsection.

5.5.1 Initial Stress of Backfill during Backfilling

In an ideal case where the backfill material had zero internal angle of friction ($\phi \approx 0$), the geostatic stress could be express as Equation 5.1. Geostatic stress is defined as the stress exerted to any direction in the filling due to gravitational force. Hence, the vertical stress, σ_v equals to horizontal stress, σ_v.

$$\sigma_{geostatic} = \sigma_v = \sigma_h = h\gamma \qquad \text{[Equation 5.1]}$$

where, h is the current height of backfill, γ is the unit weight of the backfill material

However, as the internal friction angle increases, the interfacial friction angle also increases since they are correlated with the coefficient of lateral earth pressure, K. The current state-of-the-art on the stress distribution within NW with particular reference to non-cemented slurry was given by Pirapakaran and Sivakugan (2007) and it was verified with numerical model using FLAC. From Equation 5.2, the resulting vertical stress, σ_v could be

predicted with respect to the height of filling (Figure 5.19) and the consideration of dimension of NW, height, unit weight, and friction angle of the backfill material.

$$\sigma_v = \gamma lw \frac{1-\exp\left\{-2K \tan\varphi h \frac{(l+w)}{lw}\right\}}{2K \tan\varphi \ (l+w)} \quad \text{[Equation 5.2]}$$

where, γ is the unit weight of the backfill material, l is the length of the NW, w is the width of the NW, h is the height of backfilling, ϕ is the friction angle of the backfill material, and K is lateral earth pressure coefficient at rest.

After the deposition was completed, the equation showed that there will be no change in stress when there is no change in the height of deposition. Figure 5.20 shows the comparison of geostatic stress, stress prediction based on the model and actual stress from experimental data. The rate of the increase in stress was higher for actual data because of the rate of filling was calculated based on the total time of filling. This showed that the rate of filling used in the model was an average rate of filling whereas in the actual condition the later stage of the filling will be slowed down to avoid overfilling. The stress recorded from the experimental testing showed that it is similar to the values of geostatic stress. As both backfill mix was prepared in a slurry form which was in a free-flowing state with low yield shear stress, insignificant effects of arching was generated during the pouring stage. Since that the volume of backfill material and the cross-section of the NW were kept to be the same for every testing, the differences in unit weight of CPB and UCPB resulted in differences in vertical stress. Therefore, the resulting initial peak stress at the completion of backfilling were different between UCPB and CPB as the unit weight of CPB was found to be higher than UCPB based on its properties testing. As the backfill consolidates and densifies, the gain in arching effects should affect the vertical stress.

The cross-section of the NW's opening plays a vital role in determining the stress transfer. Comparison of normalised stress, ($\sigma_v/\sigma_{geostatic}$) based on different cross-section is

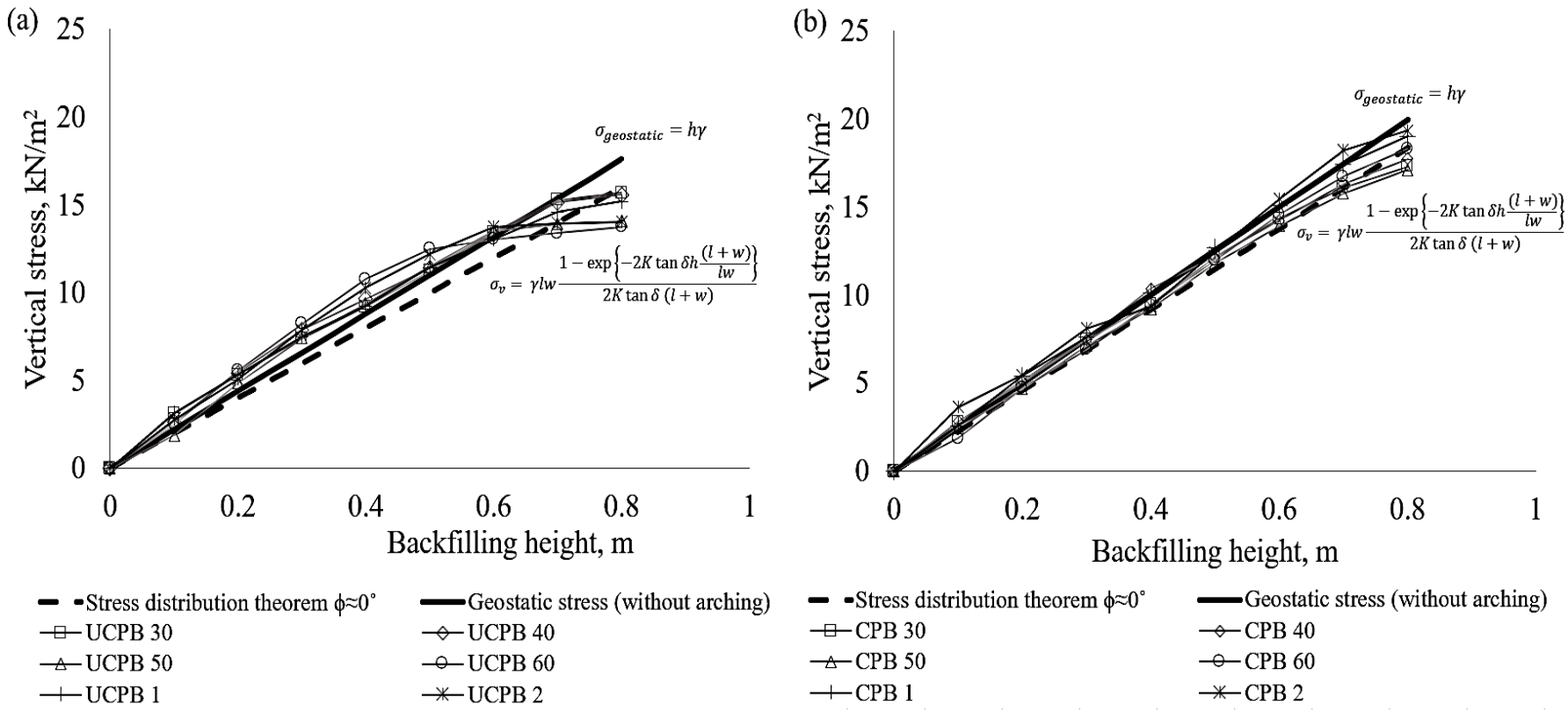

Figure 5.19: Vertical stress vs height of backfill (a) UCPB and (b) CPB

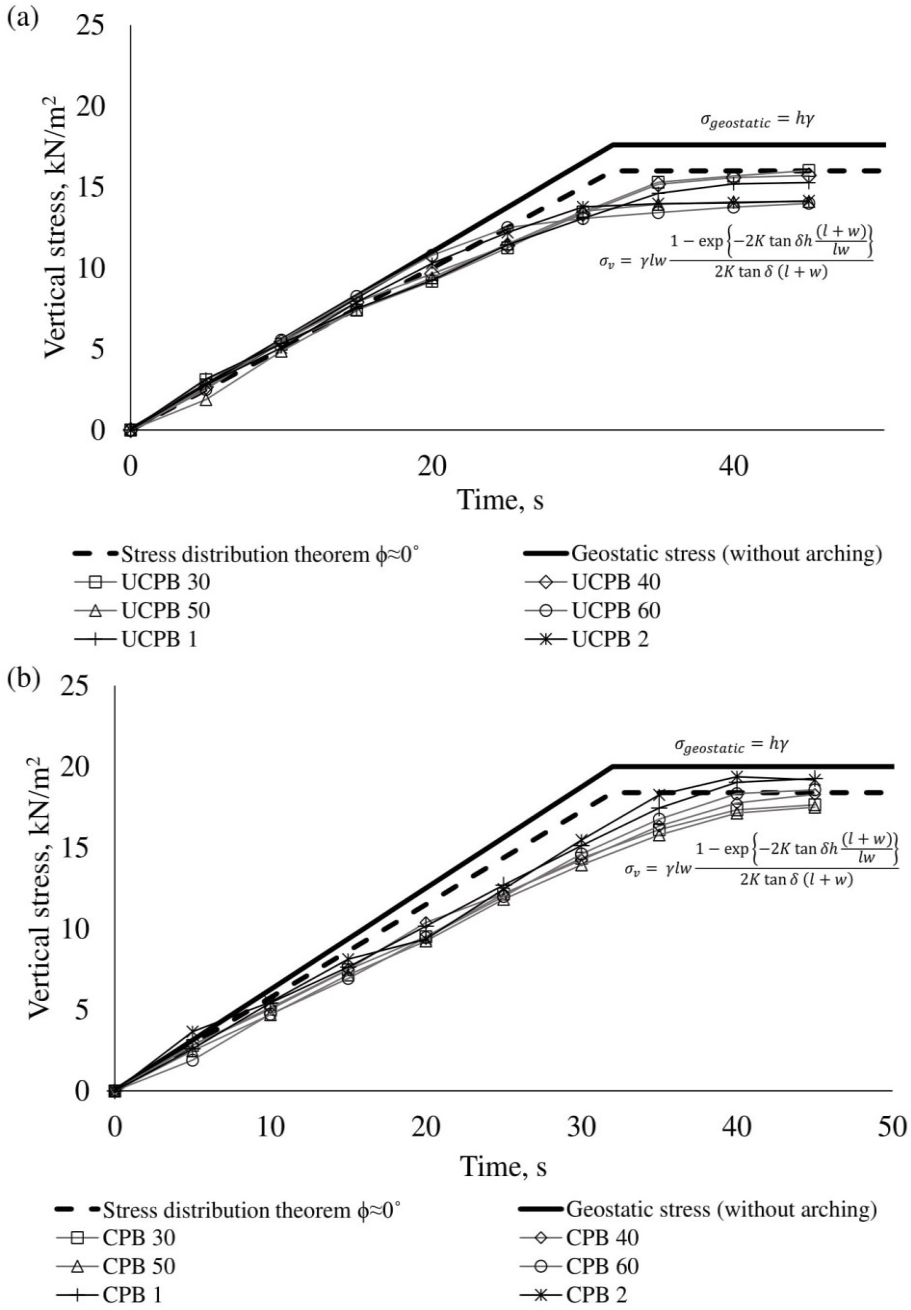

Figure 5.20: Comparison of actual and predicted data of stress generation during deposition (a) UCPB and (b) CPB

predicted using the state-of-the-art model by Pirapakaran and Sivakugan (2007) and displayed in Figure 5.21. It shows that only the dimension of the shorter span will significantly contribute to the generation of arching in comparison to the longer span. In a general term, the narrower the wall, the greater the arching effects. Therefore, the dimensional effects must be taken into account.

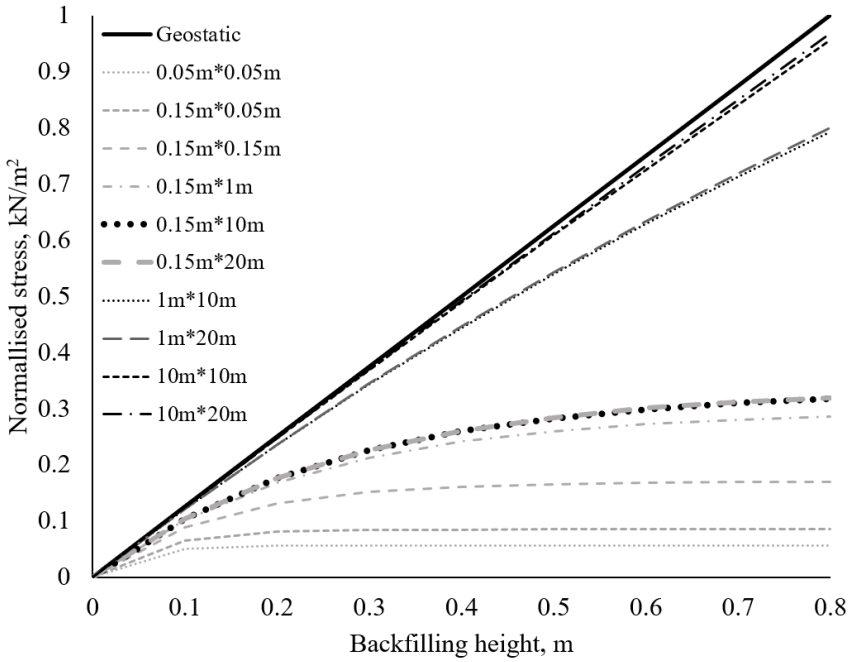

Figure 5.21: Prediction of stress through the model by varying the cross-section of stope (After Pirapakaran and Sivakugan, 2007)

The relationship of frictional angle (internal friction angle or interfacial frictional angle) with the normalised stress was predicted with the state-of-the-art model and is shown in Figure 5.22. As the friction angle of the material approaches zero, the predicted vertical stress is almost equal to the geostatic stress. Inversely, the vertical stress should reduce with the increase in friction angle.

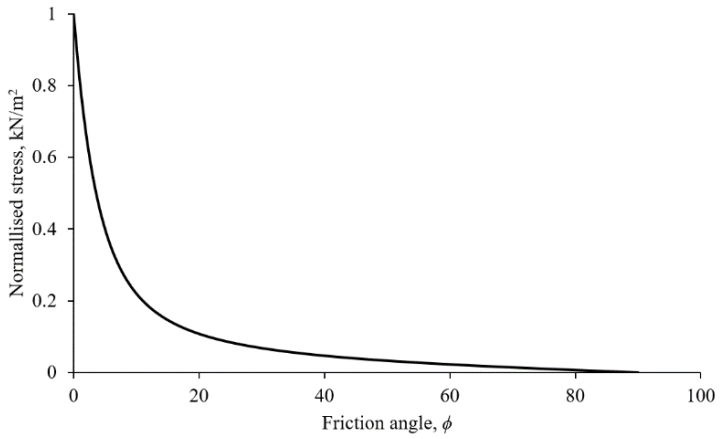

Figure 5.22: Normalised stress vs friction angle based on the model prediction (After Pirapakaran and Sivakugan, 2007)

The current state-of-the-art model was accurate and able to be used in predicting the initial vertical stress within the NW and was proven to be suitable for granular material, soil and slurry provided the input parameter is accurately defined. Most of the granular material stored in narrow silo or soil backfilled into shallow trenches does not experience an extreme change in the internal temperature but backfilling of CPB into narrow stope is subjected to various change in temperature as discussed in Section 2.6.1. The heat transfer occurred not only during the backfilling but also after its completion. As a result, the stress behaviour does not stabilise upon completion of backfilling in comparison to the granular application. Therefore, a model capable of predicting the stress behaviour throughout the backfilling processes (before and after completion of backfill) were investigated through current study.

5.5.2 Stress-Strain Behaviour of Backfill during Consolidation

The reduction of stress that occurred during full-scale monitoring and laboratory testing after completion of backfilling at constant temperature was due to the self-weight consolidation of CPB and UCPB. As both backfill material was prepared as a free-flowing slurry, consolidation and effective stress gain of CPB and UCPB should occur progressively. As time progress, consolidation of CPB was affected due to the hydration process of cement within CPB mix. Figure 5.23 shows the comparison on stress behaviour of CPB and UCPB at a controlled temperature of 30 °C. CPB took a shorter time to attain stable stress state while UCPB requires approximately 10 times amount of time to be fully consolidated. Within the first 20 minutes after the completion of CPB backfilling, the material underwent brief consolidation and volumetric reduction due to self-desiccation where water was used up for the hydration process. This resulted in a reduction in volumetric strain and pore water pressure in comparison to UCPB which only experience consolidation. As the effect of consolidation diminished at after 20 minutes, the stress remained stable while volume

continues to reduce at slower rate. This showed that CPB was experiencing self-desiccation as time goes. The strain behaviour of CPB and UCPB are shown in Figure 5.24. The volumetric change (%) is the change in volume over the initial volume after completion of deposition. The volume change of the backfill during the consolidation showed that both UCPB and CPB experience reduction in volume over time due to consolidation for UCPB and additional of self-desiccation for CPB. Strain data was shown as a reference was not thoroughly explained as the objective was to improve empirical model on stress prediction.

Based on the stress change over time, an empirical model could be established based on the consolidation data of UCPB and CPB. The model fitting line in Figure 5.23 represents the best curve fitting to represent the empirical relationship between the change in vertical stress ($\Delta\sigma_v$), with the change in time (t). Equation 5.3 is proposed:

$$\Delta\sigma_{v(t)} = \sigma_{v(peak)}(A-1)(1-e^{-ct}) \qquad \text{[Equation 5.3]}$$

where, $\sigma_{v(peak)}$ is the vertical stress upon completion of deposition (maximum height of backfill), A is an average factor of stress residual at the end of consolidation over the peak stress and c is the coefficient of reduction in stress over time constants based on self-weight consolidation of backfill, and t is the time elapsed. Respective parameters of UCPB and CPB to fulfil Equation 5.3 is shown in Table 5.1. The effect of A and c is shown in Figure 5.25.

Table 5.1: Corresponding parameter for Equation 5.3

Backfill material	$\sigma_{v(peak)}$, kN/m^2	A	c
UCPB	16	0.542	0.23
CPB	17.6	0.574	12.12

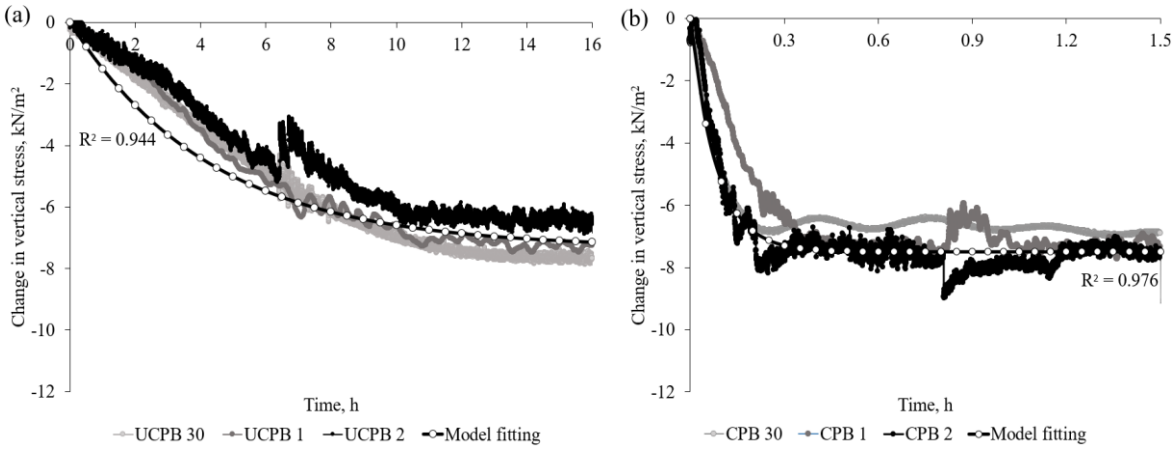

Figure 5.23: Stress behaviour of (a) CPB and (b) UCPB at controlled temperature of 30 °C

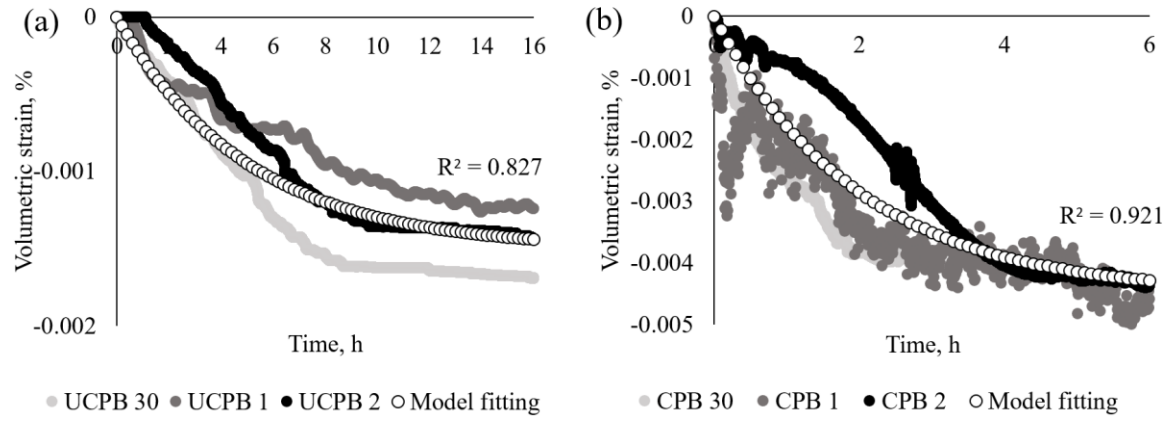

Figure 5.24: Strain behaviour of (a) CPB and (b) UCPB at controlled temperature of 30 °C

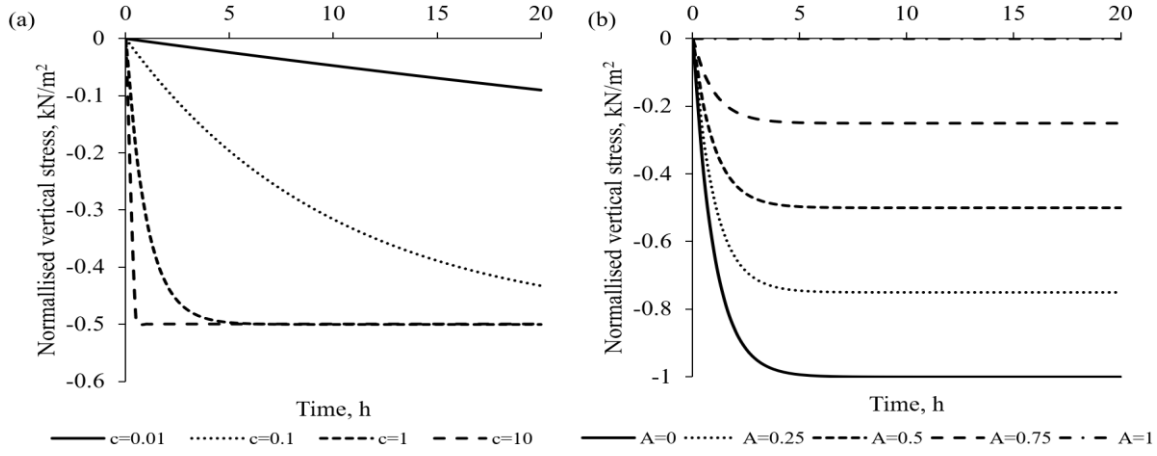

Figure 5.25: Normalised vertical stress with respect to (a) *c* and (b) *A*

5.5.3 Effect of Temperature on Stress-Strain Behaviour of Backfill

The effect of temperature change and fixed temperature on stress behaviour throughout the deposition test were studied. The strain behaviour of the backfill material was used as a reference to explain the stress behaviour. Based on the data shown in Section 5.4, Both UCPB and CPB exerted additional stress upon heating and reduced upon cooling. The magnitude of change in stress may vary due to the properties, initial peak stress, shear behaviour, and physical state of CPB and UCPB during the same temperature change. The main difference in the stress-temperature relationship between CPB and UCPB was the stress change during soak phase (temperature kept to be constant).

5.5.3.1 Effect of varying temperature on the stress-strain behaviour of backfill

Upon completion of consolidation and/or hardening of backfill material, the effect of temperature change was investigated by allowing the sample to experience various heating pattern and condition. The rate of heating and cooling were controlled for every testing. According to the temperature pattern proposed from Table 3.5, data from a specific region such as heating, soaking, and cooling were extracted and compared via stress-stress-temperature relationship.

Heating was divided into multiple steps heating (every 10 ℃ increments) and one step heating (30 ℃ increments) within the range of study from 30 ℃ to 60 ℃. Figure 5.26 and Figure 5.27 show the stress behaviour of backfill at every elevation of 10 ℃ and an elevation of 30 ℃ for all CPB and UCPB temperature varying deposition test. The change in vertical stress, $\Delta\sigma_v$ is the difference of vertical stress of initial vertical stress at 30 ℃ and final vertical stress recorded at elevated temperature. The change in temperature, ΔT is the differences between initial temperature and final elevated temperature.

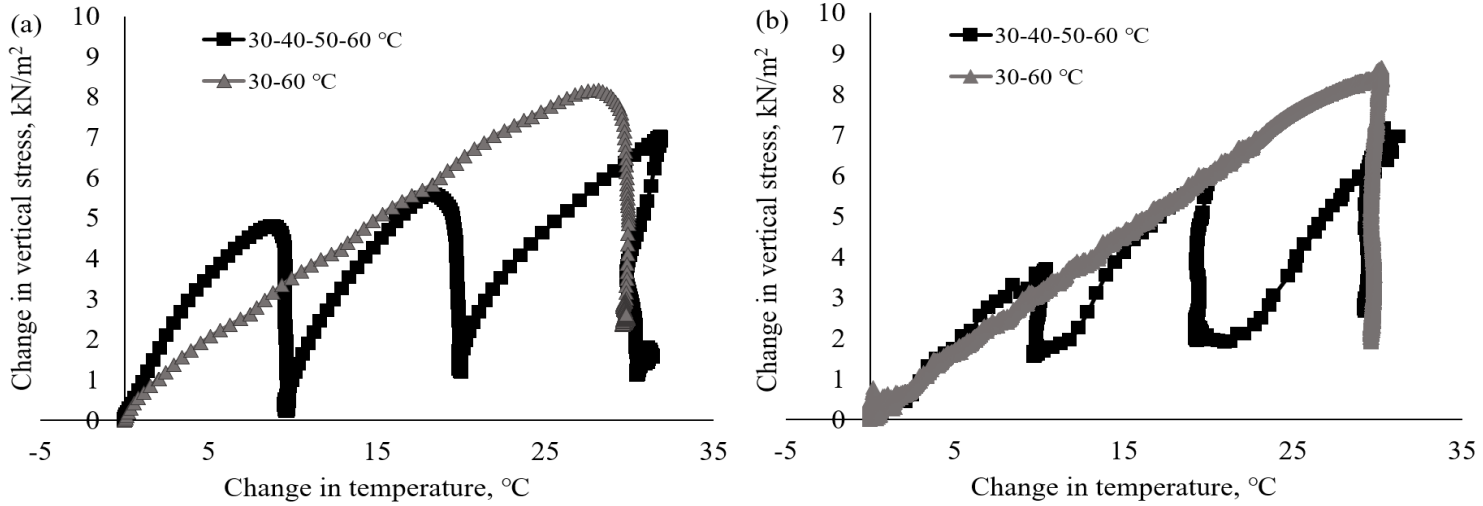

Figure 5.26: Overview of heating and soaking phase of (a) UCPB 1 and (b) UCPB 2

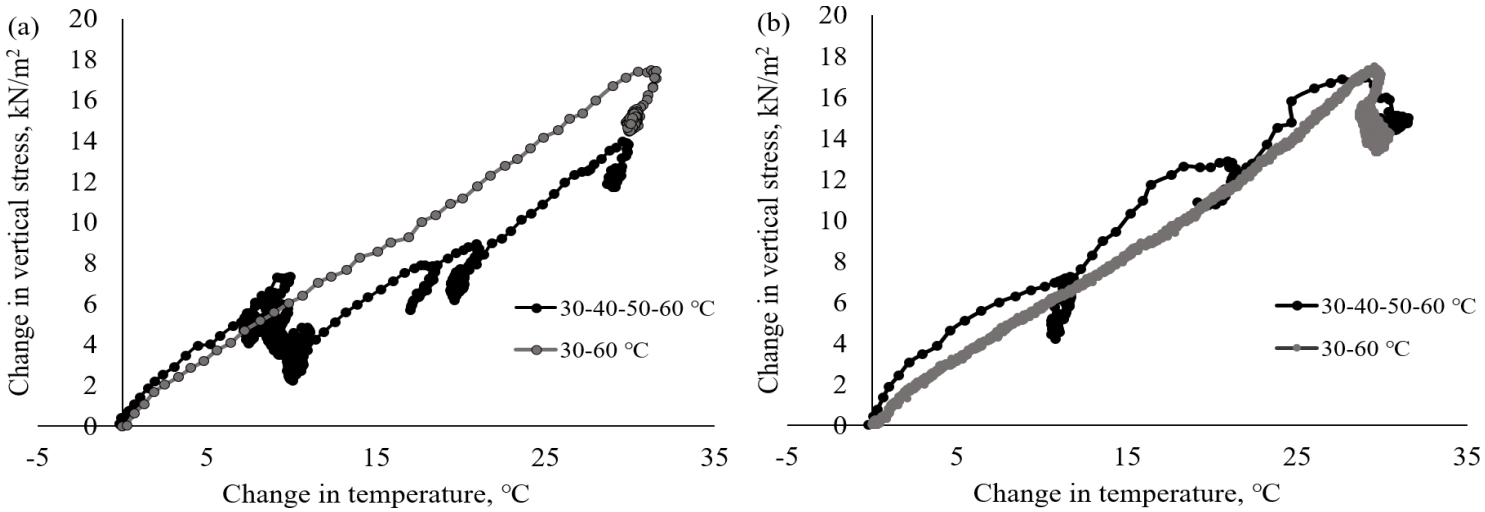

Figure 5.27: Overview of heating and soaking phase of (a) CPB 1 and (b) CPB 2

Generally, every deposition test comprising of either UCPB or CPB at any temperature exerted additional stress when there was an increase in temperature. This showed that the temperature change is responsible for the stress change. Theoretically, when the volume of a mass was allowed to expand freely (unconfined) upon temperature change, it shall not exert additional pressure (stress). However, the NW was considered as semi-confined where only the top part was unconfined.

In the case of mine backfilling where the backfilling dimension is narrow, and the backfill material is frictional and cohesive, arching will occur. Due to the friction behaviour of backfill and cohesive properties of CPB towards its adjacent sidewall, thermal expansion due to temperature change was resisted by the shear within the material and along the interface (sidewall). This showed that the particles must overcome some of the resisting force (frictional behaviour) as a response to expand thermally. While the backfill material was held up by the resisting force, stress were exerted to the opposite direction of the NW where one of the directions was to the bottom (base). Thus, some of the thermal expansion held up by the arching was converted into thermal stress. Such stress was lower than the actual stress of the backfill material if the material were to be tested on a fully confined condition. Depending on the properties of the backfill material and the geometry of the stope, the intensity of arching varies.

In contrast with the heating process, the soaking process showed a drop in the total vertical stress, which brings back the total vertical stress to its consolidated state. This implies that the change in the total vertical stress with respect to its consolidated state equals to zero ($\Delta\sigma_v = 0$) if there is no change in temperature ($\Delta T = 0$). Therefore, UCPB is speculated to experience stress reducing mechanism namely relaxation during soak phase.

Figure 5.28 and Figure 5.29 show the relationship between the change in vertical stress ($\Delta\sigma_v$) and the change in temperature (ΔT) for the three steps during the temperature heating period. The patterns for the three steps were the same, and the empirical formulation of the relationship could be established. The thermal stress generated by both UCPB and CPB were dependent on the total change in temperature and independent on initial temperature prior to heating.

Figure 5.30 highlight the comparison of stress change in both material after heated by 30 ℃. As the heating time was longer, the change in stress was more linear to the change in temperature. Figure 5.31 shows the strain behaviour of UCPB and CPB at an elevation of 10 ℃. Generally, the volume of backfill increases during heating.

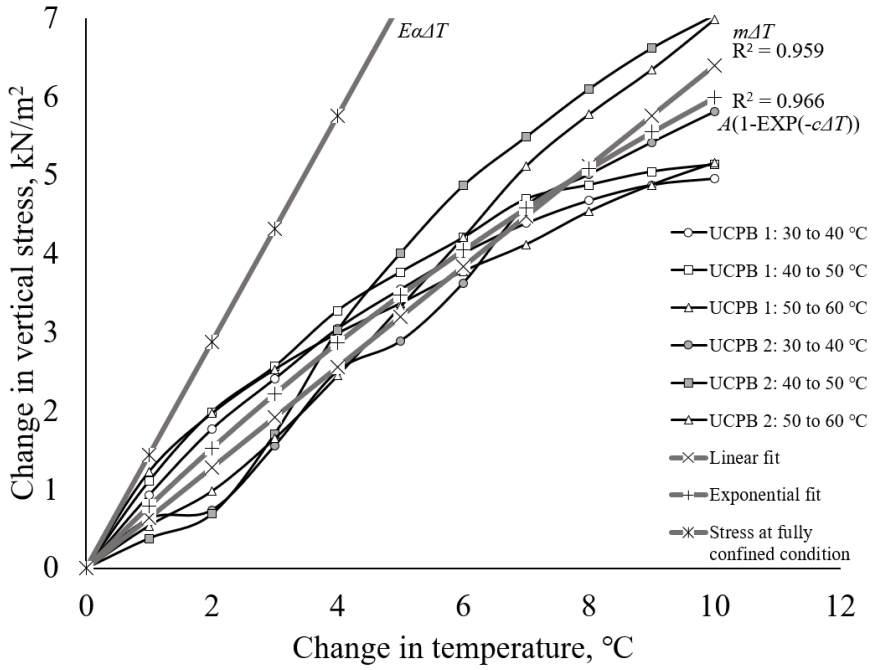

Figure 5.28: Stress behaviour of UCPB at every elevation of 10 ℃

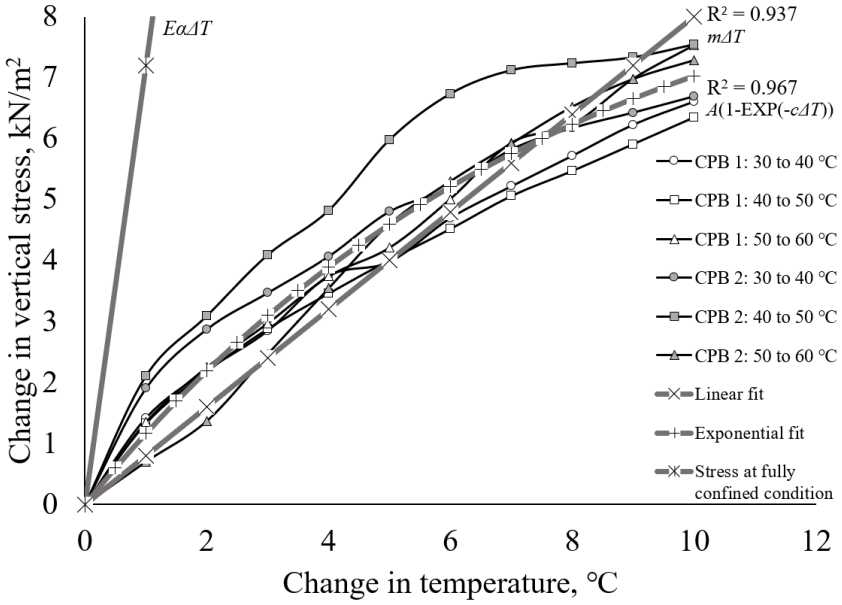

Figure 5.29: Stress behaviour of CPB at every elevation of 10 °C

Attempts had been made to curve fit the experimental data points. The linear fit in Figure 5.29 and 5.30 represents the best curve fitting to represent the empirical relationship between the change in vertical stress ($\Delta\sigma_v$) and the change in temperature (ΔT). The following form of the equation is proposed:

$$\Delta\sigma_{v(\Delta T)} = m\Delta T \qquad \text{[Equation 5.4]}$$

where, m is the average stress-temperature gradient obtained from the average of stress change per Celsius (kN/m2 / °C) for each of the backfill material. The model fitting showed a linear relationship between stress change and temperature change. The predicted stress was higher than the actual stress because the thermal stress generated at the beginning of heating experienced stress relaxation mechanism. At low-temperature change, the thermal stress generated was also low. Therefore, the relaxation occurred at the beginning of heating was low as relaxation was dependent on the thermal stress and properties of the material. As

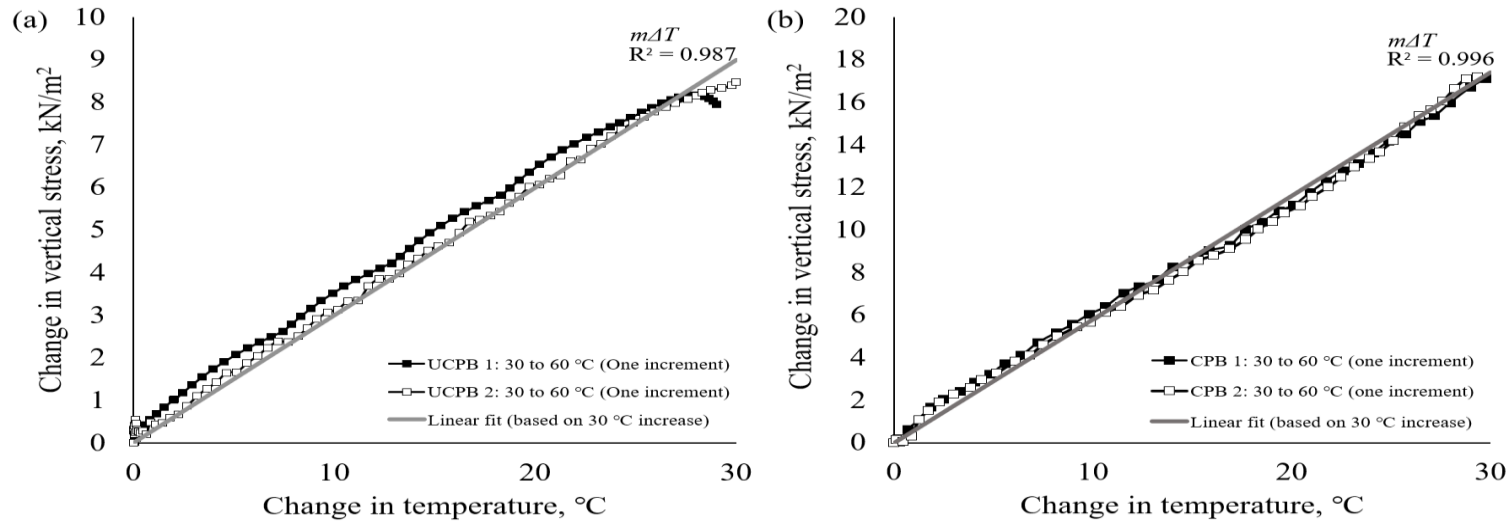

Figure 5.30: Stress behaviour of (a) UCPB and (b) CPB at an elevation of 30 °C

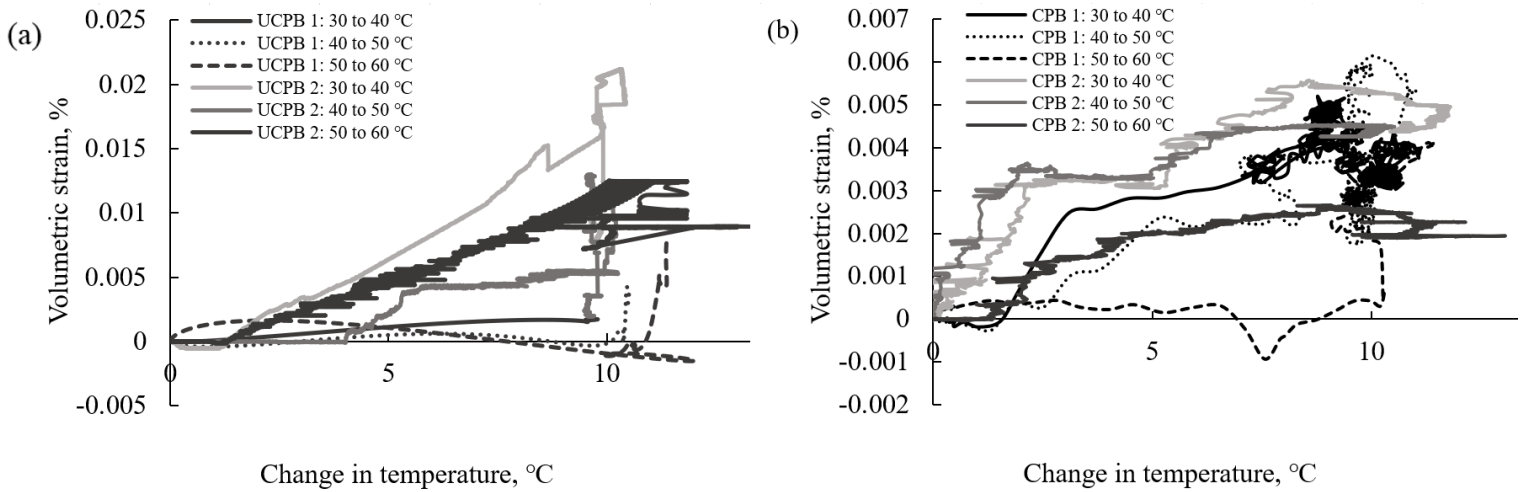

Figure 5.31: Strain behaviour of (a) UCPB and (b) CPB at an elevation of 10 °C

relaxation occurred with the function of time, the reduction in stress when there was no more gain in thermal stress at the soaking stage could be clearly seen for both materials as time elapsed.

Soaking behaviour was investigated and compared at different soaking temperature. After heating or cooling, the test was also controlled (soak) at a targeted temperature until no further change in vertical stress, and volumetric strain was observed.

Figure 5.32a and Figure 5.32c show that there was a significant reduction in stress when the temperature was kept constant (±2 °C) after heating it for 10 or 30 °C. Note that both UCPB and CPB experienced an insignificant reduction in stress when it was kept at a constant temperature after cooling. The reduction in stress due to relaxation was lesser when soaked after heating to a higher temperature which was found to be true for both UCPB and CPB test. UCPB which did not undergo hydration experiences stress reducing mechanism namely relaxation also known as creep. As the backfill material was fully consolidated at 30 °C before any temperature change, the backfill material is assumed to be in closely packed form. During heating, the material thermally expanded but some of the expansion were restricted by arching which resulted in additional pressure within the material. This additional pressure was generated when the thermal stress from the thermal expansion was restrained by the arching effects. When the material was kept at a constant temperature after heating, the excessive thermal stress reduced due to relaxation. Relaxation was a time-dependent phenomenon where the thermal stress was relieved over time (Figure 5.33).

Figure 5.32b and Figure 5.32d show that CPB experience lesser reduction in stress while soaking within the targeted constant temperature (±2 °C). The magnitude of reduction in stress was dependent on the current state of the backfill material which showed that UCPB

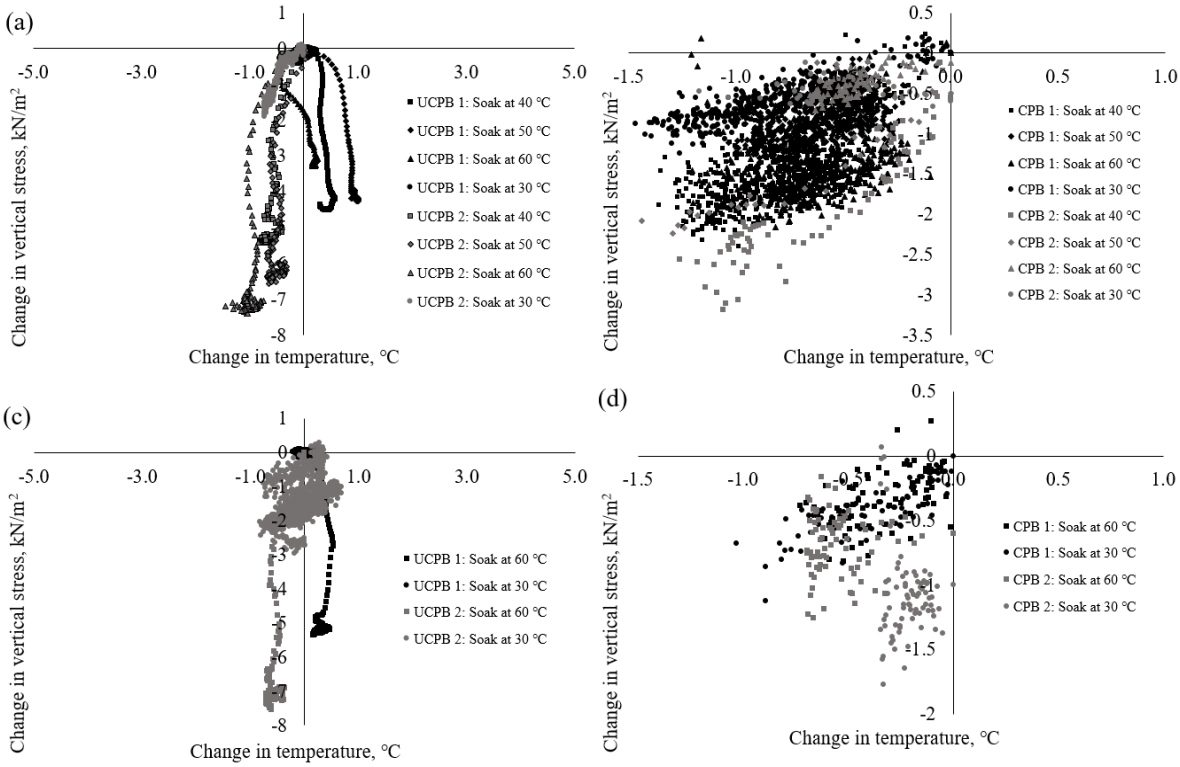

Figure 5.32: Stress behaviour at constant temperature: (a) UCPB after 10 °C, (b) CPB after 10 °C, (c) UCPB after 30 °C and (d) CPB after 30 °C temperature change (ramp)

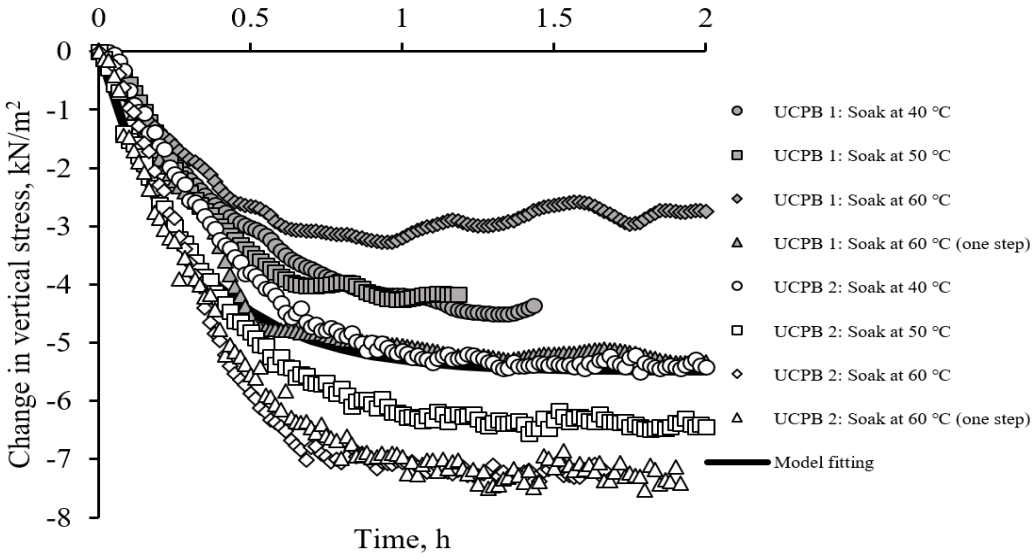

Figure 5.33: Change in the vertical stress of UCPB over time during soaking

clearly had greater reduction in stress in comparison to CPB regardless the soak temperature. CPB is a hydrating material that will harden over time. As CPB hardens, it shall behave elastically which hinders the stress reducing mechanism (relaxation).

According to Figure 5.9 and Figure 5.10, relaxation while CPB was soaking diminish at later time of the testing due to the hardening properties of CPB. Therefore, the magnitude of relaxation was less dependent on the soaking temperature and was much more dependent on the properties of the material as shown in Figure 5.34. The relaxation mechanism of CPB was less pronounced compared to UCPB due to the hydration process that hinders the capability of particle rearrangement. Yilmaz (2010) claims that as hydration progresses, cemented sample particles may be partially locked by the cement bonds based on 1-D consolidation test with UCPB and CPB at different curing days.

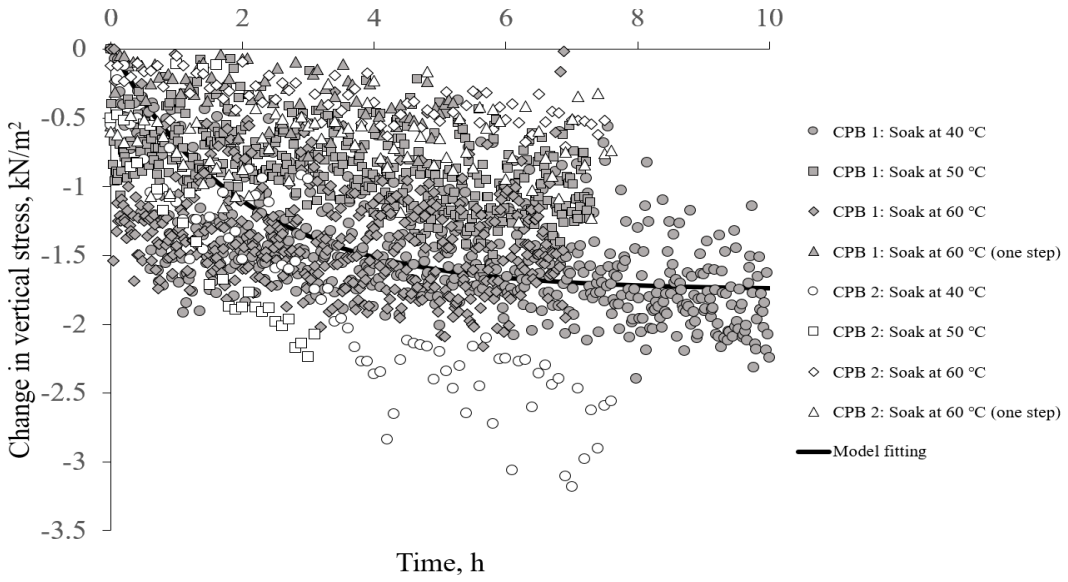

Figure 5.34: Change in the vertical stress of CPB over time during soaking

During cooling, the volume of the backfill material reduced according to the change in temperature. Due to the relaxation that occurred during soaking after heating to a higher temperature, the net stress was considerably lower than the stress recorded at the end of consolidation at 30 °C. Only one step cooling (60 to 30 °C) was practised in this experimental approach as steps cooling may results in undesirable spike in stress-strain behaviour due to the limitation of the temperature controller. Figure 5.35 shows the cooling behaviour of UCPB and CPB. As CPB was elastic, the change in stress was nearly linear to the change in

temperature. The behaviour of UCPB during cooling was inconsistent but generally still showing a reduction in stress during cooling. The inconsistency could be due to the coupled effect of thermal shrinkage and rapid relaxation. The reduction in stress during cooling was lesser in UCPB because most of the thermal stress gain has been dissipated by the relaxation mechanism during the soaking phase. Thus, only the remaining thermal stress was reduced during cooling. From Figure 5.7 and Figure 5.8, the final net stress after the UCPB was cooled back to 30 °C was lesser than the net stress after completion of consolidation and after the first-time cooling to 30 °C. This was found to be true for both UCPB 1 and 2 tests. Arching effect was not evident in the cooling behaviour of CPB as thermal shrinkage occurred at all inward direction, but it is still evident within the particles of UCPB. It was assumed that the magnitude of arching effect when UCPB was cooling is insignificant. Since UCPB is a non-hydrating material, it shall remain in paste form throughout the experiment. When UCPB was volumetrically reduced due to thermal shrinkage during cooling, re-establishment of arching effects occurred due to gravitational consolidation in order to fill out the space created during consolidation which results in possible extension of stress reduction after completion of cooling.

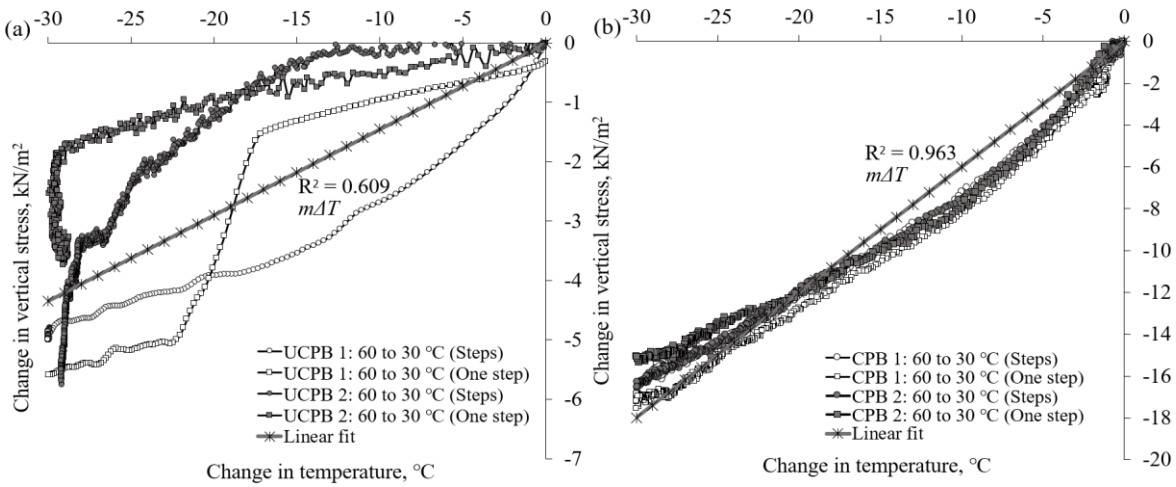

Figure 5.35: Stress behaviour of (a) UCPB and (b) CPB during cooling by 30 °C

Figure 5.36 shows the strain behaviour of UCPB and CPB during cooling. The volumetric strain reduced with respect to temperature decrease. This showed that the stress reduction was due to the volumetric shrinkage of the backfill material that reduces the thermal stress generated during the heating period. The reduction in volume recorded by the potentiometer was inconsistent due to the ability of the probe to extrude smoothly.

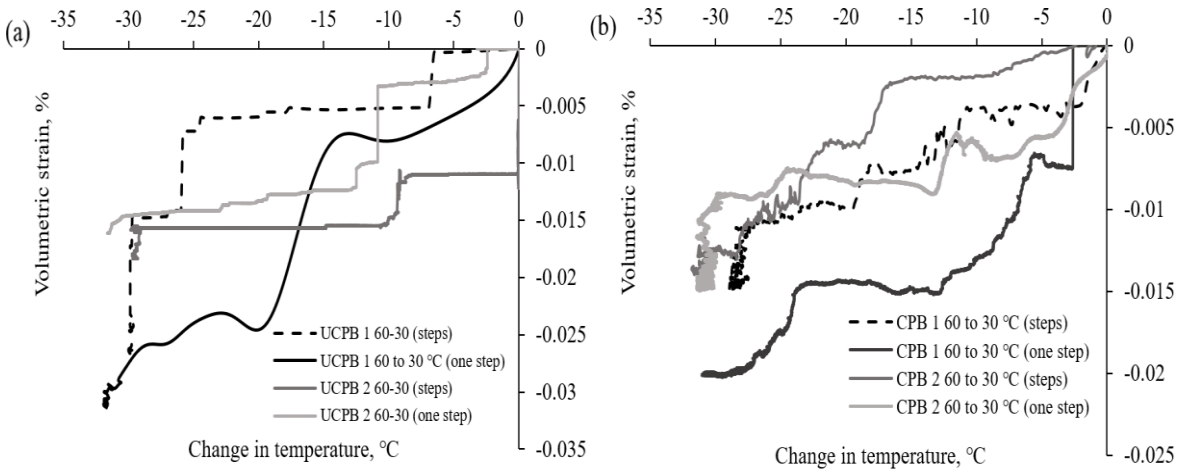

Figure 5.36: Strain behaviour of (a) UCPB and (b) CPB during cooling by 30 °C

5.5.3.2 Effect of fixed temperature on the stress-strain behaviour of backfill

In the actual practice of mine backfill, CPB was usually backfilled into a stope without controlling the current temperature of the stope wall. The effect of curing temperature for the deposition tests conducted at a controlled temperature was studied by analysing the behaviour of backfill material when it was heated, soaked, and cooled. The effect of temperature on stress-strain behaviour could be seen in Figure 5.11 to Figure 5.18.

Figure 5.37 shows the stress behaviour of CPB and UCPB when deposited into the NW that were controlled at the targeted temperature. Heat transfer into the backfill material from the narrow was allowed from the beginning of the deposition until the backfill material reached the targeted temperature. The backfill material underwent different change in stress when backfilled into the NW at different target temperature. The higher the target

temperature, the greater the final stress upon reaching the targeted temperature. CPB showed a greater effect on stress gain when the temperature was increased in comparison to UCPB. The reduction in stress due to consolidation in CPB 50 had been overcame by the thermal stress generated. As for CPB 60, the thermal stress exceeded the stress reducing mechanism and resulted in higher stress than the initial peak stress. As higher temperature would promote hydration process, CPB deposited at a higher temperature would establish higher strength at an earlier stage in comparison to CPB cured at a lower temperature. The shear strength of CPB 60 was higher, and it had been established that the friction angle and cohesion of the same material were higher when tested at a higher temperature. This resulted in a greater arching effect and thus greater resistance to thermal expansion that resulted in greater thermal stress.

As for UCPB, the stress generated is lower in comparison to the stress generated by UCPB that was fully consolidated. These UCPB tests had not established proper arching effects at the early stage of deposition. In comparison to the time required for UCPB to be fully consolidated which was about 16 hours (based on Figure 5.23), the longest time required for UCPB to be heated to a higher temperature that is a total gain of 30 ℃ (30 ℃ to 60 ℃) only took around 1 hour. This showed that the arching effect was not well established and the UCPB which was in the slurry state had less constraint from thermally expand in comparison to UCPB test that is fully consolidated. This was true when the variety of temperature does not affect stress generation at an earlier stage. Since UCPB 60 takes a longer time to be heated to 60 ℃, some arching may have been established. Therefore, some gain in thermal stress is observed when the temperature approaches 60 ℃.

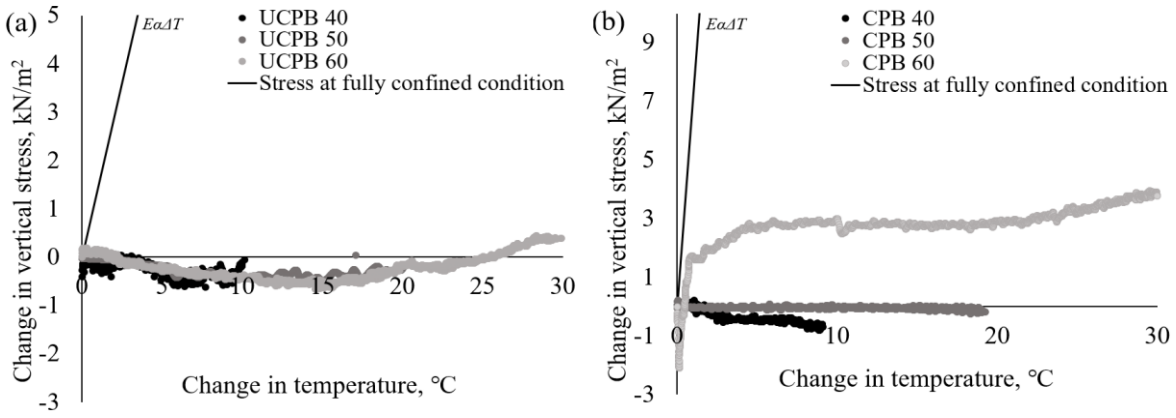

Figure 5.37: Initial stress behaviour of (a) CPB (b) UCPB when backfilled into the NW at a controlled temperature

Upon reaching the targeted temperature, the backfill material was left to soak until the responding variable stabilised. As the backfill material was not allowed to consolidate before any change in temperature, the backfill material was still consolidating during the soaking phase at the respective targeted temperature. For UCPB, the coupled effect self-weight consolidation, thermal expansion and relaxation occurred simultaneously which resulted in a great reduction in stress for every UCPB samples. The reduction in stress was lesser at a higher temperature because of the higher friction angle as the intensified arching prevents further relaxation by retaining more the thermal stress generated during temperature increase. As for CPB, consolidation was still possible as the testing was still in the early stage of cement hydration. But upon curing at a higher temperature, it would accelerate the reaction process of hydration. Therefore, it promotes early strength development. As early strength was developed by CPB that was tested at a higher temperature, the frictional properties of CPB was enhanced too. In addition to the increase of friction angle and cohesion due to accelerated hydration, higher curing temperature also increased the friction angle and cohesion of CPB as discussed in Section 4.3.4. This showed that when CPB was cured within a NW at elevated temperature, the improvement of its shear behaviour could intensify arching that was even greater than UCPB. Furthermore, CPB at higher temperature

was more likely to behave like elastic material instead of paste due to early strength development which also showed that the elastic modulus of CPB is greater than CPB at lower temperature. Therefore, CPB should experience less relaxation and generate more thermal stress due to greater thermal expansion and arching effects at higher temperature.

Figure 5.38 shows the change in stress at a constant temperature of ±2 °C while Figure 5.39 shows the change in stress with respect to time elapsed. After heating, UCPB experience more reduction in stress due to relaxation in comparison to CPB.

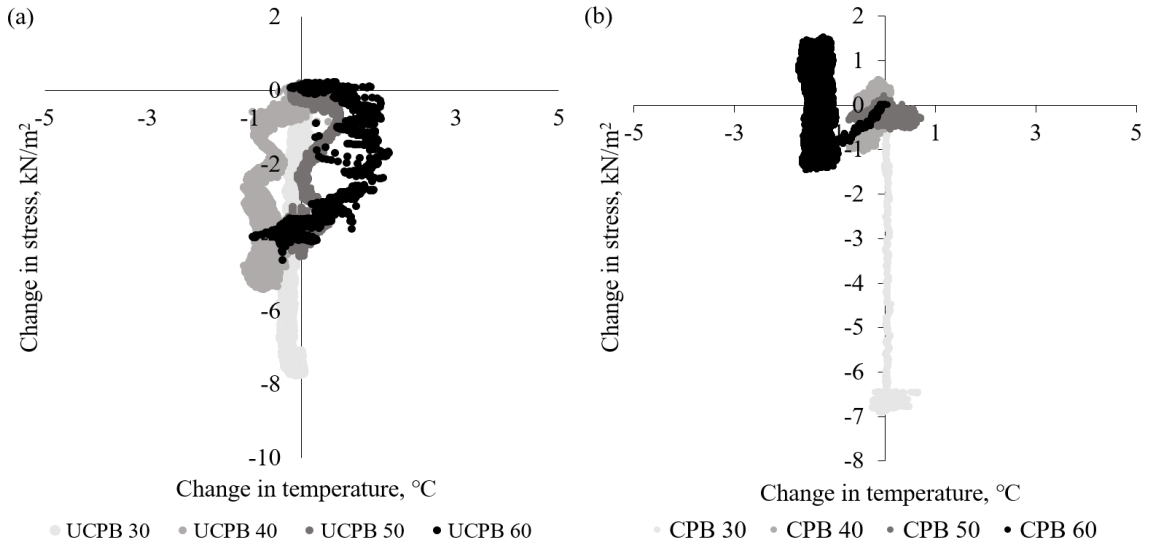

Figure 5.38: Change in vertical stress over temperature change for (a) UCPB and (b) CPB

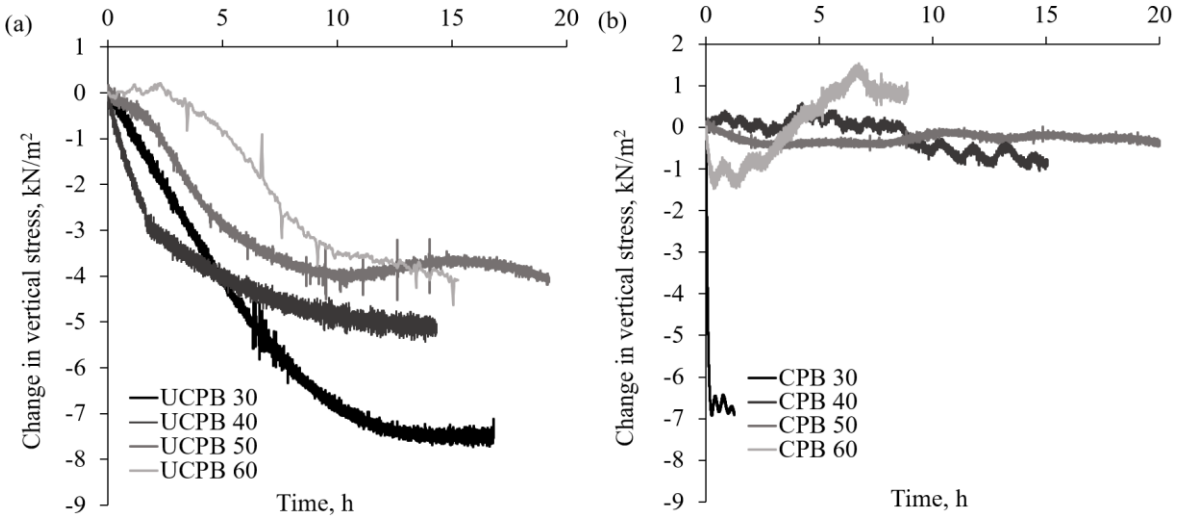

Figure 5.39: Change in vertical stress over time for (a) UCPB and (b) CPB

Once the stress behaviour stabilised (fully consolidated, relaxed, and thermally expanded) during the soaking phase, the temperature was reduced back to 30 ℃ to investigate the effect of cooling. All backfill material experienced a reduction in stress during cooling (As shown in Figure 5.40). UCPB 60 has the greatest reduction due to the relief of thermal stress that was retained during soaking, and same goes to CPB 60. The effect of cooling was scattered due to insignificant volumetric strain and thermal stress generated upon low-temperature change.

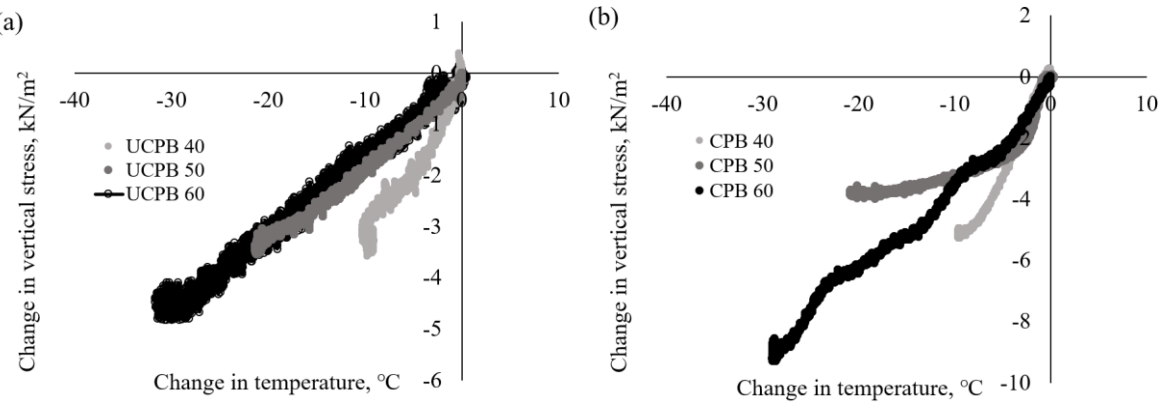

Figure 5.40: Change in stress while cooling (a) CPB and (b) UCPB

The data collected from the deposition test conducted at fixed temperature could serve as a great reference. But due to the complexity of multiple factors that simultaneously contribute to stress changes, the data and analysis from backfill that was fully consolidated prior any temperature change was used to generate a model that could predict the stress behaviour with respect to temperature change.

5.6 Generation of Model

The slurry was low in friction during deposition prior to consolidation. Therefore, vertical stress generated upon deposition was predicted using friction angle near to zero. The peak vertical stress, ($\sigma_{v(peak)}$) of the backfill was obtained upon the maximum height of backfilling. Assuming that friction angle is negligible at deposition stage and insignificant

consolidation due to short deposition period, horizontal stress is negligible as there is no transfer due to arching effects that is based on the friction angle of the material. The vertical stress upon of deposition, ($\sigma_{v(dpst)}$) and peak vertical stress, ($\sigma_{v(peak)}$) is expressed in Equation 5.5 and Equation 5.6 below.

$$\sigma_{v(dpst)} = \gamma lw \frac{1-\exp\left\{-2K\tan\varphi h\frac{(l+w)}{lw}\right\}}{2K\tan\varphi\ (l+w)} \quad \text{[Equation 5.5]}$$

$$\sigma_{v(peak)} = \gamma lw \frac{1-\exp\left\{-2K\tan\varphi h_{max}\frac{(l+w)}{lw}\right\}}{2K\tan\varphi\ (l+w)} \quad \text{[Equation 5.6]}$$

where, γ is the unit weight of the backfill material, l is the length of the NW, w is the width of the NW, h is the height of backfill during backfilling, h_{max} is the maximum height of backfill upon completion of backfilling, ϕ is the friction angle of the backfill material, and K is the earth pressure coefficient at rest.

Upon completion of the deposition, the slurry began to consolidate due to the self-weight of the backfill particles that resulted in the reduction in stress observed in full-scale monitoring and laboratory-scale testing. As the material consolidates, the frictional properties of the material are intensified. This allowed the stress transfer phenomenon or arching effects to occur which resulted in a reduction of vertical stress recorded at the bottom of the backfilling. The reduction of stress due to consolidation is mainly associated with time and properties of the material. UCPB is an inert material where its physical and chemical properties do not change over time, but CPB is a hydrating material that is subjected to chemical processes such as hydration/cementation that will chemically alter the properties and state of matter of CPB over time. For this study, the effect of self-weight consolidation for CPB and UCPB was only associated with time and unit weight of the respective material. The peak stress obtained from Equation 5.6 is used as the reference point to indicate the

maximum stress at the beginning of consolidation (t = 0). Therefore, the resulting vertical stress ($\sigma_{v(t)}$) at time (t = *t*) could be express as Equation 5.7 below.

$$\sigma_{v(t)} = A\sigma_{v(peak)} + \sigma_{v(peak)}(1 - A)(e^{-ct}) \quad \text{[Equation 5.7]}$$

where, $\sigma_{v(peak)}$ is the vertical stress upon completion of deposition (maximum height of backfill), A is an average factor of stress residual at the end of consolidation over the peak stress and *c* is the curvature of reduction in stress over time constants, and *t* is the time elapsed. The change in vertical stress due to consolidation phase could be express as Equation 5.8 below.

$$\Delta\sigma_{v(t)} = \sigma_{v(t)} - \sigma_{v(peak)} \quad \text{[Equation 5.8]}$$

$$\Delta\sigma_{v(t)} = \sigma_{v(peak)}(A - 1)(1 - e^{-ct}) \quad \text{[Equation 5.9]}$$

The change in stress due to temperature change could be predicted using Equation 5.4. The reduction in stress during soaking due to relaxation was known as plastic strain that is non-recoverable. Therefore, it was not considered in the generation of the model. Since relaxation was found to be inconsistent throughout the testing program, the model was designed to be able to predict the stress generation at a safe level. This showed that the model shown in Equation 5.10 below is capable of predicting maximum vertical stress, ($\sigma_{v(spp)}$) based on the type of backfill and its properties (Equation 5.5), effect of consolidation time (Equation 5.9), and temperature change (Equation 5.4).

$$\sigma_{v(spp)} = \sigma_{v(dpst)} + \Delta\sigma_{v(t)} + \Delta\sigma_{v(\Delta T)} \quad \text{[Equation 5.10]}$$

The proposed model was generated based on UCPB and CPB data that was tested at the fully consolidated condition. Therefore, the model was checked with its actual data based on the same properties and parameters input for both UCPB and CPB. Figure 5.41 and Figure 5.42 show predicted vertical stress generated from the model and compared with actual data.

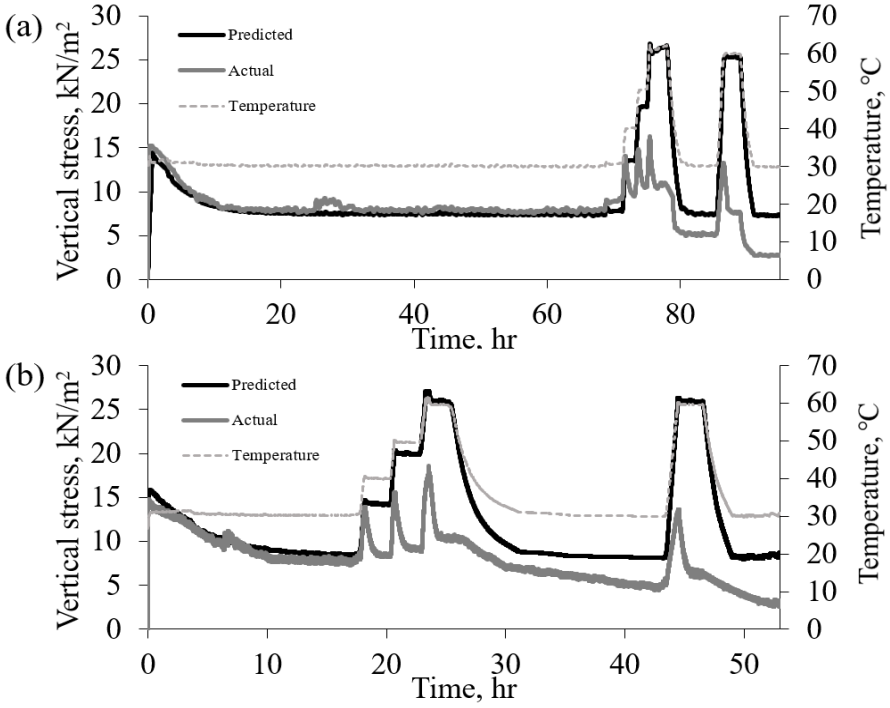

Figure 5.41: Predicted vs actual vertical stress with respect to change in temperature and time of (a) UCPB 1 and (b) UCPB 2

The predicted data for UCPB deposition test showed good correlation with the actual data for the deposition phase and consolidation phase. During heating, the maximum thermal stress generation predicted similar with the actual data. But, the model did not incorporate the stress reducing mechanism (relaxation) which is known as non-recoverable plastic strain of the material. At the end of the cooling, the model predicted slightly higher stress than the actual data. Whereas, the predicted stress at the end of cooling was similar to the stress before heating (at the same temperature). This showed that the model was stating that the thermal stress is fully recoverable. Such higher stress prediction was accepted as safety factor because the relaxation mechanism was inconsistent (especially for UCPB) throughout the temperature change period which may result in underestimation of stress if the estimation of relaxation were to be incorporated. The model showed a good prediction of maximum vertical stress to be expected when UCPB was deposited into a specific dimension of the NW and underwent temperature change during the curing period.

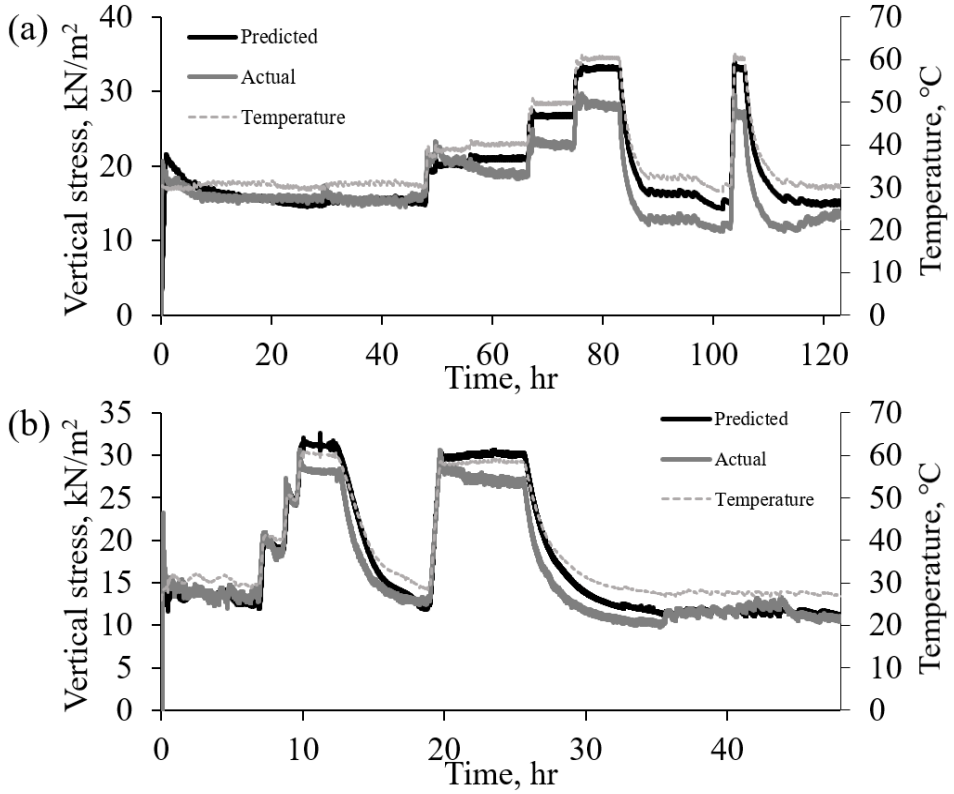

Figure 5.42: Predicted vs actual vertical stress with respect to change in temperature and time of (a) CPB 1 and (b) CPB 2

Similar with UCPB, CPB also experienced stress relaxation when there was additional thermal stress. Therefore, the predicted vertical stress during soaking was slightly higher than the actual data. Figure 5.43 shows the adequacy of predicted vertical stress was checked by comparing the actual vertical stress versus predicted vertical stress with actual versus actual vertical stress. Similarly with Figure 5.41 and Figure 5.42, the proposed model was shown to be suitable for CPB with a higher coefficient of determination in comparison to UCPB. Generally, the predicted data for CPB also showed a good correlation with the actual data for every phase. This showed that the proposed model was capable of predicting vertical stress change with respect to temperature change for both of the backfill material under controlled condition (heating occur after the material is fully consolidated).

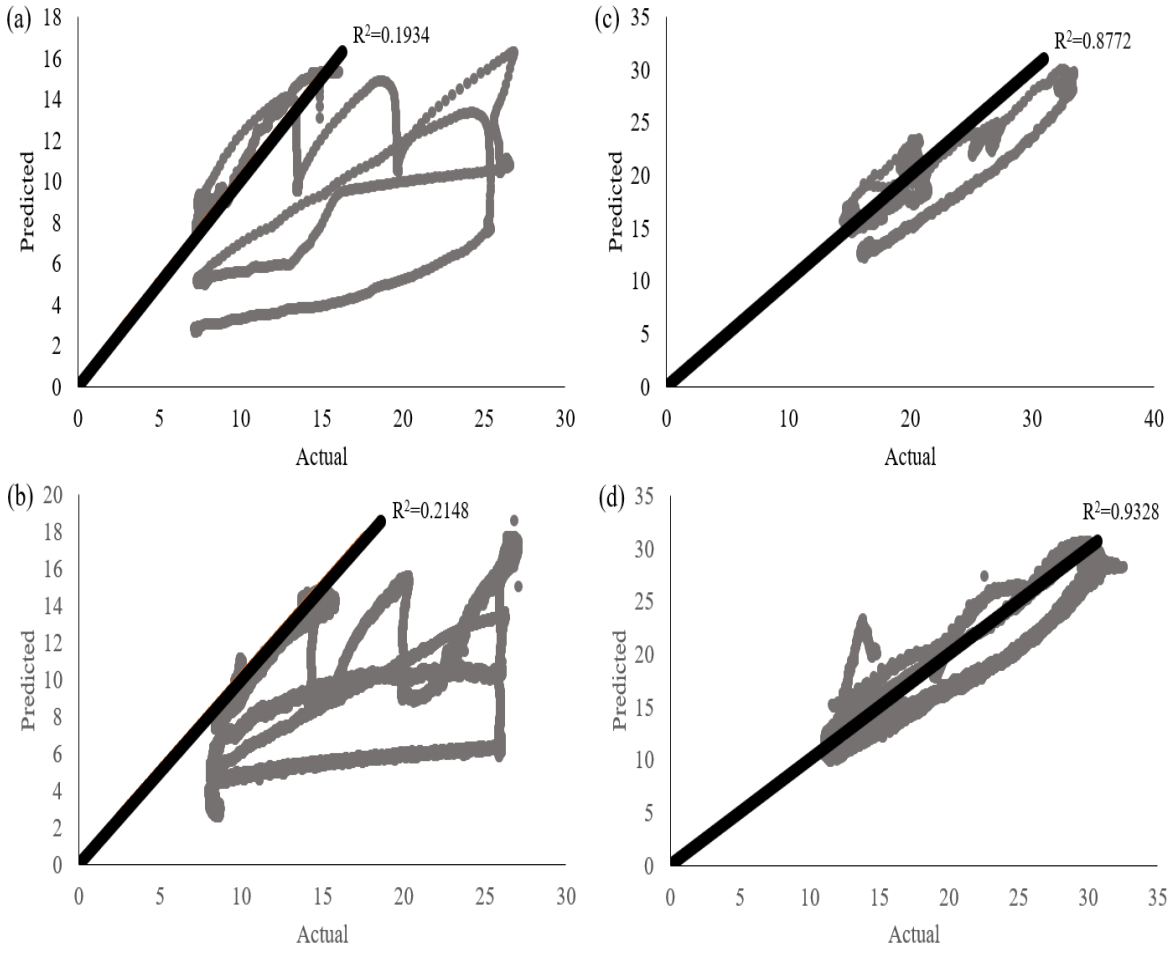

Figure 5.43: Adequacy of vertical stress prediction for (a) UCPB 1, (b) UCPB 2, (c) CPB 1, and (d) CPB 2

5.7 Diagnostics of Model Adequacy

The model was used to predict the stress behaviour of laboratory deposition test conducted at a fixed temperature (consolidation and temperature change concurrently) and full-scale monitoring data from the published work to determine the adequacy of the model.

5.7.1 Experimental Data

The fixed temperature deposition test was conducted to show greater similarity to actual mine backfill where the temperature was induced before the initiation of deposition and completion of consolidation. The changes in stress behaviour were subjected to multiple known factors (i.e. temperature change and consolidation) that prevent accurate analysis or

modelling on the effect of each contributing factors towards its stress behaviour. Thus, based on the model generated from the temperature varying deposition test, the model was expected to be able to predict the stress behaviour of the deposition test conducted at a fixed temperature. With the correct inputs of parameter into the proposed model, the predicted versus actual stress behaviour of every fixed temperature deposition test is shown in Figure 5.44.

For UCPB 30 and CPB 30 tests, the proposed model could predict the vertical stress generated from deposition and stress reduction due to the consolidation of backfill material over time. As for UCPB 40, UCPB 50 and UCPB 60, the model predicted that there shall be a significant gain in thermal stress during the short heating period. But, the actual data showed the otherwise where the vertical stress at the end of the heating is rather similar for each test. It was speculated to be caused by the coupled effect of consolidation and volumetric expansion (temperature change). The state of the material was still in slurry form (not consolidated and low in friction angle) where the material was free to expand upward without much restriction from arching effects. Thus, there was insignificant thermal stress generated. As for UCPB 60, the heating time to 60 ℃ was longer which allows the material to establish more arching effects due to greater consolidation and frictional properties at elevated temperature as discussed in Section 4.3.4. Thus, there was some gain in thermal stress when the temperature was about to reach 60 ℃, and it was proven to be true when UCPB 60 experience steep reduction in stress due to relaxation at the soaking period which did not incur to UCPB 40 and 50 that does not have significant thermal stress generated from temperature change. The stress reduction curve due to consolidation was found to be similar for both predicted and actual data during the soaking period.

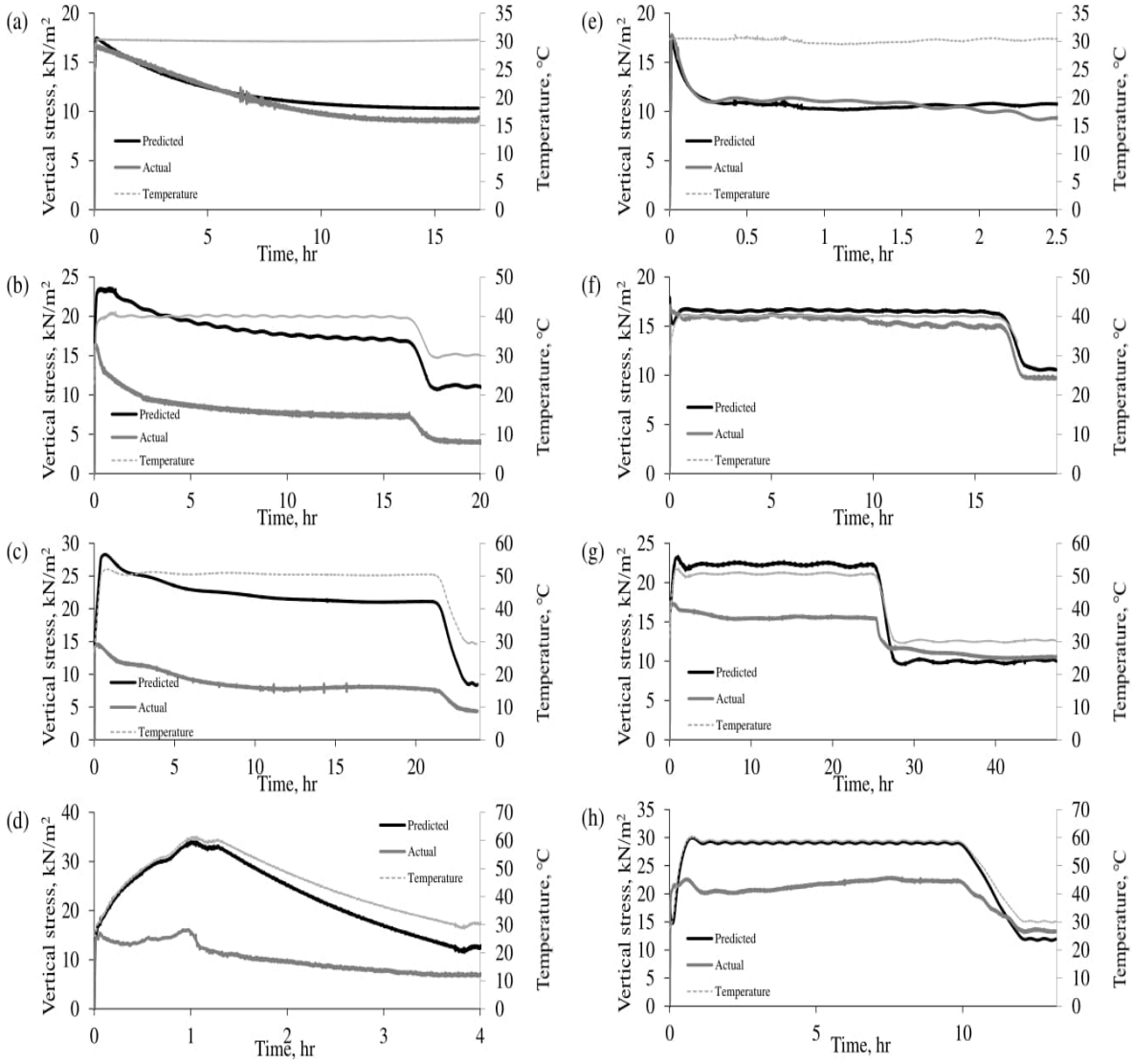

Figure 5.44: Predicted vs actual vertical stress of (a) UCPB 30, (b) UCPB 40, (c) UCPB 50, (d) UCPB 60, (e) CPB 30, (f) CPB 40, (g) CPB 50, and (h) CPB 60

As for CPB 40, CPB 50, and CPB 60, the same phenomenon to UCPB occurred. The short heating period where the CPB was not properly consolidated and harden which allowed the CPB to expand without exerting much thermal stress. Instead of reduction in stress due to consolidation as the time elapsed, CPB rapidly hydrates at higher temperature which hinders the effect of consolidation. Due to the limitation of the thermocouple placement, some temperature increase at the other region of the NW was not captured. Therefore, the self-heating mechanism of hydration (exothermic reaction) was speculated to induce additional heat and trapped mostly at the centre of the backfilling which generate minor volumetric expansion in the upward direction (observed in Figure 5.44) and some thermal stress (observed at Figure 5.44h) due to established arching effects and more volumetric expansion at harden or elastic state of CPB during the later period of deposition. Such additional stress caused the model to slightly underestimate the final stress upon cooling due to the temperature gain during hydration was not fully captured and predicted. Such shall not be an issue as the underestimation only occurred at the end of the cooling where the maximum stress was still predicted in a safe range upon higher temperature.

Figure 5.45 shows the adequacy of predicted vertical stress was checked similarly as Figure 5.43. The proposed model was shown to be suitable for CPB with a higher coefficient of determination in comparison to UCPB. Whenever UCPB experience additional heating, the stress prediction differs greater due to stress reduction from relaxation was greater at higher temperature. The coefficient of determination for CPB drops when CPB was tested at higher initial temperature. Other than the stress reduction due to relaxation, the predicted stress data for CPB showed a good correlation with the actual data for every phase. This showed that the proposed model was capable of predicting vertical stress change at coupled situation where temperature change occurred while the material was still consolidating and/or hydrating.

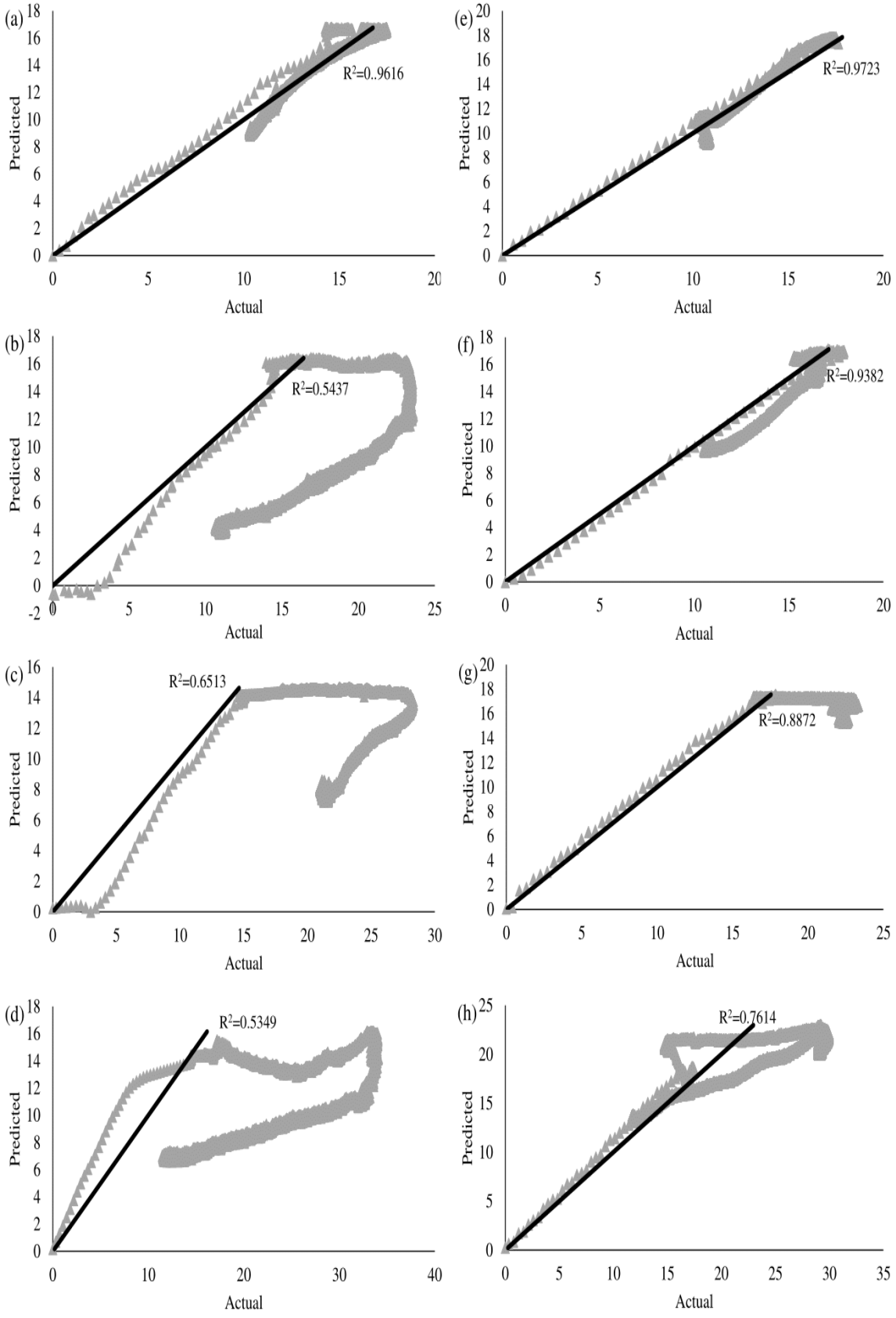

Figure 5.45: Adequacy of vertical stress prediction for (a) UCPB 30, (b) UCPB 40, (c) UCPB 50, (d) UCPB 60, (e) CPB 30, (f) CPB 40, (g) CPB 50, and (h) CPB 60

5.7.2 Full-Scale Data

The proposed model also aimed to be able to predict the stress behaviour of actual mine backfill. Based on one of the full-scale monitoring data by Thompson et al. (2012), appropriate parameters of backfill material and dimension of the stope were extracted and optimised as the inputs for the proposed model. The opening of the stope (i.e. width and length) was idealised as the adjacent wall is not perfectly shaped. Since that the CPB for the backfilling was initially in a free-flowing slurry state, the frictional angle of CPB was assumed to be very low during the deposition. The rest of the CPB properties and parameters of the backfilling were provided and used for the model prediction.

The stress behaviour of the backfill was investigated in a hydrostatic state where there was no reduction of pore water pressure. As for CPB, there might be a reduction of pore water pressure due to hydration processes. In the actual mine backfill, the adjacent wall of the stope was very stiff due to long-term exertion of pressure. Therefore, slurry with high water content could not reduce its pore water pressure by dissipating to its surrounding medium. But, in order to reduce the total pressure exerted by the backfill, barricade that allows discharge of water was usually design and used in actual mine backfill. This only applies to the deposition at the lower level. As the time elapsed, the hydration process and the increasing height of the backfilling will reduce the hydraulic conductivity, k of CPB. In this experimental approach, the testing was conducted at hydrostatic state throughout the testing. Therefore, the model generated shall predict slightly higher total vertical stress in comparison to actual full-scale monitoring data.

The monitoring was conducted at three different height at approximately the centre of each stope. The actual data (only vertical stress and temperature) was regenerated based on their finding displayed in graphs. Figure 5.46a to Figure 5.46c shows the vertical stress

versus time and temperature versus time relationship of stope 685 (one time pour) at different height while Figure 5.46d to Figure 5.46f shows the vertical stress versus time and temperature versus time relationship of stope 685 (two times pour) at different height. Note that Figure 5.46f only experience single pour.

The predicted vertical stress from the model was generally accurate, and the difference could be explained based on the understanding of the previously discussed mechanism at Section 5.5. Basically, the model showed an accurate prediction for every pouring stage (either single pour or multiple pours). The main reason behind the differences between predicted data and full-scale data was due to the time of temperature change. It was observed when the temperature changes rapidly during the backfilling stage, the backfill sample was allowed to thermally expand without generating any significant thermal stress which resulted in lower actual stress than the prediction.

When the was change in temperature after the completion of backfilling (Figure 5.46c), the thermal stress was not dissipated whereas it was generated with temperature gain as the CPB was consolidated and harden at some time after the backfilling. For most of the cases, the temperature increased during the backfilling due to the higher initial temperature of the stope. Therefore, most of the thermal stress generation was avoided due to the free to expand state of CPB. This showed that the model could predict a safe vertical stress generation with respect to temperature change, time and number of backfilling stage. In any backfilling case where more than one pour were intended, Equation 5.10 could be derived into Equation 5.11 below that was capable to predict the vertical stress generation from multiple pours backfilling. Note that $\sigma_{v(spp)}$ is vertical stress from single pour prediction (*ssp*) and $\sigma_{v(mpp)}$ is vertical stress from multiple pour prediction (*mpp*).

$$\sigma_{v(mpp)} = \sum_{i=1}^{p} \sigma_{v(spp)_{t=i}} = \sigma_{v(spp)_{t=i}} + \sigma_{v(spp)_{t=i+1}} + \cdots + \sigma_{v(spp)_{t=p-1}} + \sigma_{v(spp)_{t=p}} \quad \text{[Equation 5.11]}$$

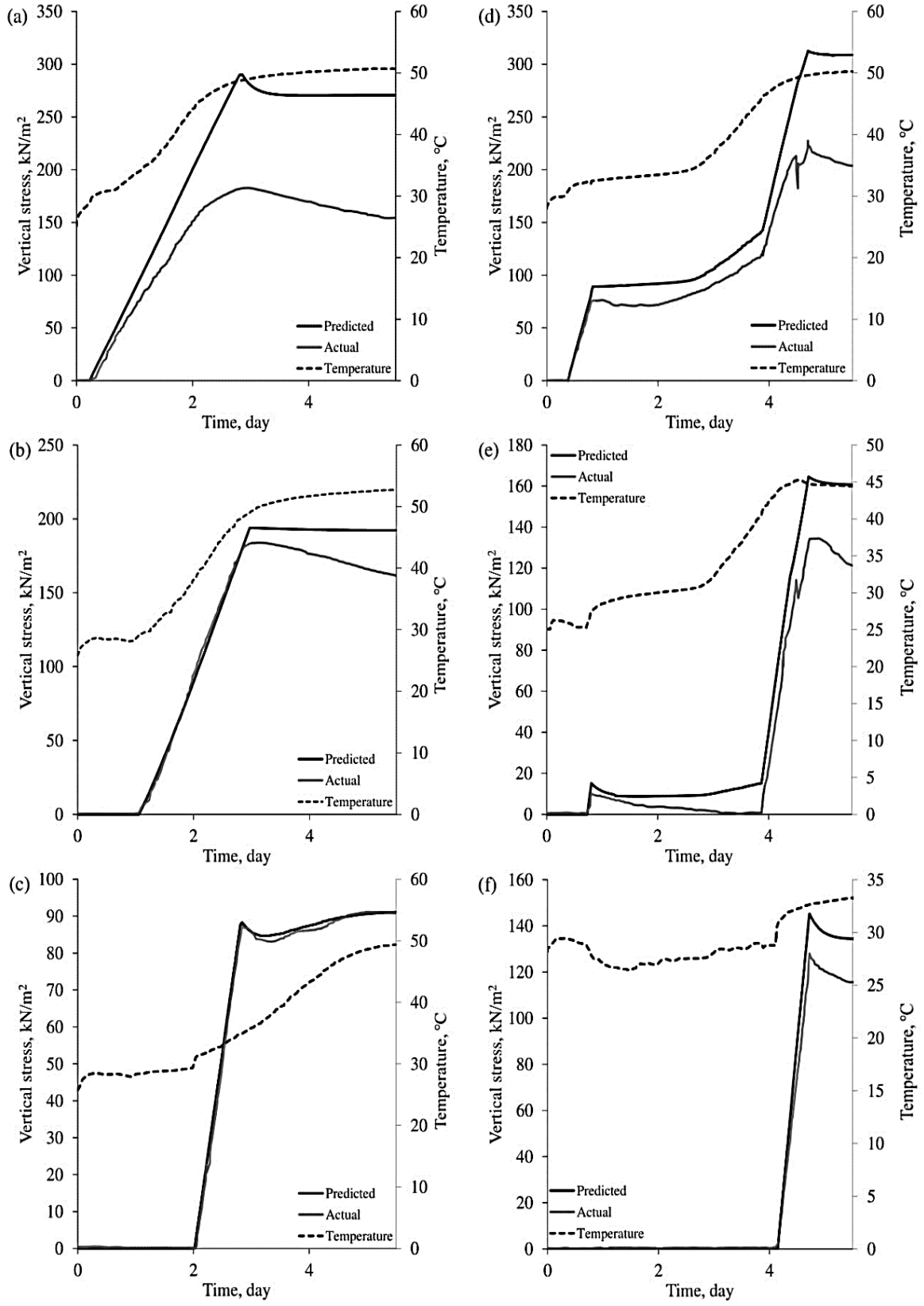

Figure 5.46: Predicted vertical stress vs full-scale monitoring data of stope 685 at (a) 2.4 m, (b) 6.4 m, (c) 11.4 m and stope 715 (d) 3 m, (e) 6 m, (f) 9 m elevation height (after Thompson et al., 2012)

Figure 5.47 shows the proposed model adequacy check with full-scale monitoring data. Similarly with the tests conducted at a fixed temperature, any temperature gain during deposition resulted in lower final stress. This caused some overprediction of stress due to the aforementioned situation. Generally, the proposed model was able to accurately predict the stress behaviour according to the full-scale data, and it was also able to prove that the stress anomaly was partly caused by the change in temperature during and after deposition. Such model was able to improve the understanding on the stress behaviour during deposition at elevated temperature and to provide a safer prediction of total stress prior structural design.

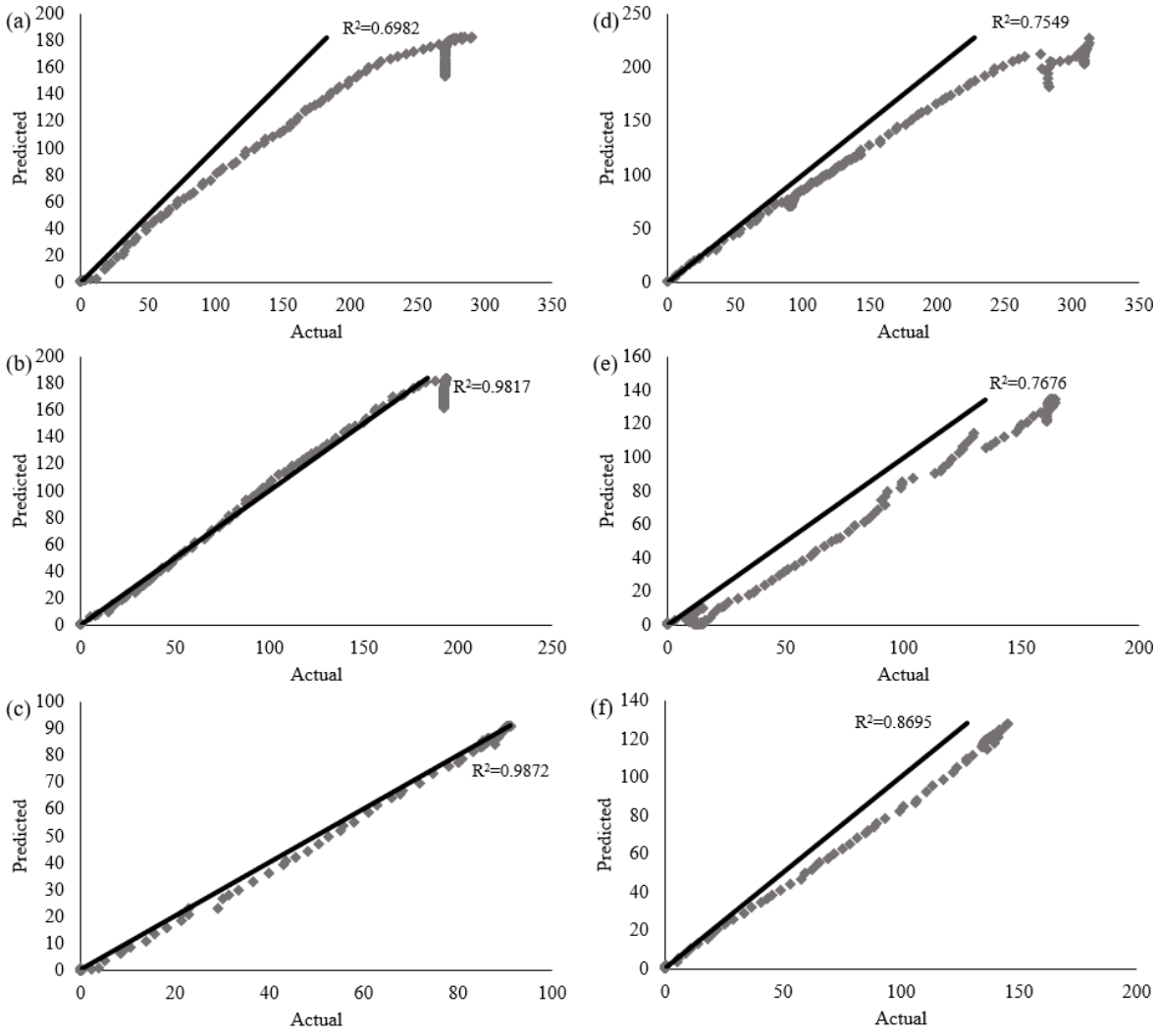

Figure 5.47: Adequacy of vertical stress prediction for stope 685 at (a) 2.4 m, (b) 6.4 m, (c) 11.4 m and stope 715 (d) 3 m, (e) 6 m, (f) 9 m elevation height

5.8 Summary of Findings

With a properly calibrated and preliminary tested narrow wall model, the stress-strain-temperature behaviour of CPB as well as UCPB were able to be captured and analysed. Generally, both material experience thermal expansion and exerts additional stress (thermal stress) onto its adjacent wall. After investigating via two different heating patterns (i.e. varying and fixed temperature), the effect of temperature change towards stress propagation were affected by the heating pattern.

CPB and UCPB experienced thermal expansion semi-confined condition and thus generating some thermal stress coupled with relaxation of thermal stress during heating. While soaking, the intensity of thermal stress relieved (relaxation) is different for CPB and UCPB due to the presence of hydration that alter the state of matter as time passes. The remains of thermal stress generated is retained by the presence of arching between the material and the narrow wall. Both materials relieved the thermal stress generated during cooling by thermal shrinkage.

As the backfill material is tested at fixed temperature throughout the deposition, both CPB and UCPB only generate smaller amount of stress at the same temperature in comparison to varying temperature test. The backfill materials were allowed to rearrange the particles during thermal expansion as there is insignificant arching effects when the material is still in slurry state. When the time taken for the temperature change I longer, the generation of thermal stress is more pronounced due to the establishment of arching effects through consolidation and hydration over time. The soaking and cooling behaviour behaves similarly with the varying temperature tests.

Based on the collected data, the stress distribution during deposition phase is similar to the prediction generated from the state-of-the-art prediction model. During the

consolidation phase, an empirical model is proposed that is befitting to the experimental data by considering the max vertical stress generation, coefficient of consolidation and stress reduction factor due to establishment of arching effects at the end of consolidation for both backfill materials. By considering the temperature change, coefficient of volumetric expansion, and arching effects, the change in stress due to temperature change is predicted using temperature-stress gradient that is coupled with arching effects based on the data analysis.

By utilising three of the empirical formula at three different phase of backfill, a new mathematical model is proposed and proven to be able to accurately predict stress propagation throughout the backfilling processes. The mathematical model is able to predict the stress propagation at the safe level for both CPB and UCPB. Overestimation only occurred under one condition that was when the backfill material experience temperature change during deposition stage where the material was still in slurry state. The mathematical model is also tested using full-scale monitoring data from actual mine backfill activities that was recently published. Once again, the proposed mathematical model is able to predict the stress change accurately throughout the backfilling phases.

CHAPTER 6

CONCLUSION AND RECOMMENDATIONS

6.1 Conclusion

Stress anomaly in mine backfilling could potentially cause devastating failure due to unexpected overload. The causes of the stress anomaly must be investigated and understood to come out with a preventive measure. As temperature change is speculated to be one of the causes of stress anomaly, a new narrow wall (NW) model was proposed and designed to be able to capture the stress-strain-temperature behaviour of backfill at controlled temperature.

The physical and mechanical properties of the proposed material were studied and suitable mix design to prepare UCPB and CPB was then acquired. Backfill material was deposited into the NW model that has been calibrated and functionality checked. Based on the preliminary test and actual test, the collected data showed that the NW model was functioning as design.

The stress-strain-temperature behaviour of CPB, as well as UCPB, were successfully captured with the proposed NW model. The general findings showed that the changes in temperature were responsible for the changes in stress (anomaly) during and after the deposition of backfill material. This explained that the stress anomaly observed from the full-scale monitoring of mine backfilling. From present studies, the resulting stress was dependent on the properties of backfill, geometry of stope, the intensity of arching effects and the change in temperature.

Based on the analysed data, an empirical model was proposed and its adequacy was checked by applying into the experimental data and full-scale monitoring data. The proposed model could predict the stress behaviour of backfill from the beginning of deposition to the end of the deposition, after the end of the deposition (curing period) and incorporate the

effects of temperature change throughout the process. The proposed model showed good prediction for CPB in comparison to UCPB as the proposed model does not consider the effects of relaxation. The proposed model showed slightly overestimate the stress behaviour if the backfill was heated during the deposition phase due to insignificant arching effect of backfill in slurry state. The proposed model did not underestimate the stress behaviour for every case but only will only slightly overestimate during the aforementioned situation. Therefore, the proposed model is feasible to be used as a reference to predict the evolution of stress and possible stress gain due to temperature change during mine backfill design.

The main conclusions are as follows:

i. The physical and mechanical properties of the material used to replicate the backfill material is identified and studied. Shear parameter is also identified at different temperature level.

ii. Designed and constructed a new narrow wall model that can simulate backfilling in a laboratory scale under controlled temperature and capture the stress-strain-temperature behaviour of backfill material upon temperature change.

iii. General finding shows that elevation of curing temperature shall result in additional stress due to thermal expansion characteristic of backfill material. Significant amount of stress approximately 50% is generated in addition to the self-weight of CPB when the temperature is elevated by 30°C. Such increment is undesired as it may result in failure of structure in the actual mining site.

iv. From the analysed data, empirical formulation was generated based on each factor. A new model is established by considering the conventional theorem used to predict stress distribution during deposition stage, stress reduction due to consolidation, and empirical formula to predict change in stress corresponding to change in temperature

on the material. The new formulation can safely predict the stress change throughout the backfilling process and applicable to field data.

6.2 Recommendations

Empirical model with greater accuracy on the prediction of stress behaviour of backfill material could be generated by collecting additional data based on the following recommendations;

i. The effects of arching over the height of deposition could be studied by varying the height of deposition. To capture the consolidation profile that is affected by arching, electrical resistivity method could be implemented into the NW design to capture the density profile over time and temperature change. The intensity of arching could be adjusted to generate greater stress by altering the interfacial friction of the NW.

ii. The effect of relaxation and establishment of arching effect could be studied by varying the rate of temperature change. It is speculated that low rate of temperature increase allows coupled stress change based on thermal expansion and relaxation that will result will lower final stress. Relaxation could be further investigated by allowing the backfill material to be tested at a fully confined condition.

iii. The behaviour of granular material should be studied with the proposed model as a transitional knowledge between the slurry and granular material

iv. The model could be studied with the Discrete Element Method (DEM), where each distinctive particle of backfill could be defined and simulated according to user's input. The force saturation, packing fraction, thermal expansion, and stress distribution could be studied with DEM. DEM allows further clarification on the experimental findings and allows simulation that is not physically restricted in laboratory-scale.

REFERENCES

Abdul-Hussain, N., & Fall, M. (2012). Thermo-hydro-mechanical behaviour of sodium silicate-cemented paste tailings in column experiments. *Tunnelling and Underground Space Technology*, *29*, 85-93.

Aubertin, M., Li, L., Arnoldi, S., Belem, T., Bussière, B., Benzaazoua, M., & Simon, R. (2003). Interaction between backfill and rock mass in narrow stopes. In: *39th U.S. Rock Mechanics Symposium*. Symposium conducted at 12th Panamerican Conference on Soil Mechanics and Geotechnical Engineering, USA, 1157-1164.

Battery and Energy Technologies. (2017). Retrieved January 15, 2017, from http://www.mpoweruk.com/geothermal_energy.htm

Bayat, M., Asgari, M. R., & Mousivand, M. (2013). Effects of cement and lime treatment on geotechnical properties of a low plasticity clay. In: *International Conference on Civil Engineering Architecture & Urban Sustainable Development*, Tabriz, Iran.

Belem, T., Benzaazoua, M., Bussière, B., & Dagenais, A. M. (2002). Effects of settlement and drainage on strength development within mine paste backfill. In: *Conference of Tailings and Mine Waste '02*. Sets & Zeitlinger, Colorado, USA, 139-148.

Belem, T., & Benzaazoua, M. (2008). Design and Application of Underground Mine Paste Backfill Technology. *Geotechnical and Geological Engineering*, *26*(2), 147-174.

Belem, T., Benzaazuoa, M., & Bussière, B. (2000). Mechanical behaviour of cemented paste backfill. In: *Proceeding of 53rd Candadian Geotechnical Conference*, Montreal, Canada, 373–380.

Benzaazoua, M., Ouellet, J., Servant, S., Newman, P., & Verburg, R. (1999). Cementitious backfill with high sulfur content: physical, chemical and mineralogical characterization. *Cement and Concrete Research, 29*, 719–725.

Benzaazoua, M., Fall, M., & Belem, T. (2004). A contribution to understanding the hardening process of cemented pastefill. *Minerals Engineering*, *17*(2), 141-152.

Benzaazoua, M., Perez, P., Belem, T., & Fall, M. (2004). A laboratory study of the behaviour of surface paste disposal. In: *Proceedings of the Minefill 2004*, Beijing, China, 180-192.

Bernier, L. R., & Li, M. (2003). High temperature oxidation (heating) of sulfide paste backfill: A mineralogical and chemical perspective. In: *Mining and the Environment*, Sudbury, Canada, CD.

Bouasker, M., Mounanga, P., Turcry, P., Loukili, A., & Khelidj, A. (2008). Chemical shrinkage of cement pastes and mortars at very early age: Effect of limestone filler and granular inclusions. *Cement and Concrete Composites*, *30*(1), 13-22.

Brackebusch, F. W. (1995). Basics of paste backfill systems. *International Journal of Rock Mechanics and Mining Sciences and Geomechanics Abstracts, 32*(3), 1175-1178.

Brooker, E. H., & Ireland, H. O. (1965). Earth pressures at rest related to stress history. *Canadian Geotechnical Journal, 2*(1), 1-15.

Brouwers, H. J. H. (2004). The work of Powers and Brownyard revisited: Part 1. *Cement and Concrete Research, 34*, 1697-1716.

Burghignoli, A., Desideri, A., & Miliziano, S. (2000). A laboratory study on the thermomechanical behaviour of clayey soils. *Canadian Geotechnical Journal, 37*(4), 764-780.

Cayouette, J. (2003). Optimization of the paste backfill plant at Louvicourt mine. *Canadian Institute of Mining Bulletin, 96*, 51-57.

Cekerevac, C. (2003). *Thermal effects on the mechanical behaviour of saturated clays: an experimental and constitutive study*. Ph.D. Dissertation, EPFL, Lausanne, Switzerland.

Chang, S. (2016). *Strength and Deformation Behaviour of Cemented Paste Backfill in Sub-Zero Environment*. Master thesis, University of Ottawa, Canada.

Chevalier, B., & Otani, J. (2011). Arching observation in three-dimensional trapdoor problem with x-ray CT and discrete element method. *Soils and Foundations*, *51*(3), 459-469.

Choktaweekarn, P., & Tangtermsirikul, S. (2009). A model for predicting coefficient of thermal expansion of cementitious paste. *Science Asia, 35*, 57-63.

Cooke, R. (2008). Pipeline design for paste and thickened tailings systems. In: *Proceedings of the 12th International Conference of Tailings and Mine Waste '08*, Vail, Colorado, USA, 95-100.

Cui, L., & Fall, M. (2015). A coupled thermo–hydro-mechanical–chemical model for underground cemented tailings backfill. *Tunnelling and Underground Space Technology*, *50*, 396-414.

Cui, L., & Fall, M. (2016). An evolutive elasto-plastic model for cemented paste backfill. *Computers and Geotechnics*, *71*, 19-29.

Célestin, J. C., & Fall, M. (2009). Thermal conductivity of cemented paste backfill material and factors affecting it. *International Journal of Mining, Reclamation and Environment*, *23*(4), 274-290.

Davies, M. P. (2002). Tailings impoundment failures: are geotechnical engineers listening? *Waste Geotechnics*, *20*, 31-36.

Di Felice, R., & Scapinello, C. (2009). On the interaction between a fixed bed of solid material and the confining column wall: the Janssen approach. *Granular Matter*, *12*(1), 49-55.

Doherty, J. P. (2015). A numerical study into factors affecting stress and pore pressure in free draining mine stopes. *Computers and Geotechnics*, *63*, 331-341.

Doherty, J. P., Hasan, A., Suazo, G. H., & Fourie, A. (2015). Investigation of some controllable factors that impact the stress state in cemented paste backfill. *Canadian Geotechnical Journal*, *52*(12), 1901-1912.

El Mkadmi, N., Aubertin, M., & Li, L. (2013). Effect of drainage and sequential filling on the behavior of backfill in mine stopes. *Canadian Geotechnical Journal, 51*(1), 1-15.

Emanuel, J. H., & Hulsey, J. L. (1977). Prediction of the thermal coefficient of expansion of concrete. *Journal - American Concrete Institute, 74*, 149-155.

Fahey, M., Helinski, M., & Fourie, A. (2009). Some aspects of the mechanics of arching in backfilled stopes. *Canadian Geotechnical Journal*, *46*(11), 1322-1336.

Fahey, M., Helinski, M., & Fourie, A. (2011). Development of specimen curing procedures that account for the influence of effective stress during curing on the strength of cemented mine backfill. *Geotechnical and Geological Engineering, 29*, 709-723.

Fall, M., Adrien, D., Célestin, J., Pokharel, M., & Touré, M. (2009). Saturated hydraulic conductivity of cemented paste backfill. *Minerals Engineering*, *22*(15), 1307-1317.

Fall, M., Belem, T., Samb, S., & Benzaazoua, M. (2007). Experimental characterization of the stress-strain behaviour of cemented paste backfill in compression. *Journal of Material Science*, *42*(11), 3914-3922.

Fall, M., & Benzaazoua, M. (2005). Modeling the effect of sulphate on strength development of paste backfill and binder mixture optimization. *Cement and Concrete Research, 35*(2), 301-314.

Fall, M., Benzaazoua, M., & Ouellet, S. (2005). Experimental characterization of the influence of tailings fineness and density on the quality of cemented paste backfill. *Minerals Engineering*, *18*(1), 41-44.

Fall, M., Benzaazoua, M., & Saa, E. (2008). Mix proportioning of underground cemented tailings backfill. *Tunnelling and Underground Space Technology*, *23*(1), 80-90.

Fall, M., Célestin, J., Pokharel, M., & Touré, M. (2010). A contribution to understanding the effects of curing temperature on the mechanical properties of mine cemented tailings backfill. *Engineering Geology*, *114*(3-4), 397-413.

Fall, M., & Pokharel, M. (2010). Coupled effects of sulphate and temperature on the strength development of cemented tailings backfills: Portland cement-paste backfill. *Cement and Concrete Composites*, *32*(10), 819-828.

Fall, M., & Samb, S. (2009). Effect of high temperature on strength and microstructural properties of cemented paste backfill. *Fire Safety Journal*, *44*(4), 642-651.

Gawin, D., Pesavento, F., & Schrefler, B. A. (2008). Modeling of cementitious materials exposed to isothermal calcium leaching, considering process kinetics and advective water flow. Part 1: theoretical model. *International Journal of Solids and Structures, 45*, 6221–6240.

Geiker, M., & Knudsen, T. (1982). Chemical Shrinkage of Portland Cement Pastes. *Cement and Concrete Research*, *12*, 603–610.

Ghirian, A., & Fall, M. (2014). Coupled thermo-hydro-mechanical–chemical behaviour of cemented paste backfill in column experiments. *Engineering Geology*, *170*, 11-23.

Ghirian, A., & Fall, M. (2015). Coupled Behavior of Cemented Paste Backfill at Early Ages. *Geotechnical and Geological Engineering*, *33*(5), 1141-1166.

Ghirian, A., & Fall, M. (2016). Strength evolution and deformation behaviour of cemented paste backfill at early ages: Effect of curing stress, filling strategy and drainage. *International Journal of Mining Science and Technology*, *26*(5), 809-817.

Goodey, R., Brown, C., & Rotter, J. (2003). Verification of a 3-dimensional model for filling pressures in square thin-walled silos. *Engineering Structures*, *25*(14), 1773-1783.

Goodey, R., Brown, C., & Rotter, J. (2006). Predicted patterns of filling pressures in thin-walled square silos. *Engineering Structures*, *28*(1), 109-119.

Grabinsky, M., & Simms, P. (2006). Self-desiccation of cemented paste backfill and implications for mine design. In: *Symposium of the International Thickened Tailings and Paste*, Australian Centre for Geomechanics, Perth, Australia, 323-332.

Grabinsky, M. W., & Thompson, B. D. (2009). Thermally induced stresses in cemented paste backfill. *Geotechnical News*, *27*(3), 36–40.

Hartman, H. L. (1992). *SME Mining Engineering Handbook.* Society for Mining, Metallurgy, and Exploration, Incorporate, Volume 2, Colorado, USA.

Hasan, A., Suazo, G., & Fourie., A. (2013). Full scale experiments on the effectiveness of a drainage system for cemented paste backfill. In: *Proceedings of the 16th International Seminar on Paste and Thickened Tailings*. Nedlands, Western Australia, Australia, 379-392.

Hasan, A., Suazo, G., Doherty, J., & Fourie., A. (2014). In-stope measurements at two Western Australian mine sites. In: *Proceedings of the 17th International Seminar on Paste and Thickened Tailings*. Vancouver, Canada, 355-368.

Hassani, J. F., & Archibald, J. (1998). Mine Backfill, An Operator's Guide. An interactive CD-ROM for mine operators and engineers., *Metallurgy and Petroleum*, Canadian Institute of Mine, Canada.

Hassani, F., Mortazavi, A., & Shabani, M. (2008). An investigation of mechanisms involved in backfill-rock mass behaviour in narrow vein mining. *The Journal of The Southern African Institute of Mining and Metallurgy*, *108*, 463-472.

Helinski, M., Fahey, M., & Fourie, A. (2007). Numerical modeling of cemented mine backfill deposition. *Journal of Geotechnical and Geoenvironmental Engineering*, *133*(10), 1308-1319.

Helinski, M., Fahey, M., & Fourie, A. (2010). Coupled two-dimensional finite element modelling of mine backfilling with cemented tailings. *Canadian Geotechnical Journal*, *47*(11), 1187-1200.

Helinski, M., Fahey, M., & Fourie, A. (2011). Behavior of cemented paste backfill in two mine stopes: Measurements and modeling. *Journal of Geotechnical and Geoenvironmental Engineering*, *137*(2), 171-182.

Helinski, M., Fourie, A., Fahey, M., & Ismail, M. (2007). Assessment of the self-desiccation process in cemented mine backfills. *Canadian Geotechnical Journal*, *44*(10), 1148-1156.

Helms, W. (1988). Preparation and transportation systems for cemented backfill. *Mining Science and Technology*, *7*(2), 183-193.

Hoek, E., & Diederichs, M. S. (2006). Empirical estimation of rock mass modulus. *International Journal of Rock Mechanics and Mining Sciences, 43*, 203-215.

Huang, S. (2009). *Dynamic Testing of Soft and Ultra-Soft Materials.* Master thesis, University of Toronto, Canada.

Hueckel, T., & Baldi, G. (1990). Thermoplasticity of saturated clays: experimental constitutive study. *Journal of Geotechnical Engineering, 116*(12), 1778-1796.

Hustrulid, W. A., & Holmberg, R. (1991). Drilling and Blasting, *Underground Structures Design and Construction*, Elsevier.

James, M., Aubertin, M., Wijewickreme, D., & Wilson, G. W. (2011). A laboratory investigation of the dynamic properties of tailings. *Canadian Geotechnical Journal*, *48*(11), 1587-1600.

Janssen, H. (1895). Versuche uber Getreidedruck in Silozellen. Zeitschrift des Vereines deutscher Ingenieure. *39*, 1045-1049. Translated by Sperl. M. (2006). *Granular matter, 8,* 59-65.

Jarrett, N. D. (1991). *A Study of the Influence of Wall Flexibility on Pressure in Rectangular Silos.* Doctoral dissertation, Brunel University, London.

Karademir, T. (2011). *Elevated temperature effects on interface shear behaviour*. Ph.D. Dissertation, Georgia Institute of Technology, Georgia.

Kjellsen, K., Detwiler, R., & Gjørv, O. (1991). Development of microstructures in plain cement pastes hydrated at different temperatures. *Cement and Concrete Research, 21*, 179-189.

Landriault, D. A. (1995). Paste backfill mix design for Canadian underground hard rock mining. In*: Proceeding of the 97th Annual General Meeting of the CIM Rock Mechanics and Strata Control Session*, Halifax, Nova Scotia, Canada.

Landry, W., Grest, S., & Plimpton, J. (2004). Discrete element simulations of stress distributions in silos: crossover from two to three dimensions. *Powder Technology*, *139*(3), 233-239.

Le Roux, K., Bawden, W. F., & Grabinsky, M. F. (2005). Field properties of cemented paste backfill at the Golden Giant mine. *Transactions of the Institution of Mining and Metallurgy*, *114*(2), 65-80.

Li, L., Aubertin, M., Simon, R., Bussière, B., & Belem, T. (2003). Modeling arching effects in narrow backfilled stopes with FLAC. In: *Proceedings of 3rd international FLAC symposium,* Sudbury, Canada, 211-218.

Li, L., Aubertin, M., & Belem, T. (2005). Formulation of a three dimensional analytical solution to evaluate stresses in backfilled vertical narrow openings. *Canadian Geotechnical Journal*, *42*(6), 1705-1717.

Li, L., Aubertin, M., & Belem, T. (2006). Formulation of a three dimensional analytical solution to evaluate stresses in backfilled vertical narrow openings. *Canadian Geotechnical Journal*, *43*(3), 338-339.

Li, L., & Aubertin, M. (2008). An improved analytical solution to estimate the stress state in subvertical backfilled stopes. *Canadian Geotechnical Journal*, *45*(10), 1487-1496.

Li, L., & Aubertin, M. (2010). An analytical solution for the nonlinear distribution of effective and total stresses in vertical backfilled stopes. *Geomechanics and Geoengineering*, *5*(4), 237-245.

Li, L., & Yang, P. (2015). A numerical evaluation of continuous backfilling in cemented paste backfilled stope through an application of wick drains. *International Journal of Mining Science and Technology*, *25*(6), 897-904.

Li, Y., Jin, L., & Zhang, L. (2016). Mechanical Parameters of Cemented Paste Backfilling and Its Failure Modes Under Different Loading Rates. *Electronic Journal of Geotechnical Engineering*, *21*(3), 969-978.

Liu, Z., Lan, M., Xiao, S., & Guo, H. (2015). Damage failure of cemented backfill and its reasonable match with rock mass. *Transactions of Nonferrous Metals Society of China*, *25*(3), 954-959.

Lura, P., Winnefeld, F. & Klemm, S., (2010). Simultaneous measurements of heat of hydration and chemical shrinkage on hardening cement pastes. *Journal of Thermal Analysis and Calorimetry, 101*(3), 925-932.

Marston, A. (1930). The theory of external loads on closed conduits in the light of latest experiments. *Bulletin No. 96*, Iowa Engineering Experiment Station, Ames, Iowa, USA.

Mehta, P. K., & Monteiro, P. J. (2006). *Concrete Microstructure, Properties, and Materials* (Third ed.). McGraw-Hill.

Mindess, S., Young, J. F., & Darwin, D. (2003). *Concrete* (Second ed.). Prentice Hall, Pearson Education, Inc., Upper Saddle River, New Jersey, USA.

Mitchell, R. J., Olsen, R. S., & Smith, J. D. (1982). Model studies on cemented tailings used in mine backfill. *Canadian Geotechnical Journal*, *19*(1), 14-28.

Mozaffaridana, M. (2011). *Using Thermal Profiles of Cemented Paste Backfill to Predict Strength*. Master's thesis, University of Toronto, Canada.

Nasir, O., & Fall, M. (2008). Shear behaviour of cemented pastefill-rock interfaces. *Engineering Geology*, *101*(3-4), 146-153.

Nasir, O., & Fall, M. (2009). Modeling the heat development in hydrating CPB structures. *Computers and Geotechnics*, *36*(7), 1207-1218.

Nasir, O., & Fall, M. (2010). Coupling binder hydration, temperature and compressive strength development of underground cemented paste backfill at early ages. *Tunnelling and Underground Space Technology*, *25*(1), 9-20.

Orejarena, L., & Fall, M. (2008). Mechanical response of a mine composite material to extreme heat. *Bulletin of Engineering Geology and the Environment*, *67*(3), 387-396.

Orejarena, L., & Fall, M. (2011). Artificial neural network based modelling of the coupled effects so sulphate and temperature on the strength of cemented paste backfill. *Canadian Journal of Civil Engineering, 38*(1), 100-109.

Ovarlez, G., Fond, C., & Clément, E. (2003). Overshoot effect in the Janssen granular column: A crucial test for granular mechanics. *Physical Review E*, *67*(6), 1-4.

Pengyu, Y., & Li, L. (2014). A 3D analytical solution for the short-term stress distribution in backfilled stopes and on barricades. In: *67th Canadian Geotechnical Conference, Regina, Canada*.

Pengyu, Y., & Li, L. (2015). Investigation of the short-term stress distribution in stopes and drifts backfilled with cemented paste backfill. *International Journal of Mining Science and Technology*, *25*(5), 721-728.

Pirapakaran, K. (2008). *Load-deformation characteristics of minefills with particular reference to arching and stress developments*. Doctoral dissertation, James Cook University, Australia.

Pirapakaran, K., & Sivakugan, N. (2007). Arching within hydraulic fill stopes. *Geotechnical and Geological Engineering*, *25*(1), 25-35.

Pokharel, M., & Fall, M. (2011). Coupled Thermochemical Effects on the Strength Development of Slag-Paste Backfill Materials. *Journal of Materials in Civil Engineering*, *23*(5), 511-525.

Potvin, Y., Thomas, E., & Fourie, A. (2005). *Handbook on mine fill*. Australian Centre for Geomechanics.

Powers, T. C. (1935). Absorption of Water by Portland Cement Paste during the Hardening Process. *Industrial and Engineering Chemistry*, *27*(7), 790-794.

Powers, T. C., & Brownyard, T. L. (1947). Studies of the physical properties of hardened Portland cement paste. *American Concrete Institute Journal Proceeding*, *43*(9), 249-336.

Ramlochan, T., Grabinsky, M., & Hooton, R. (2004). Microstructural and chemical investigations of cemented paste backfills. In: *57th Canadian geotechnical conference*, Quebec City, Canada.

Rankine, R. M., & Sivakugan, N. (2007). Geotechnical properties of cemented paste backfill from Cannington Mine, Australia. *Geotechnical and Geological Engineering*, *25*(4), 383-393.

Revell, M. B. (2004). Paste-how strong is it?. In: *Proceedings of 8th International Symposium on Mining with Backfill*. Beijing, China.

Rotter, J., Brown, C., & Lahlouh, E. (2002). Patterns of wall pressure on filling a square planform steel silo. *Engineering Structures*, *24*(2), 135-150.

Sant, G., Lura, P., and Weiss, J. (2006). Measurement of volume change in cementitious materials at early ages: Review of testing protocols and interpretation of results. *Journal of the Transportation Research Board*, *1979*(1), 21-29.

Sellevold, E. J., & Bjøntegaard, Ø. (2006). Coefficient of thermal expansion of cement paste and concrete: mechanisms of moisture interaction. *Materials and Structures, 39*, 809-815.

Sheshpari, M. (2015). A review of underground mine backfilling methods with emphasis on cemented paste backfill. *Electronic Journal of Geotechnical Engineering*, *20*(13), 5183-5208.

Simon, D. (2005). *Microscale Analysis of Cemented Paste Backfill*. Doctoral dissertation, University of Toronto, Canada.

Sivakugan, N., Widisinghe, S., & Wang, V. Z. (2014). Vertical Stress Determination within Backfilled Mine Stopes. *International Journal of Geomechanics*, *14*(5), 06014011.

Souza, P., Soares, R., Anjos, M., Freitas, J., Martinelli, A., & Melo, D. (2012). Cement slurries of oil wells under high temperature and pressure: The effects of the use of ceramic waste and silica flour. *Brazilian Journal of Petroleum and Gas*, *6*(3), 105-113.

Tazawa, E., Miyazawa, S., & Kasai, T. (1995). Chemical shrinkage and autogenous shrinkage of hydrating cement paste. *Cement and Concrete Research*, *25*(2), 288-292.

Terzaghi, K. (1943). *Theoretical soil mechanics*. New York: J. Wiley and Sons, Inc.

Thompson, B. D., Bawden, W. F., & Grabinsky, M. W. (2011a). In-situ pressures in cemented paste backfill – a review of fieldwork from three mines. In: *Proceedings of the 14th International Seminar on Paste and Thickened Tailings*, Perth, Australia, 491-504.

Thompson, B. D., Bawden, W. F., & Grabinsky, M. W. (2011b). In-situ monitoring of cemented paste backfill pressure to increase backfilling efficiency. *Canadian Institute of Mining Journal, 2*(4), 1-10.

Thompson, B. D., Bawden, W., & Grabinsky, M. (2012). In-situ measurements of cemented paste backfill at the Cayeli Mine. *Canadian Geotechnical Journal*, *49*(7), 755-772.

Thompson, B. D., Grabinsky, M. W., Bawden, W. F., & Counter, D. B. (2009). In-situ measurements of cemented paste backfill in long-hole stopes. In: *CANUS Rock Mechanics Symposium*, Toronto, Canada, 1-10.

Vanel, L., Claudin, P., Bouchaud, J., Cates, M. E., Clément, E., & Wittmer, J. P. (2000). Stresses in Silos: Comparison Between Theoretical Models and New Experiments. *Physical Review Letters*, *84*(7), 1439-1442.

Vanel, L., & Clément, E. (1999). Pressure screening and fluctuations at the bottom of a granular column. *The European Physical Journal B*, *11*(3), 525-533.

Van Horn A. D. (1963). A study of loads on underground structures, part III. Iowa Engineering Experiment Station, Ames, Iowa, USA.

Walske, M. L. (2014). *An Experimental Study of Cementing Paste Backfill.* Doctoral dissertation, The University of Western Australia, Australia.

Wang, X., Li, J., Xiao, Z., & Xiao, W. (2004). Rheological properties of tailing paste slurry. *Journal of Central South University of Technology*, *11*(1), 75-79.

Widisinghe, S., & Sivakugan, N. (2014). Vertical stresses within granular materials in containments. *International Journal of Geotechnical Engineering*, *8*, 431-435.

Witteman, M. L. (2013). *Unsaturated Flow in Hydrating Porous Media: Application to Cemented Paste Backfill*. Master's thesis, Carleton University Ottawa, Ontario, Canada.

Wu, A., Wang, Y., Zhou, B., & Shen, J. (2016). Effect of Initial Backfill Temperature on the Deformation Behavior of Early Age Cemented Paste Backfill That Contains Sodium Silicate. *Advances in Materials Science and Engineering*, *2016*, 1-10.

Wu, D., & Cai, S. (2015). Coupled effect of cement hydration and temperature on hydraulic behavior of cemented tailings backfill. *Journal of Central South University*, *22*(5), 1956-1964.

Wu, D., Fall, M., & Cai, S. (2013). Coupling temperature, cement hydration and rheological behaviour of fresh cemented paste backfill. *Minerals Engineering*, *42*, 76-87.

Xie, Y., & Leshchinsky, B. (2016). Active earth pressures from a log-spiral slip surface with arching effects. *Géotechnique Letters*, *6*(2), 149-155.

Yilmaz, E., Kesimal, A., Ercikdi, B., & Alp, I. (2003). Determination of the Optimum Cement Content for Paste Backfill Samples. In: *18th International Mining Congress and Exhibition of - IMCET 2003*, Turkey, 119-125.

Yilmaz, E., Kesima, A., & Ercidi, B. (2004). Strength development of paste backfill simples at long term using different binders. In: *Proceedings of 8th symposium MineFill04*, China, 281-285.

Yilmaz, E., Belem, T., Bussiere, B., & Benzaazoua, M. (2008), Consolidation characteristics of early age cemented paste backfill. In: *Proceedings of the 61st Canadian Geotechnical Conference*, Edmonton, Alberta, Canada.

Yilmaz, E., Belem, T., Benzaazoua, M., & Bussière, B., (2010). Assessment of the modified CUAPS apparatus to estimate in situ properties of cemented paste backfill. *Geotechnical Testing Journal*, *33*(5), 1-12.

Yilmaz, E., Belem, T., & Benzaazoua, M. (2014). Effects of curing and stress conditions on hydromechanical, geotechnical and geochemical properties of cemented paste backfill. *Engineering Geology*, *168*, 23-37.

Yilmaz, E., Belem, T., & Benzaazoua, M. (2015). Specimen size effect on strength behavior of cemented paste backfills subjected to different placement conditions. *Engineering Geology*, *185*, 52-62.

Yin, S., Wu, A., Hu, K., Wang, Y., & Zhang, Y. (2012). The effect of solid components on the rheological and mechanical properties of cemented paste backfill. *Minerals Engineering*, *35*, 61-66.

APPENDICES

Appendix A: Full-scale monitoring results from published literature

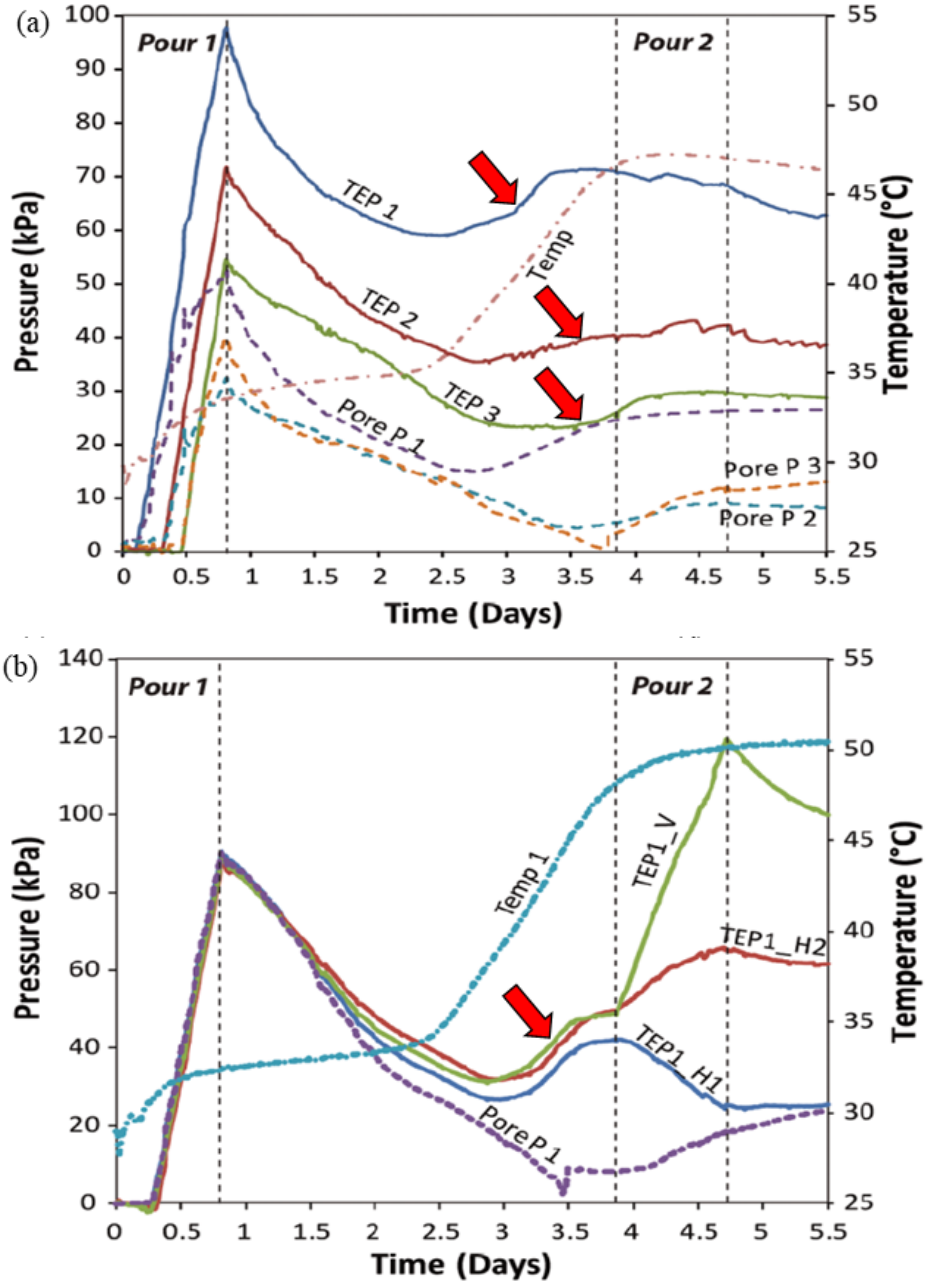

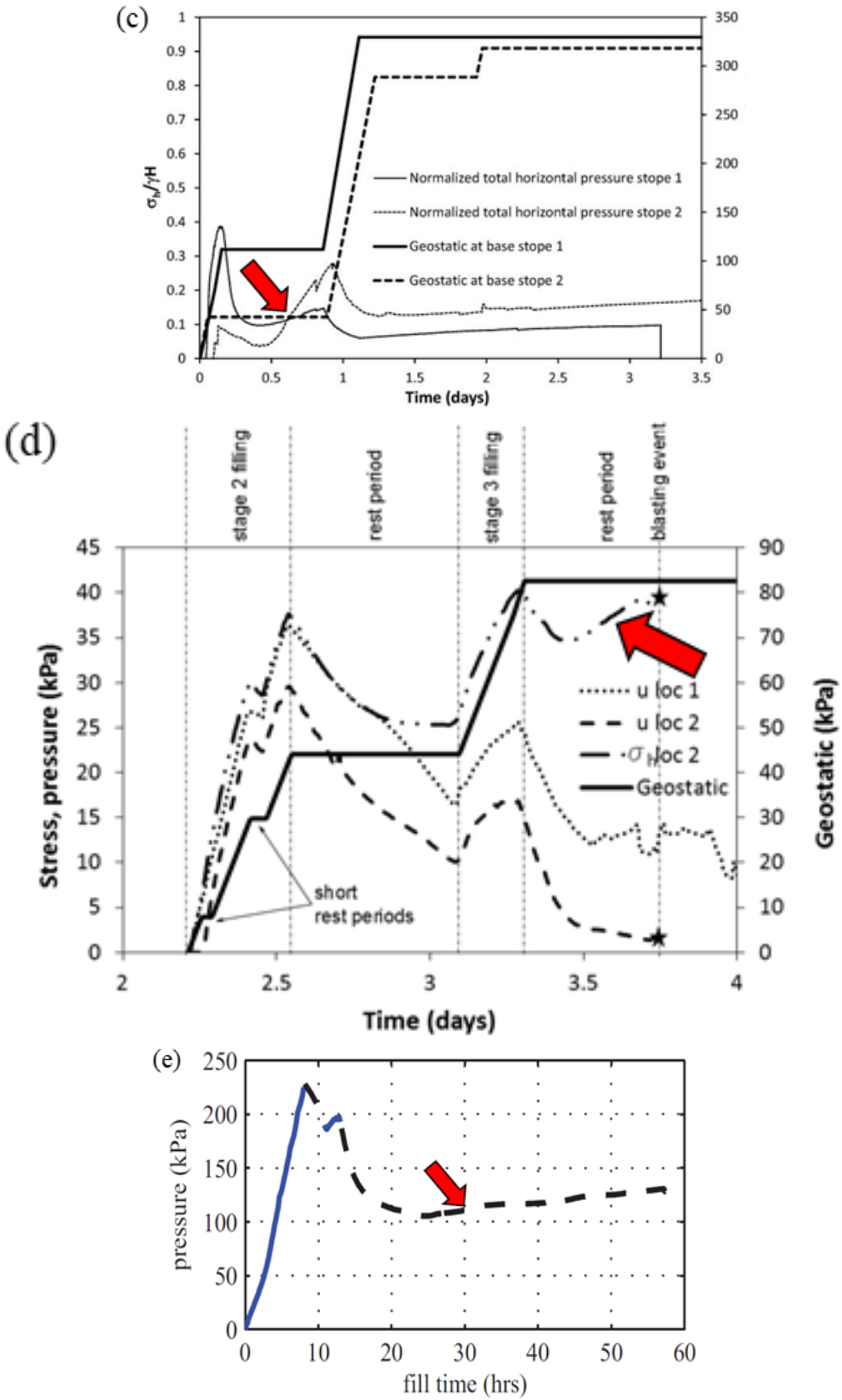

(a) Thompson et al., 2012; (b) Thompson et al., 2012; (c) Hasan et al., 2013; (d) Hasan et al., 2014; and Doherty et al., 2015

Appendix B: Detailed hydration process

Stages	Equation
Dissolution hydration of tricalcium silicate with water	$2Ca_3SiO_5 + 6H_2O \rightarrow 6Ca^{2+} + 8OH^- + 2H_2SiO_4^{2-}$
Precipitation hydration process Tricalcium aluminate reacts with the gypsum in the presence of water to generate ettringite and heat	$C_3A + 3CSH_2 + 26H \rightarrow CASH_{32}$, $\Delta H = 207cal/g$
Tricalcium silicate is hydrated to produce calcium silicate hydrates and lime, as well as heat	$2C_3S + 6H \rightarrow C_3S_2H_3 + 3CH$, $\Delta H = 120cal/g$
Ettringite will become unstable and react with the remaining tricalcium aluminate to produce monosulphate aluminate hydrate crystals	$2C_3A + 3C_6AS_3H_32 + 22H \rightarrow 3C_4ASH_{18}$
Dicalcium silicate also hydrates to form calcium silicate hydrates and heat	$C_2S + 4H \rightarrow C_3S_2H_3 + CH$, $\Delta = 62cal/g$
Ferrite reacts with gypsum	$C_4AF + 3CSH_2 + 3H \rightarrow C_6(A, F)S_3H_32 + (A, F)H_3 + CH$
Ferrite reacts with ettringite	$C_4AF + C_6(A, F)S_3H_32 + 2CH + 23H \rightarrow 3C_4(A, F)SH_18 + (A, F)H_3$

Appendix C: Specification and unit count of model parts

Parts	Material	Position	Nos	Dimension in mm				
				w	*t*	*h*	*l*	*d*
Narrow wall	Aluminium	Front / rear	2	176	5	800	-	-
		Side	2	51.3	13.3	800	-	-
		Bottom	1	176	5	-	61.3	-
L-angle support	Steel	All	4	50	10	50	60	-
Vertical support	Steel thread rod	Both side	2	-	-	-	1200	21.6
Base platform	Mild-steel	-	1	510	5	150	700	-
Base level support	Steel thread rod	All corners	4	-	-	-	370	21.6
Smooth base plate	Stainless steel	Centre	1	200	6	-	195	-
Load cell platform	Steel	Centre	1	100	12	-	175	-
Load cell level	Steel thread rod	All corners	4	-	-	-	150	5.5
Load cell support	Steel thread rod	Centre	1	-	-	-	50	5.5
Ceramic holder	Aluminium	As schematic	6	25.3	2.3	26.3	125	-
Holder clamp	Steel thread rod	Both side	6	-	-	-	150	5.5
Nuts	Stainless steel	As schematic	20	-	-	40	-	21.6
			30	-	-	5	-	5.5
Bolts	Stainless steel	Front / rear	28	-	-	-	10	5
		Side	16	-	-	-	10	5

Appendix D: Instruments for deposition test

Instrument	Manufacturer	Model	Function
Load cell	OMEGA Engineering	LC101-50	50lbs detection
		LCM101-100	100kg detection
Linear Potentiometer	OMEGA Engineering	LP804-01	Linear measurement
Temperature controller	OMEGA Engineering	CN7263	Temperature control
Thermocouple	OMEGA Engineering	Type-J	Temperature detection
Ceramic heater	HongTai	-	Heat generation
Data acquisition unit	OMEGA Engineering	OM-DAQ-USB-2401	Data logging

APPENDIX E: In-depth specifications of selected instruments

Instrument	Specification
	Model LC101-50 and LCM101-100 S-load cell manufactured by OMEGA® with a capacity of 50 lb or 22.68 kg and 100 kg are used for the vertical stress measurement. It has a safe overload and ultimate overload of 150% and 300% of its predesigned capacity which is beneficial upon unexpected results from our test program. It could operate within -40 to +93 °C which is able to cope with our target temperature range.
	Model LP804-01 miniature linear potentiometer with a 25mm range manufactured by OMEGA Engineering is used to monitor the expansive behaviour of fill material during deposition test. LP804-01 could be used in a confined space, high accuracy with 0.00127mm resolution and operate within -40 to 80°C which is compatible with our usage. The initiating force (in terms of weight) require to displace the rod is lesser than 2.8 g which allows it to be used on soft material without denting the sample.
	Temperature controller model CN7262 manufactured by OMEGA® is used for temperature control by having a relay function on real-time temperature monitoring and feedback by generating appropriate heat to maintain the pre-set temperature. It could accept a wide range of thermocouple which includes our proposed thermocouple (Type-J). The output has a maximum load of 250VAC, 5A resistive load which is suitable for our ceramic heater and allows up to 10 ceramic heaters to be used simultaneously. It has a configurable data logging interface once it is connected to a computer with RS-485.

	A thermocouple is a simple, robust and cost-effective temperature sensor used in a wide range of temperature measurement processes. It consists of two dissimilar metal wires, joined at one end. When properly configured, thermocouples could provide measurements over a wide range of temperatures. Type-J thermocouple with a detection range of -100 to 1300°C is used to monitor the temperature of the model. It is compatible with the temperature controller and data acquisition unit. Thermocouples are placed at every critical point to ensure that the heat is equally distributed.
	Half Through Element (HTE) ceramic heater manufactured by HongTai is used for heat generation purposes. It could generate up to 700 °C with 125 W requirement. It will be connected to the temperature controller for power supply and relay control. The size of the ceramic heater is rather small compared to the narrow wall. Thus, multiple ceramic heaters are used at a different height from both sides of the wall. Trial test of heat conductivity and distribution will be performed to find out the proper height of placement of ceramic heaters to ensure that the heat is equally distributed throughout the narrow wall and into the deposition.
	Data acquisition model OM-DAQ-USB-2401 is a portable USB 2.0 full speed thermocouple or voltage input data acquisition module that could be used with a computer. This stand-alone module draws power from the USB port to operate. An external power supply (optional) could be used. All of the inputs are configurable through its software. The DAQ unit is compatible with thermocouple types J/K/T/E/R/S/B/N and voltage input ranging from ±30mV to ±10V. All analogue input channels could be measured sequentially at about 1ms per channel. A total of 1000 samples per second could be taken, divided across all active channels. It has a software namely DAQ Central which allows charting, data logging, file storage and real-time virtual monitoring (digital meters, dial meters, bar graphs) of data.

Appendix F: Recommended test preparation and paste backfilling test procedure:

1. Assemble the narrow wall with its wall support.
2. Install the load cell as in the schematic diagram and conduct calibration on the load cell (using external load).
3. Lower the vertical support to allow the narrow wall to touch the load cell and conduct stress transfer check on the wall support to ensure no stress could be transferred to the load cell by adding weight on top of the narrow wall.
4. Remove the load and disassemble the narrow wall with its vertical support from the base.
5. Construct the expansion joint in between of the narrow wall and its base plate.
6. Surround the narrow wall with a flexible latex from its base plate to the side wall and sealed the ending with waterproofing adhesive (epoxy). Clamp the latex onto the narrow wall surface to prevent water pressure from stripping off the adhesive from the latex.
7. Install the narrow wall with its wall support (rods) onto the base support after the epoxy achieves its initial strength after 20 minutes.
8. Put a spirit level on top of the narrow wall, adjust four adjustable sides of base support until the model is levelled and adjust the level of the load cell to have good contact with the base plate.
9. Leave the epoxy to set for at least 24 hours in order to attain its full strength before any testing.
10. Start the data acquisition prior conducting base plate pressure test by adding water into the narrow wall. Water needs to be drained using a vacuum pump and ensure that the interior of the narrow wall is dry.

11. Place the ceramic heaters and thermocouples according to the schematic diagram. Place another thermocouple at one meter away from the set-up to monitor the room temperature.
12. Preheat the narrow using the temperature controller and ceramic heater until targeted temperature and ensure that no stress contribution from the expansion of narrow wall by observing the load cell reading.
13. Ensure that the DAQ and temperature controller software is ready prior preparation of slurry.
14. Mix the paste either cemented or non-cemented using a portable mixer according to the designed proportion until it is homogenised which takes about 7 – 10 minutes.
15. Upon completion of filling, the level of the paste should be recorded as some of the paste may be lost during the transfer or mixing process.
16. Quickly lower the support hanger for the potentiometer and thermocouple. Place a piece of acrylic (pad) at the end of the potentiometer probe within the narrow wall on top of the deposited material. Insert the thermocouple into the paste.
17. Cover the top opening of the narrow wall with plastic wrap to minimise evaporation.
18. Monitor every parameter according to the test plan.
19. Stop the data acquisition upon completion.
20. Dismantle the set-up to allow post-test sample collection and cleaning work prior to next experiment with the different test plan.

Appendix G: Publication

1. Ting, W. K., Hasan, A., Sahdi, F., Taib, S. N. L., Sutan, N. M., Aziz, B. A., and Fourie, A. (2018). A narrow wall system to capture temperature-stress-strain behavior in paste backfill. *Geotechnical Testing Journal, 43.* https://doi.org/10.1520/GTJ20170383
   Status: Accepted and In Press.

2. Ting, W. K., Hasan, A., Sahdi, F., Taib, S. N. L., Sutan, N. M., Aziz, B. A., and Fourie, A. (2018). Interfacial friction behaviour in narrow wall paste backfill system. *Malaysian Construction Research Journal, Special Issue, 5*(3). pp. 52-56. ISSN 2590 - 4140.
   Status: Published.

3. Hasan, A., Ting, W. K., Sahdi, F., Taib, S. N. L., Sutan, N. M., Aziz, B. A., and Fourie, A. (2018). Temperature change and the total stress anomaly in paste backfill. *International Journal of GEOMATE, 14*(44), 90-95.
   Status: Published